MODELING, OPTIMIZATION AND ANALYSIS OF WIRELESS INFORMATION AND ENERGY TRANSFER IN BEYOND 5G IOT NETWORKS

A Thesis

Submitted in Partial Fulfilment

of the Requirements for the Degree of

Doctor of Philosophy

by

Chandan Kumar

Department of Electronics and Electrical Engineering
Indian Institute of Technology Guwahati
Guwahati - 781039, Assam, India

September 2023

To

My Family

Certificate

This is to certify that the thesis entitled "**Modeling, Optimization and Analysis of Wireless Information and Energy Transfer in Beyond 5G IoT Networks**", submitted by **Chandan Kumar**, a research scholar in the *Department of Electronics and Electrical Engineering, Indian Institute of Technology Guwahati*, for the award of the degree of **Doctor of Philosophy**, is a record of an original research work carried out by him under my supervision and guidance. The thesis has fulfilled all requirements as per the regulations of the institute and in my opinion has reached the standard needed for submission. The results embodied in this thesis have not been submitted to any other University or Institute for the award of any degree or diploma.

Date:

Place: Guwahati

Dr. Salil Kashyap

Dept. of Electronics and Electrical Engg.,

Indian Institute of Technology Guwahati,

Guwahati - 781 039, Assam, India.

Acknowledgements

First and foremost, I would like to express my deepest and most sincere gratitude to my supervisor *Dr. Salil Kashyap* for his excellent guidance throughout my study. His kindness, dedication, hard work and attention to detail have been a source of great inspiration to me. My heartfelt thanks to him for the unlimited support and patience shown to me. I sincerely thank him for the pain he undertook in scrutinizing every work I presented to him and offering critical comments to refine my work.

I am very thankful to my doctoral committee members *Prof. Ratnajit Bhattacharjee, Prof. Prabin Kumar Bora* and *Dr. Kalpana Dhaka* for sparing their precious time out of their busy schedule to evaluate my progress and enrich this work with their invaluable suggestions and feedback. I thank *Dr. Rimalapudi Sarvendranath* for his feedback and comments on the work done in Chapter 3 during our collaboration.

I would also like to thank the Head of the Department and other faculty members for their kind help in carrying out this work. Thanks are also due to the Science and Engineering Research Board (SERB), Government of India for funding my research studies during the later half of my PhD.

I sincerely thank my *parents, brothers* and *other family members* for their limitless efforts, unending support and blessings. I express a deep sense of gratitude to my *wife* and *son* for their tremendous support, patience and love.

(Chandan Kumar)

Abstract

This thesis focuses on system modeling, optimization and comprehensive performance analysis of wireless information and energy transfer to the Internet-of-Things (IoT) devices. These devices are likely to form a core component of beyond fifth generation (5G) wireless systems in order to support numerous applications foreseen in such systems. We first investigate whether a base station (BS) with massive number of antennas can support joint machine-centric communication among the IoT devices and human-centric communication among the mobile terminals. To this end, we derive downlink spectral efficiency (SE) of the IoT devices with maximum ratio precoding when channel estimates are acquired via the proposed distance-dependent grouping based hybrid pilot assignment strategy. As benchmarks, we also evaluate SE under non-orthogonal pilot assignment and distance-independent grouping. We show that under channel inversion based power control at the BS, the proposed pilot assignment and channel estimation strategy yields the highest sum SE and can serve the largest number of IoT devices when compared to the benchmarks. The corresponding performance under max-min power allocation is also presented.

We then elucidate feasibility of wireless energy transfer (WET) with the help of an intelligent reflecting surface (IRS). We consider a source equipped with multiple antennas and a single radio-frequency (RF) chain. And propose a low complexity rule that does joint antenna selection (AS) at source and passive beamforming at IRS. We derive new expressions for probability of outage in WET under perfect and estimated channel knowledge and for both single and multiple users. For a system with M antennas at source and N passive elements at IRS, we prove that

the diversity order equals $M+N$. Generalizations to subset AS, discrete phase shift design, and performance under limited scattering are also presented. Our results show that the proposed AS rule yields near-optimal performance while requiring only $M+N$ pilot transmissions compared to $M+MN$ pilot transmissions required by the optimal AS rule in literature. We illustrate that active RF chains at source can be traded with passive elements at IRS to obtain improved performance both in terms of outage probability (OP) and power transfer efficiency (PTE). And 3-bit IRS is sufficient to obtain good performance at lower complexity.

Thereafter, we study viability of WET from a source that is assisted by double IRS. To this end, we derive new closed-form analytical expressions for OP under non-linear energy harvesting (EH) at the user for different channel fading scenarios. We also generalize our outage analysis to a scenario where all links via the direct path and via the cascaded paths along the two IRSs undergo Rician fading. This analysis involves developing a novel statistical model based on Gamma distribution for the sum of product of Rician fading envelopes corresponding to cascaded paths. We then study the impact of four communication links between source and user on OP. To this end, we develop two algorithms, one based on manifold optimization and the other based on alternating optimization to design the phase shift matrices at two IRSs. Furthermore, we determine the optimal number of IRS elements that maximizes PTE under double IRS-assisted configuration. As benchmarks, we also derive the corresponding results for single IRS-assisted WET and massive multiple input multiple output enabled WET. The operational regimes in which double IRS aided WET provides improved performance are characterized.

We then investigate simultaneous wireless information and energy transfer to multiple IoT users using IRS under spatial correlation and optimal phase configuration. We derive a new and fairly tight upper bound on OP using Boole-Fréchet inequality when the IoT users are served based on round-robin scheduling strategy, share common source to IRS links and adopt non-linear EH at their end. We then de-

rive the diversity order for this system. A new upper bound on SE is also derived. The analysis involves developing a statistical model based on the Gamma distribution for the sum of product of Rayleigh fading envelopes that are correlated across reflected paths via the IRS. We determine the shape and scale parameters of this distribution using moment matching method and express them as hypergeometric function of the correlation coefficient. We present results to validate the accuracy of our statistical modeling and novel analytical bounds. The gain in performance relative to random and equal phase shift configurations is also quantified.

Contents

List of Figures

List of Tables

List of Abbreviations

AO	Alternating Optimization
AS	Antenna Selection
BS	Base Station
CDF	Cumulative Distribution Function
CLT	Central Limit Theorem
CSI	Channel State Information
DL	Downlink
EE	Energy Efficiency
EH	Energy Harvesting
IoT	Internet-of-Things
IRS	Intelligent Reflecting Surface
LAS	Low Complexity Antenna Selection
MIMO	Multiple Input Multiple Output
MMSE	Minimum Mean Square Error
MO	Manifold Optimization
MR	Maximum Ratio
OAS	Optimal Antenna Selection
OP	Outage Probability
PDF	Probability Density Function
PIN	Positive-Intrinsic-Negative

PTE	Power Transfer Efficiency
RF	Radio-Frequency
RR	Round-Robin
RV	Random Variable
SE	Spectral Efficiency
SWIET	Simultaneous Wireless Information and Energy Transfer
TDD	Time Division Duplex
UL	Uplink
WET	Wireless Energy Transfer
5G	Fifth Generation

List of Publications

Journal Papers

- **Chandan Kumar** and Salil Kashyap, "Intelligent Reflecting Surface Aided Simultaneous Wireless Information and Energy Transfer to IoT Users Under Spatial Correlation" Under review, *IEEE Transactions on Green Communications and Networking*, Jul. 2023.
- **Chandan Kumar** and Salil Kashyap, "On the Power Transfer Efficiency and Feasibility of Wireless Energy Transfer Using Double IRS" *IEEE Transactions on Vehicular Technology*, vol. 72, no. 5, pp. 6165-6180, May 2023.
- **Chandan Kumar**, Salil Kashyap, Rimalapudi Sarvendranath and Supreet Kumar Sharma, "On the Feasibility of Wireless Energy Transfer Based on Low Complexity Antenna Selection and Passive IRS Beamforming" *IEEE Transactions on Communications*, vol. 70, no. 8, pp. 5663–5678, Aug. 2022.
- **Chandan Kumar** and Salil Kashyap, "Massive MIMO enabled joint unicast transmission to IoT devices and mobile terminals" *IET Communication*, vol. 14, no. 13, pp. 2048–2059, Jul. 2020.

Conference Papers (Publications outside Thesis)

- **Chandan Kumar**, Aman Kumar and Salil Kashyap, "Intelligent Reflecting Surface Enabled Wireless System with Antenna Selection at Source Under Transceiver Hardware Impairments" in *Proc. Workshop on Smart Antennas and the Conference on Systems, Communications and Coding (WSA & SCC)*, Braunschweig, Germany, Feb. 2023, pp. 1–6.
- **Chandan Kumar**, Aman Kumar and Salil Kashyap, "Bit Error Rate Analysis of Double IRS Assisted Communication System Under Transceiver Hardware Impairments," in *Proc. National Conference on Communications (NCC)*, Guwahati, India, Feb. 2023, pp. 1–6.

1

Introduction

Contents

It is predicted that an exceptionally large number of Internet-of-things (IoT) devices will be part of the cellular network in the next five years [1, 2]. These IoT devices include sensors that sense data and communicate over a network. They find wide applications in consumer electronics, intelligent transportation, telecommunications, smart grids, home automation, intrusion detection for security, and autonomous monitoring of health, environment and structures. The current generation cellular network does not have the potential to handle concurrent machine-centric communication among these massive number of IoT devices and human type communication among these cellular or mobile terminals [3, 4]. The requirement to provide high aggregate data rates and reliable connectivity to such a huge number of IoT devices in addition to the mobile terminals is the main driver behind evolution of fifth generation (5G) and beyond 5G cellular networks.

Furthermore, most of these IoT devices operate on limited capacity batteries. Hence, their batteries need to be replaced or recharged from time-to-time for continued operation. This may not be feasible when these devices are placed in hazardous or inaccessible locations. Wireless energy transfer (WET), in which these energy-constrained IoT devices harvest energy from electromagnetic signals is one potential solution that can help charge the batteries of these massive number of IoT devices [5].

1.1 Challenges in Implementing Wireless Information and Energy Transfer

There are several challenges associated with supporting machine type communication among these IoT devices in addition to concurrently serving the mobile terminals. Firstly, these IoT devices may have diverse requirements in terms of data rates, latency, reliability and energy budget [3]. Secondly, acquisition of channel state information (CSI) for such a large number of IoT devices poses a significant training overhead and gives rise to challenges in pilot assignment and channel estimation. This is the first aspect that needs to be addressed.

The other aspect is that a completely different and unique set of challenges need to be addressed in order to efficiently implement WET to these IoT devices. Firstly, only a very small percentage of the power radiated by a source can be potentially harvested by an IoT device due

to severe path loss and limitations associated with the energy harvesting (EH) circuitry. Secondly, design of WET systems must ensure that the sensors harvest more energy than what they consume in sensing, computation, channel estimation and communication. Thirdly, the receive power levels that are sufficient for reliable data transfer and decoding may not be sufficient for WET and for activating the harvester in these sensors.[1] Fourthly, in order to make WET an economically viable alternative, it is highly likely that WET may happen in conjunction or concurrently with information transfer [7].

To address these challenges, massive multiple input multiple output (MIMO) systems, where the base station (BS) is equipped with hundreds of antennas, has been identified as one of the key 5G technologies in the emerging wireless standards [8, 9]. These systems offer huge degrees of freedom and have the potential to serve both mobile terminals and the IoT devices simultaneously over the same time-frequency resource through spatial multiplexing [10–12]. Furthermore, canonical massive MIMO operates in the time division duplex (TDD) mode. This makes these systems scalable in the sense that channel estimates obtained at the BS through transmission of pilots on the uplink (UL) may be used to precode data on the downlink (DL) [8]. Furthermore, it is shown that WET to IoT devices is feasible with massive number of antennas at the BS [6, 13]. However, these systems require as many radio-frequency (RF) chains as the number of antennas at the source. Since each of these RF chains consists of signal converters, up-converters, filters and power amplifiers. This increases the power consumption, hardware complexity and cost at the source in these systems.

Intelligent reflecting surface (IRS), which uses an array of passive low-cost reflecting elements and does not have any dedicated RF chains, is shown to enable WET [14, 15]. Furthermore, it has the potential to enhance spectral efficiency (SE) and energy efficiency (EE), security and coverage of a wireless network. It is being envisioned as a promising 6G technology and a core component of emerging wireless standards [16, 17]. Each of the passive IRS elements can be programmed to induce amplitude and phase shift to the incident signal. Programming these

[1] Unlike wireless information transfer, it is the absolute received power that is of interest in WET and not the signal-to-noise ratio (SNR) [6].

low cost passive elements to ensure coherent combination of signals at the receiver improves the receive signal energy. It thus enhances reliability and enables wireless charging.

1.2 Focus of Thesis and Our Contributions

This thesis focuses on system modeling, optimization and comprehensive performance analysis of wireless information and energy transfer to the IoT devices. We first investigate concurrent machine centric-communication among IoT devices and human-centric communication among cellular terminals from a BS equipped with massive number of antennas. We then analyze the feasibility of WET to IoT devices from a source that is equipped with fewer RF chains than the number of antennas and is assisted by an IRS. Thereafter, we extend this work to characterize the regimes in which double IRS aided WET can give improved performance relative to single IRS or massive MIMO enabled WET. Towards the end of this thesis, we also explore simultaneous wireless information and energy transfer (SWIET) to these devices under spatial correlation and optimal phase configuration at IRS. We present a brief background of each of these problems below and state our specific contributions.

1.2.1 Massive MIMO Enabled Joint Transmission to IoT Devices and Cellular terminals

We consider the DL of a massive MIMO system where a BS equipped with massive number of antennas serves two heterogeneous sets of user terminals, namely the mobile terminals and the IoT devices simultaneously over the same time and frequency. In order to construct precoders to transmit distinct data streams on the DL to mobile terminals and the IoT devices over a channel that varies over time, the CSI must be learnt at the BS every coherence interval. To facilitate this, we consider orthogonal pilot assignment strategy for mobile terminals where every mobile terminal is allocated an orthogonal pilot for channel estimation.

Since the number of IoT devices is expected to be high and the coherence interval has finite time-frequency samples, we consider two different low overhead pilot assignment and channel estimation strategies for the IoT devices to address the infeasibility of assigning an orthogonal pilot to every IoT device. In the first strategy, which we refer to as the distance-dependent grouping based hybrid pilot assignment strategy, the IoT devices are grouped based on their

relative distances (path losses) from the BS, for example, the farthest IoT device is grouped with the nearest, the second farthest is grouped with the second nearest and so on and every group is assigned an orthogonal pilot sequence, while IoT devices within a group share the same pilot sequence. In the second strategy, every IoT device is assigned a unique non-orthogonal pilot sequence. We also consider power control during the pilot phase which ensures that the average channel gain estimate of every IoT device is the same irrespective of its distance relative to the BS. During the data transmission phase, we consider two different power control policies, namely, channel inversion based power control and max-min power control that ensures uniform service to all.

Given this model, we make the following contributions:

- We first develop an expression for the channel estimate of every IoT device in a group for the proposed distance-dependent grouping based hybrid pilot assignment strategy. We then derive a new expression for the DL SE of the IoT devices when channel estimates are acquired using the hybrid strategy and maximum ratio (MR) precoding is used at the BS. Our analysis takes into account the correlation among the channel estimates of IoT devices within a group and also the interference that arises due to the presence of cellular users in the network.
- As a baseline, we also derive a new expression for the DL SE of IoT devices when channel estimates are acquired using non-orthogonal pilot assignment strategy.
- We then analyze the SE of mobile terminals when they are served jointly along with the IoT devices on the DL. We show that the SE of mobile terminals is independent of the pilot assignment strategy employed for IoT devices.
- We prove that under channel inversion based power control at the BS, distance-dependent grouping based hybrid pilot assignment strategy achieves the highest DL sum SE for IoT devices since it causes the least pilot contamination induced interference during data transmission when compared against the benchmarks.
- Furthermore, we also prove that for lower number of IoT devices, orthogonal pilot assignment strategy achieves the highest sum SE. However, as the number of IoT devices

grow, the sum SE with orthogonal strategy eventually reduces to zero and the distance-dependent grouping based hybrid strategy can the serve the largest number of IoT devices, when compared against non-orthogonal or distance-independent strategy.

- We numerically obtain the max-min power control coefficients and show that the SE obtained by the IoT devices is independent of the pilot assignment and channel estimation strategy used. This is because IoT devices also employ channel inversion based power control during pilot transmission phase, which makes the channel gain estimate of every IoT device roughly the same.

1.2.2 Single IRS-Assisted WET

We then study a practically relevant model where a source equipped with fewer RF chains than the number of transmit antennas is assisted by an IRS to transfer energy wirelessly. Each transmit RF chain, which is made up of digital-to-analog converters, up-converters, filters, and power amplifiers makes the source power hungry, bulky and costly. Antenna selection (AS) employed by the source reduces the number of RF chains required, thus reducing hardware complexity, power consumption, and the associated cost[2]. For this model, our main objective is to ascertain whether the receive power level at the user can be maintained at the same level by trading-off active RF chains at the source with passive elements at the IRS that do not require dedicated RF chains. Our model includes as a special case, the full-complexity system in which the source is equipped with as many RF chains as the number of antennas. We next summarize our key contributions:

- *AS Rule:* For a system with M antennas and N passive elements at IRS, we propose a joint AS and passive beamforming rule that requires only $M+N$ pilot transmissions for channel estimation. This is significantly lower than $M + MN$ pilot transmissions required by the optimal rule in [19, 20]. Therefore, the proposed AS rule reduces the pilot transmissions significantly and increases the time available for WET in a coherence interval.
- *Performance Analysis:* We derive a new analytical expression for probability of outage in WET with perfect CSI. This is an appropriate performance metric to ascertain feasibility

[2]This is the reason why it is a part of next generation wireless standards [18].

of WET in a wireless system with static or limited mobility users [6, 13, 21–23]. It helps identify operational regimes where users harvest more than what they consume in tasks related to channel estimation, sensing, computation, and communication. We also derive new expressions for minimum number of IRS elements required to avoid outage. These expressions provide key insights related to WET system design.

- *Estimated CSI:* We also derive a novel mathematical expression that approximates probability of outage in WET under linear minimum mean square error (MMSE) estimate of the cascaded and the direct channels. Our analysis helps in understanding the robustness of WET in practical scenarios in which the channel estimates are likely to be imperfect. The analysis involves order statistics of the magnitude of the estimated direct path channel gains and depends on IRS phase shifts that are designed based on estimated CSI.
- *Diversity Order:* We prove that diversity order of a joint AS and IRS-assisted WET is equal to sum of the number of antennas at the source and number of passive reflecting elements at the IRS, i.e., the diversity order equals $M + N$.
- *Subset AS:* We next generalize our model to include a source that is equipped with more than one RF chain and selects a subset of antennas based on strength of the direct channels to the user. We apply alternating optimization (AO) to obtain the beamformer at the source and phase shifts at the IRS. And elucidate the trade-off between probability of outage in WET and power transfer efficiency (PTE) under AS and full-complexity based energy beamforming.
- *Discrete Phase Shifts:* We then study the impact of practically relevant and implementation-friendly discrete phase shift design at IRS on performance. We show that a 3-bit programmable IRS is sufficient to achieve good trade-off between complexity and outage performance.
- *Multi-User Scenario:* We derive novel analytical bounds on probability of outage in WET to multiple users under both perfect and estimated CSI, where users are served based on round-robin (RR) scheduling strategy. This analysis takes into account the correlation that is expected to arise due to common source to IRS links for different users.

- *Limited Scattering:* We also study the impact of limited number of scatterers and inter-element spacing on outage probability (OP) [24]. We show how by exploiting the underlying spatial correlation, the pilot overhead can be reduced further from $M+N$ to $M+\frac{N}{G}$, where G denotes number of adjacent IRS elements that are configured with identical phase shifts.

While this part of the thesis focuses on fundamental aspects related to system modeling, optimization and comprehensive performance analysis to elucidate the feasibility of single IRS-assisted WET from a source that is equipped with fewer RF chains than the number of antennas. We next delve deeper into ascertaining the use of double IRS for WET and quantifying the gain in performance that can be achieved in terms of OP and PTE relative to single IRS-enabled WET and massive MIMO enabled WET.

1.2.3 Double IRS-Enabled WET

In this part of the thesis, we consider a wireless scenario where a single antenna source assisted by double IRS transfers DL energy to a single antenna user via reflected paths and the direct path. We design the passive beamforming at both the IRSs to maximize the received power at the user. We consider practically-relevant channel fading scenarios between different hops of the cascaded and direct channels to obtain a well-rounded and thorough understanding of the practical feasibility of double IRS-assisted WET. Our key contributions are listed as follows:

- *OP Analysis:* We derive new expressions for OP with double IRS-assisted configuration under non-linear EH at the user. Our analysis considers the presence of direct channel between the source and the user. This is justified and practically relevant, since there is a higher likelihood that the direct channel would also exist between the source and the user at typical distances foreseen in most WET scenarios. We note that this analysis entails designing the phases at the two IRSs in order to maximize the received power at the user and finding the joint probability density function (PDF) of the direct and the cascaded paths. As benchmarks, we derive new expressions for OP with single IRS-assisted configuration and with massive MIMO enabled WET.

- *Outage Analysis for Generic Channel Fading Scenario:* We generalize our analysis to also include the case when each link via the direct and the cascaded paths between the source and the user follows Rician fading. This analysis involves developing a novel statistical model based on Gamma distribution for the sum of product of Rician fading envelopes and rigorously deriving its shape and scale parameters through moment matching. We also validate the accuracy of this statistical modeling. Based on this, we derive a novel expression for OP for this scenario.
- *Extension to Four Communication Links:* We then study the impact of modeling four communication links between the source and the user on OP. Specifically, we develop two algorithms: one based on manifold optimization (MO) and the other based on AO in order to determine the phase shift configurations at the two IRSs to maximize the received power and obtain the corresponding OP.
- *PTE Analysis:* We also determine the optimal number of IRS elements that minimizes total power consumption for a given received power, thus optimizing PTE with double IRS-assisted WET under non-linear EH at the user. As benchmarks, we also derive new closed-form expressions for the optimal number of IRS elements and the optimal number of antennas that minimize total power consumption for a given received power for single IRS and massive MIMO enabled WET.
- *Extensive Numerical Results:* We prove that significant savings of power radiated by the source can be obtained through the use of two IRSs when compared to single IRS or massive MIMO while keeping OP fixed at a specific level. We also show that double IRS-assisted WET achieves about 10x and 1000x improved PTE compared to single IRS-assisted WET and massive MIMO enabled WET, respectively under pure line-of-sight (LoS) channels. Furthermore, we show that fewer number of elements are required in a double IRS configuration relative to single IRS and the number of antennas in massive MIMO to obtain the same received power.
- *New Design Insights:* Based on asymptotic analysis, we also determine the minimum number of elements that are required in double IRS-enabled WET in order to overcome

the effective path loss of the cascaded channel and give improved received power when compared to single IRS or massive MIMO-aided WET.

While the goal in this part of the thesis was to investigate the viability of WET from a double IRS-assisted source. We wish to emphasize that to make WET an economically viable alternative, one option is to integrate WET with the existing wireless information transfer system such that the same source and waveform can be harnessed to enable WET and make it a reality [7]. To this end, in the last part of the thesis, we consider IRS-assisted SWIET to IoT devices.

1.2.4 IRS-Enabled SWIET

In the last part of the thesis, we consider a novel and a practically well-motivated model in which a source assisted by an IRS performs SWIET over spatially correlated channels to multiple IoT users. Our model is comprehensive in the sense that we consider non-linear EH and power splitting architecture at the user end and optimal phase configuration at the IRS. We consider that the source adopts the channel unaware but fair RR scheduling strategy to perform SWIET to multiple users over equal duration time-orthogonal slots. We wish to emphasize that this is a practically appealing strategy that guarantees uniform quality of service to all the users. It enables real-time phase configuration at the IRS based on the direct and the cascaded channels to the user being served in the specific slot. It also avoids the necessity of running computationally intensive algorithms at the source to configure phases at the IRS when all users are served simultaneously. For this model, we summarise our key contributions below:

- *OP Analysis:* We derive a new upper bound on OP using Boole-Fréchet inequality [25] when IoT users are scheduled based on the RR strategy and share common source to IRS links. This rigorous analysis[3] takes into account the spatial correlation among the channels via the IRS elements. It also captures the correlation that arises in the energy harvested by different IoT users due to common source to IRS links. Furthermore, it involves developing a statistical model based on Gamma distribution for the sum of product of Rayleigh fading envelopes that are correlated across the reflected channels via the IRS. And computing the shape and scale parameters of the Gamma distributed random

[3]Our analysis is generic and applicable to any arbitrary correlation model.

variable (RV) as functions of the channel statistics using moment matching method and expressing them as hypergeometric function of the correlation coefficient.

- *Diversity Analysis:* We derive the diversity order for this system as $1 + \frac{k_u}{2}$, where k_u denotes the shape parameter of the Gamma distributed RV.
- *SE Analysis:* A new and simple closed-form upper bound on SE is also developed for this model. This result exploits concavity of the logarithm function and uses the new statistical model based on Gamma distribution described above.
- *Extension to Multi-Antenna Systems:* To obtain well-rounded understanding, we generalize our system to study the impact of multiple antennas at the source on OP. For this scenario, we obtain the transmit beamforming at the source and passive beamforming at IRS using AO with the objective of maximizing the received power at the IoT user being served.
- *Numerical Results and Novel Insights:* We present numerical results to validate the accuracy of our modeling and analytical bounds. We quantify and benchmark the gain in performance in terms of OP and SE, that can be achieved by systems that employ optimal phase shift configuration at IRS relative to systems that employs either random or equal phase shift configurations in a multi-user scenario under spatial correlation. We also elucidate that larger number of users can be supported by increasing number of IRS elements while maintaining OP at a specific level. Furthermore, by adding multiple antennas at the source, one can obtain the target OP at much lower transmit power.

1.3 Organisation of Thesis

The rest of the thesis is organized as follows. In Chapter 2, we analyze whether a BS with massive number of antennas can support joint machine type communication among IoT devices and human type communication among mobile terminals and address challenges in doing so. In Chapter 3, we develop low complexity AS rule, active and passive beamforming design based on the selected antennas and present comprehensive performance analysis under both perfect and estimated CSI for joint AS and IRS-assisted WET. Thereafter, in Chapter 4,

we extend our study to analyze the feasibility of WET from a double IRS-assisted source under non-linear EH and characterize regimes where they outperform single IRS-enabled WET and massive MIMO enabled WET. We then generalize our model to study SWIET to multiple IoT users under spatial correlation and optimal phase configuration at the IRS in Chapter 5. This is followed by conclusions and directions for future research in Chapter 6.

2

Massive MIMO Enabled Joint Transmission to IoT Devices and Cellular Terminals

Contents

In this Chapter, we consider the DL of a massive MIMO system where a BS with massive number of antennas serves two heterogeneous sets of user terminals, namely the cellular terminals and the IoT devices simultaneously over the same time and frequency. To construct precoders to transmit distinct data streams on the DL to mobile terminals and the IoT devices over a channel that varies over time, the CSI must be learnt at the BS every coherence interval. For this, we focus on orthogonal pilot assignment for mobile terminals where every mobile terminal is allocated an orthogonal pilot to enable channel estimation. Since the number of IoT devices is expected to be high and considering the fact the coherence interval has finite time-frequency samples, we analyze two different low overhead pilot assignment and channel estimation strategies for the IoT devices.

Given this model, we ask and delve deeper into answering the following questions: What is the DL sum SE that can be achieved by the IoT devices (interested in machine type communication) given that (1) they are served jointly with the mobile terminals (interested in human type communication) and (2) it is infeasible to assign an orthogonal pilot to each IoT device for channel estimation since very little time will be left for data transmission otherwise in a coherence interval? And how does the answer to the question above depend on the pilot assignment, channel estimation and power control strategies adopted.

We first review few papers related to massive MIMO enabled machine type communication.

2.1 Related Literature

While the authors in [26] discussed random access protocols for massive MIMO systems, in [27], a joint pilot assignment and data transmission protocol based on random access was proposed and UL sum-rate expressions were derived under pilot collisions and intermittent device activity. In [28, 29], the authors considered UL communication with massive number of devices and characterized the impact of imperfections in activity detection and channel estimation on the average achievable rates. The authors in [30] proposed the use of compressed sensing approaches like approximate message passing for device activity detection in order to ensure that grant free access schemes for pilot allocation remain scalable. In [31], deep learn-

ing based pilot assignment scheme was proposed for massive MIMO 5G systems. In [12], the authors considered a single-cell scenario and analyzed the UL achievable rates when both machines and cellular users are served simultaneously using massive MIMO technology. In [32], the authors derived the achievable rates for each user terminal in a single cell for both unicast and multigroup-multicast scenarios.

In [33], the authors developed solution for the weighted max-min fairness problem for a multigroup-multicast system under a per-antenna peak transmit power constraint. The authors in [34] considered a multicast scenario and proposed a pilot transmission scheme in order to estimate the sum channel of users interested in a common message within a group. A multigroup-multicast system where a common message is transmitted to all users within a group was also considered in [35], where the objective was to provide a low complexity solution to the weighted max-min problem in order to ensure uniform service to all. In [36], the design of precoding matrix which maximized the minimum SE of the users in every group for multicast and unicast transmissions was proposed. While for multicast transmission, joint precoding matrix was designed for the users in every group, for unicast transmission, a distinct precoding matrix was designed for each user in every group. As before, the users in every group were interested in common message and across groups distinct messages were transmitted.

Based on the discussion above, we conclude that grouping users to reduce the pilot signaling overhead has been considered before. However, every user in a group was considered to be interested in a common message and the precoder design for this multicast transmission was based on the sum channel estimate of the users within the group obtained via shared pilot signaling [32–36]. And for unicast transmission, the precoders were designed based on channel estimates acquired via orthogonal pilot signaling [32, 36]. We also observe that joint UL transmission to IoT devices and cellular users has also been considered before. However, to the best of our knowledge, this is the first work which considers DL unicast transmission from a BS with a massive number of antennas that transmits distinct messages jointly to two heterogeneous sets of user terminals, namely, the mobile terminals and the IoT devices [12]. To facilitate DL data transmission, the precoder, unlike the existing works has been designed based on estimates

obtained via low overhead channel estimation strategies where the pilot sequences assigned to all the user terminals need not be orthogonal. This is relevant since an orthogonal pilot cannot really be assigned to every IoT device which may be interested in distinct messages and which are expected to be huge in number in beyond 5G networks.

Notations: Boldface uppercase and lowercase letters denote matrices and vectors, respectively. The conjugate of a complex number and transpose are denoted by $(\cdot)^*$ and $(\cdot)^T$, respectively. The expectation and variance operators are denoted by $\mathbb{E}(\cdot)$ and var$(\cdot)$, respectively. A complex Gaussian RV Y with mean μ and variance σ^2 is denoted as $Y \sim \mathcal{CN}(\mu, \sigma^2)$. An $l \times l$ identity matrix is denoted by I_l.

2.2 System Model

We consider the DL of a single cell massive MIMO system where a BS equipped with L antennas serves M mobile terminals and D IoT devices simultaneously over the same time-frequency resource as shown in Figure 2.1. The two heterogeneous sets of user terminals, namely, mobile and IoT devices are expected to have different data rate requirements. We assume that number of IoT devices is much larger than number of mobile terminals, i.e., $D \gg M$ [12]. We model the channel vector $\boldsymbol{h}_m \in C^{L\times 1}$ between the BS and the m^{th} mobile terminal as Rayleigh faded, i.e., $\boldsymbol{h}_m \sim \mathcal{CN}(\boldsymbol{0}, \beta_m \boldsymbol{I}_L)$, for all $m \in \{1, 2, \ldots, M\}$, where β_m denotes the path loss between the BS and the m^{th} mobile terminal. Similarly, the channel vector $\boldsymbol{g}_d \in C^{L\times 1}$ between the BS and the d^{th} IoT device is modeled as Rayleigh faded, i.e., $\boldsymbol{g}_d \sim \mathcal{CN}(\boldsymbol{0}, \beta_d \boldsymbol{I}_L)$, for all $d \in \{1, 2, \ldots, D\}$, where β_d captures the path loss between the BS and the d^{th} IoT device. The path loss to any user is independent of the BS antenna index since the array length is considered to be much less than the distance between the BS and the users [8].

The channels are assumed to be time-invariant over a coherence interval of τ_c samples. Furthermore, we assume TDD mode of communication between the BS and the user terminals (mobile or IoT devices) in order to exploit channel reciprocity [8, 11]. This ensures that the channel estimates acquired during UL training phase may be used to precode data to user terminals on the DL.

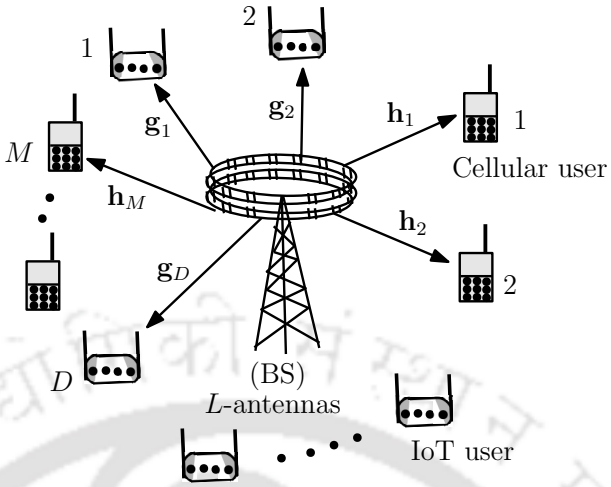

Fig. 2.1: System Model

The communication between the BS and the user terminals occurs in three different phases as shown in Figure 2.2. In a coherence interval of τ_c samples, the first τ_{pd} samples are used for UL pilot signaling by the IoT devices. The next τ_{pm} samples are used for UL pilot signaling by the mobile terminals. This is followed by the data transmission phase of τ_s samples, wherein the BS based on the channel estimates acquired during the first two phases precodes data to both mobile terminals and the IoT devices. Thus, $\tau_{pd} + \tau_{pm} + \tau_s = \tau_c$.

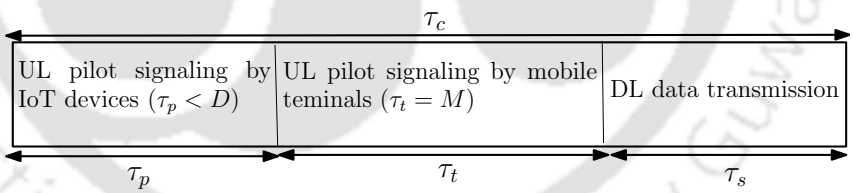

Fig. 2.2: Frame structure for UL pilot and DL data transmission.

2.2.1 UL Pilot Signaling and Channel Estimation

In order to multiplex data streams to both the mobile terminals and the IoT devices, the BS must acquire CSI through UL pilot transmission. We consider a scenario where every mobile terminal is assigned an orthogonal pilot sequence for channel estimation. Furthermore, for the IoT devices that have relatively low data rate requirements and are relatively huge in number, we consider two different pilot assignment strategies with the objective of reducing the training overhead. While in the first strategy, which we refer to as the distance-dependent grouping based hybrid pilot assignment strategy, the IoT devices are grouped together based on their

relative distances from the BS and every group is allocated an orthogonal pilot sequence while devices within a group share the same pilot. In the second strategy, every IoT device is assigned a dedicated non-orthogonal pilot sequence whose length is less than D.

2.2.1.1 By IoT Devices Using the Proposed Distance-Dependent Grouping Based Hybrid Pilot Assignment Strategy

In this strategy, the IoT devices are grouped together based on relative distances from the BS and every group is assigned an orthogonal pilot sequence. However, devices within a group share the same pilot. Let N IoT devices be grouped together, so that we have $\frac{D}{N}$ groups.[1]

Let $\boldsymbol{\phi}_D^{G_i} \in C^{\tau_{pd}\times 1}$ denote the pilot sequence assigned to G_i^{th} group such that $\tau_{pd} \geq \frac{D}{N}$. This condition ensures that every group of IoT devices is assigned an orthogonal pilot for channel estimation, i.e., these pilot sequences are allocated such that $\left(\boldsymbol{\phi}_D^{G_i}\right)^H \boldsymbol{\phi}_D^{G_j} = \delta_{ij}$, where $\delta_{ij} = 1$ if $i = j$ and is 0 otherwise. Let $q_d^{G_k}$ denote the pilot power of d^{th} IoT device in G_k^{th} group.

The signal $\boldsymbol{Y}_p^G \in C^{L\times\tau_{pd}}$ received at the BS based on this pilot transmission strategy by the IoT devices is given by

$$\boldsymbol{Y}_p^G = \sum_{k=1}^{D/N} \sqrt{\tau_{pd}} \left(\sum_{d\in G_k} \sqrt{q_d^{G_k}}\, \boldsymbol{g}_d^{G_k} \right) \left(\boldsymbol{\phi}_D^{G_k}\right)^H + \boldsymbol{N}_p^G, \tag{2.1}$$

where $\boldsymbol{g}_d^{G_k} \in C^{L\times 1}$ denotes the channel vector between the BS and the d^{th} IoT device belonging to the G_k^{th} group, $\boldsymbol{N}_{pd}^G \in C^{L\times\tau_{pd}}$ is the noise introduced at the BS, each of whose entries is independent and identically distributed (i.i.d.) $\mathcal{CN}(0,\sigma^2)$. In order to estimate the channel of the d^{th} IoT device in the G_k^{th} group, de-spreading of the received signal is performed. Let $\boldsymbol{y}_{pd}^{G_k} \in C^{L\times 1}$ denote the de-spreaded signal for the d^{th} IoT device in G_k^{th} group. Then,

$$\boldsymbol{y}_{pd}^{G_k} = \boldsymbol{Y}_p^G \boldsymbol{\phi}_D^{G_k}, \tag{2.2}$$

$$= \sqrt{\tau_{pd} q_d^{G_k}}\, \boldsymbol{g}_d^{G_k} + \sum_{d'\in G_k\setminus\{d\}} \sqrt{\tau_{pd} q_{d'}^{G_k}}\, \boldsymbol{g}_{d'}^{G_k} + \boldsymbol{n}_{pd}^{G_k}, \tag{2.3}$$

where $\boldsymbol{n}_{pd}^{G_k} = \boldsymbol{N}_p^G \boldsymbol{\phi}_D^{G_k}$. Each entry of $\boldsymbol{n}_{pd}^{G_k}$ is also i.i.d. $\mathcal{CN}(0,\sigma^2)$ owing to the rotational invariance property of circular symmetric complex Gaussian RVs.

Analyzing the signal at the l^{th} BS antenna from the d^{th} IoT device in the G_k^{th} group would be

[1] We assume $\frac{D}{N}$ to be an integer.

enough, since the elements of the channel and noise matrices are statistically independent [37]. Hence, using (2.3), the signal received at the l^{th} BS antenna from the d^{th} IoT device in the G_k^{th} group

$$y_{pdl}^{G_k} = \sqrt{\tau_{pd} q_d^{G_k}} g_{dl}^{G_k} + \sum_{d' \in G_k \setminus \{d\}} \sqrt{\tau_{pd} q_{d'}^{G_k}} g_{d'l}^{G_k} + n_{pdl}^{G_k}, \tag{2.4}$$

where $g_{dl}^{G_k}$ denotes the l^{th} element of $\boldsymbol{g}_d^{G_k}$ and $n_{pdl}^{G_k}$ denotes the l^{th} element of $\boldsymbol{n}_{pd}^{G_k}$. Based on this, the MMSE estimate[2] of the channel $g_{dl}^{G_k}$ between the l^{th} BS antenna and the d^{th} IoT device in the G_k^{th} group can be obtained and is stated in a simplified form in the Lemma below.

Lemma 2.1. *The channel estimate $\hat{g}_{dl}^{G_k}$ from the d^{th} IoT device of the G_k^{th} group to the l^{th} BS antenna, where every group is allocated an orthogonal pilot sequence while IoT devices within a group share the same pilot sequence is given by*

$$\hat{g}_{dl}^{G_k} = g_{dl}^{G_k} + \tilde{g}_{dl}^{G_k}, \tag{2.5}$$

where $\tilde{g}_{dl}^{G_k}$ is the channel estimation error that is uncorrelated to $\hat{g}_{dl}^{G_k}$ and is given by

$$\tilde{g}_{dl}^{G_k} = -g_{dl}^{G_k} \left(\frac{\sigma^2 + \sum\limits_{d' \in G_k \setminus \{d\}} \tau_{pd} q_{d'}^{G_k} \beta_{d'}^{G_k}}{\sigma^2 + \sum\limits_{d' \in G_k} \tau_{pd} q_{d'}^{G_k} \beta_{d'}^{G_k}} \right) + \frac{\sqrt{q_d^{G_k} \tau_{pd}} \beta_d^{G_k}}{\sigma^2 + \sum\limits_{d' \in G_k} \tau_{pd} q_{d'}^{G_k} \beta_{d'}^{G_k}} \left(\sum_{d' \in G_k \setminus \{d\}} \sqrt{\tau_{pd} q_{d'}^{G_k}} g_{d'l}^{G_k} + n_{pdl}^{G_k} \right). \tag{2.6}$$

Furthermore, the variance $\gamma_d^{G_k}$ of the channel estimate equals $\mathbb{E}\left[\left|\hat{g}_{dl}^{G_k}\right|^2\right] = \frac{q_d^{G_k} \tau_{pd} {\beta_d^{G_k}}^2}{\sigma^2 + \sum\limits_{d' \in G_k} \tau_{pd} q_{d'}^{G_k} \beta_{d'}^{G_k}}$ and the variance of the estimation error equals $\mathbb{E}\left[\left|\tilde{g}_{dl}^{G_k}\right|^2\right] = \beta_d^{G_k} - \gamma_d^{G_k}$.

Proof. The proof is given in Appendix A.1. □

Remark: Note that the channel estimate of the d^{th} IoT device belonging to the G_k^{th} group is a linear combination of the true channels of all the N IoT devices that belong to the G_k^{th} group. Therefore, the channel estimates are correlated within the group. Furthermore, these estimates are also valid for the distance independent strategy where IoT devices are grouped irrespective of their distances from the BS.

2.2.1.2 By IoT Devices Using Non-Orthogonal Pilot Assignment Strategy

We now consider the strategy where every IoT device as shown in Figure 2.1 is assigned a unique non-orthogonal pilot sequence. Let $\boldsymbol{\phi}_d \in C^{\tau_{pd} \times 1}$ denote the unique non-orthogonal pilot

[2]The computational complexity involved in estimating the channel vector to all D IoT devices based on this strategy requires $\frac{4L\tau_p D}{N} + 2LD + 3D$ real multiplications, $(4L\tau_p - 2L)\frac{D}{N} + D$ real additions and D real divisions.

sequence assigned to d^{th} IoT device such that $\tau_{pd} < D$. Furthermore, the pilot sequences are chosen such that $\boldsymbol{\phi}_d^H \boldsymbol{\phi}_{d'} = 1$, if $d' = d$ and $\boldsymbol{\phi}_d^H \boldsymbol{\phi}_{d'} \neq 0$, if $d' \neq d$. Let q_d denote the pilot power of d^{th} IoT device.

The signal $\boldsymbol{Y}_p \in C^{L \times \tau_{pd}}$ received at the BS when every IoT device transmits a unique non-orthogonal pilot sequence is given by

$$\boldsymbol{Y}_p = \sum_{d=1}^{D} \sqrt{\tau_{pd} q_d} \boldsymbol{g}_d \boldsymbol{\phi}_d^H + \boldsymbol{N}_p, \tag{2.7}$$

where $\boldsymbol{N}_p \in C^{L \times \tau_{pd}}$ is the noise introduced at the BS, each of whose entries is i.i.d. $\mathcal{CN}(0, \sigma^2)$. In order to estimate channel of d^{th} IoT device, we de-spread $\boldsymbol{Y}_p$ using $\boldsymbol{\phi}_d$ to obtain

$$\boldsymbol{y}_{pd} = \boldsymbol{Y}_p \boldsymbol{\phi}_d = \sqrt{\tau_{pd} q_d} \boldsymbol{g}_d + \sum_{\substack{d'=1 \\ d' \neq d}}^{D} \sqrt{\tau_{pd} q_{d'}} \boldsymbol{g}_{d'} \boldsymbol{\phi}_{d'}^H \boldsymbol{\phi}_d + \boldsymbol{n}_{pd}, \tag{2.8}$$

where $\boldsymbol{n}_{pd} = \boldsymbol{N}_p \boldsymbol{\phi}_d$. Each entry of $\boldsymbol{n}_{pd}$ is also i.i.d. $\mathcal{CN}(0, \sigma^2)$. It is sufficient to consider the de-spreaded signal from the d^{th} IoT device to the l^{th} BS antenna as given by [37]

$$y_{pdl} = \sqrt{\tau_{pd} q_d} g_{dl} + \sum_{\substack{d'=1 \\ d' \neq d}}^{D} \sqrt{\tau_{pd} q_{d'}} g_{d'l} \boldsymbol{\phi}_{d'}^H \boldsymbol{\phi}_d + n_{pdl}, \tag{2.9}$$

where g_{dl} denotes the l^{th} element of $\boldsymbol{g}_d$ and n_{pdl} denotes the l^{th} element of $\boldsymbol{n}_{pd}$. Based on this observable, the MMSE estimate[3] of the channel from the d^{th} IoT device to the l^{th} BS antenna is given by the classic conditional mean [38] and is stated in a simplified form as a Lemma below.

Lemma 2.2. *The channel estimate $\hat{g}_{dl}$ from the d^{th} IoT device to the l^{th} BS antenna when every IoT device transmits a unique non-orthogonal pilot sequence is given by*

$$\hat{g}_{dl} = g_{dl} + \tilde{g}_{dl}, \tag{2.10}$$

[3]The computational complexity involved in estimating the channel vector to all D IoT devices based on this strategy requires $4L\tau_p D + 2LD + 4\tau_p D^2 + 4D^2$ real multiplications, $(4L\tau_p - 2L)D + 4\tau_p D^2$ real additions and D real divisions.

where $\tilde{g}_{dl}$ is the channel estimation error that is uncorrelated to $\hat{g}_{dl}$ and is given by

$$\tilde{g}_{dl} = -g_{dl}\left(\frac{\sigma^2 + \sum_{\substack{d'=1 \\ d'\neq d}}^{D} q_{d'}\tau_{pd}\beta_{d'}|\boldsymbol{\phi}_{d'}^H\boldsymbol{\phi}_d|^2}{\sigma^2 + \sum_{d'=1}^{D} q_{d'}\tau_{pd}\beta_{d'}|\boldsymbol{\phi}_{d'}^H\boldsymbol{\phi}_d|^2}\right) + \frac{\sqrt{\tau_{pd}q_d}\beta_d}{\sigma^2 + \sum_{d'=1}^{D} q_{d'}\tau_{pd}\beta_{d'}|\boldsymbol{\phi}_{d'}^H\boldsymbol{\phi}_d|^2}\left(\sum_{\substack{d'=1 \\ d'\neq d}}^{D}\sqrt{\tau_{pd}q_{d'}}g_{d'l}\boldsymbol{\phi}_{d'}^H\boldsymbol{\phi}_d + n_{pdl}\right). \tag{2.11}$$

Furthermore, the variance γ_d of the channel estimate equals $\mathbb{E}\left[|\hat{g}_{dl}|^2\right] = \frac{\tau_{pd}q_d\beta_d^2}{\sigma^2+\tau_{pd}\sum_{d=1}^{D} q_d\beta_{d'}|\boldsymbol{\phi}_{d'}^H\boldsymbol{\phi}_d|^2}$ and the variance of the estimation error equals $\mathbb{E}\left[|\tilde{g}_{dl}|^2\right] = \beta_d - \gamma_d$.

Proof. This can be proved using standard results on conditional Gaussian RVs. □

Remark: Note that the channel estimate of the d^{th} IoT device obtained above is a linear combination of the true channels of all IoT devices. The estimates of different IoT devices are thus correlated to each other.

2.2.1.3 By Mobile Terminals Using Orthogonal Pilot Assignment Strategy

Let $\boldsymbol{\phi}_m \in C^{\tau_{pm}\times 1}$ be the pilot signal assigned to the m^{th} mobile terminal such that $\tau_{pm} \geq M$. Furthermore, $\boldsymbol{\phi}_m^H\boldsymbol{\phi}_{m'} = \delta_{mm'}$, where $\delta_{mm'} = 1$ if $m' = m$ and is 0 otherwise. Let q_m denote the pilot power of the m^{th} mobile terminal. The signal $\boldsymbol{R}_p \in C^{L\times\tau_{pm}}$ received at the BS when every mobile terminal transmits an orthogonal pilot is given by

$$\boldsymbol{R}_p = \sum_{m=1}^{M}\sqrt{\tau_{pm}q_m}\boldsymbol{h}_m\boldsymbol{\phi}_m^H + \boldsymbol{W}_p, \tag{2.12}$$

where $\boldsymbol{W}_p \in C^{L\times\tau_{pm}}$ is the noise introduced at the BS each of whose each entries is i.i.d. $\mathcal{CN}(0,\sigma^2)$.

Based on the observables in (2.12) at the BS, the MMSE estimate of the channel h_{ml} between the m^{th} mobile terminal and the l^{th} BS antenna is given by [37, 38]

$$\hat{h}_{ml} = h_{ml} + \tilde{h}_{ml}, \tag{2.13}$$

where $\tilde{h}_{ml}$ is the channel estimation error that is uncorrelated to the $\hat{h}_{ml}$. Furthermore, $\tilde{h}_{ml} = -h_{ml}\left(\frac{\sigma^2}{\sigma^2+\tau_{pm}q_m\beta_m}\right) + \frac{\sqrt{q_m\tau_{pm}}\beta_m}{\sigma^2+\tau_{pm}q_m\beta_m}w_{pml}$, where w_{pml} denotes the l^{th} element of $\boldsymbol{w}_{pm} = \boldsymbol{W}_p\boldsymbol{\phi}_m$. It can be shown that the variance γ_m of the channel estimate equals $\mathbb{E}\left[\left|\hat{h}_{ml}\right|^2\right] = \frac{\tau_{pm}q_m\beta_m^2}{\sigma^2+\tau_{pm}q_m\beta_m}$ and variance of

the estimation error equals $\mathbb{E}\left[\left|\tilde{h}_{ml}\right|^2\right] = \beta_m - \gamma_m$. Note that the channel estimates of the mobile terminals are uncorrelated to each other.

The channel estimates obtained in this section will be referred to in the analysis in Section 2.3.

2.2.2 DL Data Transmission

Let $\boldsymbol{x} \in C^{L\times 1}$ denote the signal vector transmitted by the BS. Then,

$$\boldsymbol{x} = \sum_{d=1}^{D} \sqrt{p_d}\boldsymbol{a}_d s_d + \sum_{m=1}^{M} \sqrt{p_m}\boldsymbol{a}_m s_m, \tag{2.14}$$

where $\boldsymbol{a}_d$ denotes the precoding vector corresponding to the d^{th} IoT device, $\boldsymbol{a}_m$ denotes the precoding vector corresponding to the m^{th} mobile terminal, p_d denotes the data power of d^{th} IoT device, p_m denotes the power with which data is sent to the m^{th} mobile terminal, s_d denotes the symbol transmitted to d^{th} IoT device and s_m denotes symbol transmitted to the m^{th} mobile terminal. Every symbol is independently transmitted and is assumed to have unit variance. We assume that the BS is transmit power constrained, i.e., $\mathbb{E}\left[\|\boldsymbol{x}\|^2\right] \leq P$.

Collectively, the signal $\boldsymbol{y} \in C^{(D+M)\times 1}$ received at the user terminals during DL data transmission is given by

$$\boldsymbol{y} = \boldsymbol{G_c}^T\boldsymbol{x} + \boldsymbol{w}, \tag{2.15}$$

where $\boldsymbol{w} \in C^{(D+M)\times 1}$ is the noise introduced at the users during data transmission, each of whose entries is i.i.d. $\mathcal{CN}(0, \sigma^2)$ and $\boldsymbol{G_c} \in C^{L\times(D+M)}$ denotes the composite true channel matrix given by $\boldsymbol{G_c} = [\boldsymbol{G}\ \ \boldsymbol{H}]$. The d^{th} column of $\boldsymbol{G}$ is $\boldsymbol{G}(:, d) = \boldsymbol{g}_d$, for $1 \leq d \leq D$ and the m^{th} column of $\boldsymbol{H}$ is $\boldsymbol{H}(:, m) = \boldsymbol{h}_m$, for $1 \leq m \leq M$.

2.3 SE Analysis

In this section, we derive new expressions for the DL achievable SE first for the IoT devices and then for the mobile terminals. The expressions are derived for the case when MR precoding is deployed at the BS and channel estimates for mobile terminals are obtained using orthogonal pilots while that for the IoT devices are obtained based on either of the two different pilot

$$y_d^{G_k} = \sqrt{p_d^{G_k}} \left(\boldsymbol{g}_d^{G_k}\right)^T \boldsymbol{a}_d^{G_k} s_d^{G_k} + \sum_{d' \in G_k \setminus \{d\}} \sqrt{p_{d'}^{G_k}} \left(\boldsymbol{g}_d^{G_k}\right)^T \boldsymbol{a}_{d'}^{G_k} s_{d'}^{G_k} + \sum_{\substack{k'=1 \\ k' \neq k}}^{D/N} \sum_{d' \in G_{k'}} \sqrt{p_{d'}^{G_{k'}}} \left(\boldsymbol{g}_d^{G_k}\right)^T \boldsymbol{a}_{d'}^{G_{k'}} s_{d'}^{G_{k'}} + \sum_{m'=1}^{M} \sqrt{p_{m'}} \left(\boldsymbol{g}_d^{G_k}\right)^T \boldsymbol{a}_{m'} s_{m'} + w_d^G, \quad (2.16)$$

$$y_d^{G_k} = \sqrt{\frac{p_d^{G_k}}{L\gamma_d^{G_k}}} \left(\hat{\boldsymbol{g}}_d^{G_k}\right)^T \left(\hat{\boldsymbol{g}}_d^{G_k}\right)^* s_d^{G_k} + \sum_{d' \in G_k \setminus \{d\}} \sqrt{\frac{p_{d'}^{G_k}}{L\gamma_{d'}^{G_k}}} \left(\boldsymbol{g}_d^{G_k}\right)^T \left(\hat{\boldsymbol{g}}_{d'}^{G_k}\right)^* s_{d'}^{G_k} + \sum_{\substack{k'=1 \\ k' \neq k}}^{D/N} \sum_{d' \in G_{k'}} \sqrt{\frac{p_{d'}^{G_{k'}}}{L\gamma_{d'}^{G_{k'}}}} \left(\boldsymbol{g}_d^{G_k}\right)^T \left(\hat{\boldsymbol{g}}_{d'}^{G_{k'}}\right)^* s_{d'}^{G_{k'}} + \sum_{m'=1}^{M} \sqrt{\frac{p_{m'}}{L\gamma_{m'}}} \left(\boldsymbol{g}_d^{G_k}\right)^T \hat{\boldsymbol{h}}_{m'}^* s_{m'} + \left(w_d^G - \sqrt{\frac{p_d^{G_k}}{L\gamma_d^{G_k}}} \left(\tilde{\boldsymbol{g}}_d^{G_k}\right)^T \left(\hat{\boldsymbol{g}}_d^{G_k}\right)^* s_d^{G_k} \right). \quad (2.17)$$

signaling strategies aimed at reducing the training overhead as discussed in Section 2.2.

2.3.1 For IoT Devices Based on the Proposed Distance-Dependent Grouping Based Hybrid Pilot Assignment Strategy

Based on (2.15) and upon simplification, the data signal $y_d^{G_k}$ received on the DL by the d^{th} IoT device in group G_k is given by (2.16) given at the top of the next page, where $p_d^{G_k}$ denotes the data power for the d^{th} IoT device in G_k^{th} group, the MR precoding vector for the m^{th} mobile terminal is $\boldsymbol{a}_m = \frac{1}{\sqrt{L}} \frac{\hat{\boldsymbol{h}}_m^*}{\sqrt{\gamma_m}}$, while the MR precoding vector for the d^{th} IoT device in group G_k equals $\boldsymbol{a}_d^{G_k} = \frac{1}{\sqrt{L}} \frac{\left(\hat{\boldsymbol{g}}_d^{G_k}\right)^*}{\sqrt{\gamma_d^{G_k}}}$. Substituting the corresponding precoding vectors and $g_{dl}^{G_k} = \hat{g}_{dl}^{G_k} - \tilde{g}_{dl}^{G_k}$ for all l from (2.5) in (2.16), we get (2.17).

In order to apply use and forget bound to evaluate the signal to interference plus noise ratio (SINR) [39], we rearrange (2.17) to obtain (2.18). Note that the first term in (2.18) corresponds to the desired signal for the d^{th} IoT device in group G_k, the second term captures the interference due to all other users within the group G_k, the third term captures the interference due to IoT devices in all other groups except G_k. The other three terms capture the interference due to mobile terminals, receiver noise, channel estimation error, and the penalty due to the application

$$y_d^{G_k} = \underbrace{\sqrt{\frac{p_d^{G_k}}{L\gamma_d^{G_k}}}\mathbb{E}\left\{\left\|\hat{\boldsymbol{g}}_d^{G_k}\right\|^2\right\} s_d^{G_k}}_{I} + \underbrace{\sum_{d'\in G_k\setminus\{d\}} \sqrt{\frac{p_{d'}^{G_k}}{L\gamma_{d'}^{G_k}}}\left(\boldsymbol{g}_d^{G_k}\right)^T\left(\hat{\boldsymbol{g}}_{d'}^{G_k}\right)^* s_{d'}^{G_k}}_{II}$$
$$+ \underbrace{\sum_{\substack{k'=1\\k'\neq k}}^{D/N}\sum_{d'\in G_{k'}} \sqrt{\frac{p_{d'}^{G_{k'}}}{L\gamma_{d'}^{G_{k'}}}}\left(\boldsymbol{g}_d^{G_k}\right)^T\left(\hat{\boldsymbol{g}}_{d'}^{G_{k'}}\right)^* s_{d'}^{G_{k'}}}_{III} + \underbrace{\sum_{m'=1}^{M}\sqrt{\frac{p_{m'}}{L\gamma_{m'}}}\left(\boldsymbol{g}_d^{G_k}\right)^T\hat{\boldsymbol{h}}_{m'}^* s_{m'}}_{IV}$$
$$+ \underbrace{\left(w_d^G - \sqrt{\frac{p_d^{G_k}}{L\gamma_d^{G_k}}}\left(\tilde{\boldsymbol{g}}_d^{G_k}\right)^T\left(\hat{\boldsymbol{g}}_d^{G_k}\right)^* s_d^{G_k}\right)}_{V} + \underbrace{\sqrt{\frac{p_d^{G_k}}{L\gamma_d^{G_k}}}\left[\left\|\hat{\boldsymbol{g}}_d^{G_k}\right\|^2 - E\left\|\hat{\boldsymbol{g}}_d^{G_k}\right\|^2\right] s_d^{G_k}}_{VI}. \quad (2.18)$$

of use and forget bound. Using (2.18), we obtain the DL achievable SE of the d^{th} IoT device in the G_k^{th} group and state that next as a theorem.

Theorem 2.1. *The DL achievable SE $R_d^{G_k}$ of the d^{th} IoT device in the G_k^{th} group when the IoT devices adopt the hybrid pilot assignment strategy for channel estimation while mobile terminals adopt orthogonal pilot assignment strategy is given by*

$$R_d^{G_k} = \left(1 - \frac{\tau_{pd} + \tau_{pm}}{\tau_c}\right)\log_2\left(1 + \text{SINR}_d^{G_k}\right), \quad (2.19)$$

where,

$$\text{SINR}_d^{G_k} = \frac{L\gamma_d^{G_k} p_d^{G_k}}{\sigma^2 + \sum\limits_{d'\in G_k\setminus\{d\}} \frac{p_{d'}^{G_k}}{L\gamma_{d'}^{G_k}}\chi_{d'}^{G_k} + \beta_d^{G_k}\sum\limits_{m'=1}^{M} p_{m'} + \beta_d^{G_k} p_d^{G_k} + \sum\limits_{\substack{k'=1\\k'\neq k}}^{D/N}\sum\limits_{d'\in G_{k'}} \frac{p_{d'}^{G_{k'}}}{L\gamma_{d'}^{G_{k'}}}\xi_{d'}^{G_{k'}}}, \quad (2.20)$$

$$\chi_{d'}^{G_k} = \left(\eta_{d'}^{G_k}\right)^2\left(\tau_{pd} q_d^{G_k} L(L+1)\left(\beta_d^{G_k}\right)^2 + \sum_{u\in G_k\setminus\{d\}} \tau_{pd} q_u^{G_k} L\beta_d^{G_k}\beta_u^{G_k} + L\beta_d^{G_k}\sigma^2\right),$$
$$\xi_{d'}^{G_{k'}} = \left(\eta_{d'}^{G_{k'}}\right)^2\left(\sum_{u\in G_{k'}} \tau_{pd} q_u^{G_{k'}} L\beta_d^{G_k}\beta_u^{G_{k'}} + L\beta_d^{G_k}\sigma^2\right) \text{ and } \eta_{d'}^{G_k} = \frac{\sqrt{\tau_{pd} q_{d'}^{G_k}}\beta_{d'}^{G_k}}{\sigma^2 + \sum\limits_{v\in G_k}\tau_{pd} q_v^{G_k}\beta_v^{G_k}}.$$

Proof. The proof is given in Appendix A.2. □

The achievable SE analysis of the d^{th} IoT device in the G_k^{th} group accounts for the correlation among the channel estimates of the IoT devices within a group due to pilot sharing within the group and also accounts for the interference that arises due to the mobile terminals in the network.

$$y_d = \underbrace{\sqrt{\frac{p_d}{L\gamma_d}}\mathbb{E}\{\|\hat{\boldsymbol{g}}_d\|^2\}s_d}_{I} + \underbrace{\sum_{\substack{d'=1\\d'\neq d}}^{D}\sqrt{\frac{p_{d'}}{L\gamma_{d'}}}\boldsymbol{g}_d^T\hat{\boldsymbol{g}}_{d'}^* s_{d'}}_{II} + \underbrace{\sum_{m'=1}^{M}\sqrt{\frac{p_{m'}}{L\gamma_{m'}}}\boldsymbol{g}_d^T\hat{\boldsymbol{h}}_{m'}^* s_{m'}}_{III}$$
$$+ \underbrace{\left(w_d - \sqrt{\frac{p_d}{L\gamma_d}}\tilde{\boldsymbol{g}}_d^T\hat{\boldsymbol{g}}_d^* s_d\right)}_{IV} + \underbrace{\sqrt{\frac{p_d}{L\gamma_d}}\left[\|\hat{\boldsymbol{g}}_d\|^2 - \mathbb{E}\{\|\hat{\boldsymbol{g}}_d\|^2\}\right]s_d}_{V}. \quad (2.23)$$

2.3.2 For IoT Devices Based on Non-Orthogonal Pilot Assignment Strategy

Based on (2.15), the signal received at the d^{th} IoT device can be written as

$$y_d = \sqrt{p_d}\boldsymbol{g}_d^T\boldsymbol{a}_d s_d + \sum_{\substack{d'=1\\d'\neq d}}^{D}\sqrt{p_{d'}}\boldsymbol{g}_d^T\boldsymbol{a}_{d'}s_{d'} + \sum_{m'=1}^{M}\sqrt{p_{m'}}\boldsymbol{g}_d^T\boldsymbol{a}_{m'}s_{m'} + w_d, \quad (2.21)$$

where the MR precoding vector for the d^{th} IoT device under this strategy equals $\boldsymbol{a}_d = \frac{1}{\sqrt{L}}\frac{\hat{\boldsymbol{g}}_d^*}{\sqrt{\gamma_d}}$. Substituting the corresponding precoding vectors and $g_{dl} = \hat{g}_{dl} - \tilde{g}_{dl}$ for all l from (2.10) in (2.21), we get

$$y_d = \sqrt{\frac{p_d}{L\gamma_d}}\hat{\boldsymbol{g}}_d^T\hat{\boldsymbol{g}}_d^* s_d + \sum_{\substack{d'=1\\d'\neq d}}^{D}\sqrt{\frac{p_{d'}}{L\gamma_{d'}}}\boldsymbol{g}_d^T\hat{\boldsymbol{g}}_{d'}^* s_{d'} + \sum_{m'=1}^{M}\sqrt{\frac{p_{m'}}{L\gamma_{m'}}}\boldsymbol{g}_d^T\hat{\boldsymbol{h}}_{m'}^* s_{m'} + w_d - \sqrt{\frac{p_d}{L\gamma_d}}\tilde{\boldsymbol{g}}_d^T\hat{\boldsymbol{g}}_d^* s_d. \quad (2.22)$$

We invoke the use and forget bound to evaluate the SINR [39], and re-write the above equation as (2.23) shown at the top of this page. Note that the first term in (2.23) is the desired signal for the d^{th} IoT device, the second term represents the interference due to other IoT devices, the third term represents the interference due to mobile terminals, the fourth term captures noise and the error incurred in channel estimation while the fifth term captures the beamforming gain uncertainty. It is the penalty incurred due to the application of use and forget bound. We state the SE achieved by the d^{th} IoT device in this scenario below.

Theorem 2.2. *The DL SE R_d achieved by the d^{th} IoT device when every IoT device is assigned a dedicated non-orthogonal pilot sequence and every mobile terminal is assigned an orthogonal pilot sequence for channel estimation is given by*

$$R_d = \left(1 - \frac{\tau_{pd} + \tau_{pm}}{\tau}\right)\log_2\left(1 + \text{SINR}_d\right), \quad (2.24)$$

$$y_m = \underbrace{\sqrt{\frac{p_m}{L\gamma_m}}\mathbb{E}\{\|\hat{\boldsymbol{h}}_m\|^2\}s_m}_{I} + \underbrace{\sum_{\substack{m'=1\\m'\neq m}}^{M}\sqrt{\frac{p_{m'}}{L\gamma_{m'}}}\boldsymbol{h}_m^T\hat{\boldsymbol{h}}_{m'}^*s_{m'}}_{II} + \underbrace{\sum_{d'=1}^{D}\sqrt{\frac{p_{d'}}{L\gamma_{d'}}}\boldsymbol{h}_m^T\hat{\boldsymbol{g}}_{d'}^*s_{d'}}_{III}$$
$$+ \underbrace{\left(w_m - \sqrt{\frac{p_m}{L\gamma_m}}\tilde{\boldsymbol{h}}_m^T\hat{\boldsymbol{h}}_m^*s_m\right)}_{IV} + \underbrace{\sqrt{\frac{p_m}{L\gamma_m}}[\|\hat{\boldsymbol{h}}_m\|^2 - \mathbb{E}\{\|\hat{\boldsymbol{h}}_m\|^2\}]s_m}_{V}. \quad (2.27)$$

where $\text{SINR}_d = \frac{L\gamma_d p_d}{\sigma^2 + \sum\limits_{\substack{d'=1\\d'\neq d}}^{D}\frac{p_{d'}}{L\gamma_{d'}}\chi_{d'} + \beta_d\sum\limits_{m'=1}^{M}p_{m'} + \beta_d p_d}$, $\chi_{d'} = \eta_{d'}^2\left(q_d\tau_{pd}L(L+1)\beta_d^2\left|\boldsymbol{\phi}_d^T\boldsymbol{\phi}_{d'}^*\right|^2\right.$
$\left. + \sum\limits_{\substack{u=1\\u\neq d}}^{D}q_u\tau_{pd}L\beta_d\beta_u\left|\boldsymbol{\phi}_u^T\boldsymbol{\phi}_{d'}^*\right|^2 + L\beta_d\sigma^2\right)$ *and* $\eta_{d'} = \left(\frac{\sqrt{q_{d'}\tau_{pd}}\beta_{d'}}{\sigma^2 + \sum\limits_{v=1}^{D}q_v\tau_{pd}\beta_v|\boldsymbol{\phi}_v^H\boldsymbol{\phi}_{d'}|^2}\right)$.

Proof. The proof is given in Appendix A.3. □

The achievable SE analysis of the d^{th} IoT device accounts for the correlation among the channel estimates due to non-orthogonal pilots based channel estimation and also the interference arising due to the presence of the mobile terminals in the network.

2.3.3 For Mobile Terminals Based on Orthogonal Pilot Assignment Strategy

From (2.15), the signal received at the m^{th} mobile terminal equals

$$y_m = \sqrt{p_m}\boldsymbol{h}_m^T\boldsymbol{a}_m s_m + \sum_{\substack{m'=1\\m'\neq m}}^{M}\sqrt{p_{m'}}\boldsymbol{h}_m^T\boldsymbol{a}_{m'}s_{m'} + \sum_{d'=1}^{D}\sqrt{p_{d'}}\boldsymbol{h}_m^T\boldsymbol{a}_{d'}s_{d'} + w_m, \quad (2.25)$$

where $\boldsymbol{a}_m = \frac{1}{\sqrt{L}}\frac{\hat{\boldsymbol{h}}_m^*}{\sqrt{\gamma_m}}$ and $\boldsymbol{a}_d = \frac{1}{\sqrt{L}}\frac{\hat{\boldsymbol{g}}_d^*}{\sqrt{\gamma_d}}$. Substituting $h_{ml} = \hat{h}_{ml} - \tilde{h}_{ml}$ for all l from (2.13) in the first term in (2.25), we get

$$y_m = \sqrt{\frac{p_m}{L\gamma_m}}\hat{\boldsymbol{h}}_m^T\hat{\boldsymbol{h}}_m^*s_m + \sum_{\substack{m'=1\\m'\neq m}}^{M}\sqrt{\frac{p_{m'}}{L\gamma_{m'}}}\boldsymbol{h}_m^T\hat{\boldsymbol{h}}_{m'}^*s_{m'} + \sum_{d'=1}^{D}\sqrt{\frac{p_{d'}}{L\gamma_{d'}}}\boldsymbol{h}_m^T\hat{\boldsymbol{g}}_{d'}^*s_{d'} + w_m - \sqrt{\frac{p_m}{L\gamma_m}}\tilde{\boldsymbol{h}}_m^T\hat{\boldsymbol{h}}_m^*s_m. \quad (2.26)$$

In order to invoke use and forget bound to evaluate the SINR [39], we re-write (2.26) as (2.27) shown at the top of this page. Note that the third term in (2.27) arises due to the presence of the IoT devices. The achievable SE for the m^{th} mobile terminal can be found by computing the

variances of each of the terms in (2.27) and is stated in a simplified form below.

Theorem 2.3. *The DL achievable SE R_m for the m^{th} mobile terminal when every mobile terminal is assigned an orthogonal pilot sequence for channel estimation and irrespective of the channel estimation strategy employed by the IoT devices is given by*

$$R_m = \left(1 - \frac{\tau_{pm} + \tau_{pd}}{\tau_c}\right) \log_2 (1 + \text{SINR}_m), \tag{2.28}$$

where $\text{SINR}_m = \dfrac{L\gamma_m p_m}{\sigma^2 + \beta_m \sum\limits_{m'=1}^{M} p_{m'} + \beta_m \sum\limits_{d'=1}^{D} p_{d'}}$.

Proof. The proof is given in Appendix A.4. □

Note that the achievable SE of the m^{th} mobile terminal is independent of the choice of the pilot assignment and channel estimation strategy employed by the IoT devices.

2.4 Numerical Results

In this section, we present numerical results to illustrate the impact of the proposed distance-dependent grouping based hybrid pilot assignment strategy for channel estimation of IoT devices on the achievable DL sum SE of IoT devices and the mobile terminals. As benchmarks, we also compare the performance of the proposed strategy against non-orthogonal, orthogonal and distance-independent grouping based hybrid pilot assignment. We consider two different power control techniques at the BS, namely, the channel inversion based power control [40] and the max-min power control. Out of the total power P available at the BS, a fraction λP is given to the mobile terminals and $(1 - \lambda)P$ is given to the IoT devices, where $0 \leq \lambda \leq 1$. The power allocation parameter λ can be chosen based on the sum SE requirements of the mobile terminals and the IoT devices.

Furthermore, we assume that the mobile terminals transmit with full available power during the pilot phase whereas the IoT devices employ channel inversion based power control during the pilot phase in order to counter the near-far effect and benefit the relatively weaker IoT devices [40]. Specifically, if every IoT device has a maximum transmit power constraint of $q_{\max}$, then the pilot power $q_d^{G_k}$ of the d^{th} IoT device in the G_k^{th} group equals $q_d^{G_k} = q_{\max} \frac{\beta_{\min}}{\beta_d^{G_k}}$, where $\beta_{\min}$ denotes the large-scale fading coefficient of the farthest IoT device. We consider a

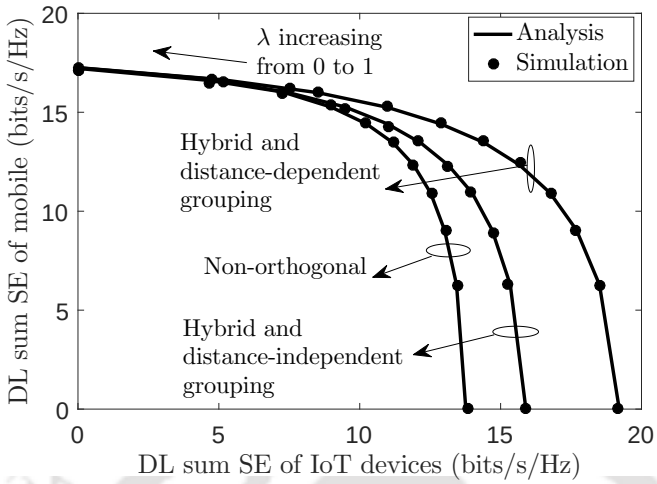

Fig. 2.3: DL sum SE of mobile terminals vs. DL sum SE of IoT devices ($M = 5$, $D = 20$, $\tau_c = 200$, $L = 100$ and $P = 40$ W).

single cell scenario where the mobile terminals and the IoT devices are uniformly distributed over an annular ring of inner radius $r_{\min} = 20$ m and outer radius $r_{\max} = 250$ m [12]. We model the large-scale fading coefficient β_u between the BS and the user terminals as $\beta_u = 130 + 37.6 \log 10(d)$, where d is the distance of the user (mobile/IoT) terminals from the BS in Kms. Unless mentioned otherwise, we take $P = 40$ W, the maximum transmit power $q_{\max}$ during training as 1 W, $\sigma^2 = 2 \times 10^{-20}$ W/Hz and the bandwidth equal to 10 MHz. For the distance-dependent grouping based hybrid pilot assignment strategy, we consider $N = 2$. For the non-orthogonal pilot assignment strategy, we consider non-orthogonal pilot sequences of length $\frac{D}{2}$ which satisfy the Welch bound equality (WBE) [41], since such sequences minimize the maximum mean square error of the channel estimates [12].

2.4.1 Based on Channel Inversion Power Control at BS

Under channel inversion based power control during the data transmission phase, the power allocated to the d^{th} IoT device belonging to the G_k^{th} group equals $p_d^{G_k} = \frac{(1-\lambda)P}{\sum_{k'=1}^{D/N} \sum_{d' \in G_{k'}} \left(\frac{1}{\beta_{d'}^{G_{k'}}}\right)} \frac{1}{\beta_d^{G_k}}$ and the power allocated to the k^{th} mobile terminal equals $p_m = \frac{\lambda P}{\sum_{m'=1}^{M} \frac{1}{\beta_{m'}}} \frac{1}{\beta_m}$. This power control ensures that the user terminals that are far-off from the BS are allocated relatively more power than those that are nearer. It thus improves the performance of relatively weaker user terminals, however, unlike max-min power control, it does not ensure uniform service to all the user terminals.

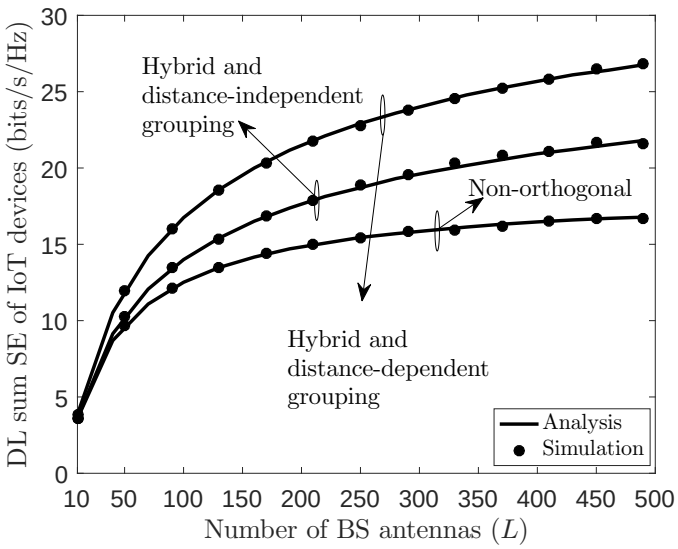

Fig. 2.4: DL sum SE of IoT devices vs. L ($M = 5$, $D = 20$, $\tau_c = 200$, $\lambda = 0.3$ and $P = 40$ W).

Figure 2.3 plots the DL sum SE of mobile terminals in (bits/s/Hz) vs. the DL sum SE of IoT devices (averaged over user locations) by varying the power allocation parameter λ from 0 to 1. Note that $\lambda = 0$ corresponds to the case when the BS allocates all its power to serve IoT devices and $\lambda = 1$ corresponds to the case when the BS allocates all its power to serve mobile terminals. We obtain these curves for three different cases, namely distance-dependent grouping based hybrid channel estimation, distance-independent grouping based hybrid channel estimation, and non-orthogonal channel estimation strategy. For each of the three cases, both the analysis and simulation results are plotted and we observe that they are in close agreement with each other. We observe that while keeping the sum SE of the mobile terminals at the same level, distance-dependent grouping based hybrid pilot assignment strategy yields the highest sum SE for the IoT devices among the three strategies. This is because the proposed channel estimation strategy produces the least pilot contamination induced interference during the data transmission phase. It can be observed that non-orthogonal channel assignment strategy yields the lowest sum SE because of highest pilot contamination induced interference among the three.

Figure 2.4 plots the DL sum SE of IoT devices (averaged over user locations) vs. L for the three different pilot assignment strategies employed by IoT devices. As expected, the sum SE increases with L and the proposed strategy gives the highest sum SE among the three.

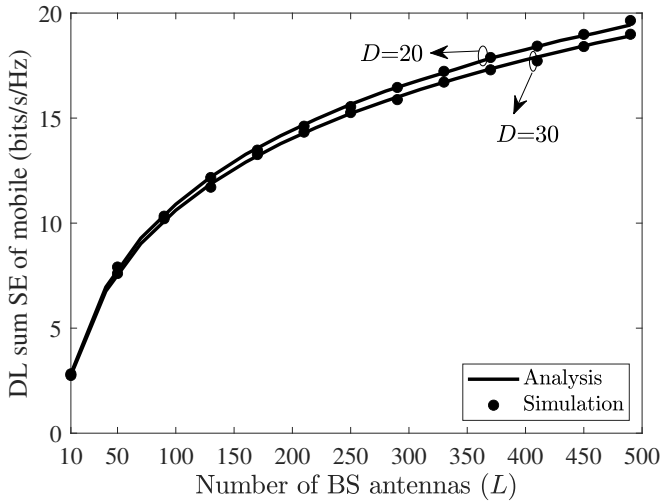

Fig. 2.5: DL sum SE of mobile terminals vs. L (M = 5, τ_c = 200, λ = 0.3 and P = 40 W).

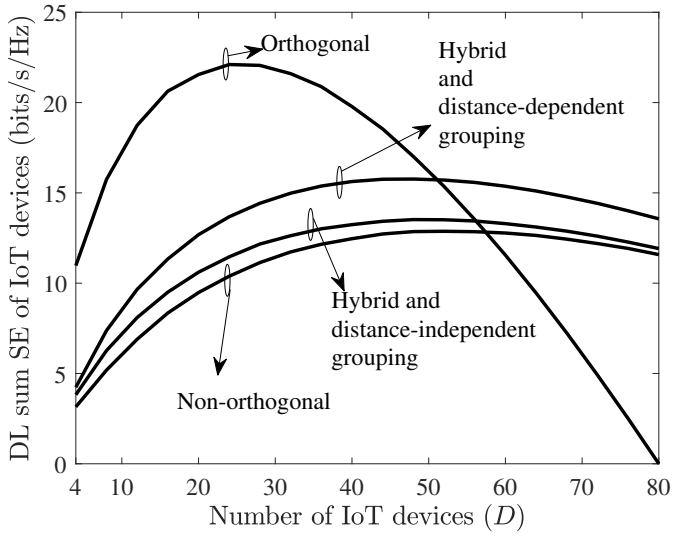

Fig. 2.6: DL sum SE of IoT devices vs. D (M = 20, τ_c = 100, λ = 0.3, L = 100 and P = 40 W).

Figure 2.5 plots the DL sum SE of the mobile terminals (averaged over user locations) vs. L for two different values of D. Note that the sum SE of mobile terminals is independent of the choice of the pilot assignment and channel estimation strategy used by the IoT devices. It can also be observed that just by deploying a few more additional antennas at the BS, more number of IoT devices can be supported in the network without deteriorating the sum SE of mobile terminals.

Figure 2.6 plots the DL sum SE of IoT devices averaged over device locations vs. D for three different pilot assignment strategies. In addition, we also benchmark against orthogonal pilot

assignment, where the IoT devices are also assigned orthogonal pilots for channel estimation. We clearly observe that when the number of IoT devices is small, then orthogonal strategy yields the highest sum SE for IoT devices due to no pilot contamination. As the number of IoT devices increases which is likely to be the case in beyond 5G networks, the sum SE falls down sharply and hits zero at $D = 80 = \tau_c - M$, since all the samples are lost in learning the channel. However, the proposed distance-dependent grouping based strategy can clearly support larger number of IoT devices with reasonable DL sum SE without affecting the achievable SE of the mobile terminals when also compared against non-orthogonal and distance-independent grouping.

2.4.2 Based on Max-Min Power Control at the BS

Under max-min power control, the objective is to maximize the minimum SINR among all user terminals thus providing uniform service to all. The optimization problem can be stated mathematically in a generic form as follows:

$$\max_{\{p_u\}} \quad \min_k \text{SINR}_k,$$

$$\text{s.t.} \sum_{k=1}^{U} p_u \leq \delta P, \tag{2.29}$$

$$p_u \geq 0, \text{ for all } k, \tag{2.30}$$

where $k \in \{d, m\}$, $\text{SINR}_k \in \{\text{SINR}_d^{G_k}, \text{SINR}_d, \text{SINR}_m\}$ depending respectively on whether we want to maximize the minimum SE of IoT devices using distance-dependent grouping based hybrid channel estimation or non-orthogonal training or that of mobile terminals based on orthogonal training, $p_u \in \{p_d^{G_k}, p_d, p_m\}$, $U \in \{D, M\}$, and $\delta \in \{\lambda, (1-\lambda)\}$. Note that in case of hybrid pilot assignment strategy, the power constraint in (2.29) gets modified to $\sum_{k=1}^{D/N} \sum_{d \in G_k} p_d^{G_k} \leq \delta P$. This problem can be stated in the epigraph form as follows [42]:

$$\max_{\{p_u\}} \overline{\text{SINR}},$$

$$\text{s.t. } \text{SINR}_k \geq \overline{\text{SINR}}, \text{ for all } k,$$

$$\sum_{k=1}^{U} p_u \leq \delta P,$$

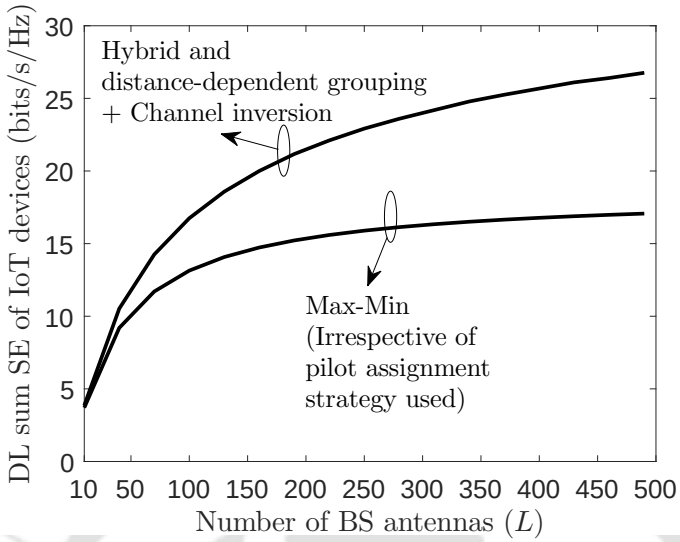

Fig. 2.7: DL sum SE of IoT devices vs. L ($M = 5$, $D = 20$, $\tau_c = 200$, $\lambda = 0.3$ and $P = 40$ W).

$$p_u \geq 0, \text{ for all } k, \tag{2.31}$$

where $\overline{\text{SINR}}$ is the common SINR target for all the user terminals. The problem as stated above is a linear feasibility problem and its solution is obtained numerically based on bisection search using a standard optimization tool such as CVX [42–44].

Figure 2.7 plots the DL sum SE of IoT devices (averaged over user locations) vs. L for both max-min and channel inversion power control. Note that under max-min power control during data transmission phase, the power is allocated to IoT devices in such a manner that every IoT device gets the same SE irrespective of its location. Furthermore, since IoT devices also employ channel inversion based power control during the pilot phase, it essentially makes the strength of the channel estimates of these IoT devices nearly the same. This results into identical sum SE irrespective of the pilot allocation strategy employed. Moreover, the DL sum SE of IoT devices under channel inversion is higher than their performance under max-min since the IoT devices that are far-off are benefitted in two ways when channel inversion based power control is employed jointly with grouping based hybrid pilot assignment. First, the way these IoT devices are grouped under the proposed strategy, the far-off IoT devices experience relatively less interference from the other IoT devices within a group. Secondly, under channel inversion control, far-off IoT devices get relatively more power.

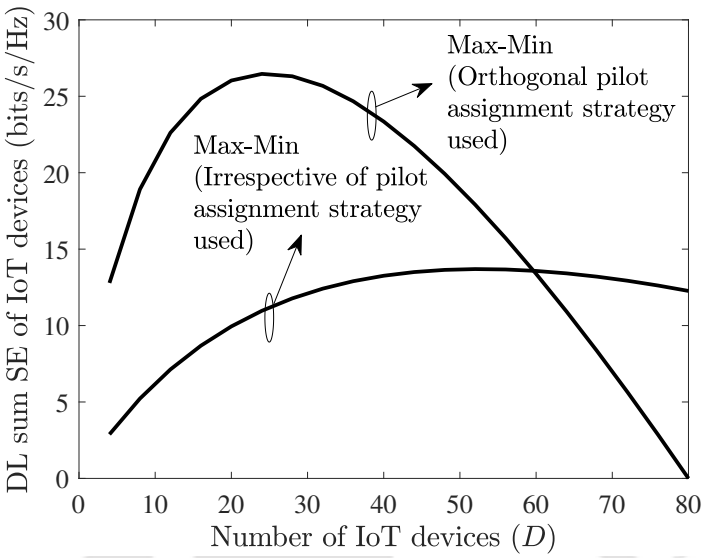

Fig. 2.8: Under Max-Min power control DL sum SE of IoT devices vs. D (M = 20, τ_c = 100, λ = 0.3, L = 100 and P = 40 W).

Figure 2.8 plots the DL sum SE of IoT devices averaged over user locations vs. D when max-min power control is deployed at the BS. Note again that under max-min power control, the DL sum SE of IoT devices is independent of the channel estimation strategy deployed by the IoT devices. And that with orthogonal training during data phase and no pilot power control, the DL sum SE reduces to zero when $D = \tau_c - M$, since the number of samples left for data transmission reduces to zero. Furthermore, with the proposed lower overhead channel estimation strategy, a relatively larger number of IoT devices can be supported.

2.5 Summary

We investigated DL unicast transmission from a massive MIMO BS jointly to IoT devices and mobile terminals. To facilitate MR precoding, the channel estimates were obtained using orthogonal pilot assignment strategy for mobile and two different low overhead channel estimation strategies, namely, grouping based hybrid pilot assignment (distance-dependent or distance-independent) and non-orthogonal pilot assignment for IoT devices. We derived new expression for the DL sum SE for the IoT devices when estimates are acquired based on grouping based hybrid pilot assignment strategy. As a baseline, we also derived new DL sum SE for IoT devices based on non-orthogonal strategy. The analysis accounted for the correlation

among the channel estimates and the interference due to mobile.

We proved that under channel inversion based power control at the BS, distance-dependent grouping based hybrid strategy achieves the highest DL sum SE for IoT devices when compared against non-orthogonal or distance-independent grouping based hybrid strategy since it causes least pilot contamination induced interference during the data phase. We also showed that the distance-dependent grouping based hybrid strategy can serve the largest number of IoT devices among all the strategies considered. A new expression for the DL sum SE of mobile terminals taking into account the interference due to IoT devices was also developed. We showed that the sum SE achieved by the mobile terminals is independent of the pilot assignment strategy employed by the IoT devices. Furthermore, under max-min power control at the BS during data transmission phase, we observe that the performance of IoT devices remains unaffected irrespective of the estimation strategy due to power control used during estimation.

While this Chapter focused on the first aspect related to system modeling and performance analysis of joint machine-centric communication among IoT devices and human-centric communication among mobile terminals and addressed challenges associated with pilot assignment and channel estimation, the next Chapter considers the second aspect and addresses challenges associated with efficient wireless charging of these IoT devices.

3

Single IRS Enabled WET

Contents

In this Chapter, we focus on a practically well-motivated model where a source equipped with fewer RF chains than the number of transmit antennas is assisted by an IRS to transfer energy wirelessly to IoT users. Each transmit RF chain, which is made up of signal converters, up-converters, filters, and power amplifiers makes the source power hungry, bulky and costly. AS employed by source is a low hardware complexity solution that reduces the number of RF chains required, thus reducing power consumption and the associated cost. For this model, our main objective is to identify the operational regimes that guarantee feasibility of WET and to determine if the receive power level at the user can be maintained at the same level by trading-off active RF chains at the source with passive elements at the IRS that do not require dedicated RF chains.

We first present a near-optimal joint AS and passive beamforming rule that requires fewer pilot transmissions than the optimal rule in the literature. We then analyze probability of outage in WET with both perfect and estimated CSI for both single and multiple users. Diversity analysis for the joint AS and IRS enabled WET is also presented. Thereafter, we present extensive numerical results, discuss extensions to subset AS, discrete phase-shift design and evaluate the performance under limited scattering.

3.1 Related Literature

We now present some key related references on IRS-aided WET and IRS-aided SWIET system.

IRS-Assisted WET System: The authors in [14] proposed a channel estimation protocol and designed near-optimal beamformers at BS and at IRS. Active beamformer at BS and constant envelope precoding based passive beamformer at IRS were designed to maximize sum received power at IoT users in [15]. Average symbol error and outage probabilities were derived with perfect CSI in [45]. The authors in [46] designed active beamforming at source and passive beamforming at IRS to maximize minimum harvested power among users. In [47], the authors jointly optimized beamformers at the source and at the IRS to maximize the total power received by the users. The authors in [48] maximized weighted sum direct current under a transmit power

constraint at source and unit modulus constraint at IRS.

IRS-Assisted SWIET: The authors in [49] maximized the common throughput of the information and energy users by jointly optimizing transmit time, power allocation, and reflection coefficients at IRS. In [50], the authors jointly optimized beamformer at the BS and transmission mode at the IRS to minimize total BS transmit power. In [51], the authors designed active beamforming at the BS and phase shifts at the IRS to minimize transmit power under SINR constraint at the information user and EH constraint at the energy user. In [52], the authors determined the optimal power splitting ratio, active beamforming at the BS, and phase shifts of the IRS to maximize the EE. Transmit beamformer and covariance matrix of the artificial noise at the BS were optimized in order to maximize the system EE in [53].

Analytical bounds on achievable rate and harvested energy were derived for time switching and power splitting protocols in [54]. Transmit power at the BS is minimized with minimum rate and harvested energy constraints at every user in [55]. The authors in [56] optimized the active beamforming at the BS and phase shifts at the IRS to maximize the minimum rate of the information users subject to minimum EH constraint at the energy users. The authors in [57] studied the trade-off between sum data rate maximization and sum harvested energy maximization by jointly optimizing the information/energy beamforming vectors at the BS and phase shifts at IRS. An extensive survey of works that consider IRS-aided wireless information and/or energy transfer without spatial correlation can be found in [7] and the references therein.

Based on the discussion above, we observe that most of the works considered IRS assisted transmission from a source that is equipped with as many RF chains as the number of antennas. This increases hardware complexity, power consumption and cost at the source. AS is a low complexity technique that reduces the cost and power consumption at the source. There are limited works available on joint AS-IRS beamforming. While [19] studied joint AS at the BS and passive beamforming at the IRS to maximize received signal power under perfect CSI. The authors in [20] considered joint AS and IRS beamforming to maximize the ergodic sum data rate and in [58], algorithms were developed for joint AS and passive beamforming at the IRS to maximize channel capacity under unit modulus constraints of all IRS elements assuming

perfect CSI. However, system modeling, developing low complexity AS rule, active and passive beamforming design based on the selected antennas, and comprehensive performance analysis in terms of OP and PTE under both perfect and estimated CSI for joint AS and IRS-assisted WET to single and/or multiple users is still in its infancy, remains an open problem and is the focus of this work.

Notations: We denote an $N \times N$ diagonal matrix with diagonal elements $a_1, \ldots, a_N$ by $\text{diag}(a_1, \ldots, a_N)$. The probability of an event A is denoted by $\Pr(A)$ and PDF of a RV X is denoted by $f_X(\cdot)$. Real and imaginary parts of a complex variable are denoted by $\Re(\cdot)$ and $\Im(\cdot)$, respectively.

Organization: This Chapter is organized as follows. We present the system model in Section 3.2. We propose our joint AS and passive beamforming rule, analyze its probability of outage with perfect CSI and extend this analysis to multi-user scenario in Section 3.3. We analyze the corresponding performance with estimated CSI in Section 3.4. The numerical results and summary are presented in Sections 3.5 and 3.6, respectively.

3.2 System Model

We consider an IRS-assisted WET system as shown in Figure 3.1. It has a source S equipped with M antennas and a single RF chain that transmits RF signal to a single antenna user U. We consider that the passive reflecting elements of IRS I are arranged in a planar array of dimension $N_x \times N_y$, where N_x and N_y denote the number of IRS elements along length and breadth, respectively. Therefore, total number of IRS elements $N = N_x N_y$. The source dynamically switches its RF chain to the antenna selected based on instantaneous CSI. It also computes the IRS reflection coefficients, which are communicated to IRS through a dedicated control link. We consider a block fading model, in which the wireless channel remains constant over a coherence interval of duration τ_c and varies independently across different coherence intervals. We consider TDD[1] mode of communication to exploit channel reciprocity. The CSI acquired through UL pilot signaling is used to select an antenna at S and compute reflection coefficients

[1]Indoor/outdoor field trials confirmed that UL and DL channels are reciprocal in TDD mode even in IRS-aided wireless communications [59]. Furthermore, this has been widely adopted in literature [14, 60–63].

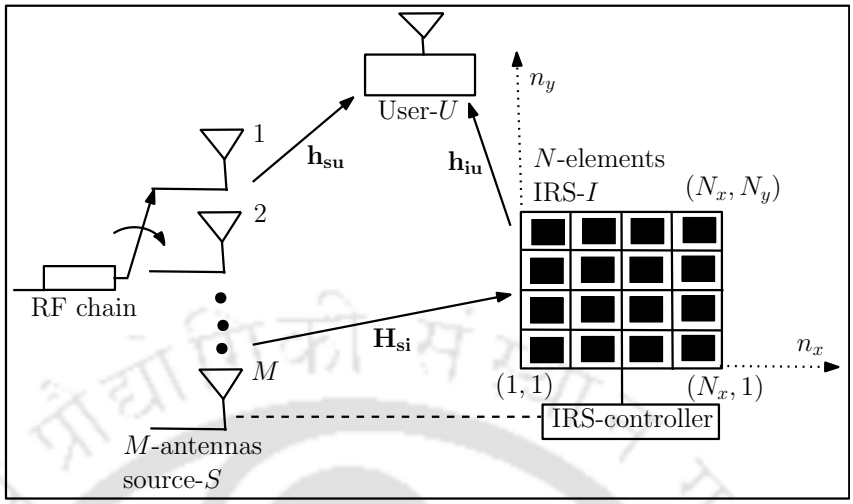

Fig. 3.1: System model: Joint AS and IRS-assisted WET.

at I. We consider that the IRS is completely passive in nature and does not have dedicated RF chains connected to it. Let $\boldsymbol{h}_{su} \in C^{M\times 1}$ denote the complex channel gain vector of direct path from S to U. We model it as Rayleigh fading. Therefore, $\boldsymbol{h}_{su} \sim \mathcal{CN}(\mathbf{0}, \beta_{su}\boldsymbol{I}_M)$, where β_{su} denotes distance-dependent path loss. Let $\boldsymbol{H}_{si} \in C^{M\times N}$ denote complex channel gain matrix from S to I. We model it as Rician fading. It can be written as

$$\boldsymbol{H}_{si} = \sqrt{\frac{K_{si}\zeta_{si}}{K_{si}+1}}\overline{\boldsymbol{H}}_{si} + \sqrt{\frac{\zeta_{si}}{K_{si}+1}}\widetilde{\boldsymbol{H}}_{si}, \tag{3.1}$$

where ζ_{si} and K_{si} denote the distance-dependent path loss and the Rician factor, respectively. Furthermore, the $(m,n)^{\text{th}}$ element of the line-of-sight (LoS) component $\overline{\boldsymbol{H}}_{si} \in C^{M\times N}$ is given by $\overline{H}_{si}^{mn} = \exp\left[j\frac{2\pi}{\lambda}d\left((m-1)\sin(\psi_1)\cos(\phi_1)+(n_x-1)\sin(\psi_2)\cos(\phi_2)+(n_y-1)\sin(\psi_2)\sin(\phi_2)\right)\right]$, where the index $n = (n_x-1)+1+\left(n_y-1\right)N_x$, λ denotes the wavelength, d denotes the inter-element spacing at S and I, $\psi_1, \phi_1, \psi_2, \phi_2 \in (0, 2\pi)$ denote the elevation angle of departure (AoD) and azimuthal AoD at S, elevation angle of arrival (AoA), and azimuthal AoA at I, respectively, $1 \le m \le M$, $1 \le n_x \le N_x$, and $1 \le n_y \le N_y$ [24]. The elements of the non-LoS component $\widetilde{\boldsymbol{H}}_{si} \in C^{M\times N}$ are i.i.d. circular symmetric complex Gaussian RVs with zero mean and unit variance, i.e., $\widetilde{H}_{si}^{mn} \sim \mathcal{CN}(0,1)$. Thus, $H_{si}^{mn} \sim \mathcal{CN}(\mu_{si}^{mn}, \beta_{si})$, where $\mu_{si}^{mn} = \sqrt{\frac{K_{si}\zeta_{si}}{K_{si}+1}}\overline{H}_{si}^{mn}$ and $\beta_{si} = \frac{\zeta_{si}}{K_{si}+1}$. The elements of the channel matrix $\boldsymbol{H}_{si}$ are independent across m and n.

Let $\boldsymbol{h}_{iu} \in C^{N\times 1}$ denote the complex channel gain vector from I to U. It is modeled as

$$\boldsymbol{h}_{iu} = \sqrt{\frac{K_{iu}\zeta_{iu}}{K_{iu}+1}}\overline{\boldsymbol{h}}_{iu} + \sqrt{\frac{\zeta_{iu}}{K_{iu}+1}}\widetilde{\boldsymbol{h}}_{iu}, \tag{3.2}$$

where ζ_{iu} and K_{iu} denote the distance-dependent path loss and the Rician factor, respectively. The n^{th} element of the LoS component $\overline{\boldsymbol{h}}_{iu} \in C^{N\times 1}$ is given by

$$\overline{h}_{iu}^{n} = \exp\left[j\frac{2\pi}{\lambda}d\left((n_x-1)\sin(\psi_3)\cos(\phi_3) + (n_y-1)\sin(\psi_3)\cos(\phi_3)\right)\right], \tag{3.3}$$

where $\psi_3, \phi_3 \in (0, 2\pi)$ denote the elevation AoD and azimuthal AoD at I, respectively [24]. Furthermore, $\widetilde{\boldsymbol{h}}_{iu} \in C^{N\times 1}$ denotes the non-LoS component with i.i.d. $\mathcal{CN}(0,1)$ elements. Thus, $h_{iu}^{n} \sim \mathcal{CN}(\mu_{iu}^{n}, \beta_{iu})$, where $\mu_{iu}^{n} = \sqrt{\frac{K_{iu}\zeta_{iu}}{K_{iu}+1}}\overline{h}_{iu}^{n}$ and $\beta_{iu} = \frac{\zeta_{iu}}{K_{iu}+1}$. The elements of the channel vector $\boldsymbol{h}_{iu}$ are independent of each other. Let $\alpha_n \in [0,1]$ and $\theta_n \in [0, 2\pi]$ denote the amplitude and phase coefficients of the n^{th} IRS element. Then, the phase shift matrix of the IRS is given by $\boldsymbol{\Theta} = \text{diag}(\alpha_1 e^{j\theta_1}, \alpha_2 e^{j\theta_2}, \ldots, \alpha_N e^{j\theta_N})$.

Let $a \in \{1, 2, \ldots, M\}$ denote the index of the antenna selected at S. Furthermore, let h_{su}^{a} and $\boldsymbol{h}_{si}^{a} \in C^{1\times N}$ denote a^{th} element of $\boldsymbol{h}_{su}$ and a^{th} row of $\boldsymbol{H}_{si}$, respectively. Then, the DL signal received at the user is given by

$$y_u = \left(h_{su}^{a} + \boldsymbol{h}_{si}^{a}\boldsymbol{\Theta}\boldsymbol{h}_{iu}\right)x_s + w_u, \tag{3.4}$$

where x_s denotes the transmit symbol and w_u denotes circular symmetric complex additive white Gaussian noise (AWGN) with variance σ^2. Therefore, $w_u \sim \mathcal{CN}(0, \sigma^2)$. Let $\boldsymbol{g}_{siu}^{a} = \left[g_{siu}^{a1}, \ldots, g_{siu}^{aN}\right] = \boldsymbol{h}_{si}^{a}\,\text{diag}(\boldsymbol{h}_{iu}^{T}) \in C^{1\times N}$ denote the vector of cascaded channels of the reflected path. Furthermore, let $\boldsymbol{f}_i = \left[f_i^1, \ldots, f_i^N\right]^T$ denote the IRS passive beamforming vector, where f_i^n denotes the n^{th} diagonal element of $\boldsymbol{\Theta}$ and is given by $f_i^n = \alpha_n e^{j\theta_n}$. Using these notations, the signal y_u in (3.4) can be re-written as

$$y_u = \left(h_{su}^{a} + \boldsymbol{g}_{siu}^{a}\boldsymbol{f_i}\right)x_s + w_u. \tag{3.5}$$

3.3 AS Rule and its Analysis With Perfect CSI

In this section, we state our low-complexity AS rule and derive its probability of outage with perfect CSI.[2] Let ρ_{su}^m and Λ_{su}^m denote the magnitude and phase of the direct path channel gain h_{su}^m, i.e., $h_{su}^m = \rho_{su}^m e^{j\Lambda_{su}^m}$, for $m \in \{1, 2, \ldots, M\}$.

3.3.1 AS and Passive Beamforming

The source selects the antenna with the highest channel power gain along the direct path from S to U. Therefore, $a = \underset{m\in\{1,2,\ldots,M\}}{\arg\max}\{\rho_{su}^m\}$. From y_u in (3.5), the energy harvested at U in a coherence interval of duration τ_c seconds is given by

$$E_u = \eta_r \tau_c |x_s|^2 |h_{su}^a + \boldsymbol{g}_{siu}^a \boldsymbol{f}_i|^2 = \eta_r \tau_c |x_s|^2 \left| h_{su}^a + \sum_{n=1}^{N} g_{siu}^{an} f_i^n \right|^2, \tag{3.6}$$

where $0 < \eta_r < 1$ denotes the rectification efficiency of the EH circuit at the user.[3] Let $p = |x_s|^2$ and $\gamma = \eta_r \tau_c p$. The contribution of noise w_u to the harvested energy is negligibly small and is therefore not considered [6, 13–15, 66]. In terms of magnitude and phase, we can express the RVs in (3.6) as $g_{siu}^{an} = \rho_{siu}^{an} e^{j\phi_{siu}^{an}}$, where $\rho_{siu}^{an} = \rho_{si}^{an}\rho_{iu}^n$, $\rho_{si}^{an} = \left|H_{si}^{an}\right|$, $\rho_{iu}^n = \left|h_{iu}^n\right|$ and $\phi_{siu}^{an} = \angle H_{si}^{an} + \angle h_{iu}^n$. Therefore, E_u in (3.6) can be expressed as

$$E_u = \gamma \left| \rho_{su}^a e^{j\Lambda_{su}^a} + \sum_{n=1}^{N} \rho_{siu}^{an} e^{j\phi_{siu}^{an}} f_i^n \right|^2. \tag{3.7}$$

By triangle inequality, we know that programming $f_i^n = e^{-j\left(\phi_{siu}^{an} - \Lambda_{su}^a\right)}$ maximizes E_u in (3.7). This choice enables coherent combination of the direct path signal and the reflected path signals via the IRS. Therefore, our joint AS and passive beamforming rule can be written as

$$a = \underset{m\in\{1,2,\ldots,M\}}{\arg\max}\{\rho_{su}^m\}, \tag{3.8}$$

$$f_i^n = \exp\left(-j\left(\phi_{siu}^{an} - \Lambda_{su}^a\right)\right), \text{ for } n = 1, \ldots, N. \tag{3.9}$$

[2] WET with perfect CSI refers to genie-aided WET, where the CSI is error-free and no resources are spent on pilots.

[3] With a single EH circuit, the energy harvested is a non-linear function of the received energy due to saturation effects. However, it is shown that we can mitigate the non-linear behavior and also extend the range over which it is a linear function by using multiple such circuits in parallel [49, 64, 65].

We now describe the two-step procedure that implements the above AS rule. *Step 1:* The IRS is turned off and the user sends M pilots. The source estimates the direct path CSI and selects antenna a in (3.8). *Step 2:* The source switches the RF chain to the selected antenna and the IRS is turned on. Now the user sends N pilots and the source estimates the sum of direct path and the reflected path CSI corresponding to the antenna a selected. Then, the source subtracts the direct path CSI to obtain the reflected path CSI and computes the IRS passive beamforming coefficients as in (3.9). These coefficients are communicated to the IRS through the dedicated control link. The channel estimation procedure in these two steps is discussed in detail in Section 3.4.1.

Benefits of the Proposed Rule: (i) It reduces number of pilot transmissions required and increases the time available for WET. Based on the above description, we see that the proposed joint AS and passive beamforming rule requires $M + N$ pilots to obtain required CSI. This is significantly lower than the $M + MN$ pilots required by the optimal AS rule proposed in [19, 20]; (ii) In Section 3.5, we show that the proposed rule is near-optimal with fewer pilots; (iii) Furthermore, it simplifies outage analysis and brings out valuable insights.

3.3.2 Probability of Outage Analysis

Let E_{th} denote the threshold energy required at the user. We now derive an expression for the probability of outage in WET, i.e., $\Pr(E_u \leq E_{\text{th}})$, for the proposed joint AS and passive beamforming rule with perfect CSI. Substituting f_i^n from (3.9) in (3.7), we get

$$E_u = \gamma \left(\rho_{su}^a + \sum_{n=1}^{N} \rho_{siu}^{an} \right)^2 . \tag{3.10}$$

Here, E_u is square of the sum of two independent RVs ρ_{su}^a and $\sum_{n=1}^{N} \rho_{siu}^{an}$. From (3.8), we know that $\rho_{su}^a = \max\{\rho_{su}^1, \ldots, \rho_{su}^M\}$, which is the maximum of M i.i.d. Rayleigh RVs. Furthermore, $\sum_{n=1}^{N} \rho_{siu}^{an} = \sum_{n=1}^{N} \rho_{si}^{an} \rho_{iu}^{n}$ is the sum of the product of independent Rician RVs. Therefore, the probability of outage in energy transfer can be written as

$$P_{\text{outage}} = \Pr(E_u \leq E_{\text{th}}) = \Pr\left(\gamma \left(\rho_{su}^a + \sum_{n=1}^{N} \rho_{siu}^{an} \right)^2 \leq E_{\text{th}} \right). \tag{3.11}$$

Theorem 3.1. *The probability of outage for the proposed joint AS and passive beamforming rule with perfect CSI is given by*

$$P_{outage} = \sum_{m=0}^{M-1} \frac{M(-1)^m}{m+1}\binom{M-1}{m}\left[1 - \psi Q\left(\frac{\overline{E}_{th} - \mu_y}{\sigma_y}\right) - \frac{\psi e^{\frac{\xi^2 - \eta\chi}{2\eta}}}{\sqrt{\eta\sigma_y^2}}\left(Q\left(\frac{-\xi}{\sqrt{\eta}}\right) - Q\left(\frac{\overline{E}_{th} - \mu_y}{\sigma_y^2\sqrt{\eta}}\right)\right)\right], \tag{3.12}$$

where $\psi = Q^{-1}\left(\frac{-\mu_y}{\sigma_y}\right)$, $\eta = \left(\frac{2(m+1)}{\beta_{su}} + \frac{1}{\sigma_y^2}\right)$, $\xi = \left(\frac{2(m+1)\overline{E}_{th}}{\beta_{su}} + \frac{\mu_y}{\sigma_y^2}\right)$, $\chi = \left(\frac{2(m+1)\overline{E}_{th}^2}{\beta_{su}} + \frac{\mu_y^2}{\sigma_y^2}\right)$, $\overline{E}_{th} = \sqrt{\frac{E_{th}}{\gamma}}$, $\mu_y = \frac{N\pi}{4}\sqrt{\beta_{si}\beta_{iu}}L_{\frac{1}{2}}(-K_{si})\,L_{\frac{1}{2}}(-K_{iu})$, $\sigma_y^2 = N\beta_{si}\beta_{iu}(1+K_{si})(1+K_{iu}) - N\mu_0^2$, $\mu_0 = \frac{\pi}{4}\sqrt{\beta_{si}\beta_{iu}}L_{\frac{1}{2}}(-K_{si})\,L_{\frac{1}{2}}(-K_{iu})$, *$Q(\cdot)$ denotes the Q-function [67] and $L_n(\cdot)$ denotes Laguerre polynomial of order-n [68].*

Proof. The proof is given in Appendix B.1. □

The above expression brings out the dependence of the probability of outage on system parameters M, N, and E_{th} and channel parameters K_{si}, K_{iu}, β_{su}, β_{si} and β_{iu}. With $M = 1$, P_{outage} in (3.12) reduces to a form similar to [69, Eqn. (7)]

$$P_{\text{outage}} = 1 - \psi Q\left(\frac{\overline{E}_{\text{th}} - \mu_y}{\sigma_y}\right) - \frac{\psi e^{\frac{\xi_1^2 - \eta_1\chi_1}{2\eta_1}}}{\sqrt{\eta_1\sigma_y^2}}\left(Q\left(\frac{-\xi_1}{\sqrt{\eta_1}}\right) - Q\left(\frac{\overline{E}_{\text{th}} - \mu_y}{\sigma_y^2\sqrt{\eta_1}}\right)\right), \tag{3.13}$$

where $\eta_1 = \left(\frac{2}{\beta_{su}} + \frac{1}{\sigma_y^2}\right)$, $\xi_1 = \left(\frac{2\overline{E}_{\text{th}}}{\beta_{su}} + \frac{\mu_y}{\sigma_y^2}\right)$ and $\chi_1 = \left(\frac{2\overline{E}_{\text{th}}^2}{\beta_{su}} + \frac{\mu_y^2}{\sigma_y^2}\right)$.

3.3.2.1 Asymptotic Analysis

We now study the behavior of the probability of outage for large number of IRS elements. As $N \to \infty$, by law of large numbers [70], we know that $\frac{1}{N}\sum_{n=1}^{N}\rho_{siu}^{an} \to \mathbb{E}\left(\rho_{siu}^{an}\right) = \mathbb{E}\left(\rho_{si}^{an}\right)\mathbb{E}\left(\rho_{iu}^{n}\right) = \mu_0 = \frac{\pi}{4}\sqrt{\beta_{si}\beta_{iu}}L_{\frac{1}{2}}(-K_{si})\,L_{\frac{1}{2}}(-K_{iu})$. Furthermore, the outage event can be written as $\left(\frac{1}{N}\rho_{su}^{a} + \frac{1}{N}\sum_{n=1}^{N}\rho_{siu}^{an} \le \frac{1}{N}\overline{E}_{\text{th}}\right)$. For sufficiently large N, $\frac{1}{N}\sum_{n=1}^{N}\rho_{siu}^{an} \to \mu_0$ and

$$P_{\text{outage}} \to \Pr\left(\rho_{su}^{a} \le \overline{E}_{\text{th}} - N\mu_0\right). \tag{3.14}$$

Using the fact that $\rho_{su}^{a} = \max\{\rho_{su}^{1}, \ldots, \rho_{su}^{M}\}$, the probability of outage

$$P_{\text{outage}} \to \Pr\left(\rho_{su}^{1} \le \overline{E}_{\text{th}} - N\mu_0, \ldots, \rho_{su}^{M} \le \overline{E}_{\text{th}} - N\mu_0\right). \tag{3.15}$$

Since $\rho_{su}^1, \ldots, \rho_{su}^M$ are i.i.d. Rayleigh RVs, we get

$$P_{\text{outage}} \to \begin{cases} 0, & \text{if } N\mu_0 \geq \overline{E}_{\text{th}}, \\ \left[1 - \exp\left(\frac{-\left(\overline{E}_{\text{th}} - N\mu_0\right)^2}{\beta_{su}}\right)\right]^M, & \text{otherwise.} \end{cases} \tag{3.16}$$

From the analysis above, we see that $P_{\text{outage}} \to 0$ when $N\mu_0 \geq \overline{E}_{\text{th}}$. Therefore, the probability of outage can be made negligibly small when the number of IRS elements is greater than

$$\frac{4\sqrt{E_{\text{th}}}}{\pi\sqrt{p\eta_r\tau_c}\sqrt{\beta_{si}\beta_{iu}}L_{\frac{1}{2}}\left(-K_{si}\right)L_{\frac{1}{2}}\left(-K_{iu}\right)}. \tag{3.17}$$

Insights: We see that the minimum number of IRS elements required is inversely proportional to the strength of the cascaded reflected path. It decreases as the strength of the LoS components increases, i.e., as K_{si} or K_{iu} increases. This is because $L_{\frac{1}{2}}(x)$ is a monotonically decreasing function of x. Furthermore, it is independent of the strength of the direct path.

3.3.2.2 LoS Scenario

We now consider a special case when there are only LoS components from $S \to I$ and from $I \to U$, i.e., $K_{si} \to \infty$ and $K_{iu} \to \infty$. Therefore, $\boldsymbol{H}_{si} = \sqrt{\zeta_{si}}\,\overline{\boldsymbol{H}}_{si}$ and $\boldsymbol{h}_{iu} = \sqrt{\zeta_{iu}}\,\overline{\boldsymbol{h}}_{iu}$. In this case, $\sum_{n=1}^{N} \rho_{siu}^{an} = N\sqrt{\zeta_{si}\zeta_{iu}}$ and the probability of outage in (3.11) reduces to $\Pr\left(\rho_{su}^a \leq \overline{E}_{\text{th}} - N\sqrt{\zeta_{si}\zeta_{iu}}\right)$. Further simplification yields

$$P_{\text{outage}} = \begin{cases} 0, & \text{if } N\sqrt{\zeta_{si}\zeta_{iu}} \geq \overline{E}_{\text{th}}, \\ \left[1 - \exp\left(\frac{-\left(\overline{E}_{\text{th}} - N\sqrt{\zeta_{si}\zeta_{iu}}\right)^2}{\beta_{su}}\right)\right]^M, & \text{otherwise.} \end{cases} \tag{3.18}$$

Note that (3.18) is an exact expression for the probability of outage in WET. Here, employing $\sqrt{E_{\text{th}}/\left(p\eta_r\tau_c\zeta_{si}\zeta_{iu}\right)}$ number of IRS elements will yield zero OP.

3.3.2.3 Extension to Multi-User Scenario

With K users, if the source transmits energy wirelessly to every user based on RR scheduling strategy over a slot of length $\frac{\tau_c}{K}$ seconds, then the joint AS and passive beamforming rule is given

by

$$a_k = \underset{m\in\{1,2,\ldots,M\}}{\arg\max}\{\rho_{sk}^m\} \tag{3.19}$$

$$f_{i_k}^n = \exp\left(-j\left(\phi_{sik}^{a_k n} - \Lambda_{sk}^{a_k}\right)\right), \text{ for } n = 1,\ldots,N, \tag{3.20}$$

where $1 \le k \le K$ denotes index of the user being served in slot k, ρ_{sk}^m denotes magnitude of the direct path channel gain from the m^{th} antenna at the source to user k, $\Lambda_{sk}^{a_k}$ denotes phase of the direct path channel gain from the selected antenna a_k at the source to user k and $\phi_{sik}^{a_k n} = \angle H_{si}^{a_k n} + \angle h_{ik}^n$. Note that $\angle H_{si}^{a_k n}$ denotes the phase of the channel between the selected antenna a_k at S and n^{th} IRS element and $\angle h_{ik}^n$ denotes phase of the channel between n^{th} IRS element and k^{th} user. For this model, P_{outage} equals one minus the probability that every user harvests more than E_{th} amount of energy. Mathematically,

$$P_{\text{outage}} = 1 - \Pr\left(\bigcap_{k=1}^{K} E_k > E_{\text{th}}\right), \tag{3.21}$$

where E_k denotes energy harvested by k^{th} user.

Theorem 3.2. *An upper bound on probability of outage in WET with perfect CSI when users are served based on RR scheduling strategy is given by*

$$P_{outage} \le \min\left(1, \sum_{k=1}^{K} \Pr\left(E_k \le E_{th}\right)\right), \tag{3.22}$$

where $\Pr\left(E_k \le E_{th}\right)$ *is given in Theorem 3.1 with* γ *replaced by* $\frac{\gamma}{K}$.

Proof. The proof is given in Appendix B.2. □

3.4 Analysis of Probability of Outage in WET With Estimated CSI

In this section, we first present estimation of the direct and the reflected channels via the IRS using the two step procedure described in Section 3.3.1. Then we present our joint AS and IRS passive beamforming rule based on estimated CSI and derive its OP.

3.4.1 UL Pilot Transmission and Channel Estimation

Step 1: First, we estimate the direct path channel gain from S to U. In order to do that, we configure all the IRS elements to the off state, i.e., $\alpha_n = 0$ for all $n = 1,\ldots N$. The user transmits

pilot x_p with power q. Then the source receives signal y^m when it connects RF chain to the m^{th} antenna. It is given by

$$y^m = \sqrt{q} h_{su}^m x_p + w^m, \text{ for } m = 1, \ldots, M, \tag{3.23}$$

where $|x_p|^2 = 1$ and w^m is the complex AWGN with zero mean and variance σ^2. We know that

$$\overline{y}^m = y^m x_p^* = \sqrt{q} h_{su}^m + \overline{w}^m, \tag{3.24}$$

where $\overline{w}^m = w^m x_p^*$, is a sufficient statistic to estimate h_{su}^m. Based on $\overline{y}^m$, the MMSE estimate of the direct path channel gain is given by [38]

$$\hat{h}_{su}^m = \frac{\sqrt{q}\beta_{su}}{q\beta_{su} + \sigma^2} \overline{y}^m. \tag{3.25}$$

Substituting $\overline{y}^m$, it can be further simplified as

$$\hat{h}_{su}^m = h_{su}^m + \tilde{h}_{su}^m, \text{ for } m = 1, \ldots, M, \tag{3.26}$$

where the channel estimation error $\tilde{h}_{su}^m = \frac{-\sigma^2}{q\beta_{su}+\sigma^2} h_{su}^m + \frac{\sqrt{q}\beta_{su}}{q\beta_{su}+\sigma^2} \overline{w}^m$. Note that $\tilde{h}_{su}^m$ is independent of $\hat{h}_{su}^m$. Let $\gamma_{su} = \mathbb{E}\left(\left|\hat{h}_{su}^m\right|^2\right) = \frac{q\beta_{su}^2}{q\beta_{su}+\sigma^2}$ denote the variance of the channel estimate. Furthermore, the variance of the channel estimation error $\mathbb{E}\left(\left|\tilde{h}_{su}^m\right|^2\right) = \beta_{su} - \gamma_{su}$. Let $\hat{\rho}_{su}^m$ and $\hat{\Lambda}_{su}^m$ respectively denote the magnitude and phase of the channel gain estimate $\hat{h}_{su}^m$, i.e., $\hat{h}_{su}^m = \hat{\rho}_{su}^m e^{j\hat{\Lambda}_{su}^m}$, for $m \in \{1, 2, \ldots, M\}$. The source selects antenna $\hat{a}$ that has the highest channel power gain estimate. It is given by

$$\hat{a} = \underset{m \in \{1,2,\ldots,M\}}{\arg\max} \{\hat{\rho}_{su}^m\}. \tag{3.27}$$

Step 2: The source connects the RF chain to antenna $\hat{a}$ and estimates the corresponding cascaded channel gain via IRS. We turn on one IRS element at a time. The signal received at S when the n^{th} IRS element is turned on, i.e., $\alpha_n = 1$ and $\theta_n = 0$, is given by

$$y^{\hat{a}n} = \sqrt{q} h_{su}^{\hat{a}} x_p + \sqrt{q} g_{siu}^{\hat{a}n} x_p + w^{\hat{a}n}, \text{ for } n = 1, \ldots, N, \tag{3.28}$$

where $w^{\hat{a}n}$ is complex AWGN with zero mean and variance σ^2. Let $\overline{y}^{\hat{a}n}$ denote the signal component after subtracting the scaled version of the direct path channel gain estimate obtained in

$$\tilde{g}_{siu}^{\hat{a}n} = \frac{-g_{siu}^{\hat{a}n}\left[\sigma^2 + q\left(\tilde{\sigma}_{su}^{\hat{a}}\right)^2\right]}{q\left(\beta_{si} + \left|\mu_{si}^{\hat{a}n}\right|^2\right)\left(\beta_{iu} + \left|\mu_{iu}^{n}\right|^2\right) + \sigma^2 + q\left(\tilde{\sigma}_{su}^{\hat{a}}\right)^2 - q\left|\mu_{siu}^{\hat{a}n}\right|^2} + \mu_{siu}^{\hat{a}n}$$
$$+ \frac{\sqrt{q}\left(\left(\beta_{si} + \left|\mu_{si}^{\hat{a}n}\right|^2\right)\left(\beta_{iu} + |\mu_{iu}^{n}|^2\right) - \left|\mu_{siu}^{\hat{a}n}\right|^2\right)\left[\overline{w}^{\hat{a}n} - \sqrt{q}\tilde{h}_{su}^{\hat{a}} - \sqrt{q}\left(\mu_{siu}^{\hat{a}n} - \tilde{\mu}_{su}^{\hat{a}}\right)\right]}{q\left(\beta_{si} + \left|\mu_{si}^{\hat{a}n}\right|^2\right)\left(\beta_{iu} + |\mu_{iu}^{n}|^2\right) + \sigma^2 + q\left(\tilde{\sigma}_{su}^{\hat{a}}\right)^2 - q\left|\mu_{siu}^{\hat{a}n}\right|^2}. \quad (3.33)$$

Step 1, which is given by

$$\overline{y}^{\hat{a}n} = y^{\hat{a}n} - \sqrt{q}\hat{h}_{su}^{\hat{a}}x_p. \quad (3.29)$$

Using (3.26), we get

$$\overline{y}^{\hat{a}n} = \sqrt{q}g_{siu}^{\hat{a}n}x_p + w^{\hat{a}n} - \sqrt{q}\tilde{h}_{su}^{\hat{a}}x_p, \text{ for } n = 1, \ldots, N. \quad (3.30)$$

A sufficient statistic to estimate the cascaded channel $g_{siu}^{\hat{a}n}$ via the n^{th} IRS element is given by

$$\overline{\overline{y}}^{\hat{a}n} = \overline{y}^{\hat{a}n}x_p^* = \sqrt{q}g_{siu}^{\hat{a}n} + \overline{w}^{\hat{a}n} - \sqrt{q}\tilde{h}_{su}^{\hat{a}}, \quad (3.31)$$

for $n = 1, \ldots, N$, where $\overline{w}^{\hat{a}n} = w^{\hat{a}n}x_p^*$. Based on $\overline{\overline{y}}^{\hat{a}n}$, we next develop the linear MMSE estimate of the cascaded channel coefficient between S and U via the n^{th} IRS element. Since, IRS is passive, estimate of the cascaded channel coefficients can only be obtained.

Lemma 3.1. *The linear MMSE estimate of the cascaded channel coefficient $g_{siu}^{\hat{a}n}$ between the selected antenna at S and U via the n^{th} IRS element is given by [38]*

$$\hat{g}_{siu}^{\hat{a}n} = g_{siu}^{\hat{a}n} + \tilde{g}_{siu}^{\hat{a}n}, \quad (3.32)$$

where $\tilde{g}_{siu}^{\hat{a}n}$ is given in (3.33) *at the top of this page,* $\mu_{si}^{\hat{a}n} = \sqrt{\frac{K_{si}\zeta_{si}}{K_{si}+1}}\overline{H}_{si}^{\hat{a}n}$, $\mu_{iu}^{n} = \sqrt{\frac{K_{iu}\zeta_{iu}}{K_{iu}+1}}\overline{h}_{iu}^{n}$, $\mu_{siu}^{\hat{a}n} = \mu_{si}^{\hat{a}n}\mu_{iu}^{n} = \sqrt{\frac{K_{si}\zeta_{si}}{K_{si}+1}\frac{K_{iu}\zeta_{iu}}{K_{iu}+1}}\overline{H}_{si}^{\hat{a}n}\overline{h}_{iu}^{n}$, $\tilde{\mu}_{su}^{\hat{a}} = \mathbb{E}\left(\tilde{h}_{su}^{\hat{a}}\right) = \Re\left(\tilde{\mu}_{su}^{\hat{a}}\right) + j\Im\left(\tilde{\mu}_{su}^{\hat{a}}\right)$, $\Re\left(\tilde{\mu}_{su}^{\hat{a}}\right) = \Im\left(\tilde{\mu}_{su}^{\hat{a}}\right)$,

$$\Re\left(\tilde{\mu}_{su}^{\hat{a}}\right) \simeq \frac{-M\sqrt{\beta_{su} - \gamma_{su}}}{2\sqrt{\pi}}\left(\sum_{m=0}^{M-1}\binom{M-1}{m}\frac{\left(\frac{-1}{12}\right)^{M-1}3^{m+1}}{3M+m} - \sum_{m_1=0}^{M-1}\sum_{m_2=0}^{m_1}\binom{M-1}{m_1}\binom{m_1}{m_2}\frac{\left(\frac{-1}{12}\right)^{m_1}3^{m_2+1}}{3m_1+m_2+3}\right), \quad (3.34)$$

$$\left(\tilde{\sigma}_{su}^{\hat{a}}\right)^2 = var\left(\tilde{h}_{su}^{\hat{a}}\right) \simeq \frac{M(\beta_{su} - \gamma_{su})}{2}\left(\sum_{m_1=0}^{M-1}\sum_{m_2=0}^{m_1}\binom{M-1}{m_1}\binom{m_1}{m_2}\left(\frac{-1}{12}\right)^{m_1}3^{m_2+1}\frac{\sqrt{3(3m_1+m_2+3)}}{(3m_1+m_2+3)^2}\right.$$
$$\left. + \sum_{m=0}^{M-1}\binom{M-1}{m}\left(\frac{1}{12}\right)^{M-1}3^{m+1}\frac{\sqrt{3(3M+m)}}{(3M+m)^2}\right) - \left|\tilde{\mu}_{su}^{\hat{a}}\right|^2. \quad (3.35)$$

Proof. The proof is given in Appendix B.3. □

3.4.2 DL Transmission Based on Estimated CSI

Let $\hat{f}_i^n$ denote the reflection coefficient programmed at the n^{th} element based on the estimated CSI. Let $\hat{h}_{su}^{\hat{a}} = \hat{\rho}_{su}^{\hat{a}} e^{j\hat{\Lambda}_{su}^{\hat{a}}}$ and $\hat{g}_{siu}^{\hat{a}n} = \left|\hat{g}_{siu}^{\hat{a}n}\right| e^{j\hat{\phi}_{siu}^{\hat{a}n}}$ denote estimates of the direct and the reflected channels, respectively in terms of magnitude and phase. Substituting these estimates, in (3.8) and (3.9), joint AS and passive beamforming rule with estimated CSI can be written as

$$\hat{a} = \underset{m\in\{1,2,\ldots,M\}}{\arg\max}\{\hat{\rho}_{su}^{m}\}, \tag{3.36}$$

$$\hat{f}_i^n = \exp\left(-j\left(\hat{\phi}_{siu}^{\hat{a}n} - \hat{\Lambda}_{su}^{\hat{a}}\right)\right), \text{ for } n = 1,\ldots,N. \tag{3.37}$$

Let $\hat{\boldsymbol{f}}_{\boldsymbol{i}} = \left[\hat{f}_i^1, \hat{f}_i^2, \ldots, \hat{f}_i^N\right]^T$ denote the IRS passive beamforming vector based on estimated CSI. Signal received at U when source employs above joint AS and passive beamforming rule is

$$\hat{y}_u = \left(h_{su}^{\hat{a}} + \boldsymbol{g}_{siu}^{\hat{a}}\hat{\boldsymbol{f}}_{\boldsymbol{i}}\right) x_s + w_u, \tag{3.38}$$

where $w_u \sim \mathcal{CN}(0,\sigma^2)$ denotes complex AWGN at the user. Here, we spend $(M+N)\tau_p$ seconds to obtain channel estimates of the direct and reflected channel paths and energy is harvested for $\left(\tau_c - (M+N)\tau_p\right)$ seconds in each coherence interval. Therefore, from (3.38), the harvested energy with estimated CSI is given by $\hat{E}_u = \widehat{\gamma}\left|h_{su}^{\hat{a}} + \boldsymbol{g}_{siu}^{\hat{a}}\hat{\boldsymbol{f}}_i\right|^2$, where $\widehat{\gamma} = p\eta_r(\tau_c - (M+N)\tau_p)$. Expressing true channel as sum of estimate and estimation error based on (3.26) and (3.32), we get

$$\hat{E}_u = \widehat{\gamma}\left|\left(\hat{h}_{su}^{\hat{a}} + \hat{\boldsymbol{g}}_{siu}^{\hat{a}}\hat{\boldsymbol{f}}_i\right) - \left(\tilde{h}_{su}^{\hat{a}} + \tilde{\boldsymbol{g}}_{siu}^{\hat{a}}\hat{\boldsymbol{f}}_i\right)\right|^2. \tag{3.39}$$

Neglecting the estimation errors, $\hat{E}_u$ in (3.39) can be approximated as

$$\hat{E}_u \simeq \widehat{\gamma}\left|\hat{h}_{su}^{\hat{a}} + \hat{\boldsymbol{g}}_{siu}^{\hat{a}}\hat{\boldsymbol{f}}_i\right|^2 = \widehat{\gamma}\left|\hat{h}_{su}^{\hat{a}} + \sum_{n=1}^{N}\hat{g}_{siu}^{\hat{a}n}\hat{f}_i^n\right|^2 = \widehat{\gamma}\left|\hat{\rho}_{su}^{\hat{a}}e^{j\hat{\Lambda}_{su}^{\hat{a}}} + \sum_{n=1}^{N}\left|\hat{g}_{siu}^{\hat{a}n}\right| e^{j\hat{\phi}_{siu}^{\hat{a}n}}\hat{f}_i^n\right|^2. \tag{3.40}$$

By triangle inequality, we know that the choice of $\hat{f}_i^n$ in (3.37) maximizes $\hat{E}_u$ in (3.40). Therefore, substituting $\hat{f}_i^n$ from (3.37) in (3.40), the harvested energy can be written as

$$\hat{E}_u \simeq \widehat{\gamma}\left(\hat{\rho}_{su}^{\hat{a}} + \sum_{n=1}^{N}\left|\hat{g}_{siu}^{\hat{a}n}\right|\right)^2. \tag{3.41}$$

This approximation ensure analytical tractability. Furthermore, it is justified at practical operating points, since estimation errors $\tilde{h}_{su}^{\hat{a}}$ and $\tilde{\mathbf{g}}_{siu}^{\hat{a}}$ make negligibly small contribution to $\hat{E}_u$ [6, 71]. In Section 3.5, our numerical results show that the probability of outage obtained through Monte Carlo simulations based on exact $\hat{E}_u$ in (3.39) is in close agreement with the probability of outage expression derived in Theorem 3.3 based on approximate $\hat{E}_u$ in (3.41).

3.4.3 Analysis of Probability of Outage in WET

With estimated CSI, the probability of outage in WET is given by

$$\hat{P}_{\text{outage}} = \Pr\left(\hat{E}_u \le E_{\text{th}}\right) \simeq \Pr\left(\widehat{\gamma}\left(\hat{\rho}_{su}^{\hat{a}} + \sum_{n=1}^{N}\left|\hat{g}_{siu}^{\hat{a}n}\right|\right)^2 \le E_{\text{th}}\right). \tag{3.42}$$

Note that $\left|\hat{g}_{siu}^{\hat{a}n}\right|$ is magnitude of the estimate of the cascaded channel coefficient from the selected antenna at S to U via n^{th} IRS element. To simplify the analysis, we model it as a Rician RV. Figure 3.2 plots the cumulative distribution function (CDF) of $\left|\hat{g}_{siu}^{\hat{a}n}\right|$ obtained empirically from 10^5 samples through Monte Carlo simulations and the CDF of a Rician RV for three values of K_{si} and K_{iu}. We observe that for moderate and higher values of K_{si} and K_{iu}, the empirical and the Rician CDF match well. And for lower values of K_{si} and K_{iu}, we notice that the Rician approximation, while not perfect, tracks the empirical CDF of $\left|\hat{g}_{siu}^{\hat{a}n}\right|$ reasonably well. For this model, we next derive mathematical expression that approximates $\hat{P}_{\text{outage}}$ under estimated CSI.

Theorem 3.3. *With joint AS and IRS assisted passive beamforming based on estimated CSI, the probability of outage in WET is given by*

$$\hat{P}_{outage} \simeq \sum_{m=0}^{M-1}\frac{M(-1)^m}{m+1}\binom{M-1}{m}\left[1-\hat{\psi}Q\left(\frac{\hat{E}_{th}-\mu_{\hat{y}}}{\sigma_{\hat{y}}}\right)-\frac{\hat{\psi}e^{\frac{\hat{\xi}^2-\hat{\eta}\hat{\chi}}{2\hat{\eta}}}}{\sqrt{\hat{\eta}\sigma_{\hat{y}}^2}}\left(Q\left(\frac{-\hat{\xi}}{\sqrt{\hat{\eta}}}\right)-Q\left(\frac{\hat{E}_{th}-\mu_{\hat{y}}}{\sigma_{\hat{y}}^2\sqrt{\hat{\eta}}}\right)\right)\right], \tag{3.43}$$

where $\hat{\psi} = Q^{-1}\left(\frac{-\mu_{\hat{y}}}{\sigma_{\hat{y}}}\right)$, $\hat{\eta} = \frac{2(m+1)}{\gamma_{su}} + \frac{1}{\sigma_{\hat{y}}^2}$, $\hat{\xi} = \frac{2(m+1)\hat{E}_{th}}{\gamma_{su}} + \frac{\mu_{\hat{y}}}{\sigma_{\hat{y}}^2}$, $\hat{\chi} = \frac{2(m+1)\hat{E}_{th}^2}{\gamma_{su}} + \frac{\mu_{\hat{y}}^2}{\sigma_{\hat{y}}^2}$, $\hat{E}_{th} = \sqrt{\frac{E_{th}}{\hat{\gamma}}}$, $\mu_{\hat{y}} = N\sqrt{\frac{c_1^2\pi}{4c_2}}L_{\frac{1}{2}}\left(\frac{-\left|\mu_{siu}^{\hat{a}n}\right|^2c_2}{c_1^2}\right)$, $\sigma_{\hat{y}}^2 = N\left(\frac{c_1^2}{c_2}+\left|\mu_{siu}^{\hat{a}n}\right|^2-\hat{\mu}_0^2\right)$, $\hat{\mu}_0 = \sqrt{\frac{c_1^2\pi}{4c_2}}L_{\frac{1}{2}}\left(\frac{-\left|\mu_{siu}^{\hat{a}n}\right|^2c_2}{c_1^2}\right)$,

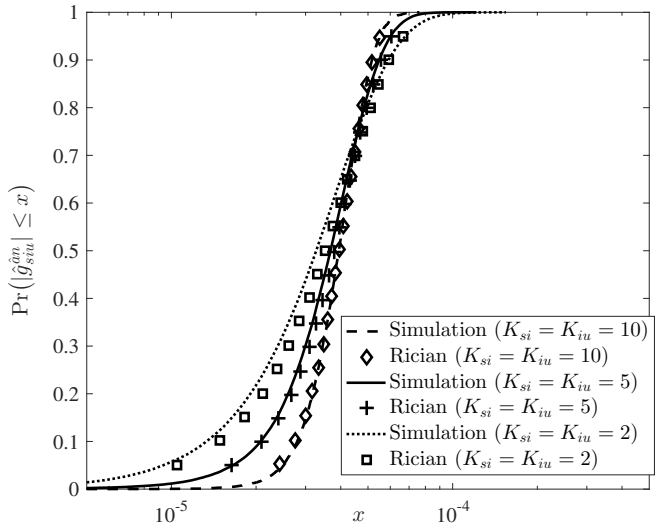

Fig. 3.2: CDF of $|\hat{g}_{siu}^{\hat{a}n}|$ compared with Rician model with similar parameters ($\beta_{su} = -45.81$ dB, $\zeta_{si} = -46.67$ dB, $\zeta_{iu} = -40.81$ dB, $\sigma^2 = -100$ dBm, and $q = 0$ dBm).

$$c_1 = \sqrt{q}\left(\left(\beta_{si} + \left|\mu_{si}^{\hat{a}n}\right|^2\right)\left(\beta_{iu} + |\mu_{iu}^{n}|^2\right) - \left|\mu_{siu}^{\hat{a}n}\right|^2\right), \text{ and } c_2 = q\left(\beta_{si} + \left|\mu_{si}^{\hat{a}n}\right|^2\right)\left(\beta_{iu} + |\mu_{iu}^{n}|^2\right) + \sigma^2 - q\left|\mu_{siu}^{\hat{a}n}\right|^2.$$

Proof. The proof is given in Appendix B.4. □

The analysis above accounts for order statistics of the magnitude of the estimated channel coefficients along the direct path and design of phase-shifts at I based on CSI estimates. Unlike the P_{outage} expression for perfect CSI in (3.12), $\hat{P}_{\text{outage}}$ in (3.43) is a function of the pilot power q, the time $\left(\tau_c - (M+N)\tau_p\right)$ that is used for DL WET, noise power σ^2 that accounts for estimation errors, and the statistics of the estimated CSI. Furthermore, the expression in (3.43) also brings out the dependence of $\hat{P}_{\text{outage}}$ on system and channel parameters. At high pilot power, $\hat{P}_{\text{outage}}$ in (3.43) reduces to P_{outage} in (3.12), since $\mu_{\hat{y}} \to \mu_y$, $\sigma_{\hat{y}}^2 \to \sigma_y^2$ and $\gamma_{su} \to \beta_{su}$.

3.4.3.1 Diversity Order

We refer to the slope of the probability of outage versus the source transmit power curve in the asymptotic regime in a log-log scale as the diversity order in WET systems. In other words, it measures the rate of decay of the probability of outage as a function of the source transmit power. We now derive the diversity order with estimated CSI in terms of number of antennas at the source and the number of passive reflecting elements at the IRS.

Theorem 3.4. *The diversity order of a joint AS and IRS passive beamforming assisted WET system with estimated CSI equals* $M + N$.[4]

Proof. The proof is given in Appendix B.5. □

3.4.3.2 Extension to Multi-User Scenario

With estimated CSI, $K(M+N)\tau_p$ seconds in a coherence interval would be spent on pilots. And AS at source and passive beamforming at IRS will be performed with estimated CSI. Therefore, based on RR scheduling strategy, the source would transfer energy wirelessly to every user over a slot of length $\frac{(\tau_c - K(M+N)\tau_p)}{K}$. Then, with estimated CSI, $\hat{P}_{\text{outage}}$ equals one minus the probability that every user harvests more than E_{th} amount of energy. Mathematically,

$$\hat{P}_{\text{outage}} = 1 - \Pr\left(\bigcap_{k=1}^{K} \hat{E}_k > E_{\text{th}}\right), \tag{3.44}$$

where $\hat{E}_k$ denotes the energy harvested by the k^{th} user with estimated CSI.

Theorem 3.5. *An upper bound on probability of outage in WET with estimated CSI when users are served based on RR scheduling strategy is given by*

$$\hat{P}_{outage} \leq \min\left(1, \sum_{k=1}^{K} \Pr\left(\hat{E}_k \leq E_{th}\right)\right), \tag{3.45}$$

where $\Pr\left(\hat{E}_k \leq E_{th}\right)$ *is given in Theorem 3.3 with* $\widehat{\gamma} = \frac{p\eta_r(\tau_c - K(M+N)\tau_p)}{K}$.

This can be proved along similar lines using ideas from Theorem 3.2 and Appendix B.4.

3.5 Numerical Results

We now present numerical results to illustrate the potential of joint low complexity AS at source and passive beamforming at IRS for WET. We present results to show the impact of the system parameters such as number of antennas M at source, number of IRS elements N, source transmit power p and pilot power q on the probability of outage. Unless mentioned otherwise, for illustration, we take $E_{\text{th}} = 10^{-7}$ J, $p = 1$ W, $q = 1$ mW, $\tau_c = 10$ ms, $\eta_r = 0.5$, $\tau_p = \frac{0.01\tau_c}{M+N}$, $\sigma^2 = 10^{-13}$ W, $K = 1$, $K_{si} = 10$, $K_{iu} = 10$, $\zeta_{ab} = \frac{G_a G_b \varpi}{d_{ab}^{\rho}}$, where $a, b \in \{s, u, i\}$, $\varpi = \left(\frac{d}{2\pi}\right)^2$ is the average channel attenuation at unit reference distance with $d = \frac{c}{2f}$ denoting the inter-element

[4]Note that this result is valid when the wireless channel offers rich scattering. It can therefore be considered as the maximal diversity gain that one can extract from such a system.

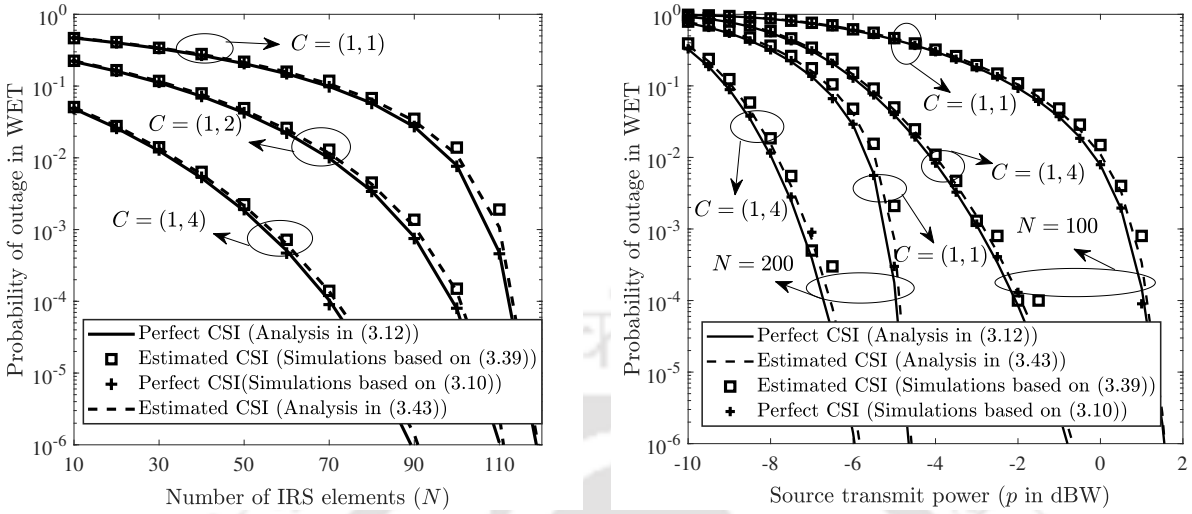

(a) (b)

Fig. 3.3: (a) Impact of N ($p = 1$ W, $q = 1$ mW, $K = 1$, and $E_{\text{th}} = 10^{-7}$ J). (b) Impact of p ($q = 1$ mW, $K = 1$, and $E_{\text{th}} = 10^{-7}$ J).

separation at the IRS, $f = 915$ MHz, $c = 3 \times 10^8$ m/s denotes speed of light and d_{ab} denotes distance between a and b. Furthermore, we take $G_s = G_u = 0$ dBi, $G_i = 5$ dBi and the path loss exponent $\rho = 2$ [14]. We consider that S, I, and U are arranged in a rectangular topology, S and I are placed opposite to each other with their coordinates (in meters) as $(0, 0)$ and $(10, 0)$ respectively, and U is placed at $(5, 1)$.

Figure 3.3 (a) plots probability of outage in WET as a function of N for three configurations, namely, $C = (1, 1)$, $C = (1, 2)$ and $C = (1, 4)$ and for both perfect and estimated CSI. Note that $C = (N_{\text{RF}}, M)$ refers to the configuration where the source is equipped with N_{RF} RF chains and M antennas. We note that the Monte Carlo simulations are in close agreement with analysis for both perfect and estimated CSI, thus validating our analysis. We observe that with $N = 70$, the probability of outage when $C = (1, 4)$ is lower by factors 100x and 1000x when compared to P_{outage} with $C = (1, 2)$ and $C = (1, 1)$, respectively. This is because the reduction in outage probability is more sensitive to changes in number of antennas M at the BS than to the changes in the number of IRS elements N since the direct path is relatively stronger than the reflected cascaded paths. We also observe that probability of outage degrades marginally with estimated CSI due to estimation errors and the fact that a part of the coherence interval is spent in estimation.

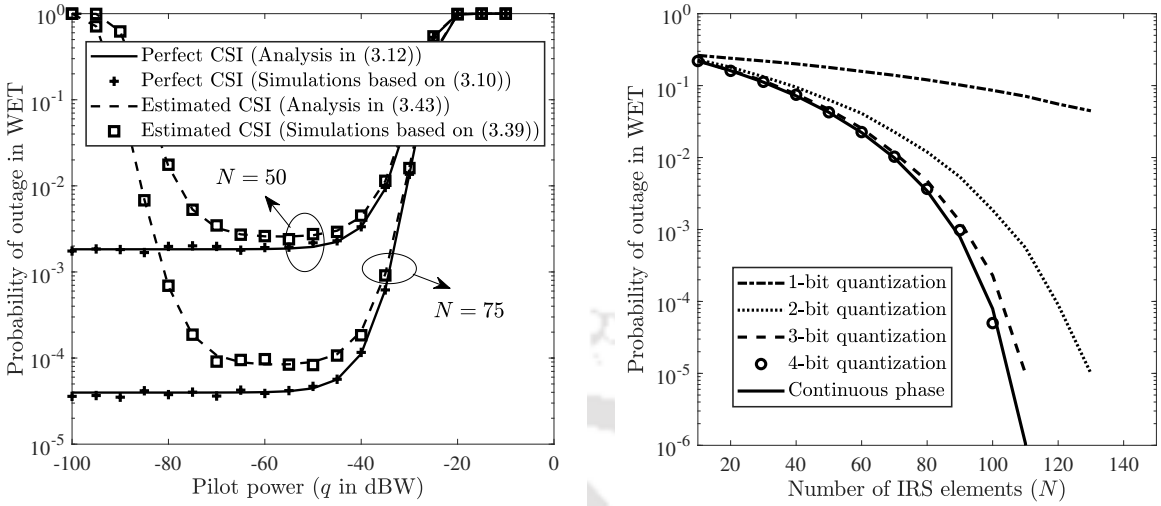

(a) (b)

Fig. 3.4: (a) Impact of q ($p = 1$ W, $E_{\text{th}} = E_p + q(M+N)\tau_p$, $C = (1,4)$, $K = 1$, and $E_p = 10^{-7}$ J), (b) Impact of discrete phase shifts ($p = 1$ W, $C = (1,2)$, $K = 1$, and $E_{\text{th}} = 10^{-7}$ J).

Figure 3.3 (b) plots probability of outage as a function of p for $C = (1,1)$ and $C = (1,4)$ and for two values of N. This is again done for both perfect and estimated CSI. As before, analysis matches well with simulations. We observe that the required transmit power at the source to achieve a given probability of outage decreases as the number of IRS elements increases. For example, with $C = (1,4)$, we can achieve P_{outage} of 10^{-6} with 5 dBW lower transmit power at S by adding 100 extra IRS elements. Moreover, the diversity order, which is equal to $M + N$, increases as M or N increase.

Figure 3.4 (a) plots probability of outage as a function of q for both perfect and estimated CSI. In general, the threshold energy E_{th} required at the user depends on the energy E_p spent on performing assigned tasks and the energy spent on channel estimation, i.e., $q(M+N)\tau_p$. To illustrate the impact of q, we consider $E_p = 10^{-7}$ J and $E_{\text{th}} = E_p + q(M+N)\tau_p$. With estimated CSI, we observe three regions of operation: i) For small values of pilot power, the probability of outage is high due to high channel estimation errors; ii) For medium values of pilot powers, i.e., -70 dBW $\leq q \leq -40$ dBW with $N = 75$, the probability of outage is relatively insensitive to the increase in pilot power; iii) For large values of pilot power, i.e., $q \geq -40$ dBW with $N = 75$, large amount of energy is spent for channel estimation. This increases E_{th}, which in turn, increases the probability of outage. Under perfect CSI, the probability of outage is

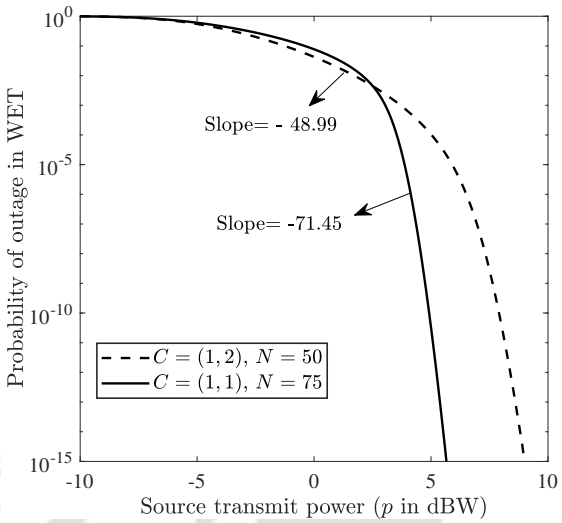

Fig. 3.5: Result to corroborate the diversity order ($q = 1$ mW, $K = 1$, and $E_{\text{th}} = 10^{-7}$ J).

constant for smaller values of q. This is because $q(M + N)\tau_p \ll E_p$ and P_{outage} does not depend on estimation errors. Furthermore, P_{outage} increases as q increases beyond -40 dBW since the threshold increases.[5]

Discrete Phase Shifts: Figure 3.4 (b) plots probability of outage in WET as a function of N under both continuous and discrete phase shifts at the IRS. We obtain the discrete phase shift by quantizing the continuous phase shift to the nearest available quantization level. We note that with j-bit discrete phase shifter at the IRS, 2^j phase-shift quantization levels are possible. As the number of quantization bits used to program the IRS increases, the performance with discrete phase shifts gets closer to the performance with continuous phase shifts. This is because an increase in the resolution of the discrete phase shifts enables better coherent combination of the reflected and direct path signals. In fact, a 3-bit programmable IRS is sufficient to achieve good trade-off between complexity[6] and performance.

Figure 3.5 plots the probability of outage in WET as a function of source transmit power with the objective of corroborating the diversity order. The diversity order based on graphical

[5]We show the outage performance with perfect CSI as well to elucidate and quantify the loss in outage performance due to estimation errors. The threshold energy under perfect CSI is kept the same as that with estimated CSI to ensure fair comparison.

[6]To configure phase shifts, positive-intrinsic-negative (PIN) diodes are used in the control circuitry at the IRS. With one PIN diode in the control circuitry at the IRS, only phase shifts of 0 and π can be induced. To induce an Q-level phase shift per IRS element, $\log_2(Q)$ PIN diodes would be required.

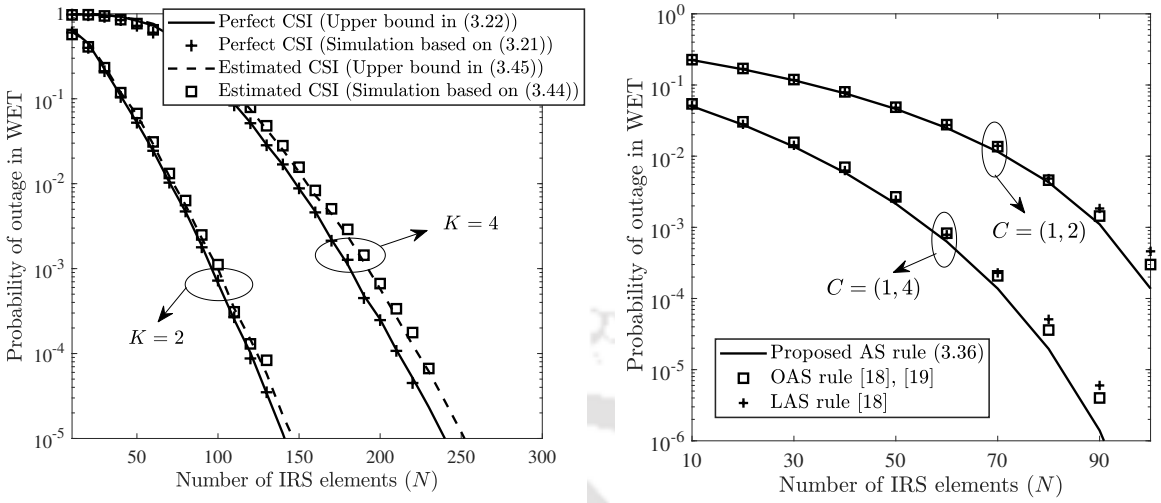

Fig. 3.6: (a) Impact of number of users ($p = 1$ W, $q = 1$ mW, $C = (1, 4)$ and $E_{\text{th}} = 10^{-7}$ J). Users are distributed uniformly between $(0, 1)$ and $(10, 1)$, (b) Performance benchmarking: Impact of different AS strategies ($p = 1$ W, $q = 1$ mW, $K = 1$, and $E_{\text{th}} = 10^{-7}$ J).

method for the curve with $(C = (1, 2), N = 50)$ is given by

$$\text{diversity order} = -\frac{10\log_{10}\left(1.10 \times 10^{-14}\right) - 10\log_{10}\left(3.59 \times 10^{-15}\right)}{8.8\ (\text{in dBW}) - 8.9\ (\text{in dBW})} = 48.99. \tag{3.46}$$

The theoretical value of diversity order corresponding to this curve is 52. While the diversity order based on graphical method for the curve with $(C = (1, 1), N = 75)$ is given by

$$\text{diversity order} = -\frac{10\log_{10}\left(1.42 \times 10^{-14}\right) - 10\log_{10}\left(2.75 \times 10^{-15}\right)}{5.5\ (\text{in dBW}) - 5.6\ (\text{in dBW})} = 71.45, \tag{3.47}$$

the theoretical value of diversity order corresponding to this curve is 76. We observe that the diversity order obtained using the graphical method deviates slightly from the theoretical value. This is because the diversity order expression that we derive theoretically is an asymptotic expression.

Figure 3.6 (a) plots probability of outage in WET vs. N for $K = 2$ and 4 with perfect and estimated CSI. Analysis matches well with simulations, thus confirming the tightness of the upper bound. We observe that by increasing N, WET to a larger number of users can be supported while maintaining the probability of outage fixed at a specific level. For example, 100 extra IRS elements are required to support WET to 4 users when compared against WET to 2 users while maintaining probability of outage fixed at 10^{-4}.

Performance Benchmarking: We benchmark the performance of the proposed AS rule with the selection rules considered in the literature.

1) *Optimal Antenna Selection (OAS) rule [19, 20]*: With estimated CSI, the OAS rule is given by $\hat{a}^{OAS} = \arg \max_{1\leq m\leq M} \left(\left|\hat{h}_{su}^{m}\right| + \sum_{n=1}^{N} \left|\hat{g}_{siu}^{mn}\right| \right)$. This rule maximizes the receive power under perfect CSI. However, it requires $M + MN$ pilot transmissions to obtain CSI. This is much higher than the $M + N$ pilot transmissions required by our proposed AS rule.

2) *Low Complexity Antenna Selection (LAS) rule [19]*: With estimated CSI, the LAS rule is given by $\hat{a}^{LAS} = \arg \max_{1\leq m\leq M} \left(\left|\hat{h}_{su}^{m}\right| + \left|\sum_{n=1}^{N} \hat{g}_{siu}^{mn}\right| \right)$. It requires $2M + N$ pilots transmission to obtain the CSI. Both OAS and LAS rules configure IRS elements as in (3.37).

Figure 3.6 (b) compares the performance of the proposed AS rule with the above two AS rules. It plots the probability of outage vs. N with estimated CSI for two different configurations. For $C = (1, 2)$, we see that the proposed AS rule[7] performs very close to OAS and LAS rules, which consider reflected channel gains in addition to the direct path channel gains. This is because the strength of the reflected channel gain via the IRS is relatively weaker compared to the strength of the direct path channel gain. We note that the proposed AS rule performs close to the optimal rule while requiring fewer number of pilot transmissions. For $C = (1, 4)$, as N increases, we see that the proposed AS rule performs better than the OAS and LAS rules. This is due to increase in the time required for the pilot transmission for both OAS and LAS rules, which in turn reduces the time available for DL energy transmission. For OAS and LAS rules, the time available for DL energy transfer is $\left(\tau_c - (M + MN)\tau_p\right)$ and $\left(\tau_c - (2M + N)\tau_p\right)$ seconds, respectively, while the proposed AS rule has $\left(\tau_c - (M + N)\tau_p\right)$ seconds available for energy transfer. Furthermore, the OAS rule performs marginally better than the LAS rule despite having a smaller DL energy transmission duration since it by design maximizes the receive power under perfect CSI.

[7]Unlike information transfer, in which the range is of the order of hundreds of meters, the range of WET is very limited and typically varies from few meters to few tens of meters [5, 6, 13–15, 72]. In most WET scenarios, it is, therefore, more likely that the direct channel between the source and the user would be present. And in WET, it is the absolute receive power that matters, unlike information transfer where the receive SNR is of interest. And by using IRS-assisted beamforming, the receive power can be boosted significantly to compensate the loss in performance due to AS.

Subset AS: Figure 3.7 (a) plots the PTE[8] as a function of the number of RF chains at the source for $M = 32$ and $N = 50,\ 75,$ and 100. We observe that the PTE increases initially as the number of RF chains increase and reaches a maxima. This is because the power harvested by the user increases as more number of antennas are selected[9] for energy beamforming. However, beyond a certain number of RF chains, the PTE decreases as the power consumption at the source dominates the harvested power at the user. Therefore, employing subset AS with a certain number of RF chains yields optimal PTE when compared to employing full complexity energy beamforming where number of RF chains must equal the number of antennas. For a given number of RF chains at the source, the PTE improves as N increases.

Figure 3.7 (b) plots the probability of outage as a function of p for $N = 50$ and $N = 150$ and for different configurations. We observe that for a given source transmit power, the probability of outage of single AS $(1, 4)$ with $N = 150$ is lower than even a full complexity $(4, 4)$ system with $N = 50$. Thus, one can trade-off active RF chains at the source with passive elements at the IRS to obtain improved outage performance. We also note that for a given configuration, substantial savings of radiated power is obtained by adding few passive elements at the IRS while maintaining the same probability of outage.

Limited Scattering: To study the impact of limited scattering on the probability of outage in WET, we model and decompose the channels as in [24]. Note that this modeling accounts for the number of scatterers that are present in the wireless environment. Based on this physics based generic model [24, 50], the n^{th} entry of the phase shift matrix is given by $[\boldsymbol{\Theta}]_{nn} = \alpha_n e^{j\theta_n}$, where $\alpha_n^2 = \left(\frac{\sqrt{4\pi}}{\lambda}\left|g_i\left(\Phi_t, \Phi_r\right)\right|\right)^2$, for all n, captures the amount by which the product of the path

[8]It is defined as the ratio of the average power harvested by the user to the total average power consumed at the source. Please note that we model the total average power consumed at the source as $P_c = p_{\text{tx}} + p_{\text{fix}} + N_{\text{RF}} p_{\text{s}} + p_{\text{lp}} + N p_{\text{e}}$ [71,73], where $p_{\text{tx}} = \frac{p}{\eta_{\text{pa}}}$, p denotes the source transmit power, η_{pa} denotes the efficiency of the power amplifier at the source, p_{fix} denotes the fixed power required to run the source, p_{s} denotes the circuit power consumed in every RF chain at the source, N_{RF} denotes the number of RF chains, $p_{\text{lp}} = \frac{3N_{\text{RF}}KB}{S_c k_{\text{s}}}$ denotes the total power consumed in computing active beamformer at the source, B denotes the system bandwidth, $S_c = B_c \tau_c$ denotes the number of samples in a coherence block, B_c denotes the coherence bandwidth, τ_c denotes the length of the coherence interval, K denotes the number of users, k_{s} denotes the source computational efficiency (in flops/watt) and p_{e} denotes the power spent in configuring the phase shift at each IRS element.

[9]For subset AS, the direct link channel power gains are arranged in descending order and N_{RF} antennas with the highest channel gains are selected. The active beamformer at the source and the phase-shifts at the IRS for both subset AS and the full-complexity system are obtained to maximize the received power based on AO, which is given in Appendix B.6.

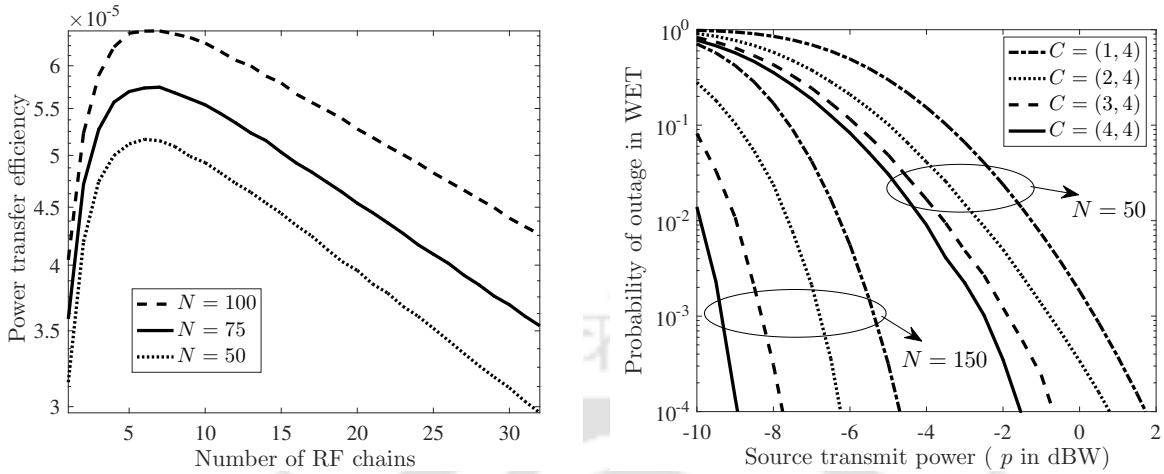

(a) (b)

Fig. 3.7: Illustration of trade-off between RF chains at source and passive elements at IRS (a) PTE vs. number of RF chains ($M = 32$, $p = 1$ W, $p_{\text{s}} = 1$ W, $p_{\text{fix}} = 1$ W, $\eta_{\text{pa}} = 0.39$, $p_{\text{e}} = 5$ mW, $K = 1$, $B = 10$ MHz, $B_c = 10$ KHz, and $k_s = 20 \times 10^9$ flops/W), (b) P_{outage} vs. p ($K = 1$ and $E_{\text{th}} = 10^{-7}$ J).

losses from source to IRS and IRS to user would get affected due to the amplitude change induced by the IRS.[10] Note that

$$g_i(\Phi_t, \Phi_r) = j\frac{\sqrt{4\pi}}{\lambda}\tau' l_i^2 \widetilde{g}_i(\Phi_t, \Phi_r) \tag{3.48}$$

denotes the response of each reflection element at IRS, τ' denotes amplitude of the reflection coefficient, l_i^2 captures the area of an IRS element, Φ_t denotes the direction of the incident signal, Φ_r denotes the direction of the reflected signal, and $\widetilde{g}_i(\Phi_t, \Phi_r)$ is given in [24, Eqn. (11)].

Figure 3.8 (a) plots probability of outage in WET as a function of N under limited scattering. Note that L_{su}, L_{si}, and L_{iu} denote the number of scatterers in the channel from S to U, S to I, and I to U, respectively. We observe that probability of outage increases as number of scatterers in the channel reduce. This is because the channel becomes more and more spatially correlated as the number of scatterers decrease.

The channel correlation can be exploited to further reduce the number of pilot transmissions by considering grouping based channel estimation.[11] We configure the phase shift of

[10] For this model, μ_0 in Section 3.3.2.1 can be expressed in a generic form as $\mu_0 = \frac{\pi}{4}\sqrt{\alpha_n^2 \beta_{si}\beta_{iu}} L_{\frac{1}{2}}(-K_{si}) L_{\frac{1}{2}}(-K_{iu})$. Using this, (3.17) is modified as $\frac{\lambda^2\sqrt{E_{\text{th}}}}{\tau' l_i^2 \widetilde{g}_i(\Phi_t,\Phi_r)\pi^2\sqrt{p\eta_r\tau_c}\sqrt{\beta_{si}\beta_{iu}} L_{\frac{1}{2}}(-K_{si}) L_{\frac{1}{2}}(-K_{iu})}$. This expression brings out dependence on the size l_i of each reflecting element at the IRS, and also gives insight that as size of IRS elements decreases, we need more IRS elements to avoid outage. The corresponding analysis under LoS scenario can be done along similar lines.

[11] The authors in [74] exploit the sparse structure of the wireless channel at mmWave frequencies to reduce

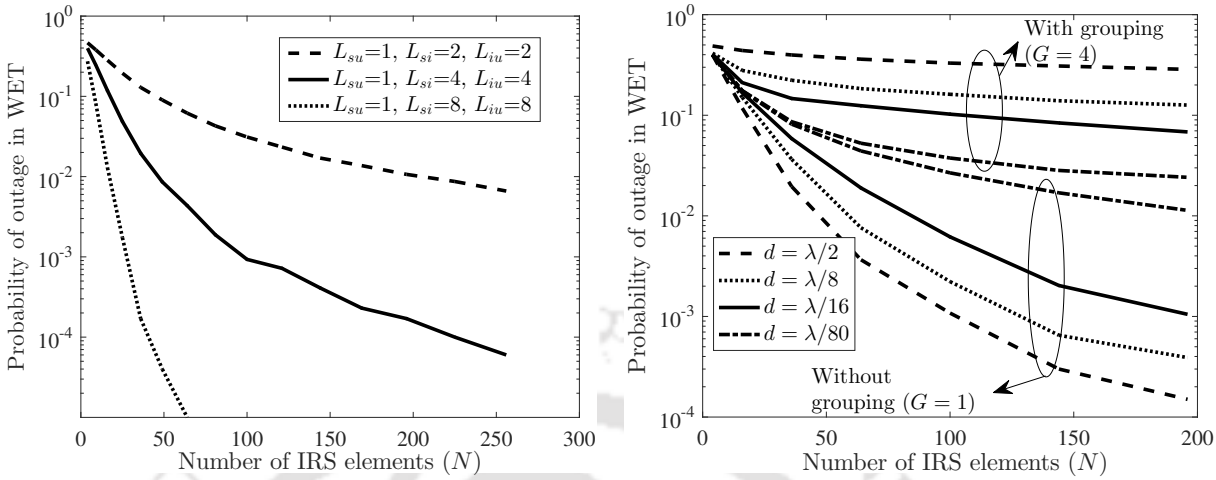

(a) (b)

Fig. 3.8: (a) Impact of limited scattering (p = 1 W, K = 1, τ' = 0.8, C = (1, 4), E_{th} = 10^{-7} J, and $l_i = d = \frac{\lambda}{2}$), (b) Impact of d (p = 1 W, K = 1, τ' = 0.8, E_{th} = 10^{-7} J, $l_i = \frac{\lambda}{2}$, C = (1, 4), L_{su} = 1, and $L_{si} = L_{iu}$ = 4).

any element in a group of size G as $f_i^g = \exp\left(-j\left(\phi_{siu}^{aG} - \Lambda_{su}^{a}\right)\right)$, for all $g \in \{1, \ldots, G\}$, where $\phi_{siu}^{aG} = \angle H_{si}^{aG} + \angle h_{iu}^{G}$, $\Lambda_{su}^{a} = \angle h_{su}^{a}$ and a denotes the strongest antenna along the direct path to the user. This grouping further reduces the number of pilot transmissions to $M + \frac{N}{G}$ [75]. To illustrate performance with grouping under limited scattering, Figure 3.8 (b) plots probability of outage vs. N for different inter-element spacing (d) and for two values of G. We observe that the gap between probability of outage with $G = 1$ and $G = 4$ decreases as d decreases. This is due to increase in spatial correlation as inter-element spacing decreases. This gives us an interesting design insight that the underlying correlation can be exploited to configure a larger group of adjacent elements with identical phase-shifts.

3.6 Summary

We considered a WET system in which a source with multiple antennas and a single RF chain transfers energy to an energy-constrained user and is assisted by an IRS with passive reflecting elements. We proposed a joint AS and passive beamforming rule that selects antenna based on direct path channel gains. We showed that it is near-optimal with fewer pilot transmissions. We derived new mathematical expressions for probability of outage for both perfect and estimated CSI cases and for both single and multi-user scenarios. We also proved that the

channel estimation overhead. However, we focus on WET at sub-6 GHz, where the channel is not really sparse.

diversity order of joint AS and IRS beamforming assisted system equals sum of the number of antennas at the source and the number of passive reflecting elements at the IRS.

We showed that the source transmit power required to achieve a target probability of outage decreases as the number of IRS elements or the number of transmit antennas increase. With estimated CSI, we observed that probability of outage is high both at low pilot powers due to high channel estimation errors and at high pilot powers as large fraction of the harvested energy is spent on channel estimation. We proved that we can trade-off active RF chains at source with passive elements at IRS to obtain improved performance both in terms of probability of outage and PTE. We also showed that by adding few passive IRS elements, WET to a larger number of users can be supported. Furthermore, a 3 bit programmable IRS gives near-identical probability of outage as a continuous phase shift IRS. We also elucidated the impact of limited scattering and inter-element spacing at the IRS on performance.

Based on the comprehensive characterization and evaluation of the WET system presented in this Chapter, a wireless system designer can identify operational regimes where the users harvest more than what they consume in sense, estimate, compute and communicate. In other words, this study gives an idea about the probability that the user may suffer from a blackout due to insufficient energy [21] and can help design systems that are robust to blackouts and ensure feasibility of WET. This can have potential applications in areas related to health monitoring where an implantable medical device would require perpetual supply of energy to continuously monitor vital parameters. Another potential application where systems designed based on this metric could prevent sensor nodes from going into sleep state due to insufficient energy is intrusion detection, which is again very critical to ensure security.

In this Chapter, we focussed on system modeling, optimization and performance analysis with perfect and estimated channel knowledge to elucidate the feasibility of single IRS assisted WET from a source that is equipped with fewer RF chains than the number of antennas. In the next Chapter, we extend our study and delve deeper into understanding the use of double IRS for WET and identify operational regimes where double IRS-aided WET outperforms single IRS-aided WET and massive multiple input multiple output (MIMO) enabled WET.

4

Double IRS Enabled WET

Contents

In this Chapter, we focus on a wireless scenario where a single antenna source assisted by double IRS transfers energy on the DL to a single antenna user via reflected paths and the direct path. We design the phase shift matrices at both the IRSs to maximize the received power at the user. We analyze OP for this model under non-linear EH at the user and for different practically relevant channel fading scenarios between different hops of the cascaded and direct channels. We also present the outage analysis for the generic scenario where each link via the direct and the cascaded paths between the source and the user follows Rician fading.

This analysis entails developing a novel statistical model based on Gamma distribution for the sum of product of Rician fading envelopes. We then generalize our study to also understand the impact of four communications links on OP and develop algorithms based on MO and AO to design the phase shifts at the two IRSs. Thereafter, we determine the optimal number of IRS elements that optimizes PTE for double IRS-assisted WET. Benchmarking against single IRS and massive MIMO enabled WET is also presented. We first discuss some key state-of-the-art literature related to massive MIMO, single-IRS and double-IRS enabled WET.

4.1 Related Literature

Massive MIMO Enabled Systems: Upper bounds on OP in WET were derived for a multi-user scenario in [13]. Authors in [76] optimized the transmit time switching factor and power allocation coefficient to maximize the minimum throughput of users. EE and PTE were maximized over number of BS antennas and number of users in [71]. Power allocation at the BS and power splitting factor at the receivers were designed to maximize the EE in [77]. A detailed survey of WET based on multi-antenna beamforming can be found in [78] and the references therein.

Single IRS Enabled Systems: In [52], the authors obtained the optimal power splitting ratio, active beamforming at BS and phase shifts at IRS to maximize the EE for a simultaneous wireless information and power transfer (SWIPT) system. The authors in [79] analyzed coverage, probability of signal-to-noise ratio (SNR) gain, and delay outage in an IRS-aided single input single output (SISO) communication network. In [14], active beamformer at the source and

passive beamformer at the IRS were designed for a multiple input single output WET system. An exhaustive survey of IRS-assisted WET and IRS-assisted SWIPT can be found in [7] and the references therein.

Double IRS Enabled Systems: In [80], passive beamforming at IRSs were designed to analyze the power gain at the user. Coverage probability of double IRS assisted SISO system was analyzed in [81]. In [82], the authors optimized the beamforming at the source and phase shifts at IRSs to maximize the secrecy rate at the intended user. Authors in [83] optimized receive beamforming at the source and passive beamforming at IRSs to maximize the minimum SINR in a MIMO system. In [84], transmit beamforming at source and phase shift at IRSs were optimized to maximize the DL sum rate subject to a minimum rate constraint per user in a MIMO system. The active beamforming at the source and passive beamforming at IRSs were designed to maximize the received signal in a multi-IRSs assisted communication scenario in [85].

Unlike existing works, the main objective of this work is to ascertain whether the use of double IRS can help save radiated power at the source while keeping OP fixed at a specific level and improve PTE. We ask and answer the following fundamental questions: 1) Under non-linear EH at the user, how does the harvested energy scale as a function of the number of elements in the double IRS configuration? The basic objective is to determine the scaling laws for WET using double IRS configuration; 2) How does the number of elements required at the two IRSs depend on the distance-dependent path loss and the channel propagation model used? 3) How does double IRS-assisted WET compare to single IRS assisted WET and massive MIMO assisted WET in terms of OP and PTE? The answer to these open questions require thorough investigation and would help us understand the fundamentals of double IRS enabled WET.

Notations: The $(m,n)^{\text{th}}$ element of a matrix $\boldsymbol{H}$ and the n^{th} element of a vector $\boldsymbol{h}$ are denoted by H^{mn} and h^n, respectively. The inner product between $\boldsymbol{a}$ and $\boldsymbol{b}$ is denoted as $\langle \boldsymbol{a}, \boldsymbol{b} \rangle$. Element-wise product of two matrix/vector is denoted by $\odot$.

Organization: This Chapter is organized as follows. We present the system model in Section 4.2. We design the passive beamformer and analyze the probability of outage for different

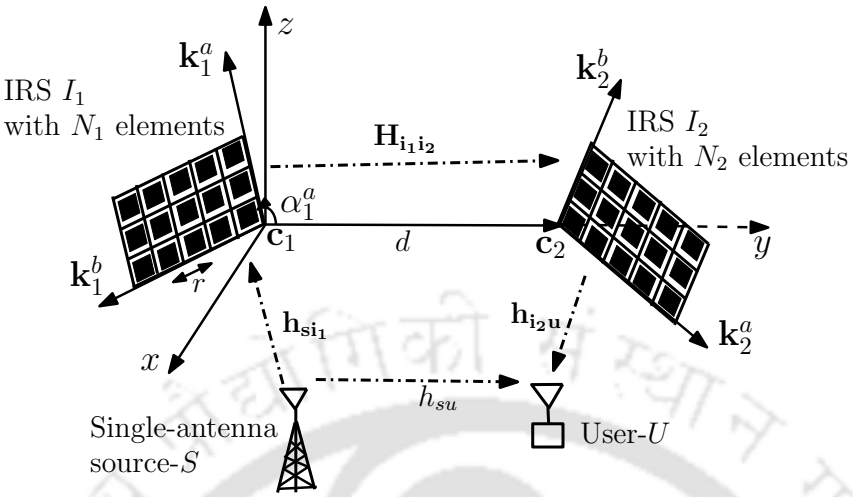

Fig. 4.1: Double IRS enabled WET

fading scenarios in Section 4.3. The outage analysis discussion is extended for four communication links in Section 4.4. The PTE is analyzed in Section 4.5. The numerical results and summary follow in Sections 4.6 and 4.7, respectively.

4.2 System Model

We consider a wireless scenario where a single-antenna source serves a single-antenna user via the direct path and via the cascaded path through IRS I_1 consisting of N_1 passive reflecting elements and another IRS I_2 consisting of N_2 passive reflecting elements as shown in Figure 4.1. We consider that I_1 is located at $\boldsymbol{c}_1$ and its elements are arranged along the orthonormal vectors $\boldsymbol{k}_1^a$ and $\boldsymbol{k}_1^b$. And I_2 is located at $\boldsymbol{c}_2$ and its elements are arranged along the orthonormal vectors $\boldsymbol{k}_2^a$ and $\boldsymbol{k}_2^b$. We denote the distance between $\boldsymbol{c}_1$ and $\boldsymbol{c}_2$ by d and the inter element distance at both IRSs is denoted by r. We denote the angles between $\boldsymbol{k}_i^o$ and $\boldsymbol{c}_2 - \boldsymbol{c}_1$ by α_i^o for $i \in \{1, 2\}$ and $o \in \{a, b\}$. The channel between S and U via the direct path is represented by $h_{su} \in C$. We denote the channel between S and I_1 by $\boldsymbol{h}_{si_1} \in C^{1\times N_1}$, the channel between I_1 and I_2 by $\boldsymbol{H}_{i_1 i_2} \in C^{N_1\times N_2}$ and the channel between I_2 and U by $\boldsymbol{h}_{i_2 u} \in C^{N_2\times 1}$. We model the phase shifts induced by the N_1 elements at I_1 by $\boldsymbol{\Theta} = \text{diag}(e^{j\theta_1}, e^{j\theta_2}, \ldots, e^{j\theta_{N_1}})$ and the phase shifts induced at I_2 by $\boldsymbol{\Phi} = \text{diag}(e^{j\phi_1}, e^{j\phi_2}, \ldots, e^{j\phi_{N_2}})$. Given this model, the signal received at the user is given by

$$y_u = \sqrt{p}\,(h_{su} + \boldsymbol{h}_{si_1}\boldsymbol{\Theta}\boldsymbol{H}_{i_1 i_2}\boldsymbol{\Phi}\boldsymbol{h}_{i_2 u})\, s_u + w_u, \tag{4.1}$$

$$= \sqrt{p}\left(h_{su} + \sum_{n_1=1}^{N_1}\sum_{n_2=1}^{N_2} h_{si_1}^{n_1}\Theta^{n_1 n_1}H_{i_1 i_2}^{n_1 n_2}\Phi^{n_2 n_2}h_{i_2 u}^{n_2}\right)s_u + w_u, \tag{4.2}$$

where p denotes the source transmit power, s_u denotes the transmit symbol chosen such that $|s_u|^2 = 1$ and w_u denotes complex additive white Gaussian noise.

4.3 Analysis of OP

Based on (4.2), the power of the signal received at the user is given by

$$P_u = p\left|h_{su} + \sum_{n_1=1}^{N_1}\sum_{n_2=1}^{N_2} h_{si_1}^{n_1}\Theta^{n_1 n_1}H_{i_1 i_2}^{n_1 n_2}\Phi^{n_2 n_2}h_{i_2 u}^{n_2}\right|^2. \tag{4.3}$$

Since, the contribution of noise to the received power is negligibly small, it is ignored [6,13,66]. We configure the phases at both the IRSs by considering a pure LoS channel between the two IRS. To ensure that the LoS channel between the two IRS is rank one, the distance d between two IRS must be such that $d > \frac{\sqrt{N_2}r^2}{\lambda}$, where λ denotes the wavelength [80]. The phases at both the IRSs are configured to ensure that the signal reaching the user via the direct path adds up coherently with the signal reaching the user via the reflected paths through I_1 and I_2. For this, we express the channel between the two IRSs as [80]

$$H_{i_1 i_2}^{n_1 n_2} = \rho_{i_1 i_2}^{n_1 n_2}\exp\left(\frac{-j2\pi d_{i_1 i_2}^{n_1 n_2}}{\lambda}\right) = \rho_{i_1 i_2}^{n_1 n_2}\exp\left(\frac{-j2\pi d}{\lambda}\right)h_1^{n_1}h_2^{n_2}, \tag{4.4}$$

where $\rho_{i_1 i_2}^{n_1 n_2} = \left|H_{i_1 i_2}^{n_1 n_2}\right|$, $d_{i_1 i_2}^{n_1 n_2}$ denotes the distance between element n_1 in I_1 and element n_2 in I_2, $h_1^{n_1} = \exp\left(\frac{j2\pi}{\lambda}\left(n_1^a r\cos\left(\alpha_1^a\right) + n_1^b r\cos\left(\alpha_1^b\right)\right)\right)$, and $h_2^{n_2} = \exp\left(\frac{-j2\pi}{\lambda}\left(n_2^a r\cos\left(\alpha_2^a\right) + n_2^b r\cos\left(\alpha_2^b\right)\right)\right)$. Furthermore, the index n_i is given by $n_i = n_i^a + 1 + n_i^b N_i^a$, where $i \in \{1,2\}$, $n_i^a \in \{0,\ldots,N_i^a - 1\}$, $n_i^b \in \{0,\ldots,N_i^b - 1\}$, and N_i^a and N_i^b are the number of elements along $\boldsymbol{k}_i^a$ and $\boldsymbol{k}_i^b$ directions of the IRS, respectively. Thus, $N_i = N_i^a N_i^b$ denotes the total number of elements at i^{th} IRS. To maximize the received power in (4.3), the phases at I_1 can be configured as follows:

$$\Theta^{n_1 n_1} = \left(\frac{h_{si_1}^{n_1}h_1^{n_1}}{\left|h_{si_1}^{n_1}\right|}\right)^*, \text{ for all } n_1 = 1,\ldots,N_1, \tag{4.5}$$

and the phases at I_2 can be configured as

$$\Phi^{n_2 n_2} = \left(\frac{h_2^{n_2} h_{i_2 u}^{n_2}}{\left|h_{i_2 u}^{n_2}\right|}\right)^* \frac{h_{su}}{|h_{su}|} \exp\left(\frac{j2\pi d}{\lambda}\right), \text{ for all } n_2 = 1, \ldots, N_2. \tag{4.6}$$

Substituting $\Theta^{n_1 n_1}$ from (4.5), $\Phi^{n_2 n_2}$ from (4.6) and $H_{i_1 i_2}^{n_1 n_2}$ from (4.4) in (4.3), the power of the signal received at the user equals

$$P_u = p\left(\rho_{su} + \sum_{n_1=1}^{N_1} \sum_{n_2=1}^{N_2} \rho_{si_1}^{n_1} \rho_{i_1 i_2}^{n_1 n_2} \rho_{i_2 u}^{n_2}\right)^2, \tag{4.7}$$

where $\rho_{su} = |h_{su}|$, $\rho_{si_1}^{n_1} = \left|h_{si_1}^{n_1}\right|$, and $\rho_{i_2 u}^{n_2} = \left|h_{i_2 u}^{n_2}\right|$.

Based on the received power in (4.7) the harvested power considering the practically relevant non-linear EH model at the user is given by [86, 87]

$$P_h = \frac{P_0}{(1 + \exp(-a_0(P_u - b_0)))\,(1 - \Omega)} - \frac{P_0 \Omega}{1 - \Omega}, \tag{4.8}$$

where a_0, b_0 are parameters that are determined by active and passive components of the EH circuit, P_0 is the maximum power that can be harvested when the circuit enters into saturation and $\Omega = \frac{1}{1+\exp(a_0 b_0)}$. The constants a_0, b_0 and P_0 are obtained through curve fitting of the experimental data obtained from the EH circuit in [88].

We declare an outage in energy transfer when the user harvests energy below a threshold. Mathematically, the OP in the context of energy transfer is given by

$$P_{\text{out}} = \Pr\left(E_h \leq E_{\text{th}}\right), \tag{4.9}$$

where $E_h = P_h \tau_c$ denotes the harvested energy, τ_c denotes the length of the coherence interval and E_{th} denotes the threshold energy. We next analyze this metric for different fading scenarios.

4.3.1 Scenario 1: When the Reflected Links $S - I_1$, $I_1 - I_2$ and $I_2 - U$ are LoS and Direct Channel $S - U$ is Rayleigh Faded

We consider that the direct channel between S and U is Rayleigh faded, i.e., $h_{su} \sim \mathcal{CN}(0, \beta_{su})$, where β_{su} denotes the path loss corresponding to this link. The n_1^{th} entry of the LoS channel between S and I_1 is given by $h_{si_1}^{n_1} = \sqrt{\beta_{si_1}} \exp\left(\frac{-j2\pi d_{si_1}^{n_1}}{\lambda}\right)$, for all $1 \leq n_1 \leq N_1$, where β_{si_1} denotes the path loss and $d_{si_1}^{n_1}$ denotes the distance between S and the n_1^{th} element of I_1. The LoS channel

between I_1 and I_2 is given in (4.4), where $\rho_{i_1 i_2}^{n_1 n_2} = \sqrt{\beta_{i_1 i_2}}$, for all $1 \leq n_1 \leq N_1$ and $1 \leq n_2 \leq N_2$, and $\beta_{i_1 i_2}$ denotes the path loss. The n_2^{th} entry of the LoS channel between I_2 and U is given by $h_{i_2 u}^{n_2} = \sqrt{\beta_{i_2 u}} \exp\left(\frac{-j2\pi d_{i_2 u}^{n_2}}{\lambda}\right)$, for all $1 \leq n_2 \leq N_2$, where $\beta_{i_2 u}$ denotes the path loss and $d_{i_2 u}^{n_2}$ denotes the distance between the n_2^{th} element of I_2 and U.

Using (4.8) and (4.9), the OP equals

$$P_{\text{out}} = \Pr\left(\frac{P_0}{\left(1 + \exp(-a_0(P_u - b_0))\right)(1 - \Omega)} - \frac{P_0 \Omega}{1 - \Omega} \leq P_{\text{th}}\right), \tag{4.10}$$

where $P_{\text{th}} = \frac{E_{\text{th}}}{\tau_c}$.

Result 4.1. *Under non-linear EH at the user, OP in scenario* 1 *is given by*

$$P_{out} = 1 - \exp\left(\frac{-\left(\overline{P}_{th} - N_1 N_2 \sqrt{\beta_{si_1}\beta_{i_1 i_2}\beta_{i_2 u}}\right)^2}{\beta_{su}}\right), \tag{4.11}$$

where $\overline{P}_{th} = \sqrt{\frac{P'_{th}}{p}}$, $P'_{th} = b_0 - \frac{\ln\left(\frac{P_0 - P_{th}(1-\Omega) - P_0\Omega}{P_{th}(1-\Omega) + P_0\Omega}\right)}{a_0}$.

Proof. The proof is given in Appendix C.1. □

We next obtain the optimal values of N_1 and N_2 in terms of the total number of IRS elements $N = N_1 + N_2$ that minimizes the OP in (4.11). To do this, we need to maximize the exponential to obtain the optimal N_1 and N_2. In other words, we need to minimize $t = \overline{P}_{\text{th}} - N_1 N_2 \sqrt{\beta_{si_1}\beta_{i_1 i_2}\beta_{i_2 u}}$. Let $N_1 = \lambda_0 N$ and $N_2 = (1 - \lambda_0)N$, where $0 \leq \lambda_0 \leq 1$ denotes the fraction of the total IRS elements at I_1. Therefore, we re-write t in term of λ_0 as $t = \overline{P}_{\text{th}} - \lambda_0(1 - \lambda_0)N^2 \sqrt{\beta_{si_1}\beta_{i_1 i_2}\beta_{i_2 u}}$. To obtain the optimal λ_0 which minimizes t, we differentiate t with respect to λ_0 to obtain $\frac{\partial t}{\partial \lambda_0} = -N^2 \sqrt{\beta_{si_1}\beta_{i_1 i_2}\beta_{i_2 u}}(1 - 2\lambda_0)$, and equate this to zero. This gives us the optimal value $\lambda_0^* = \frac{1}{2}$. We note that second derivative of t with respect to λ_0 is greater than 0. This implies that λ_0^* minimizes t. Also, $\lambda_0^* = 1/2$ implies that $N_1 = N_2 = N/2$ ensures that the OP is minimized even under the practically well-motivated non-linear EH model. This is consistent with the conclusions obtained in [80].

New Insights: Under non-linear EH at the user, the product of the number of IRS elements required at I_1 and I_2 to drive OP in (4.11) to zero in scenario 1 is given by $N_1 N_2 = \frac{\overline{P}_{\text{th}}}{\sqrt{\beta_{si_1}\beta_{i_1 i_2}\beta_{i_2 u}}}$.

4.3.2 Scenario 2: When the Channel $S - I_1$ is Rician Faded, $I_1 - I_2$ and $I_2 - U$ are LoS and Direct Channel $S - U$ is Rayleigh Faded

In this scenario, the channel between S and I_1 is given by

$$\boldsymbol{h}_{si_1} = \sqrt{\frac{K_{si_1}}{K_{si_1}+1}}\overline{\boldsymbol{h}}_{si_1} + \sqrt{\frac{1}{K_{si_1}+1}}\widetilde{\boldsymbol{h}}_{si_1}, \tag{4.12}$$

where K_{si_1} denotes the Rician factor, the n_1^{th} element of the LoS component $\overline{\boldsymbol{h}}_{si_1}$ is given by $\overline{h}_{si_1}^{n_1} = \sqrt{\beta_{si_1}}\exp\left(\frac{-j2\pi d_{si_1}^{n_1}}{\lambda}\right)$ and the n_1^{th} element of the non-LoS component $\widetilde{\boldsymbol{h}}_{si_1}$ is modelled as $\widetilde{h}_{si_1}^{n_1} \sim \mathcal{CN}(0,\beta_{si_1})$. Thus, $h_{si_1}^{n_1} \sim \mathcal{CN}\left(\mu_{si_1}^{n_1}, \zeta_{si_1}\right)$, where $\mu_{si_1}^{n_1} = \sqrt{\frac{K_{si_1}}{K_{si_1}+1}}\overline{h}_{si_1}^{n_1}$ and $\zeta_{si_1} = \frac{\beta_{si_1}}{K_{si_1}+1}$ for all $1 \le n_1 \le N_1$.

Result 4.2. *Under non-linear EH at the user, OP in scenario 2 is given by*

$$P_{out} = 1 - \psi_1 Q\left(\frac{\overline{P}_{th}-\mu_1}{\sigma_1}\right) - \frac{\psi_1 e^{\frac{\xi_1^2-\eta_1\chi_1}{2\eta_1}}}{\sqrt{\eta_1\sigma_1^2}}\left(Q\left(\frac{-\xi_1}{\sqrt{\eta_1}}\right) - Q\left(\frac{\overline{P}_{th}-\mu_1}{\sigma_1^2\sqrt{\eta_1}}\right)\right), \tag{4.13}$$

where $\psi_1 = Q^{-1}\left(\frac{-\mu_1}{\sigma_1}\right)$, $\eta_1 = \left(\frac{2}{\beta_{su}} + \frac{1}{\sigma_1^2}\right)$, $\xi_1 = \left(\frac{2\overline{P}_{th}}{\beta_{su}} + \frac{\mu_1}{\sigma_1^2}\right)$, $\chi_1 = \left(\frac{2\overline{P}_{th}^2}{\beta_{su}} + \frac{\mu_1^2}{\sigma_1^2}\right)$,
$\mu_1 = N_1N_2\sqrt{\frac{\pi\zeta_{si_1}\beta_{i_1i_2}\beta_{i_2u}}{4}}L_{\frac{1}{2}}(-K_{si_1})$, $\sigma_1^2 = N_1N_2^2\beta_{i_1i_2}\beta_{i_2u}\left(\zeta_{si_1}(1+K_{si_1}) - \nu_1^2\right)$,
$\nu_1 = \sqrt{\frac{\pi\zeta_{si_1}}{4}}L_{\frac{1}{2}}(-K_{si_1})$, $Q(\cdot)$ *denotes the Q-function [67] and* $L_n(\cdot)$ *denotes Laguerre polynomial of order-n [68].*

Proof. The proof is given in Appendix C.2. □

Remark: The mathematical expression above brings out the dependence of the OP on the Rician factor K_{si_1} in addition to the system parameters such as N_1, N_2, and P_{th}, channel parameters such as β_{su}, β_{si_1}, $\beta_{i_1i_2}$ and β_{i_2u}, and the non-linear EH circuit parameters such as a_0, b_0 and P_0. If the direct channel is blocked, the expression in (4.13) simplifies to

$$P_{\text{out}} = 1 - \psi_1 Q\left(\frac{\overline{P}_{\text{th}}-\mu_1}{\sigma_1}\right). \tag{4.14}$$

4.3.3 Scenario 3: When Channels $S - I_1$, $I_1 - I_2$ are LoS, $I_2 - U$ is Rician Faded and the Direct Channel $S - U$ is Rayleigh Faded

In this wireless scenario, the channel between I_2 and U is given by

$$\boldsymbol{h}_{i_2u} = \sqrt{\frac{K_{i_2u}}{K_{i_2u}+1}}\overline{\boldsymbol{h}}_{i_2u} + \sqrt{\frac{1}{K_{i_2u}+1}}\widetilde{\boldsymbol{h}}_{i_2u}, \tag{4.15}$$

where K_{i_2u} denotes the Rician factor, the n_2^{th} element of the LoS component $\overline{\boldsymbol{h}}_{i_2u}$ is given by $\overline{h}_{i_2u}^{n_2} = \sqrt{\beta_{i_2u}} \exp\left(\frac{-j2\pi d_{i_2u}^{n_2}}{\lambda}\right)$ and the n_2^{th} element of the non-LoS component $\widetilde{\boldsymbol{h}}_{i_2u}$ is modelled as $\widetilde{h}_{i_2u}^{n_2} \sim \mathcal{CN}(0, \beta_{i_2u})$. Thus, $h_{i_2u}^{n_2} \sim \mathcal{CN}\left(\mu_{i_2u}^{n_2}, \zeta_{i_2u}\right)$, where $\mu_{i_2u}^{n_2} = \sqrt{\frac{K_{i_2u}}{K_{i_2u}+1}}\overline{h}_{i_2u}^{n_2}$ and $\zeta_{i_2u} = \frac{\beta_{i_2u}}{K_{i_2u}+1}$ for all $1 \leq n_2 \leq N_2$.

Result 4.3. *Under non-linear EH at the user, OP in scenario* 3 *is given by*

$$P_{out} = 1 - \psi_2 Q\left(\frac{\overline{P}_{th} - \mu_2}{\sigma_2}\right) - \frac{\psi_2 e^{\frac{\xi_2^2 - \eta_2\chi_2}{2\eta_2}}}{\sqrt{\eta_2\sigma_2^2}}\left(Q\left(\frac{-\xi_2}{\sqrt{\eta_2}}\right) - Q\left(\frac{\overline{P}_{th} - \mu_2}{\sigma_2^2\sqrt{\eta_2}}\right)\right), \tag{4.16}$$

where ψ_2, η_2, ξ_2 *and* χ_2 *are obtained from* ψ_1, η_1, ξ_1 *and* χ_1, *respectively, in* (4.13), *just by replacing* μ_1 *with* μ_2 *and* σ_1 *with* σ_2, $\mu_2 = N_1N_2\sqrt{\frac{\pi\beta_{si_1}\beta_{i_1i_2}\zeta_{i_2u}}{4}}L_{\frac{1}{2}}(-K_{i_2u})$,
$\sigma_2^2 = N_1^2N_2\beta_{si_1}\beta_{i_1i_2}\left(\zeta_{i_2u}(1+K_{i_2u}) - \nu_2^2\right)$, $\nu_2 = \sqrt{\frac{\pi\zeta_{i_2u}}{4}}L_{\frac{1}{2}}(-K_{i_2u})$.

Proof. This can be proved using similar ideas as in Appendix C.2. □

New Insights: Note that σ_2^2 scales as $N_1^2N_2$ unlike theorem 4.2 where σ_1^2 scales as $N_1N_2^2$. Based on (4.7), we observe that the OP as given in (4.13) and (4.16) for wireless scenarios 2 and 3, respectively would be identical provided N_1 and N_2 are sufficiently large and the Rician factors $K_{si_1} = K_{i_2u}$. This is because for sufficiently large N_1 and N_2, the term $\frac{1}{N_1N_2}\sum_{n_1=1}^{N_1}\sum_{n_2=1}^{N_2}\rho_{si_1}^{n_1}\rho_{i_1i_2}^{n_1n_2}\rho_{i_2u}^{n_2}$ approaches $\sqrt{\frac{\pi\zeta_{si_1}\beta_{i_1i_2}\beta_{i_2u}}{4}}L_{\frac{1}{2}}(-K_{si_1})$ in scenario 2 and in scenario 3, it approaches $\sqrt{\frac{\pi\beta_{si_1}\beta_{i_1i_2}\zeta_{i_2u}}{4}}L_{\frac{1}{2}}(-K_{i_2u})$. And these terms for scenarios 2 and 3 turn out to be the same if the Rician factors K_{si_1} and K_{i_2u} are equal. If the direct channel is blocked, the expression in (4.16) simplifies to

$$P_{\text{out}} = 1 - \psi_2 Q\left(\frac{\overline{P}_{\text{th}} - \mu_2}{\sigma_2}\right). \tag{4.17}$$

4.3.4 Scenario 4-Generic Channel Fading: When Channels $S-U$, $S-I_1$, I_1-I_2 and I_2-U are Rician Faded

We generalize our mathematical analysis to also consider a generic wireless scenario where the channel from $S-U$ via the direct path and the channels from $S-I_1$, I_1-I_2 and I_2-U via the cascaded path undergo Rician fading. The channel between $S-I_1$ and I_2-U are given in

sections 4.3.2 and 4.3.3, respectively. The channel between I_1 and I_2 is given by

$$\boldsymbol{H}_{i_1 i_2} = \sqrt{\frac{K_{i_1 i_2}}{K_{i_1 i_2}+1}}\overline{\boldsymbol{H}}_{i_1 i_2} + \sqrt{\frac{1}{K_{i_1 i_2}+1}}\widetilde{\boldsymbol{H}}_{i_1 i_2}, \tag{4.18}$$

where $K_{i_1 i_2}$ denotes the Rician factor for this link. The $(n_1, n_2)^{\text{th}}$ element of the LoS component $\overline{\boldsymbol{H}}_{i_1 i_2}$ is given by $\overline{H}_{i_1 i_2}^{n_1 n_2} = \sqrt{\beta_{i_1 i_2}} \exp\left(\frac{-j2\pi d_{i_1 i_2}^{n_1 n_2}}{\lambda}\right)$, where $\beta_{i_1 i_2}$ denotes the path loss and $d_{i_1 i_2}^{n_1 n_2}$ denotes the distance between the n_1^{th} element of I_1 and n_2^{th} element of I_2. The $(n_1, n_2)^{\text{th}}$ element of the non-LoS component $\widetilde{\boldsymbol{H}}_{i_1 i_2}$ is modelled as $\widetilde{H}_{i_1 i_2}^{n_1 n_2} \sim \mathcal{CN}(0, \beta_{i_1 i_2})$. Thus, $H_{i_1 i_2}^{n_1 n_2} \sim \mathcal{CN}\left(\mu_{i_1 i_2}^{n_1 n_2}, \zeta_{i_1 i_2}\right)$, where $\mu_{i_1 i_2}^{n_1 n_2} = \sqrt{\frac{K_{i_1 i_2}}{K_{i_1 i_2}+1}}\overline{H}_{i_1 i_2}^{n_1 n_2}$ and $\zeta_{i_1 i_2} = \frac{\beta_{i_1 i_2}}{K_{i_1 i_2}+1}$ for all $1 \le n_1 \le N_1$ and $1 \le n_2 \le N_2$. Furthermore, the direct channel between S and U also undergoes Rician fading and is given by

$$h_{su} = \sqrt{\frac{K_{su}}{K_{su}+1}}\overline{h}_{su} + \sqrt{\frac{1}{K_{su}+1}}\widetilde{h}_{su}. \tag{4.19}$$

where K_{su} denotes the Rician factor corresponding to this link. Note that $\overline{h}_{su} = \sqrt{\beta_{su}} \exp\left(\frac{-j2\pi d_{su}}{\lambda}\right)$, where β_{su} represents the path loss over this link and d_{su} denotes the distance between the source and the user via the direct path. And $\widetilde{h}_{su} \sim \mathcal{CN}(0, \beta_{su})$. Thus, $h_{su} \sim \mathcal{CN}(\mu_{su}, \zeta_{su})$, where $\mu_{su} = \sqrt{\frac{K_{su}}{K_{su}+1}}\overline{h}_{su}$ and $\zeta_{su} = \frac{\beta_{su}}{K_{su}+1}$.

Given this model and based on $\Theta^{n_1 n_1}$ in (4.5) and $\Phi^{n_2 n_2}$ in (4.6), the power of the signal received at the user can be approximated as[1]

$$P_u \approx p\left(\rho_{su} + \sum_{n_1=1}^{N_1}\sum_{n_2=1}^{N_2} \rho_{si_1}^{n_1}\rho_{i_1 i_2}^{n_1 n_2}\rho_{i_2 u}^{n_2}\right)^2, \tag{4.20}$$

Based on (4.8), (4.9) and (4.20), we obtain

$$P_{\text{out}} \approx \Pr\left(\left(\rho_{su} + \sum_{n_1=1}^{N_1}\sum_{n_2=1}^{N_2} \rho_{si_1}^{n_1}\rho_{i_1 i_2}^{n_1 n_2}\rho_{i_2 u}^{n_2}\right) \le \overline{P}_{\text{th}}\right), \tag{4.21}$$

[1]We note that the phase change induced due to the scattered component of the channel between I_1 and I_2 remains uncompensated based on the phase configuration stated above in (4.5) and (4.6). We neglect this uncompensated phase. This approximation ensures mathematical tractability while providing useful design insights. Furthermore, based on Figure 4.5 in Section 4.6, we also observe that this approximation is reasonably accurate, since the OP obtained through Monte Carlo simulations based on exact P_u in (4.3) and where phases at the two IRSs are programmed based on (4.5) and (4.6) matches well with the approximate OP expression derived in (4.26).

$$r_2 = N_1N_2\zeta_{si_1}\zeta_{i_1i_2}\zeta_{i_2u}(1+K_{si_1})(1+K_{i_1i_2})(1+K_{i_2u})+\frac{\pi^2}{16}N_1N_2(N_2-1)\zeta_{si_1}\zeta_{i_1i_2}\zeta_{i_2u}(1+K_{si_1})L^2_{\frac{1}{2}}(-K_{i_1i_2})$$
$$\times L^2_{\frac{1}{2}}(-K_{i_2u})+\frac{\pi^2}{16}N_1N_2(N_1-1)\zeta_{si_1}\zeta_{i_1i_2}\zeta_{i_2u}(1+K_{i_2u})L^2_{\frac{1}{2}}(-K_{si_1})\,L^2_{\frac{1}{2}}(-K_{i_1i_2})+\frac{\pi^3}{64}N_1N_2(N_1-1)(N_2-1)$$
$$\times\,\zeta_{si_1}\zeta_{i_1i_2}\zeta_{i_2u}L^2_{\frac{1}{2}}(-K_{si_1})\,L^2_{\frac{1}{2}}(-K_{i_1i_2})\,L^2_{\frac{1}{2}}(-K_{i_2u})\,. \quad (4.25)$$

We let $X = \rho_{su}$ and $Y = \sum_{n_1=1}^{N_1}\sum_{n_2=1}^{N_2}\rho_{si_1}^{n_1}\rho_{i_1i_2}^{n_1n_2}\rho_{i_2u}^{n_2}$. Then, OP in (4.21) can be expressed as

$$P_{\text{out}} \approx \Pr\left(X + Y \leq \overline{p}_{\text{th}}\right). \quad (4.22)$$

To simplify this further, we require the PDFs of X and Y. We know that $X = \rho_{su}$ is a Rician distributed RV. And we note that the term $Y = \sum_{n_1=1}^{N_1}\sum_{n_2=1}^{N_2}\rho_{si_1}^{n_1}\rho_{i_1i_2}^{n_1n_2}\rho_{i_2u}^{n_2}$ in (4.22) is the sum of product of three Rician RVs which are correlated across n_1 and n_2. Since the terms are correlated, central limit theorem (CLT) cannot be used to approximate the PDF of Y to a Gaussian distribution [70]. Therefore, to simplify the analysis and make it tractable while deriving useful insights, we develop a novel statistical model for Y based on Gamma distribution, where we rigorously derive the corresponding shape and scale parameters based on moment matching method.

Theorem 4.1. *When the channels $S-I_1$, I_1-I_2 and I_2-U are Rician faded, $Y = \sum_{n_1=1}^{N_1}\sum_{n_2=1}^{N_2}\rho_{si_1}^{n_1}\rho_{i_1i_2}^{n_1n_2}\rho_{i_2u}^{n_2}$ can be modeled as a Gamma RV with shape (k) and scale (t) parameters, respectively given by*

$$k = \frac{r_1^2}{r_2 - r_1^2} \text{ and } t = \frac{r_2 - r_1^2}{r_1}, \quad (4.23)$$

where r_1 denotes the first moment of Y and it equals

$$r_1 = N_1N_2\sqrt{\frac{\pi^3\zeta_{si_1}\zeta_{i_1i_2}\zeta_{i_2u}}{64}}L_{\frac{1}{2}}(-K_{si_1})\,L_{\frac{1}{2}}(-K_{i_1i_2})\,L_{\frac{1}{2}}(-K_{i_2u}), \quad (4.24)$$

and r_2 denotes the second moment of Y which is given in (4.25) *at the top of the next page.*

Proof. The proof is given in Appendix C.3. □

This result captures the correlation across n_1 and n_2 in the RV Y. Figure 4.2 plots the CDF of Y obtained empirically from 10^5 samples through Monte Carlo simulations and the CDF of a Gamma RV with shape and scale parameter as outlined in Theorem 4.1 for three different set of values of the Rician factor corresponding to each link. We observe that the empirical and the

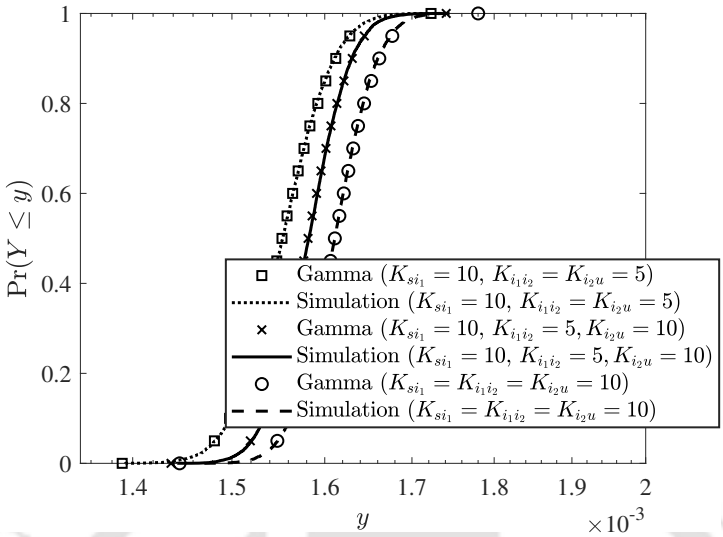

Fig. 4.2: CDF of Y compared with the Gamma model with similar parameters ($\beta_{si_1} = -30.81$ dB, $\beta_{i_1i_2} = -64.87$ dB and $\beta_{i_2u} = -48.06$ dB)

Gamma CDF are in close agreement with each other, thus validating the accuracy of statistically modeling Y as a Gamma RV. Given this statistical modeling of Y, we derive OP for this generic scenario next as a theorem.

Theorem 4.2. *Under non-linear EH at the user and when each link follows Rician fading, OP is given by*

$$P_{outage} \approx \frac{\gamma\left(k, \frac{\overline{p}_{th}}{t}\right)}{\Gamma(k)} - \frac{1}{t^k \Gamma(k)} \int_{y=0}^{\overline{p}_{th}} y^{k-1} e^{\frac{-y}{t}} Q_1\left(\sqrt{2K_{su}}, \frac{\overline{p}_{th} - y}{\sqrt{\zeta_{su}/2}}\right) dy, \tag{4.26}$$

where $\Gamma(\cdot)$ denotes the complete gamma function, $\gamma(\cdot,\cdot)$ denotes the lower incomplete gamma function [68, Eqn. (8.350.1)] and $Q_1(\cdot,\cdot)$ denotes the first order Marcum Q-function [67, Eqn. (4.34)].

Proof. The proof is given in Appendix C.4. □

We note that the second term in (4.26) is in the form of a single integral in y and probably cannot be simplified, since the integrand involves the product of an algebraic function, an exponential function and the first order Marcum-Q function. It is, however, easy to compute this numerically.

Special cases: Scenario 4, in which all links follow Rician fading reduces to scenario 1, if $K_{si_1} \to \infty$, $K_{i_1i_2} \to \infty$, $K_{i_2u} \to \infty$ and $K_{su} = 0$. And in that case, $Y = \sum_{n_1=1}^{N_1} \sum_{n_2=1}^{N_2} \rho_{si_1}^{n_1} \rho_{i_1i_2}^{n_1n_2} \rho_{i_2u}^{n_2}$ in (4.22) simplifies to $Y = N_1 N_2 \sqrt{\beta_{si_1}\beta_{i_1i_2}\beta_{i_2u}}$, as outlined in Section 4.3.1. Scenario 4 reduces to scenario 2 as $K_{i_1i_2} \to \infty$, $K_{i_2u} \to \infty$ and $K_{su} = 0$. And in that case, $Y = \sum_{n_1=1}^{N_1} \sum_{n_2=1}^{N_2} \rho_{si_1}^{n_1} \rho_{i_1i_2}^{n_1n_2} \rho_{i_2u}^{n_2}$ in (4.22)

simplifies to $Y = N_2 \sqrt{\beta_{i_1 i_2} \beta_{i_2 u}} \sum_{n_1=1}^{N_1} \rho_{si_1}$. Similarly, for the case when $K_{si_1} \to \infty$, $K_{i_1 i_2} \to \infty$ and $K_{su} = 0$, scenario 4 reduces to scenario 3 and Y simplifies to $N_1 \sqrt{\beta_{si_1} \beta_{i_1 i_2}} \sum_{n_2=1}^{N_2} \rho_{i_2 u}$. Furthermore, when I_1 is turned off and $K_{su} = 0$, scenario 4 reduces to the single IRS configuration described next.

4.3.5 Benchmark-Scenario 5: With Single IRS-Assisted WET When the Reflected Links $S - I$ and $I - U$ are Rician Faded and the Direct Channel $S - U$ is Rayleigh Faded

For benchmarking, we now consider the scenario where a single antenna source assisted by a single IRS consisting of N passive reflecting elements transfers energy to a single antenna user.[2] Given this scenario, we consider that the channels $S - I$ and $I - U$ are Rician faded, and the direct channel from S to U is Rayleigh faded. And the channel vector $\boldsymbol{h}_{si} \in C^{1\times N}$ between S and I is given by

$$\boldsymbol{h}_{si} = \sqrt{\frac{K_{si}}{K_{si}+1}} \overline{\boldsymbol{h}}_{si} + \sqrt{\frac{1}{K_{si}+1}} \widetilde{\boldsymbol{h}}_{si}, \tag{4.27}$$

where K_{si} denotes the Rician factor between S to IRS, $\overline{\boldsymbol{h}}_{si}$ denotes the LoS component and its n^{th} element is given by $\overline{h}^n_{si} = \sqrt{\beta_{si}} \exp\left(\frac{-j2\pi d^n_{si}}{\lambda}\right)$, β_{si} denotes the path loss and d^n_{si} denotes the distance between the source and the n^{th} element of IRS. Furthermore, $\widetilde{\boldsymbol{h}}_{si}$ denotes the corresponding non-LoS component and its n^{th} element is given by $\widetilde{h}^n_{si} \sim \mathcal{CN}(0, \beta_{si})$. Thus, $h^n_{si} \sim \mathcal{CN}\left(\mu^n_{si}, \zeta_{si}\right)$, where $\mu^n_{si} = \sqrt{\frac{K_{si}}{K_{si}+1}} \overline{h}^n_{si}$ and $\zeta_{si} = \frac{\beta_{si}}{K_{si}+1}$. The channel vector $\boldsymbol{h}_{iu} \in C^{N\times 1}$ between I and U can be expressed in a similar manner as in (4.27), just by replacing subscript 'si' with 'iu'.

The power of received signal at the user in this case equals

$$P'_u = p \left| h_{su} + \sum_{n=1}^{N} h^n_{si} \Lambda^{nn} h^n_{iu} \right|^2, \tag{4.28}$$

where $\boldsymbol{\Lambda} \in C^{N\times N}$ is the diagonal matrix that models the phase shift configuration at I. To maximize the power of the received signal in (4.28), the n^{th} diagonal entry of $\boldsymbol{\Lambda}$ should be programmed as follows:

$$\Lambda^{nn} = \left(\frac{h^n_{si} h^n_{iu}}{\left|h^n_{si}\right| \left|h^n_{iu}\right|} \right)^* \frac{h_{su}}{|h_{su}|}, \text{ for all } n = 1, \ldots, N. \tag{4.29}$$

[2]For benchmarking against single IRS enabled WET, we consider that I_1 is turned off and only I_2 assists WET from the single antenna source to the user.

Upon substitution of Λ^{nn} from (4.29), we obtain the power of the received signal as

$$P'_u = p\left(\rho_{su} + \sum_{n=1}^{N} \rho^n_{si}\rho^n_{iu}\right)^2, \tag{4.30}$$

where $\rho^n_{si} = \left|h^n_{si}\right|$ and $\rho^n_{iu} = \left|h^n_{iu}\right|$.

Theorem 4.3. *Under non-linear EH at the user, the OP for single IRS-assisted WET is given by*

$$P_{out} = 1 - \psi_3 Q\left(\frac{\overline{P}_{th} - \mu_3}{\sigma_3}\right) - \frac{\psi_3 e^{\frac{\xi_3^2 - \eta_3\chi_3}{2\eta_3}}}{\sqrt{\eta_3\sigma_3^2}}\left(Q\left(\frac{-\xi_3}{\sqrt{\eta_3}}\right) - Q\left(\frac{\overline{P}_{th} - \mu_3}{\sigma_3^2\sqrt{\eta_3}}\right)\right), \tag{4.31}$$

where ψ_3, η_3, ξ_3 and χ_3 are obtained respectively, from ψ_1, η_1, ξ_1 and χ_1 in (4.13)*, just by replacing μ_1 with μ_3 and σ_1 with σ_3, $\mu_3 = \frac{N\pi}{4}\sqrt{\zeta_{si}\zeta_{iu}}L_{\frac{1}{2}}(-K_{si})\,L_{\frac{1}{2}}(-K_{iu})$,*
$\sigma_3^2 = N\left(\zeta_{si}\zeta_{iu}(1+K_{si})(1+K_{iu}) - \nu_3^2\right)$, $\nu_3 = \frac{\pi}{4}\sqrt{\zeta_{si}\zeta_{iu}}L_{\frac{1}{2}}(-K_{si})\,L_{\frac{1}{2}}(-K_{iu})$.

Proof. The proof follows similar steps as given in Appendix C.2 for Theorem 4.2. □

Remark: When the direct path between source and user is absent, (4.31) simplifies to

$$P_{\text{out}} = 1 - \psi_3 Q\left(\frac{\overline{P}_{\text{th}} - \mu_3}{\sigma_3}\right). \tag{4.32}$$

4.3.6 Benchmark-Scenario 6: When the Source is Equipped with Massive Number of Antennas

For benchmarking, we now consider a scenario where the source equipped with M co-located antennas transfers energy wirelessly to the user, *and there is no IRS that assists WET from the source*.[3] We consider that the channel $\boldsymbol{h}_{su} \in C^{M\times 1}$ between source and user is Rayleigh faded. Thus, $\boldsymbol{h}_{su} \sim C\mathcal{N}(0, \beta_{su}\boldsymbol{I}_M)$. And, the received power in this scenario is given by

$$P^m_u = p\|\boldsymbol{h}_{su}\|^2. \tag{4.33}$$

Theorem 4.4. *Under non-linear EH at the user, the OP from a source with massive number of antennas is given by*

$$P_{out} = \frac{1}{(M-1)!}\gamma\left(M, \frac{P'_{th}}{\beta_{su}p}\right), \tag{4.34}$$

where P'_{th} is given in Theorem 4.1.

Proof. The proof is given in Appendix C.5. □

[3]For benchmarking against massive MIMO enabled WET, we essentially consider a source with massive number of antennas in place of a single-antenna source in Figure 4.1 and the two IRSs are treated as absent.

Remark: If the parameter $\frac{P'_{\text{th}}}{\beta_{su}p} > 1$ in (4.34), then lower incomplete gamma function increases as M increases. However, as M increases, the rate of decrease due to the factor $\frac{1}{(M-1)!}$ dominates over the rate at which $\gamma(\cdot,\cdot)$ increases with M. Therefore, OP decreases as M increases at the source.

4.3.7 Asymptotic Analysis

To obtain the same OP for a given transmit power and given locations of S and U, the harvested power at the user should be the same for all the configurations. Upon observing (4.8), we infer that to obtain the same harvested power, the received power at the user should be the same for all the configurations. Since the received power is a RV, therefore, we do asymptotic analysis to obtain the relation. In the asymptotic regime, as $M \to \infty$, $\|\boldsymbol{h}_{su}\|^2/M \to \beta_{su}$. And, therefore, the receive power P_u^m in this scenario where the source is equipped with M antennas scales as $Mp\beta_{su}$.

We consider scenario 1 of the double IRS-assisted configuration to gain insights about the number of IRS elements required to obtain the same OP as massive MIMO. The received power corresponding to this scenario is given by

$$P_u = p\left(\rho_{su} + \frac{N_d^2}{4}\sqrt{\beta_{si_1}\beta_{i_1i_2}\beta_{i_2u}}\right)^2, \tag{4.35}$$

where we have set $N_1 = N_2 = \frac{N_d}{2}$, since this choice minimizes the OP.[4] In the asymptotic regime, as $N_d \to \infty$, $\frac{1}{N_d^4}\left(\rho_{su} + \frac{N_d^2}{4}\sqrt{\beta_{si_1}\beta_{i_1i_2}\beta_{i_2u}}\right)^2 \to \frac{\beta_{si_1}\beta_{i_1i_2}\beta_{i_2u}}{16}$. And, therefore, the received power in this scenario scales as $\frac{N_d^4 p\beta_{si_1}\beta_{i_1i_2}\beta_{i_2u}}{16}$.

Similarly, we consider scenario 4 related to single IRS-assisted WET to gain insights about the number of IRS elements required to obtain the same OP as massive MIMO. The received power corresponding to this scenario is given by

$$P'_u = p\left(\rho_{su} + \sum_{n=1}^{N_s}\rho_{si}^n\rho_{iu}^n\right)^2. \tag{4.36}$$

[4]To maintain clarity, we let N_d denote the number of elements in double IRS configuration and N_s to denote the number of elements in single IRS configuration in the discussion in this section.

In the asymptotic regime as $N_s \to \infty$,

$$\frac{1}{N_s^2}\left(\rho_{su} + \sum_{n=1}^{N_s} \rho_{si}^n \rho_{iu}^n\right)^2 \to \left(\frac{\pi}{4}\sqrt{\zeta_{si}\zeta_{iu}} L_{\frac{1}{2}}\left(-K_{si}\right) L_{\frac{1}{2}}\left(-K_{iu}\right)\right)^2. \tag{4.37}$$

And, therefore, the received power in this scenario scales as

$$N_s^2 p\left(\frac{\pi}{4}\sqrt{\zeta_{si}\zeta_{iu}} L_{\frac{1}{2}}\left(-K_{si}\right) L_{\frac{1}{2}}\left(-K_{iu}\right)\right)^2. \tag{4.38}$$

Therefore, as M and N_d approach infinity,

$$\frac{P_u}{P_u^m} \to \frac{N_d^4 \beta_{si_1}\beta_{i_1 i_2}\beta_{i_2 u}}{16 M \beta_{su}}, \tag{4.39}$$

Based on this, we infer that as long as $\frac{N_d^4 \beta_{si_1}\beta_{i_1 i_2}\beta_{i_2 u}}{16 M \beta_{su}} < 1$, the performance of double IRS enabled WET will be inferior compared to massive MIMO enabled WET. In other words, in order to obtain receive power identical to scenario 6, where the source is equipped with massive number of antennas, the total number of elements that are required in double IRS configuration equals $N_d = \left(\frac{16 M \beta_{su}}{\beta_{si_1}\beta_{i_1 i_2}\beta_{i_2 u}}\right)^{\frac{1}{4}}$ so that it overcomes the effective path loss of the cascaded channel and begins to outperform massive MIMO. This is yet another novel and interesting design insight that we derive based on the asymptotic analysis.[5]

Similarly, as N_d and N_s approach infinity,

$$\frac{P_u}{P_u'} \to \frac{N_d^4 \beta_{si_1}\beta_{i_1 i_2}\beta_{i_2 u}}{16 N_s^2 \left(\frac{\pi}{4}\sqrt{\zeta_{si}\zeta_{iu}} L_{\frac{1}{2}}\left(-K_{si}\right) L_{\frac{1}{2}}\left(-K_{iu}\right)\right)^2}. \tag{4.40}$$

Based on this, we infer that as long as $\frac{N_d^4 \beta_{si_1}\beta_{i_1 i_2}\beta_{i_2 u}}{16 N_s^2 \left(\frac{\pi}{4}\sqrt{\zeta_{si}\zeta_{iu}} L_{\frac{1}{2}}\left(-K_{si}\right) L_{\frac{1}{2}}\left(-K_{iu}\right)\right)^2} < 1$, the performance of double IRS enabled WET will be inferior compared to single IRS enabled WET.

4.4 Extension to Four Communication Links

We also extend our study to a scenario where we consider that the signal reaches the user via four communication links, namely, $S - U$, $S - I_1 - I_2 - U$, $S - I_1 - U$ and $S - I_2 - U$ and is

[5]Note that we expect this trend to hold for any general channel fading scenario as well.

given by

$$y_u = \sqrt{p}(h_{su} + \boldsymbol{h}_{si_1}\boldsymbol{\Theta}\boldsymbol{H}_{i_1i_2}\boldsymbol{\Phi}\boldsymbol{h}_{i_2u} + \boldsymbol{h}_{si_1}\boldsymbol{\Theta}\boldsymbol{h}_{i_1u} + \boldsymbol{h}_{si_2}\boldsymbol{\Phi}\boldsymbol{h}_{i_2u})s_u + w_u, \tag{4.41}$$

where $\boldsymbol{h}_{i_1u} \in C^{N_1\times 1}$ denotes the channel between I_1 and U and $\boldsymbol{h}_{si_2} \in C^{1\times N_2}$ denotes the channel between S and I_2. Using (4.41), the received power at the user is given by

$$P_u = p\left|h_{su} + \boldsymbol{h}_{si_1}\boldsymbol{\Theta}\boldsymbol{H}_{i_1i_2}\boldsymbol{\Phi}\boldsymbol{h}_{i_2u} + \boldsymbol{h}_{si_1}\boldsymbol{\Theta}\boldsymbol{h}_{i_1u} + \boldsymbol{h}_{si_2}\boldsymbol{\Phi}\boldsymbol{h}_{i_2u}\right|^2. \tag{4.42}$$

The received power in (4.42), can be re-written as

$$P_u = p\left|h_{su} + \boldsymbol{h}_{si_1}\boldsymbol{\Theta}\boldsymbol{D}\boldsymbol{f}_2 + \boldsymbol{g}_{si_1u}\boldsymbol{f}_1 + \boldsymbol{g}_{si_2u}\boldsymbol{f}_2\right|^2, \tag{4.43}$$

$$= p\left|h_{su} + \sum_{n_2=1}^{N_2}\boldsymbol{h}_{si_1}\,\mathrm{diag}(\boldsymbol{d}^{n_2})\boldsymbol{f}_1 f_2^{n_2} + \boldsymbol{g}_{si_1u}\boldsymbol{f}_1 + \boldsymbol{g}_{si_2u}\boldsymbol{f}_2\right|^2, \tag{4.44}$$

$$= p\left|h_{su} + \sum_{n_2=1}^{N_2}\boldsymbol{q}^{n_2} f_2^{n_2}\boldsymbol{f}_1 + \boldsymbol{g}_{si_1u}\boldsymbol{f}_1 + \boldsymbol{g}_{si_2u}\boldsymbol{f}_2\right|^2, \tag{4.45}$$

where $\boldsymbol{D} = \boldsymbol{H}_{i_1i_2}\,\mathrm{diag}(\boldsymbol{h}_{i_2u}) = [\boldsymbol{d}^1, \ldots, \boldsymbol{d}^{N_2}]$, $\boldsymbol{f}_2 \in C^{N_2\times 1}$ comprises of the N_2 diagonal elements of $\boldsymbol{\Phi}$, $\boldsymbol{g}_{si_1u} = \boldsymbol{h}_{si_1}\,\mathrm{diag}(\boldsymbol{h}_{i_1u})$, $\boldsymbol{g}_{si_2u} = \boldsymbol{h}_{si_2}\,\mathrm{diag}(\boldsymbol{h}_{i_2u})$, $\boldsymbol{f}_1 \in C^{N_1\times 1}$ comprises of the N_1 diagonal elements of $\boldsymbol{\Theta}$, $\boldsymbol{q}^{n_2} = \boldsymbol{h}_{si_1}\,\mathrm{diag}(\boldsymbol{d}^{n_2})$ and $f_2^{n_2}$ denotes the n_2^{th} element of $\boldsymbol{f}_2$. Now, the objective is to design the two phase shift vectors: $\boldsymbol{f}_1$ at I_1 and $\boldsymbol{f}_2$ at I_2 such that the power of the signal received at the user via the four communication links is maximized. Mathematically, the optimization problem can be stated as follows:[6]

$$\begin{aligned}(\text{P1}): \quad &\max_{\boldsymbol{f}_1,\boldsymbol{f}_2}\left|h_{su} + \left(\sum_{n_2=1}^{N_2}\boldsymbol{q}^{n_2} f_2^{n_2} + \boldsymbol{g}_{si_1u}\right)\boldsymbol{f}_1 + \boldsymbol{g}_{si_2u}\boldsymbol{f}_2\right|^2 \\ &\text{subject to } |f_1^{n_1}| = 1, \ \forall n_1 = 1, \ldots, N_1, \\ &\qquad\qquad |f_2^{n_2}| = 1, \ \forall n_2 = 1, \ldots, N_2,\end{aligned} \tag{4.46}$$

where $f_1^{n_1}$ denotes the n_1^{th} element of $\boldsymbol{f}_1$. Obtaining optimal solution of the problem (P1) is difficult due to non-convex unit-modulus constraints on $f_1^{n_1}$ and $f_2^{n_2}$, and also due to coupling between $\boldsymbol{f}_1$ and $\boldsymbol{f}_2$. It is for this reason that standard convex optimization algorithms cannot be employed to solve (P1). Therefore, to obtain $\boldsymbol{f}_1$ and $\boldsymbol{f}_2$ and solve (P1), we first develop

[6]Since the transmit signal power p does not affect the maximization, it is dropped.

an algorithm based on MO technique, where the phase shift vectors $\boldsymbol{f}_1$ and $\boldsymbol{f}_2$ are optimized simultaneously and that relies on computing the Euclidean gradient of the objective function in (P1) at $\boldsymbol{f}_1$ and $\boldsymbol{f}_2$ in order to determine the updated phase shift vectors every iteration. We then also develop another algorithm where we apply AO to solve (P1) and in which the objective function is optimized alternately over one variable keeping the other fixed until convergence.

1) *MO Based Phase Shift Design:* We note that the unit modulus constraints in (P1) above form complex circle manifolds $\mathcal{M}_1 = \{\boldsymbol{f}_1 \in C^{N_1} : |f_1^{n_1}| = \cdots = |f_1^{N_1}| = 1\}$ and $\mathcal{M}_2 = \{\boldsymbol{f}_2 \in C^{N_2} : |f_2^{n_2}| = \cdots = |f_2^{N_2}| = 1\}$ of dimensions N_1 and N_2, respectively. We now define the set $\mathcal{M}$ referred to as the product of the manifolds as $\mathcal{M} = \mathcal{M}_1 \times \mathcal{M}_2$. This set denotes the set of pairs $(\boldsymbol{f}_1, \boldsymbol{f}_2)$, where $\boldsymbol{f}_1 \in \mathcal{M}_1$ and $\boldsymbol{f}_2 \in \mathcal{M}_2$. This algorithm based on MO technique[7] can therefore be used to iteratively optimize $(\boldsymbol{f}_1, \boldsymbol{f}_2)$ over the product manifold search space $\mathcal{M}$ such that the objective function is non-increasing with iteration. And the algorithm converges when the Riemannian gradient of the objective function is zero [89, 90]. Since, the unit modulus constraints form search space over the set $\mathcal{M}$ of the product of the manifolds, we can re-write the optimization problem (P1) as

$$(\text{P2}): \min_{(\boldsymbol{f}_1,\boldsymbol{f}_2)\in\mathcal{M}} g(\boldsymbol{f}_1, \boldsymbol{f}_2) = -\left|h_{su} + \left(\sum_{n_2=1}^{N_2} \boldsymbol{q}^{n_2} f_2^{n_2} + \boldsymbol{g}_{si_1u}\right)\boldsymbol{f}_1 + \boldsymbol{g}_{si_2u}\boldsymbol{f}_2\right|^2. \tag{4.47}$$

To develop an algorithm based on MO technique in order to solve (P2) and reach to a locally optimal solution for $\boldsymbol{f}_1$ and $\boldsymbol{f}_2$, we describe the concept of the tangent space corresponding to the product of the manifolds $\mathcal{M}$ at point $(\boldsymbol{f}_1, \boldsymbol{f}_2)$. For the point $\boldsymbol{f}_i \in \mathcal{M}_i$, for $i \in \{1, 2\}$, the tangent space consists of all vectors $\boldsymbol{w}_i$ that pass tangentially through the point $\boldsymbol{f}_i$ [82]. The tangent space $\mathcal{T}_{(\boldsymbol{f}_1,\boldsymbol{f}_2)}\mathcal{M}$ corresponding to the set of product of manifolds $\mathcal{M}$ can be written as $\mathcal{T}_{(\boldsymbol{f}_1,\boldsymbol{f}_2)}\mathcal{M} = \mathcal{T}_{\boldsymbol{f}_1}\mathcal{M}_1 \times \mathcal{T}_{\boldsymbol{f}_2}\mathcal{M}_2$, where $\mathcal{T}_{\boldsymbol{f}_1}\mathcal{M}_1$ denotes the tangent space at $\boldsymbol{f}_1$ and is given by $\mathcal{T}_{\boldsymbol{f}_1}\mathcal{M}_1 = \{\boldsymbol{w}_1 \in C^{N_1} : \Re\{\boldsymbol{w}_1 \odot \boldsymbol{f}_1^*\} = 0\}$, $\mathcal{T}_{\boldsymbol{f}_2}\mathcal{M}_2$ denotes the tangent space at $\boldsymbol{f}_2$ and is given by $\mathcal{T}_{\boldsymbol{f}_2}\mathcal{M}_2 = \{\boldsymbol{w}_2 \in C^{N_2} : \Re\{\boldsymbol{w}_2 \odot \boldsymbol{f}_2^*\} = 0\}$ [90].

We next describe the Riemannian gradient, which is one of the key components of the algorithm. Similar to Euclidean space, it refers to that tangent vector or direction in which the

[7]This optimization over a manifold is similar to optimization over the Euclidean space [89].

objective function in (P2) suffers the steepest descent [89]. And for $i \in \{1,2\}$, the Riemannian gradient $\text{grad}_{f_i} g$ at $\boldsymbol{f}_i$ is the orthogonal projection of the Euclidean gradient $\text{Grad}_{f_i} g$ onto tangent space $\mathcal{T}_{f_i}\mathcal{M}_i$. Therefore, for the l^{th} iteration, the Riemannian gradient of the objective function $g(\boldsymbol{f}_{1,l}, \boldsymbol{f}_{2,l})$ at $\boldsymbol{f}_{i,l}$ is given by [90]

$$\text{grad}_{f_{i,l}} g = \text{Grad}_{f_{i,l}} g - \Re\{\text{Grad}_{f_{i,l}} g \odot \boldsymbol{f}_{i,l}^*\} \odot \boldsymbol{f}_{i,l}, \text{ for all } i \in \{1,2\}, \tag{4.48}$$

where for the objective function in (P2), we derive and simplify the Euclidean gradient at $\boldsymbol{f}_{1,l}$ and $\boldsymbol{f}_{2,l}$, respectively, to obtain

$$\text{Grad}_{f_{1,l}} g = -2\left(h_{su}\boldsymbol{b}^H + \boldsymbol{b}^H \boldsymbol{g}_{si_2u} \boldsymbol{f}_{2,l} + \boldsymbol{b}^H \boldsymbol{b} \boldsymbol{f}_{1,l}\right), \tag{4.49}$$

where $\boldsymbol{b} = \left(\sum_{n_2=1}^{N_2} \boldsymbol{q}^{n_2} f_{2,l}^{n_2} + \boldsymbol{g}_{si_1u}\right)$ and

$$\text{Grad}_{f_{2,l}} g = -2\left(h_{su}\boldsymbol{c}^H + \boldsymbol{c}^H \boldsymbol{g}_{si_1u} \boldsymbol{f}_{1,l} + \boldsymbol{c}^H \boldsymbol{c} \boldsymbol{f}_{2,l}\right), \tag{4.50}$$

where $\boldsymbol{c} = \overline{\boldsymbol{q}} + \boldsymbol{g}_{si_2u}$.

Based on the Riemannian gradient, the search directions, $\boldsymbol{e}_{1,l}$ and $\boldsymbol{e}_{2,l}$ at $\boldsymbol{f}_{1,l}$ and $\boldsymbol{f}_{2,l}$, respectively can be obtained as

$$\boldsymbol{e}_{i,l} = -\text{grad}_{f_{i,l}} g + \epsilon_{i,l} \mathcal{T}_{f_{i,l-1} \to f_{i,l}}(\boldsymbol{e}_{i,l-1}), \text{ for all } i \in \{1,2\}, \tag{4.51}$$

where $\epsilon_{i,l}$ denotes the Polak-Ribiere parameter given by $\epsilon_{i,l} = \frac{\langle \text{grad}_{f_{i,l}} g, \text{grad}_{f_{i,l}} g - \text{grad}_{f_{i,l-1}} g \rangle}{\langle \text{grad}_{f_{i,l-1}} g, \text{grad}_{f_{i,l-1}} g \rangle}$, and $\mathcal{T}_{f_{i,l-1} \to f_{i,l}}(\boldsymbol{e}_{i,l-1})$ denotes the vector transport for manifold $\mathcal{M}_i$ and is given by $\mathcal{T}_{f_{i,l-1} \to f_{i,l}}(\boldsymbol{e}_{i,l-1}) = \boldsymbol{e}_{i,l-1} - \Re\{\boldsymbol{e}_{i,l-1} \odot \boldsymbol{f}_{i,l}^*\} \odot \boldsymbol{f}_{i,l}$. Since, in MO, $\boldsymbol{e}_{i,l}$ and $\boldsymbol{e}_{i,l-1}$ lie in two different tangent spaces, therefore, vector transport is required to map a vector from one tangent space to the other. Once the search directions $\boldsymbol{e}_{i,l}$, for $i \in \{1,2\}$ are obtained, the phase shift vectors $\boldsymbol{f}_{i,l+1}$ for $i \in \{1,2\}$ are updated as

$$\boldsymbol{f}_{i,l+1} = \boldsymbol{f}_{i,l} + \alpha_0 \boldsymbol{e}_{i,l}, \text{ for all } i \in \{1,2\}, \tag{4.52}$$

where α_0 denotes the step size which can be obtained using backtracking line search algorithm [90]. We note that the updated phase shift vectors may not satisfy the unit modulus constraint. Therefore, a retraction operation may be required every iteration of backtracking

Algorithm 1 MO based algorithm to solve (P2)

Input: $\overline{\epsilon} > 0$, $\boldsymbol{h}_{su}$, $\boldsymbol{g}_{si_1u}$, $\boldsymbol{g}_{si_2u}$ and $\boldsymbol{q}^{n_2}$, $\forall n_2 = 1, \ldots, N_2$, and initialize $\boldsymbol{f}_{1,0}$,$\boldsymbol{f}_{2,0}$.
1. Set $l = 0$, $\epsilon_{i,0} = 0$ and $\boldsymbol{e}_{i,0} = -\text{grad}_{\boldsymbol{f}_{i,0}} g$, where $\text{grad}_{\boldsymbol{f}_{i,0}} g$ for $i \in \{1, 2\}$ is computed based on (4.48).
repeat
2. Choose α_0 based on backtracking line search [90].
3. Set $\boldsymbol{f}_{i,l+1} = \mathcal{R}\left(\boldsymbol{f}_{i,l} + \alpha_0 \boldsymbol{e}_{i,l}\right)$ for $i \in \{1, 2\}$, where $\mathcal{R}(\cdot)$ denotes retraction.
4. For $i \in \{1, 2\}$, compute $\text{grad}_{\boldsymbol{f}_{i,l+1}} g$ based on (4.48), (4.49) and (4.50) for given $\boldsymbol{f}_{i,l+1}$.
5. For $i \in \{1, 2\}$, obtain vector transport $\mathcal{T}_{\boldsymbol{f}_{i,l} \to \boldsymbol{f}_{i,l+1}}$ and then obtain $\epsilon_{i,l+1}$.
6. Update search direction $\boldsymbol{e}_{i,l+1}$ for $i \in \{1, 2\}$ based on (4.51).
7. Set $l = l + 1$.
until $\left\| \left[\text{grad}_{\boldsymbol{f}_{1,l}} g^T, \text{grad}_{\boldsymbol{f}_{2,l}} g^T \right]^T \right\| \leq \overline{\epsilon}$.
Output: $\boldsymbol{f}_1$ and $\boldsymbol{f}_2$.

line search algorithm to ensure that the absolute value of each entry of $\boldsymbol{f}_{i,l+1}$ for $i \in \{1, 2\}$ is unity. We observe that the computation of the Euclidean gradient of the objective function at $\boldsymbol{f}_{1,l}$ and $\boldsymbol{f}_{2,l}$ that we derive in closed-form in (4.49) and (4.50) is the most expensive step in this algorithm and its complexity scales as $O\left(N_1^2 + N_2^2\right)$. We summarize the key steps in Algorithm 1 at the top of this page.

2) *AO Based Phase Shift Design:* Based on triangle inequality, the objective function in (P1) can be upper bounded as

$$\left| h_{su} + \left(\sum_{n_2=1}^{N_2} \boldsymbol{q}^{n_2} f_2^{n_2} + \boldsymbol{g}_{si_1u} \right) \boldsymbol{f}_1 + \boldsymbol{g}_{si_2u} \boldsymbol{f}_2 \right| \leq \left| \left(\sum_{n_2=1}^{N_2} \boldsymbol{q}^{n_2} f_2^{n_2} + \boldsymbol{g}_{si_1u} \right) \boldsymbol{f}_1 \right| + \left| h_{su} + \boldsymbol{g}_{si_2u} \boldsymbol{f}_2 \right|. \quad (4.53)$$

We note that if equality holds in (4.53), then it maximizes the objective function in (P1). And equality in (4.53) is achieved if and only if $\angle(\boldsymbol{b} \boldsymbol{f}_1) = \angle\left(h_{su} + \boldsymbol{g}_{si_2u} \boldsymbol{f}_2\right)$, where $\boldsymbol{b} = \left(\sum_{n_2=1}^{N_2} \boldsymbol{q}^{n_2} f_2^{n_2} + \boldsymbol{g}_{si_1u} \right)$. Therefore, for a given $\boldsymbol{f}_2$, the optimization problem (P1) can be re-formulated as

$$\begin{aligned} (\text{P2}): \quad & \max_{\boldsymbol{f}_1} \left| \left(\sum_{n_2=1}^{N_2} \boldsymbol{q}^{n_2} f_2^{n_2} + \boldsymbol{g}_{si_1u} \right) \boldsymbol{f}_1 \right|^2 \\ & \text{subject to } |f_1^{n_1}| = 1, \text{ for all } n_1 = 1, \ldots, N_1, \\ & \angle(\boldsymbol{b} \boldsymbol{f}_1) = \angle\left(h_{su} + \boldsymbol{g}_{si_2u} \boldsymbol{f}_2\right). \end{aligned} \quad (4.54)$$

Based on the constraint $\angle(\boldsymbol{b} \boldsymbol{f}_1) = \angle\left(h_{su} + \boldsymbol{g}_{si_2u} \boldsymbol{f}_2\right)$ in (P2), we obtain $\boldsymbol{f}_1$ in closed-form as

$$\boldsymbol{f}_1 = \exp\left(j \left(\angle\left(h_{su} + \boldsymbol{g}_{si_2u} \boldsymbol{f}_2\right) - \angle\left(\boldsymbol{b}^T\right) \right) \right). \quad (4.55)$$

Algorithm 2 AO based algorithm to solve (P1)

Input: $p, \boldsymbol{h}_{su}, \boldsymbol{g}_{si_1u}, \boldsymbol{g}_{si_2u}$ and $\boldsymbol{q}^{n_2}, \forall n_2 = 1, \ldots, N_2,$ and initialize $\boldsymbol{f}_2$.

1. Update $\boldsymbol{f}_1$, using (4.55), for given $\boldsymbol{f}_2$.
2. Update $\boldsymbol{f}_2$ using (4.57), for given $\boldsymbol{f}_1$.
3. Stop if increment in received power in (4.45) is below a threshold ϵ_0, where ϵ_0 is very small positive value. Else go to step 1.
4. Store $\boldsymbol{f}_1$ and $\boldsymbol{f}_2$.

Output: $\boldsymbol{f}_1$ and $\boldsymbol{f}_2$.

Again, to optimize $\boldsymbol{f}_2$ for a given $\boldsymbol{f}_1$, we re-write the objective function in (P1) as

$$\left| h_{su} + \left(\sum_{n_2=1}^{N_2} \boldsymbol{q}^{n_2} f_2^{n_2} + \boldsymbol{g}_{si_1u} \right) \boldsymbol{f}_1 + \boldsymbol{g}_{si_2u} \boldsymbol{f}_2 \right|^2 = \left| h_{su} + \left(\overline{\boldsymbol{q}} + \boldsymbol{g}_{si_2u} \right) \boldsymbol{f}_2 + \boldsymbol{g}_{si_1u} \boldsymbol{f}_1 \right|^2, \tag{4.56}$$

where $\overline{\boldsymbol{q}} = \left[\boldsymbol{q}^1 \boldsymbol{f}_1, \ldots, \boldsymbol{q}^{N_2} \boldsymbol{f}_1 \right]$. Using steps similar to (4.53), (4.54) and (4.55), we obtain

$$\boldsymbol{f}_2 = \exp\left(j \left(\angle\left(h_{su} + \boldsymbol{g}_{si_1u} \boldsymbol{f}_1 \right) - \angle\left(\overline{\boldsymbol{q}} + \boldsymbol{g}_{si_2u} \right)^T \right) \right). \tag{4.57}$$

The AO based algorithm to solve (P1) to maximize the received power in the presence of direct path between the source and the user is summarized in Algorithm 2 shown at the top of the next page. We find that it is possible to express the phase shift vectors $\boldsymbol{f}_1$ at I_1 and $\boldsymbol{f}_2$ at I_2 in closed-form as stated above in (4.55) and (4.57), respectively. Therefore, AO based technique whose complexity scales as $O(L(N_1 + N_2))$ with L representing number of iterations is an appealing technique to obtain $\boldsymbol{f}_1$ and $\boldsymbol{f}_2$ [60, 91].

Using MO based algorithm as stated in Algorithm 1 and AO based algorithm as stated in Algorithm 2, we obtain the two phase shift matrices $\boldsymbol{\Theta} = \text{diag}(\boldsymbol{f}_1)$ at I_1 and $\boldsymbol{\Phi} = \text{diag}(\boldsymbol{f}_2)$ at I_2 and substitute these in (4.42) in order to obtain the received power. Using this P_u and the non-linear EH model at the user described in (4.8), we numerically obtain OP.[8]

4.5 Analysis of PTE

As discussed in Chapter 3, the PTE is defined as the ratio of average power harvested at the user to the total power consumed. We analyze the PTE for double IRS-assisted WET,

[8]Since the problem in (P1) is non-convex, it is not possible to obtain optimal solution for the phase shift matrices. Thus, the locally optimal solution obtained may not really guarantee exact coherent addition of signal received at the user via the four communication links. This makes the outage analysis with four communication links mathematically intractable.

single IRS-assisted WET and massive MIMO enabled WET configurations to identify the most power transfer efficient configuration among the three. To ensure analytical tractability and gain insights into PTE, we consider pure LoS channels between any pair of nodes (source/IRS/user). As before, we model the total power consumed at the source as $P_{\mathrm{c}} = p_{\mathrm{tx}} + p_{\mathrm{fix}} + M\left(p_{\mathrm{s}} + p_{\mathrm{lp}}\right) + Np_{\mathrm{e}}$ [71, 73], where $p_{\mathrm{tx}} = \frac{p}{\eta_{\mathrm{pa}}}$, p denotes the power with which source transmits, η_{pa} denotes the power amplifier efficiency, p_{fix} represents the fixed power that is required to run the source, p_{s} denotes the power consumption in the circuit of each RF chain at the source, $p_{\mathrm{lp}} = \frac{3KB}{S_c k_{\mathrm{s}}}$ denotes the total power spent in linear processing at the source, B denotes the bandwidth of the system, $S_c = B_c\tau_c$ denotes the number of samples in every coherence block, B_c denotes the coherence bandwidth, M denotes number of antennas at the source, K denotes the number of users, k_{s} denotes computational efficiency of the source (in flops/W) and p_{e} denotes the power required to program the phase shift of every IRS element.

4.5.1 For Double IRS-Assisted WET

In this scenario, the direct channel between S and U is given by $h_{su} = \sqrt{\beta_{su}}\exp\left(\frac{-j2\pi d_{su}}{\lambda}\right)$, where d_{su} denotes the distance between S and U. The channel model of the reflected link in this scenario is described in Section 4.3.1.

Based on (4.7), the average received power at the user equals

$$p_1^u = p\left(\sqrt{\beta_{su}} + \frac{N^2}{4}\sqrt{\beta_{si_1}\beta_{i_1i_2}\beta_{i_2u}}\right)^2. \tag{4.58}$$

The harvested power corresponding to received power in (4.58) is given by

$$p_1^h = \frac{P_0}{\left(1 + \exp(-a_0(p_1^u - b_0))\right)(1 - \Omega)} - \frac{P_0\Omega}{1 - \Omega}. \tag{4.59}$$

Using (4.59) and the power consumption model discussed above, we define PTE mathematically as

$$\mathrm{PTE}_1^u \triangleq \frac{p_1^h}{p_{\mathrm{tx}} + p_{\mathrm{fix}} + p_{\mathrm{s}} + p_{\mathrm{lp}} + Np_e}. \tag{4.60}$$

The expression in (4.60) provide an interesting insight that for a fixed source transmit power, PTE decreases with an increase in number of IRS elements when the EH circuit enters into

saturation region of operation. This is because when the EH circuit operates in saturation, the harvested power does not increase with an increase in the number of IRS elements, however, power consumption increases linearly with N.

Theorem 4.5. *The optimal number of IRS elements N_{opt} which minimizes the average power consumption for a given received power for double IRS assisted WET can be obtained numerically by solving the following sixth degree polynomial equation in N*

$$\eta_{pa}^{bs} p_e \left(N^6 \sqrt{\beta_{si_1}^3 \beta_{i_1 i_2}^3 \beta_{i_2 u}^3} + 64 \sqrt{\beta_{su}^3} + 12N^4 \sqrt{\beta_{su}} \beta_{si_1} \beta_{i_1 i_2} \beta_{i_2 u} + 48N^2 \beta_{su} \sqrt{\beta_{si_1} \beta_{i_1 i_2} \beta_{i_2 u}} \right) - 64N p_1^u \sqrt{\beta_{si_1} \beta_{i_1 i_2} \beta_{i_2 u}} = 0, \quad (4.61)$$

Proof. The proof is given in Appendix C.6. □

Since the polynomial equation in (4.61) is of sixth degree, therefore, we evaluate its roots numerically. And from these roots, we can choose the valid root, i.e., the optimal number of IRS elements which minimizes the average power consumption. For a given received power, $N_1 = N_2 = \frac{N_{\text{opt}}}{2}$ maximizes PTE in double IRS enabled WET.

4.5.2 For Single IRS-Assisted WET

The channel model for this scenario is similar to LoS component defined in Section 4.3.5. Based on (4.30), the average received power at the user for this scenario is given by

$$p_2^u = p \left(\sqrt{\beta_{su}} + N \sqrt{\beta_{si} \beta_{iu}} \right). \quad (4.62)$$

Based on (4.62) and using steps similar to (4.59) and (4.60), we obtain PTE for this scenario.

Theorem 4.6. *The optimal number of IRS elements N_{opt} which minimizes the total average power consumption for the given received power for single IRS-assisted WET is given by*

$$N_{opt} = \sqrt[3]{\frac{2p_2^u}{\eta_{pa}^{bs} p_e \beta_{si} \beta_{iu}}} - \sqrt{\frac{\beta_{su}}{\beta_{si} \beta_{iu}}}. \quad (4.63)$$

Proof. The proof is given in C.7. □

The N_{opt} in (4.63) is usually not an integer, hence we consider the closest integer value as the optimal N. For a given received power, N_{opt} maximizes PTE in this case.

4.5.3 For Massive MIMO Enabled WET

In this scenario, the m^{th} element of the LoS channel $\boldsymbol{h}_{su}$ is given by $h_{su}^m = \sqrt{\beta_{su}} \exp\left(\frac{-j2\pi d_{su}^m}{\lambda}\right)$, where d_{su}^m denotes the distance between the m^{th} antenna at S and U. Based on (4.33), the average received power at the user for this scenario equals

$$p_3^u = p\|\boldsymbol{h}_{su}\|^2 = pM\beta_{su}. \tag{4.64}$$

Using steps similar to the previous section, we can obtain the harvested power and the PTE for this scenario based on (4.64).

Theorem 4.7. *The optimal number of antennas M_{opt} at the source which minimizes the average power consumption for a given received power with massive MIMO configuration is given by*

$$M_{opt} = \sqrt{\frac{p_3^u}{\eta_{pd}^{bs}\beta_{su}(p_s + p_{lp})}}. \tag{4.65}$$

Proof. The proof is given in Appendix C.8. □

For a given received power, M_{opt} denotes the number of antennas at the source that maximizes the PTE.

4.6 Numerical Results

We now present results to understand the performance of double IRS-assisted WET in terms of OP and PTE and to elucidate the interplay among several system parameters such as number of IRS elements, source transmit power, λ_0 and the target received power at the user. We also benchmark these results against single IRS and massive MIMO enabled WET. For fair comparison with the single IRS, I_1 is turned off, and I_2 is denoted by I. The default values of system parameters that we choose for illustration is given in Table 4.1.

Figure 4.3 plots $1 - P_{\text{out}}$ as a function of λ_0. We observe that initially, $1 - P_{\text{out}}$ increases as λ_0 increases and reaches its maximum at $\lambda_0 = 0.5$ and later it decreases as λ_0 increases for scenarios 1, 2 and 3, and for scenarios 2 and 3 with direct channel absent. This is consistent with the remark below Theorem 4.1 that at $\lambda_0 = 0.5$, i.e., $N_1 = N_2 = \frac{N}{2}$, the OP is minimized. We also observe that $1 - P_{\text{out}}$ for scenario 1 is the highest, followed by scenario 2 and scenario

Table 4.1: System Parameters.

Parameter	value
p	1 W
E_{th}	10^{-8} J
P_0, a_0, b_0	299.5 μW, 1.953×10^{-3}, -3.571×10^{3}
β_{su}	$G_s + G_u - 35.1 - 36.7 \log_{10}(d_{su})$ dB, d_{su} in meters
β_{ab}	$G_a + G_b - 37.5 - 22 \log_{10}(d_{ab})$ dB, $a, b \in \{s, i_1, i_2, u\}$, d_{ab} in meters [92, Table B.1.2.1-1]
$G_s = G_{i_1} = G_{i_2}$	5 dB
G_u	0 dB
B	1 MHz
τ_c	10 ms
k_s	20×10^{9} flops/W
K	1
r	$\frac{c}{2f}$
f, c	2.4 GHz, 3×10^{8} m/s
Coordinates (in meters) of S, I_1, I_2, U	$(1,1,0)$, $(0,0,0)$, $(0,50,0)$, $(1,45,0)$
$\boldsymbol{k}_1^a, \boldsymbol{k}_1^b, \boldsymbol{k}_2^a, \boldsymbol{k}_2^b$	$[0,0,1]$, $[\frac{\sqrt{3}}{2}, \frac{-1}{2}, 0]$, $[\frac{\sqrt{3}}{2}, \frac{1}{2}, 0]$, $[0,0,1]$ [80]
$K_{si_1}, K_{i_2u}, K_{si}, K_{iu}$	10, 5, 5, 10

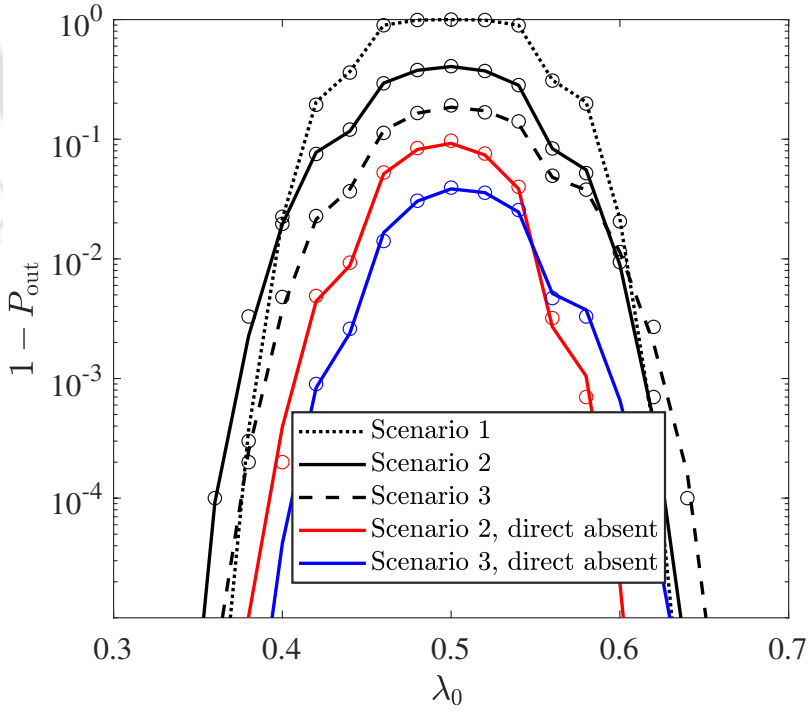

Fig. 4.3: Impact of λ_0: ($p = 1$ W, $N = 300$ $E_{\text{th}} = 1.245 \times 10^{-8}$ J, $a_0 = 1.953 \times 10^{-3}$, $b_0 = -3.571 \times 10^{3}$, and $P_0 = 299.5$ μW). Corresponding Monte Carlo simulations are shown through the marker $\circ$.

3 at $\lambda_0 = 0.5$. This is because user harvests the highest energy in scenario 1 due to dominance of LoS components. The corresponding Monte Carlo simulation results shown through the marker '$\circ$' are in close agreement with the analysis, thus validating our analysis. Since, $\lambda_0 = \frac{1}{2}$ minimizes outage, for the next set of plots we set $N_1 = N_2 = \frac{N}{2}$.

Figure 4.4 plots the OP as a function of N. We observe that OP decreases as N increases. We also observe that OP is the lowest in scenario 1, followed by scenarios 2, 3 and 4 for double IRS enabled WET. This is because the energy harvested by the user under scenario 1 is the highest due to the presence of pure LoS channels along the reflected paths, followed by scenarios 2, 3 and 4. Also, the outage performance under scenario 2 having Rician factor $K_{si_1} = 10$ is better than that of scenario 3 with Rician factor $K_{i_2u} = 5$, since scenario 2 has a relatively stronger LoS component. And outage performance with scenario 4 for double IRS enabled WET is the lowest since each link follows Rician fading. Furthermore, we observe that the OP obtained through Monte Carlo simulations based on exact P_u in (4.3) and where phases at the two IRSs are programmed based on (4.5) and (4.6) matches reasonably well with the approximate OP expression derived in Theorem 4.2 when each link follows Rician fading, thus validating the tightness of our approximation and the novel statistical modeling of Y based on Gamma distribution. We also compare the performance of the double IRS-assisted WET with scenario 5 related to single IRS-assisted WET. The system with single IRS performs poorer than all four scenarios of the double IRS system since received energy with the double IRS system scales roughly as $\left(N^4\right)$ and for single IRS, it scales roughly as $\left(N^2\right)$ as discussed in Section 4.3.7. Furthermore, we observe that to maintain the same OP, the double IRS system requires fewer IRS elements compared to the single IRS system.

Figure 4.5 plots the OP as a function of p for scenarios 1-4 related to double IRS enabled WET. We also benchmark these results against single IRS enabled WET (scenario 5) and massive MIMO enabled WET (scenario 6). We observe that double IRS-assisted WET saves significant transmit power at the source compared to single IRS-assisted WET and massive MIMO enabled WET. For example, to maintain the OP at 10^{-4}, scenario 4 requires 4 dB and 6 dB lower transmit powers compared to scenarios 5 and 6, respectively. As before, we note that the corre-

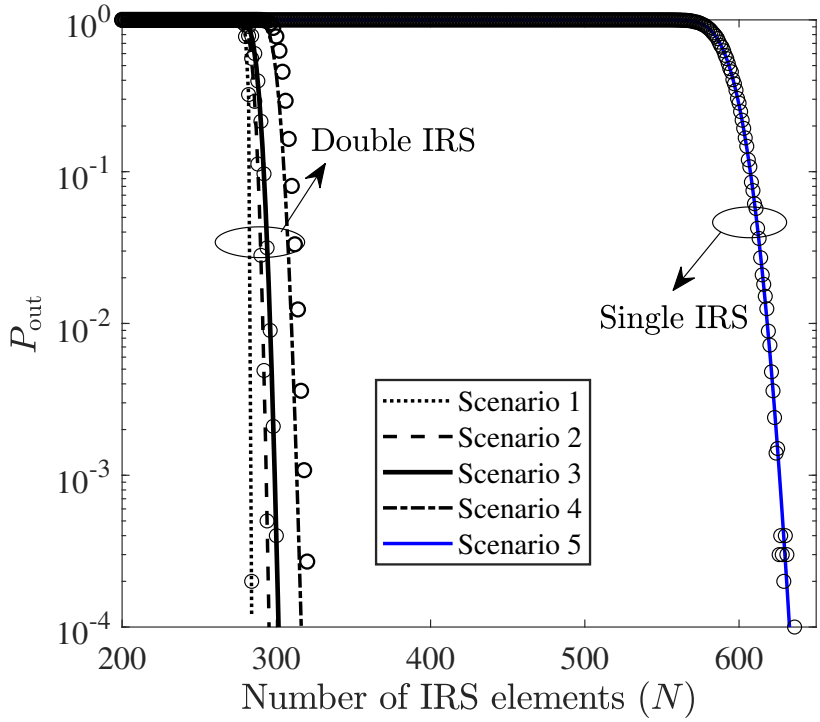

Fig. 4.4: Impact of N: ($p = 1$ W, $E_{\text{th}} = 10^{-8}$ J, $N_1 = N_2 = \frac{N}{2}$, $a_0 = 1.953 \times 10^{-3}$, $b_0 = -3.571 \times 10^3$ and $P_0 = 299.5$ μW). Corresponding Monte Carlo simulations are shown through the marker $\circ$.

sponding Monte Carlo simulation results shown through the marker '$\circ$' are in close agreement with the analysis, thus validating our analysis.

Figure 4.6 plots the OP as a function of N. In order to generate this plot, we consider that each of the links from $S-U$, $S-I_1$, I_1-I_2, I_2-U, $S-I_2$ and I_1-U follows Rician fading. We show results for three different cases: (i) when the phases at the two IRSs are designed based on MO (4 links), (ii) when the phases at the two IRSs are designed based on AO (4 links), and (iii) when the phases at the two IRSs are designed based on (4.5) and (4.6) (two links-scenario 4). We observe that the outage performance improves by considering four communication links between S and U. Furthermore, we observe that the low complexity AO based phase shift design gives identical outage performance when compared to the relatively higher complexity MO based phase shift design, while reducing the complexity and providing a locally optimal solution.

Figure 4.7 plots received power at the user as a function of $N_d = N_s = M$ based on the asymptotic analysis in Section 4.3.7. We observe that the double IRS-assisted WET requires

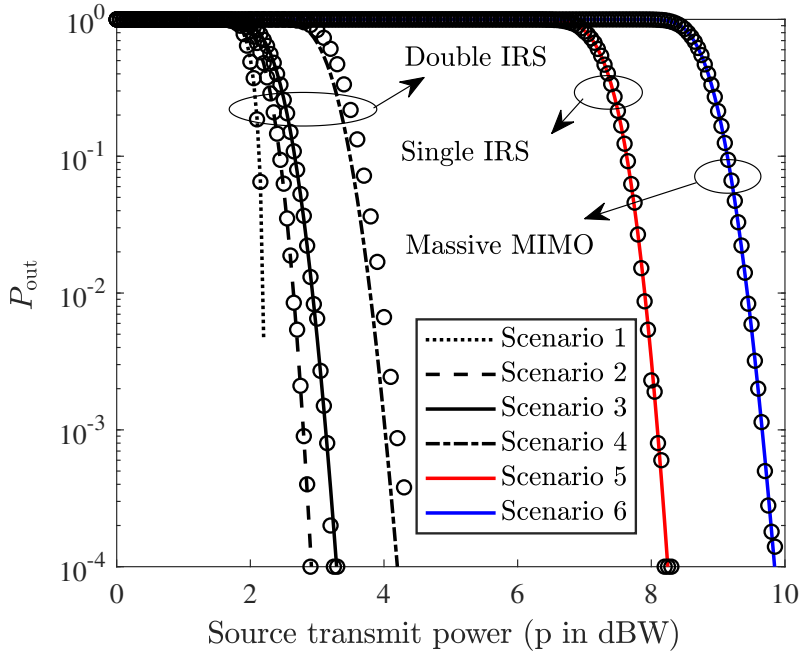

Fig. 4.5: Impact of p: ($N = 250$, $M = N$, $E_{\text{th}} = 10^{-8}$ J, $N_1 = N_2 = \frac{N}{2}$, $a_0 = 1.953 \times 10^{-3}$, $b_0 = -3.571 \times 10^{3}$ and $P_0 = 299.5$ μW). Corresponding Monte Carlo simulations are shown through the marker $\circ$ and analytical results are shown using different line types and colors.

significantly fewer IRS elements than single IRS-assisted WET and number of antennas required in massive MIMO enabled WET in order to obtain the target received power at the user. For example to receive about 1 μW power at the user, double IRS-assisted WET requires a total of 248 elements, single IRS-assisted WET requires 462 IRS elements and massive MIMO enabled WET requires 1100 antenna elements.[9] Furthermore, we observe that for lower values of $N_d = N_s = M$, massive MIMO and single IRS enabled WET outperform double IRS enabled WET. This is because double IRS enabled WET requires certain minimum number of IRS elements to overcome the effective path loss of the cascaded channel, as discussed in Section 4.3.7.

Figure 4.8 plots the PTE as a function of the given received power at the user. With double IRS-assisted WET, received power scales almost as N^4, therefore the given received power is achieved at lowest power consumption. With single IRS-assisted WET, received power scales as N^2, therefore, the given received power is achieved at relatively higher power consumption.

[9]We choose 5 dB element gain just for illustration. Our analysis is in general valid for any value of the element gain. With lower values of element gain, few extra IRS elements would be required to attain identical performance as a set-up where higher values of element gain is considered.

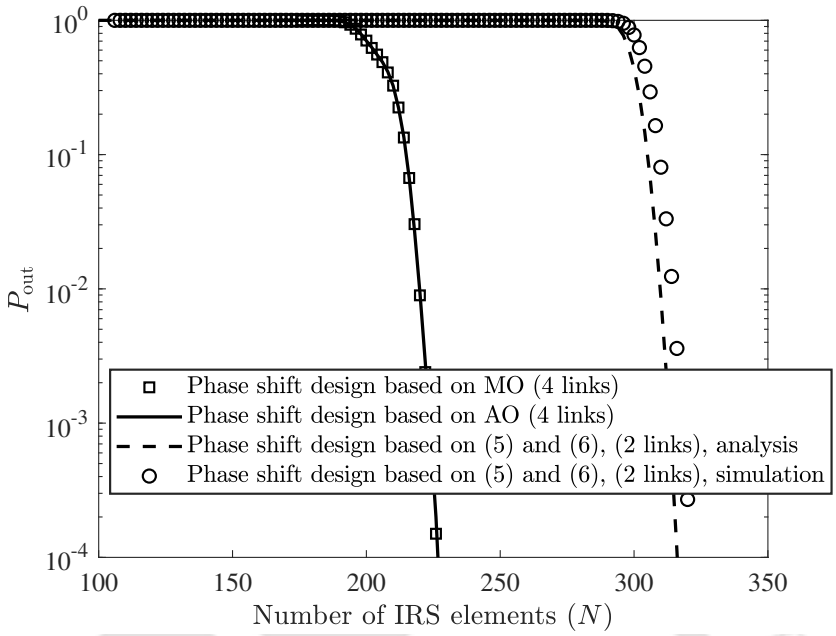

Fig. 4.6: Impact of four communication links on OP ($p = 1$ W, $E_{\text{th}} = 10^{-8}$ J, $N_1 = N_2 = \frac{N}{2}$, $a_0 = 1.953 \times 10^{-3}$, $b_0 = -3.571 \times 10^3$ and $P_0 = 299.5\ \mu$W).

With massive MIMO enabled configuration, received power scales as M, and every antenna is connected to an RF chain, which significantly increases power consumption. Therefore, the given received power is achieved at the highest power consumption for the massive MIMO configuration. Hence, we observe that the highest PTE is obtained using double IRS-assisted WET, followed by single IRS-assisted WET and massive MIMO enabled WET. We observe that the double IRS configuration achieves 10x and 1000x improved PTE compared to single IRS and massive MIMO configurations, respectively[10].

4.7 Summary

We investigated viability of double IRS enabled WET. Specifically, we derived new closed form expressions for OP under non-linear EH and different fading scenarios at the user for double IRS configuration. We also generalized the outage analysis for the scenario when the direct path and the cascaded paths via two IRSs undergo Rician fading. This analysis involved developing a new statistical model for the sum of product of Rician fading envelopes corresponding

[10]For implementing this communication network, challenges related to (i) optimal deployment of these IRSs taking into account hardware and operational cost, (ii) discrete phase shift design taking into account the number of PIN diodes that can be fabricated on each IRS element and (iii) reducing the overhead in computing the phase shifts at IRS will have to be tackled [16]. And these challenges open up interesting avenues for future research.

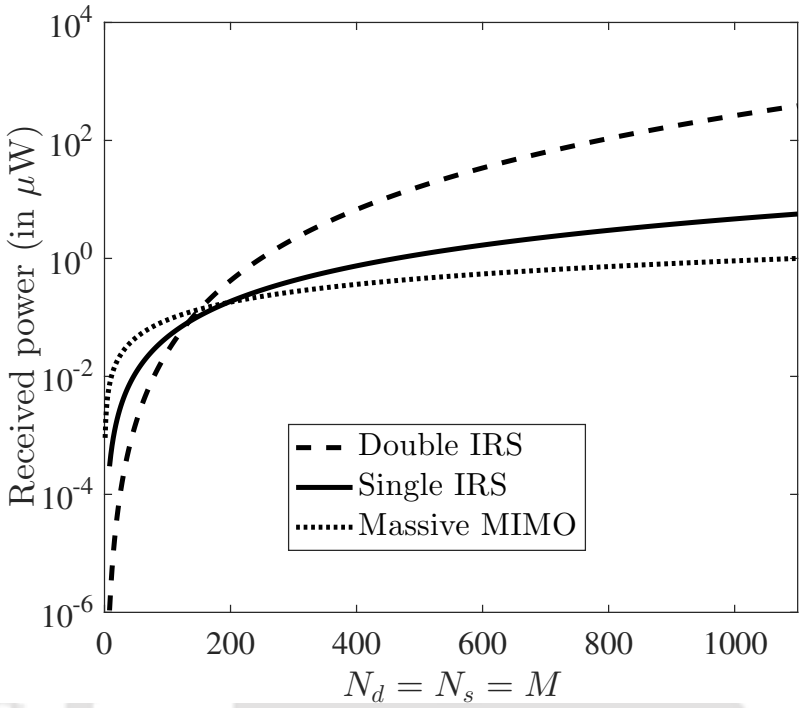

Fig. 4.7: Impact of N_d, N_s and M: (p = 1 W).

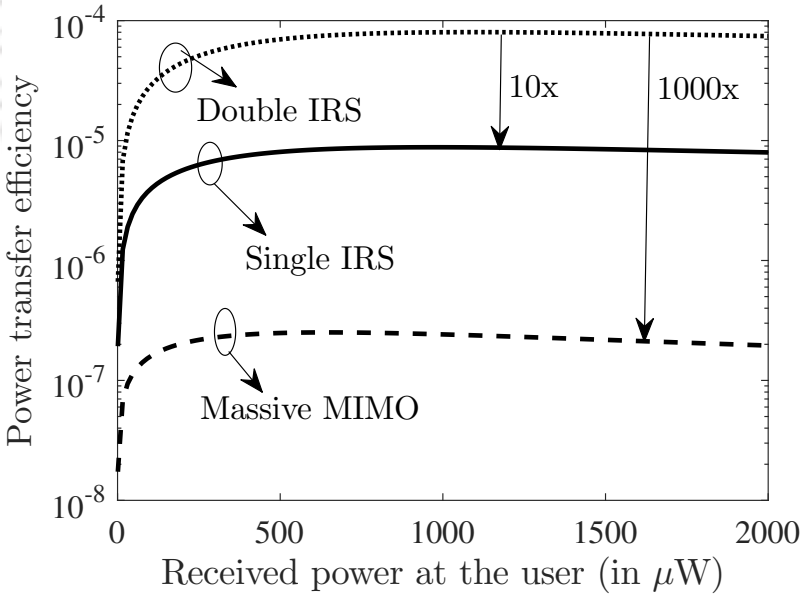

Fig. 4.8: Impact of receive power on the PTE in WET: (p_e = 5 mW, $p_s = p_{\text{fix}}$ = 100 mW, B = 1 MHz, B_c = 10 KHz, τ_c = 10 ms, $k_s = 20 \times 10^9$ flops/W, K = 1, $N_1 = N_2 = \frac{N}{2}$, $a_0 = 1.953 \times 10^{-3}$, $b_0 = -3.571 \times 10^3$ and P_0 = 299.5 μW).

to cascaded paths based on Gamma distribution. As benchmarks, we derived the corresponding new closed form expressions for single IRS and massive MIMO enabled WET configurations. We also extended our study to elucidate the impact of four communication links between source

and user on OP. We determined the optimal number of IRS elements that maximizes the PTE under both double IRS and single IRS configurations. We also derived new closed form expressions for the optimal number of antenna elements that must be used in massive MIMO enabled WET to maximize PTE. We prove that fewer IRS elements are required and substantial power savings can be obtained at the source through the use of double IRS configuration. Furthermore, we observe that double IRS enabled WET achieves 10x and 1000x improved PTE over single IRS and massive MIMO enabled WET configurations.

In the next Chapter, we take a step further, since we realize that to make WET an economically-viable alternative, it must be integrated with the existing wireless information transfer system such that the same source and waveform can be harnessed to enable WET and make it a reality [7]. Therefore, in the next chapter, we generalize the model to study simultaneous wireless information and energy transfer (SWIET) to multiple IoT users under optimal phase configuration at the IRS and correlated channels.

5

IRS Assisted SWIET

Contents

The goal in Chapter 4 was to ascertain the viability of double IRS enabled WET and characterize the regimes in which it outperforms single IRS enabled WET and massive MIMO enabled WET in terms of OP and PTE. However, as mentioned, WET must be integrated with wireless information transfer to make it an economically appealing alternative [7]. Furthermore, the design of such unified SWIET networks must ensure that IoT users harvest more energy than what they consume in sensing, computation and communication and can decode information considering factors such as path loss and limitations of the EH circuitry.

In this Chapter, we focus on modeling and performance analysis of IRS-aided SWIET to multiple IoT users under spatial correlation and optimal phase configuration at IRS. Our modeling is comprehensive in the sense that that we consider the practically relevant non-linear EH and power splitting architecture at the user end. We also consider that the source adopts the channel unaware but fair RR scheduling strategy to perform SWIET to multiple users. This strategy is practically appealing since it mandates uniform quality of service to all the users and enables real-time phase configuration at the IRS based on the direct and the cascaded channels to the user being served in the specific time slot.

We first analyze OP for this model where the source to IRS link is common to all users. We then derive the diversity order and analyze SE for this system. Our analysis captures the spatial correlation among the channels via the IRS elements and also the correlation that arises in the energy harvested by different users due to common source to IRS links. The analysis entails developing a statistical model based on gamma distribution for the sum of product of Rayleigh fading envelopes corresponding to reflected channels via the IRS. Thereafter, we extend our study to include multiple antennas at the source and design transmit beamformer at the source and phase shifts at the IRS based on AO.

We first review related literature on IRS-aided SWIET under spatial correlation.

5.1 Related Literature on IRS-Aided SWIET Under Spatial Correlation

While the authors in [93] analyzed OP in the context of information transfer, in [94], the average harvested energy and OP were analyzed under random and equal phase shift configu-

rations. The authors in [95] optimized the short term transmit beamforming at BS and the long term beamforming at IRS to maximize the sum data rate of the network. An expression for symbol error probability and an upper bound on channel capacity were derived under deterministic phase shifts at IRS in [96].

Based on the discussion above, we wish to emphasize that there are limited works available in the existing literature that study IRS-aided wireless information and/or energy transfer under spatial correlation [93–96]. Moreover, most of these works consider single antenna source and single user in the network [93,94,96] and focus on random, equal or deterministic programming of phases at the IRS that do not take into account the instantaneous channel gains to configure the phases [93–96].

Organization: The Chapter is organized as follows. We present the system model in Section 5.2. We then present the statistical modeling, analyze OP and SE, and extend our study to multiple antennas in Section 5.3. The numerical results and summary are presented in Sections 5.4 and 5.5, respectively.

5.2 System Model

We consider a wireless scenario where a single antenna[1] source S assisted by an IRS I with N passive reflecting elements performs SWIET to U single antenna IoT users according to RR scheduling strategy. Based on this strategy, the source performs SWIET to every IoT user over a slot of length $\frac{\tau}{U}$ seconds in a pre-determined manner, where τ denotes the length of the coherence interval. We consider the channel-unaware but fair RR scheduling strategy to serve the IoT users since this is a practically appealing scheduling strategy that ensures uniform quality of service to all the users while enabling real-time phase programming at the IRS.[2] We consider that the spatially correlated channel between source and IRS $\boldsymbol{h}_{si} \sim \mathcal{CN}(\boldsymbol{0}, \beta_{si}\boldsymbol{G}_{si})$, where β_{si} denotes the path loss and $\boldsymbol{G}_{si} \in \mathbb{C}^{N\times N}$ denotes the normalized correlation matrix corresponding to this link. Similarly, the spatially correlated channel between IRS and the

[1]We first focus on single antenna at the source to ensure analytical tractability under spatially correlated channels while gaining useful design insights. Extension to multiple antennas is presented in Section 5.3.5.

[2]This practically realizable strategy avoids the necessity of running computationally intensive algorithms at the source to configure phases at the IRS when users are served simultaneously.

u^{th} IoT user $\boldsymbol{h}_{iu} \sim \mathcal{CN}(\mathbf{0}, \beta_{iu}\boldsymbol{G}_{iu})$, for all $u \in \{1, \ldots, U\}$, where β_{iu} denotes the path loss and $\boldsymbol{G}_{iu} \in \mathbb{C}^{N\times N}$ denotes the normalized correlation matrix corresponding to this link. The direct channel between source and the u^{th} IoT user $h_{su} \sim \mathcal{CN}(0, \beta_{su})$, where β_{su} denotes the path loss. We model the phase configuration at the IRS corresponding to the u^{th} IoT user by $\boldsymbol{\Theta}_u \in C^{N\times N}$ and it is given by $\boldsymbol{\Theta}_u = \text{diag}(e^{j\theta_1^u}, e^{j\theta_2^u}, \ldots, e^{j\theta_N^u})$. For this model, the signal received at the u^{th} IoT user is given by

$$y_u = \sqrt{p}\left(h_{su} + \boldsymbol{h}_{si}^T\boldsymbol{\Theta}_u\boldsymbol{h}_{iu}\right)s_u + w_u, \tag{5.1}$$

$$= \sqrt{p}\left(h_{su} + \sum_{n=1}^{N} h_{si}^n e^{j\theta_n^u} h_{iu}^n\right)s_u + w_u, \tag{5.2}$$

where p denotes the source transmit power, s_u denotes the transmit symbol chosen such that $|s_u|^2 = 1$ and $w_u \sim \mathcal{CN}(0, \sigma^2)$. If we configure the phase shift of the n^{th} IRS element, when the u^{th} IoT user is served, as

$$\theta_n^u = \angle h_{su} - \angle h_{si}^n - \angle h_{iu}^n, \tag{5.3}$$

then it would maximize the received power or the receive SNR at the u^{th} IoT user.

5.3 Statistical Modeling and Performance Analysis

To perform SWIET, we consider power splitting receiver architecture at every IoT user, in which η fraction of the received power $|y_u|^2$ at the u^{th} IoT user is used for EH and the remaining $(1-\eta)$ fraction of $|y_u|^2$ is used to decode information, where $0 \le \eta \le 1$. Using (5.2) and programming phases at the IRS based on (5.3), the power p_u^e received[3] by the u^{th} IoT user is given by

$$p_u^e = \eta p\left(\rho_{su} + \sum_{n=1}^{N}\rho_{si}^n\rho_{iu}^n\right)^2, \tag{5.4}$$

where $\rho_{su} = |h_{su}|$, $\rho_{si}^n = \left|h_{si}^n\right|$ and $\rho_{iu}^n = \left|h_{iu}^n\right|$. Considering non-linear EH, the power harvested by the u^{th} IoT user equals [86]

$$p_u^h = \frac{p_0}{(1+\exp(-a(p_u^e - b)))(1-\Omega)} - \frac{p_0\Omega}{1-\Omega}, \tag{5.5}$$

[3]Since the contribution from noise power is negligibly small, it is ignored [13, 71, 97].

where a and b are parameters that are determined by active and passive components of the EH circuit, p_0 is the maximum power that can be harvested when the circuit is driven into saturation and $\Omega = \frac{1}{1+\exp(ab)}$. The constants a, b and p_0 are obtained by curve fitting of the experimental data obtained from the EH circuit in [88].

We declare outage in energy transfer when the energy harvested by any one among the several IoT users falls below a threshold. In other words, OP (P_{outage}) equals one minus the probability that every IoT user harvests energy above a certain threshold E_{th}. Mathematically,

$$P_{\text{outage}} = 1 - \Pr\left(\bigcap_{u=1}^{U}\{E_u^h > E_{\text{th}}\}\right), \tag{5.6}$$

where $E_u^h = \frac{p_u^h \tau}{U}$ denotes energy harvested by the u^{th} IoT user over an interval of length $\frac{\tau}{U}$. We note that for $1 \leq u \leq U$, the events $\{E_u^h > E_{\text{th}}\}$ are not mutually independent, since the channel between source and IRS is common to all IoT users. Therefore, we apply Boole-Fréchet inequality[4] to simplify (5.6) further and obtain an upper bound on OP as

$$P_{\text{outage}} \leq 1 - \max\left(0, \sum_{u=1}^{U} \Pr\left(E_u^h > E_{\text{th}}\right) - U + 1\right), \tag{5.7}$$

$$= \min\left(1, U - \sum_{u=1}^{U} \Pr\left(E_u^h > E_{\text{th}}\right)\right), \tag{5.8}$$

$$= \min\left(1, \sum_{u=1}^{U} \Pr\left(E_u^h \leq E_{\text{th}}\right)\right). \tag{5.9}$$

From (5.9), we observe that we need to evaluate $\psi_u \triangleq \Pr\left(E_u^h \leq E_{\text{th}}\right)$ to obtain an upper bound on OP. Thus, based on (5.4), (5.5) and the fact that $E_u^h = \frac{p_u^h \tau}{U}$,

$$\psi_u = \Pr\left(\eta p \left(\rho_{su} + \sum_{n=1}^{N} \rho_{si}^n \rho_{iu}^n\right)^2 \leq p'_{\text{th}}\right), \tag{5.10}$$

where $p'_{\text{th}} = b - \frac{\ln\left(\frac{p_0 - p_{\text{th}}(1-\Omega) - p_0\Omega}{p_{\text{th}}(1-\Omega) + p_0\Omega}\right)}{a}$ and $p_{\text{th}} = \frac{E_{\text{th}} U}{\tau}$. To simplify this further, we let $X_u = \rho_{su}$ and

[4]Let $\Pr\left(\bigcap_{i=1}^{r} A_i\right)$ be the joint probability of the events $A_1, \ldots, A_r$, then according to Boole-Fréchet inequality [25], $\max\left(0, \Pr(A_1) + \ldots + \Pr(A_r) - (r-1)\right) \leq \Pr\left(\bigcap_{i=1}^{r} A_i\right)$.

$Y_u = \sum_{n=1}^{N} \rho_{si}^n \rho_{iu}^n$. Then, (5.10) can be re-written as

$$\psi_u = \Pr\left(X_u + Y_u \leq \overline{p}_{\text{th}}\right), \tag{5.11}$$

where $\overline{p}_{\text{th}} = \sqrt{\frac{p'_{\text{th}}}{\eta p}}$.

5.3.1 Statistical Modeling

Since the term $Y_u = \sum_{n=1}^{N} \rho_{si}^n \rho_{iu}^n$ is the sum of product of Rayleigh RVs which are correlated across n, therefore, CLT cannot be applied to model Y_u as Gaussian distributed. To simplify (5.11) further, we therefore present the following statistical model for Y_u.

Lemma 5.1. *Under spatial correlation and optimal phase configuration at IRS, $Y_u = \sum_{n=1}^{N} \rho_{si}^n \rho_{iu}^n$ can be approximated as a Gamma RV with shape and scale parameters given by*

$$k_u = \frac{r_{1_u}^2}{r_{2_u} - r_{1_u}^2} \text{ and } t_u = \frac{r_{2_u} - r_{1_u}^2}{r_{1_u}}, \tag{5.12}$$

respectively, where $r_{1_u} = N\mu_{si}\mu_{iu}$ denotes the first moment of Y_u, r_{2_u} denotes the second moment of Y, which is given by

$$r_{2_u} = \sum_{m,n=1}^{N} \left(\frac{(4-\pi)\beta_{si} R_{si}^{mn}}{4} + \mu_{si}^2\right)\left(\frac{(4-\pi)\beta_{iu} R_{iu}^{mn}}{4} + \mu_{iu}^2\right), \tag{5.13}$$

$\mu_{si} = \sqrt{\frac{\pi\beta_{si}}{4}}$, $\mu_{iu} = \sqrt{\frac{\pi\beta_{iu}}{4}}$, R_{si}^{mn} denotes normalized Rayleigh envelope correlation corresponding to G_{si}^{mn}. Furthermore,

$$R_{si}^{mn} = \frac{\pi F\left(-0.5, -0.5; 1; \left|G_{si}^{mn}\right|^2\right) - \pi}{4 - \pi}, \tag{5.14}$$

where $F(x, y; z; w)$ denotes the hypergeometric function [68, Eqn. (9.100)]. Similarly R_{iu}^{mn} can be obtained just by changing the subscript 'si' to 'iu'.

Proof. The proof is given in Appendix D.1. □

Remarks: This result brings out the dependence of the shape and scale parameters of Y_u on system and channel parameters such as N, β_{si}, β_{iu}, $\boldsymbol{G}_{si}$ and $\boldsymbol{G}_{iu}$. We note that this result is valid for any arbitrary correlation model.

5.3.2 OP Analysis

We now use Lemma 5.1 to derive an upper bound on P_{outage} and state that in a simplified form next as a theorem.

Theorem 5.1. *When IoT users employ non-linear EH, share a common source to IRS link and are scheduled based on RR strategy under spatial correlation and optimal phase configuration at IRS, an upper bound on OP is given by*

$$P_{outage} \leq \min\left(1, \sum_{u=1}^{U} \psi_u\right), \tag{5.15}$$

where

$$\psi_u \approx \frac{\gamma\left(k_u, \frac{\overline{p}_{th}}{t_u}\right)}{\Gamma(k_u)} - \frac{1}{t_u^{k_u}\Gamma(k_u)} \int_{y=0}^{\overline{p}_{th}} y^{k_u-1} e^{\frac{-(y-\overline{p}_{th})^2}{\beta_{su}}} e^{\frac{-y}{t_u}} dy, \tag{5.16}$$

$\Gamma(\cdot)$ denotes complete gamma function and $\gamma(\cdot,\cdot)$ denotes the lower incomplete gamma function [68, Eqn. (8.350.1)].

Proof. The proof is given in Appendix D.2. □

Remarks: This analysis captures the mutual dependence among different events $\{E_u^h > E_{\text{th}}\}$ in (5.6) that arises due to common source to IRS links corresponding to different IoT users. It also captures the spatial correlation among the IRS elements. Furthermore, this expression helps us infer how OP scales as a function of the system and channel parameters such as N, η, $E_{\text{th}}, \beta_{su}, \beta_{si}, \beta_{iu}, \boldsymbol{G}_{si}$ and $\boldsymbol{G}_{iu}$.

5.3.3 Diversity Order

We refer to the rate of decay of OP as a function of transmit power in the asymptotic regime in a log-log scale as the diversity order [97].

Theorem 5.2. *The diversity order for this model under spatial correlation and optimal phase configuration at IRS equals $1 + \frac{k_u}{2}$, where k_u is given in* (5.12).

Proof. The proof is given in Appendix D.3. □

New Design Insights: When the correlation coefficient equals 1, i.e., for the fully correlated scenario, based on Lemma 5.1,

$$k_u = \frac{N^2\mu_{si}^2\mu_{iu}^2}{N^2\beta_{si}\beta_{iu} - N^2\mu_{si}^2\mu_{iu}^2} = \frac{\pi^2\beta_{si}\beta_{iu}}{16\beta_{si}\beta_{iu} - \pi^2\beta_{si}\beta_{iu}} = \frac{\pi^2}{16-\pi^2}. \tag{5.17}$$

Therefore, diversity order for the fully correlated channel equals $1 + \frac{\pi^2}{2(16-\pi^2)}$, where the first term corresponds to the contribution to the diversity order due to the direct path and the second term corresponds to the contribution to the diversity order due to the N elements at the IRS. On the other hand, when the correlation coefficient equals 0, i.e., for the completely uncorrelated scenario, based on Lemma 5.1,

$$k_u = \frac{N^2\pi^2\beta_{si}\beta_{iu}}{16N\beta_{si}\beta_{iu} + (N^2 - N)\pi^2\beta_{si}\beta_{iu} - N^2\pi^2\beta_{si}\beta_{iu}} = \frac{N\pi^2}{16 - \pi^2}. \tag{5.18}$$

Therefore, diversity order for the uncorrelated scenario equals $1+\frac{N\pi^2}{2(16-\pi^2)}$. Through this analysis, we obtain an interesting design insight that as the correlation coefficient decreases from 1 to 0, the shape parameter k_u increases. And we observe an N-fold jump in the contribution to the diversity order due to the N elements at the IRS.

5.3.4 SE Analysis

Based on (5.2), the fraction of the received power that is used for information decoding for the u^{th} IoT user equals $(1-\eta)|y_u|^2 + \sigma_d^2$, where σ_d^2 denotes the variance of noise added by the information decoding circuit [94]. Based on this and programming phases according to (5.3), the SE at the u^{th} IoT user which is served in u^{th} slot of duration $\frac{\tau}{U}$ is given by

$$C_u = \mathbb{E}\left\{\log_2\left(1 + \frac{(1-\eta)p\left(\rho_{su} + \sum_{n=1}^{N}\rho_{si}^n\rho_{iu}^n\right)^2}{(1-\eta)\sigma^2 + \sigma_d^2}\right)\right\}. \tag{5.19}$$

We simplify this and next obtain an upper bound on SE.

Lemma 5.2. *An upper bound on SE under spatial correlation and optimal phase configuration at IRS for the u^{th} IoT user scheduled based on RR strategy is given by*

$$C_u \leq \log_2\left(1 + \frac{(1-\eta)p\left(\beta_{su} + 2r_{1_u}\sqrt{\frac{\pi\beta_{su}}{4}} + r_{2_u}\right)}{(1-\eta)\sigma^2 + \sigma_d^2}\right). \tag{5.20}$$

Proof. The proof is given in Appendix D.4. □

Remarks: The proof exploits the concavity of the $\log(\cdot)$ function, uses Jensen's inequality [98] and the statistics of X_u and Y_u derived in Lemma 5.1. Furthermore, if we re-write the

second term of the logarithmic argument as $c_{1_u} = \frac{p\left(\beta_{su}+2r_{1u}\sqrt{\frac{\pi\beta_{su}}{4}}+r_{2u}\right)}{\sigma^2+\frac{\sigma_d^2}{(1-\eta)}}$ then, it is clear that, as the fraction η of the received power used for EH increases, c_{1_u} decreases, which in turn reduces SE. In addition, SE also depends on system parameters p and N, and channel parameters β_{su}, β_{si}, β_{iu}, $\boldsymbol{G}_{si}$ and $\boldsymbol{G}_{iu}$.

5.3.5 Extension to Multi-Antenna Source

The signal received at the u^{th} IoT user when it is served based on RR scheduling strategy and when the source is equipped with M antennas is given by

$$y_u = (\boldsymbol{h}_{su} + \boldsymbol{H}_{si}\boldsymbol{\Theta}_u\boldsymbol{h}_{iu})^T \boldsymbol{b}_u s_u + w_u, \tag{5.21}$$

where $\boldsymbol{h}_{su} \in C^{M\times 1}$, $\boldsymbol{H}_{si} \in C^{M\times N}$ and $\boldsymbol{b}_u \in C^{M\times 1}$ denotes the transmit beamformer employed at the source. Furthermore, the m^{th} row of $\boldsymbol{H}_{si}$ is given by $\boldsymbol{h}_{si}^m \sim \mathcal{CN}(\boldsymbol{0}, \beta_{si}\boldsymbol{G}_{si}^m)$, where $\boldsymbol{G}_{si}^m \in C^{N\times N}$ denotes the normalized correlation matrix corresponding to $\boldsymbol{h}_{si}^m$. Using (5.21), the power received at the u^{th} IoT user equals

$$p_u^e = \eta p \left|(\boldsymbol{h}_{su} + \boldsymbol{H}_{si}\boldsymbol{\Theta}_u\boldsymbol{h}_{iu})^T \boldsymbol{b}_u\right|^2, \tag{5.22}$$

where $p = |s_u|^2$. As before, we neglect the contribution from noise since it is negligibly small [13, 71, 97]. We obtain the transmit beamforming and the phase shifts at IRS to maximize the received power at the u^{th} IoT user based on AO [91]. Based on this, we compute p_u^e and then use the EH model in (5.5) to numerically obtain OP for the multi-antenna system.

5.4 Numerical Results

We now present results to understand the performance of IRS-assisted multi-user system in terms of OP and SE under spatial correlation and optimal phase shift configuration at IRS. We also benchmark these results against random and equal phase shift configurations at the IRS [93] and [94]. Unless mentioned otherwise, for illustration, we take $p = 1$ W, $E_{\text{th}} = 10^{-8}$ J, $\sigma^2 = \sigma_d^2 = -85$ dBW, $\tau = 10$ ms, $U = 2$, $p_0 = 299.5$ μW, $a = 1.953 \times 10^{-3}$, $b = -3.571 \times 10^3$ and $\eta = 0.5$. We consider planar structure of the IRS with $N = S \times S$

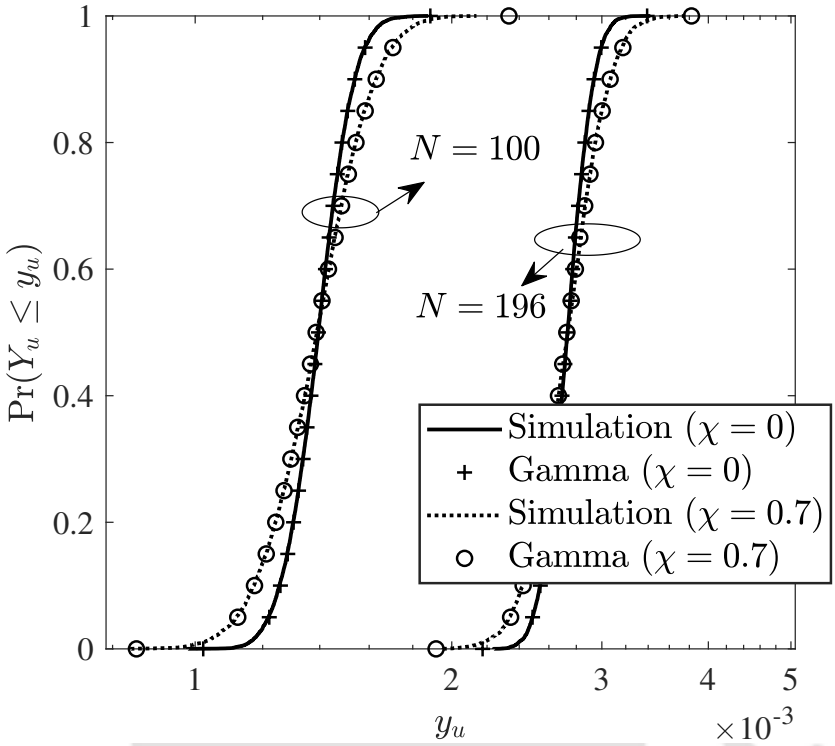

Fig. 5.1: CDF of Y_u compared with Gamma distribution.

elements. The path loss model for the direct path and the reflected paths via the IRS is given by $\beta_{lm} = G_l + G_m - 30 - 30\log_{10}(d_{lm})$ dB, where $l, m \in \{s, i, u\}$, $G_s = G_u = 0$ dB, $G_i = 5$ dB and the distance d_{lm} is in meters. For illustration, we take the $(m,n)^{\text{th}}$ entry of the correlation matrices $\boldsymbol{G}_{si}$, $\boldsymbol{G}_{iu}$ as $G_{si}^{mn} = G_{iu}^{mn} = \chi^{|m-n|}$, where $0 \leq \chi < 1$ denotes the correlation coefficient, and $1 \leq m \leq N$ and $1 \leq n \leq N$. And also for the scenario when source is equipped with multiple antennas, we take the $(j,k)^{\text{th}}$ entry of the correlation matrix $\boldsymbol{G}_{si}^{m'}$ corresponding to $\boldsymbol{h}_{si}^{m'}$ as $\chi^{|j-k|}$, for all $1 \leq m' < M$. The coordinates (in meters) of S and I are set as $(0,0)$ and $(5,0)$, respectively, and IoT users are distributed uniformly in a rectangular region with coordinates $(0, 0.5)$, $(0, 1.5)$, $(6, 0.5)$ and $(6, 1.5)$.

In order to validate the modeling of Y_u as a Gamma distributed RV, we first plot the CDF of $Y_u = \sum_{n=1}^{N} \rho_{si}^n \rho_{iu}^n$ obtained empirically from 10^5 samples through Monte Carlo simulations in Figure 5.1. We also generate Gamma distributed RVs with the shape and scale parameters as specified in Lemma 5.1, and then plot its CDF for two different values of N and two different values of correlation coefficient χ, and illustrate that using the legend 'Gamma'. We observe that the empirical CDF of Y_u tracks the CDF of Gamma RV reasonably well across a range of

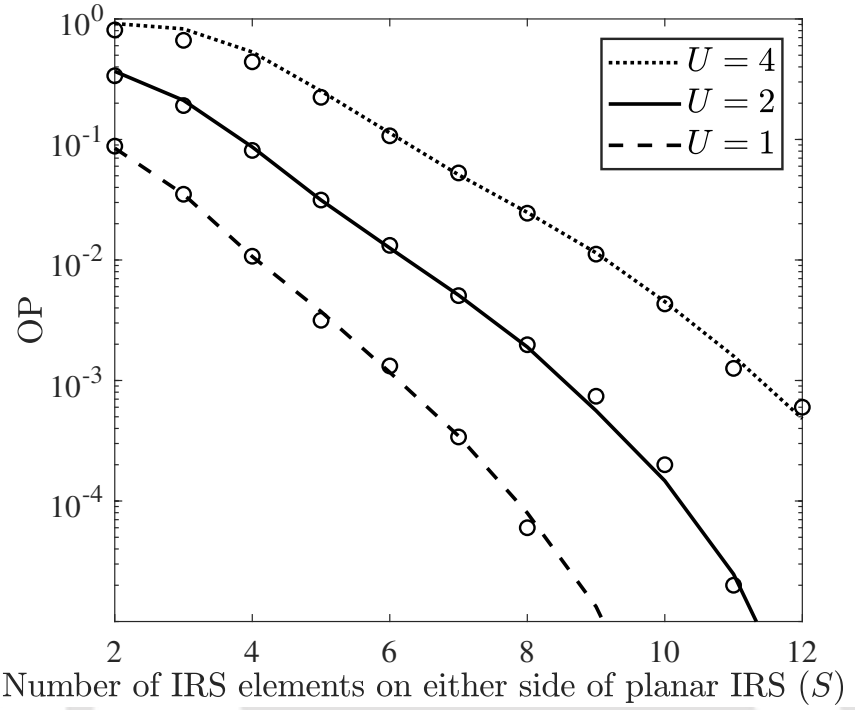

Fig. 5.2: Impact of U on OP: (p = 1 W, χ = 0.7, η = 0.5, $E_{\text{th}} = 10^{-8}$ J, $\sigma^2 = \sigma_d^2 = -85$ dBW, $a = 1.953 \times 10^{-3}$, $b = -3.571 \times 10^3$ and $p_0 = 299.5\ \mu$W). Corresponding simulations are shown through marker $\circ$.

parameter values for N and χ. This verifies the accuracy of modeling Y_u as a Gamma RV.

Figure 5.2 plots OP as a function of S under optimal phase shift configuration. We observe that by increasing number of IRS elements, one can transfer energy wirelessly to more IoT users while maintaining OP at a fixed level. For example, just by adding about 45 and 85 more IRS elements, energy can be transferred wirelessly to 1 and 3 more IoT users while maintaining OP at 10^{-3}. The corresponding analytical results shown through different line types based on the upper bound on OP are reasonably tight and in agreement with the Monte Carlo simulation results shown through markers.

Figure 5.3 plots OP as a function of S for different values of χ and different phase shift configurations. We observe that OP with optimal phase configuration at IRS is lower than OP with equal and random phase configurations under spatial correlation and in the presence of direct path. This is because, by programming the IRS with optimal phase shifts, the reflected signals add up exactly in phase with the signal coming from the direct path at every IoT user. We observe that OP increases marginally as χ increases under optimal phase configuration at

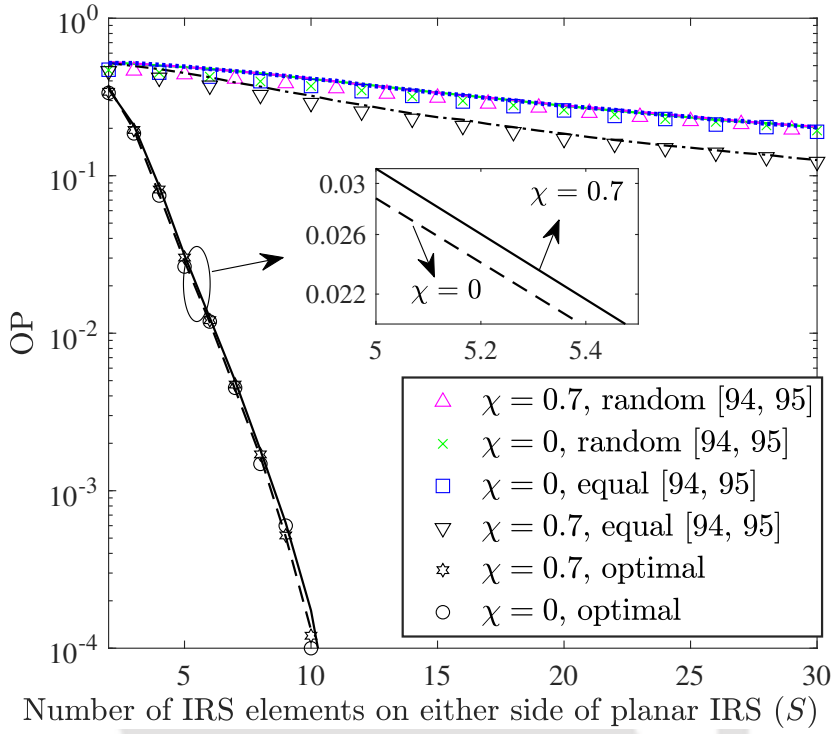

Fig. 5.3: Impact of χ on OP: (p = 1 W, $E_{\text{th}} = 10^{-8}$ J, $\eta = 0.5$, $U = 2$, $a = 1.953\times10^{-3}$, $b = -3.571\times10^{3}$, and $p_0 = 299.5$ μW). The corresponding analytical upper bound are shown through different line types.

IRS due to reduced diversity order. Furthermore, OP decreases as χ increases under equal phase shift configuration, since correlation helps in aligning the reflected signals better at every IoT user. We note that the analysis in [93] and [94] for random and equal phase configurations is done for single IoT user scenario, and we extend this analysis for multi-user scenario in order to benchmark performance. As before, the analytical results based on (5.15) shown through different line types are in agreement with the Monte Carlo simulations shown through markers, thus validating the tightness and accuracy of our modeling and analysis.

Figure 5.4 plots the CDF of SE under spatial correlation with optimal phase configuration. We also benchmark this result against random and equal phase settings at IRS [93,94]. Among the three phase configurations at IRS, we observe that the likelihood that SE exceeds a certain threshold is the highest with optimal phase configuration. This is because the system under optimal phase configuration obtains an SNR boost due to constructive interference. We also observe that the CDF of SE obtained using the upper bound in (5.20) is reasonably tight and close to the Monte Carlo simulation result under optimal phase configuration.[5]

[5]This is true even for random and equal phase configurations.

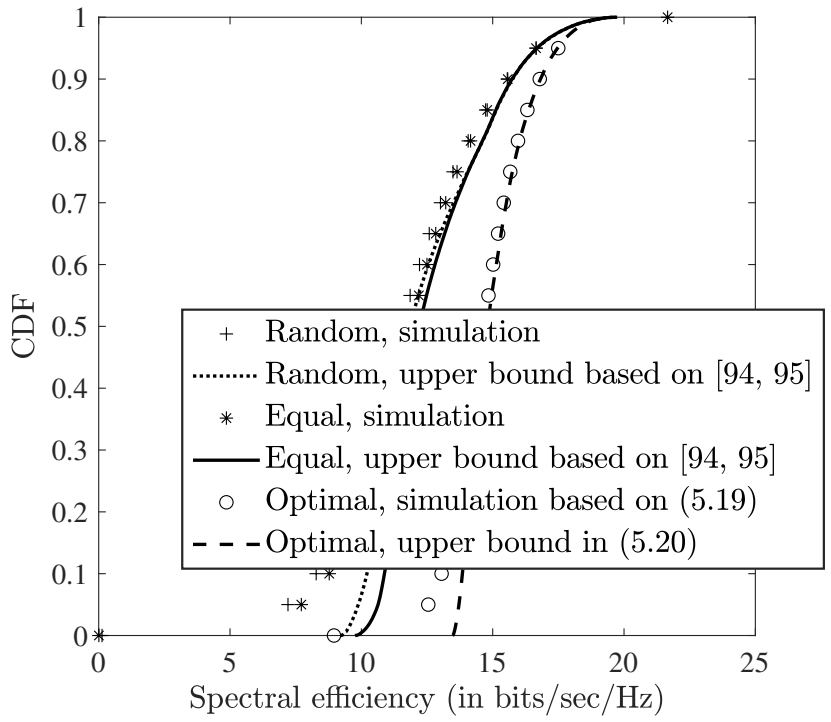

Fig. 5.4: CDF of SE: (p = 1 W, χ = 0.7, η = 0.5, U = 2, N = 100, $E_{\text{th}} = 10^{-8}$ J, $\sigma^2 = \sigma_d^2 = -85$ dBW, $a = 1.953 \times 10^{-3}$, $b = -3.571 \times 10^3$ and $p_0 = 299.5$ μW).

Figure 5.5 plots OP and SE as a function of S for optimal phase configuration at IRS. We observe that as η increases, outage performance improves, while SE reduces. This is because an increment in η increases the fraction of received power used for EH and decreases the fraction used for information decoding. However, this reduction in SE can be compensated just by adding a few more IRS elements. For example, to maintain the SE at 4 bits/sec/Hz, system with $\eta = 0.8$ requires 20 more IRS elements compared to the system with $\eta = 0.5$. We also observe that the results based on the upper bound in (5.15) and (5.20) for OP and SE are fairly tight and close to the Monte Carlo simulation results based on (5.6) and (5.19), respectively.

Figure 5.6 plots OP as a function of source transmit power (p) for different number of antennas at the source. We note that this plot is based on the discussion in Section 5.3.5 which studies the impact of multiple antennas on OP. We observe that OP decreases as the number of antennas at the source increases. In other words, by using multiple antennas at the source, one can obtain savings of radiated power. For example, just by increasing the number of antennas at the source from 2 to 4, one can save about 5 dBm of radiated power while keeping OP fixed at 10^{-3}. This is because energy beamforming with larger number of antennas improves the signal

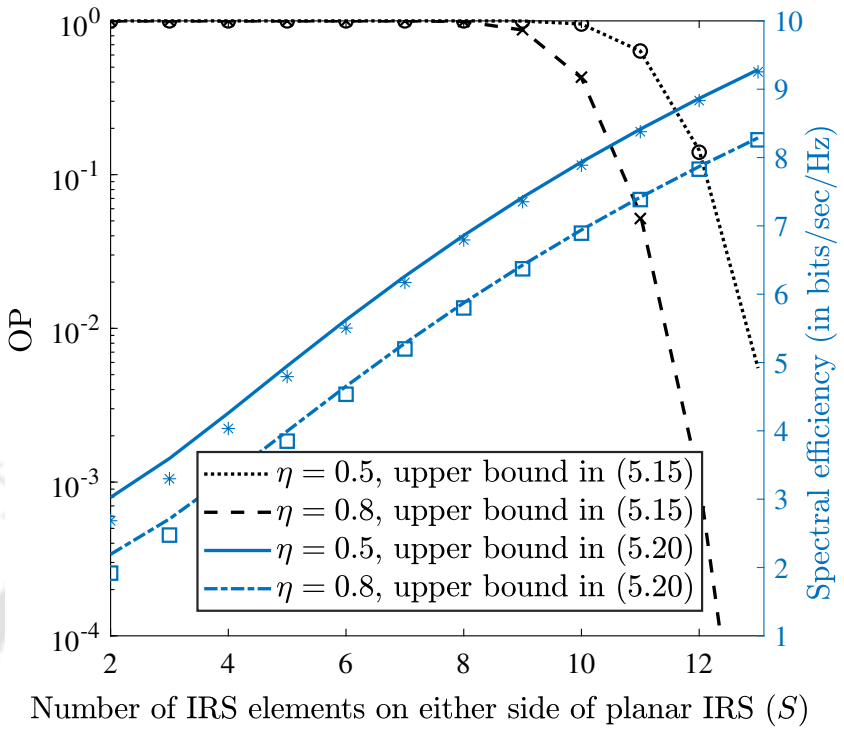

Fig. 5.5: Impact of η on OP and SE: (p = 10 mW, χ = 0.7, U = 1, E_{th} = 10^{-8} J, $\sigma^2 = \sigma_d^2$ = −85 dBW, $a = 1.953 \times 10^{-3}$, $b = -3.571 \times 10^3$ and p_0 = 299.5 μW). Corresponding simulations are shown through the different markers.

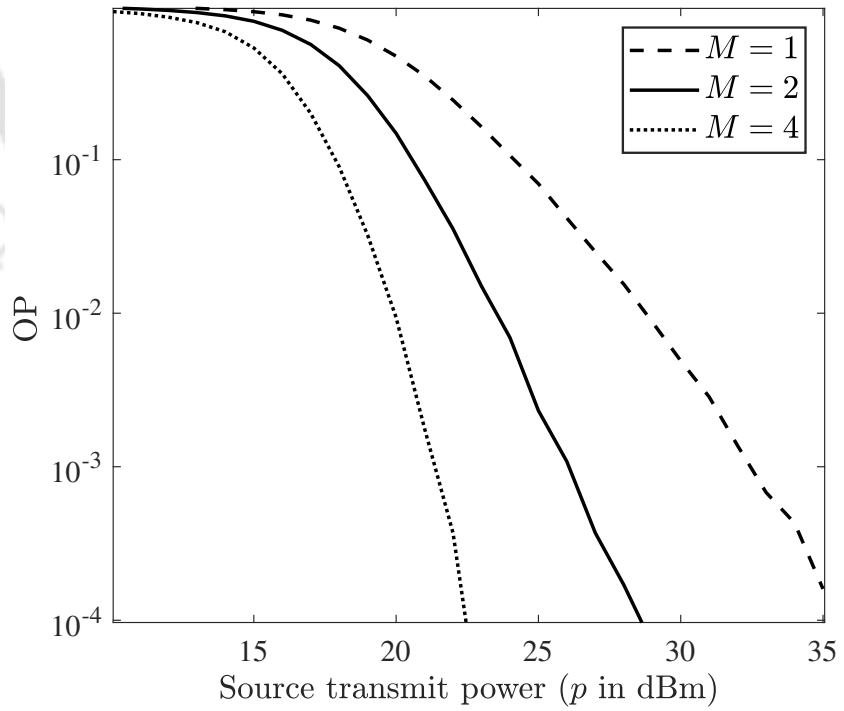

Fig. 5.6: Impact of multiple antennas on OP: (χ = 0.7, η = 0.5, U = 2, N = 49, E_{th} = 10^{-8} J, $\sigma^2 = \sigma_d^2$ = −85 dBW, $a = 1.953 \times 10^{-3}$, $b = -3.571 \times 10^3$ and p_0 = 299.5 μW).

strength at the IoT user.

5.5 Summary

We analyzed the performance of IRS assisted SWIET to multiple IoT users under spatial correlation and optimal phase configuration at IRS. We derived a new upper bound on OP based on Boole-Fréchet inequality when the IoT users are scheduled based on the practically well-motivated channel unaware but fair RR scheduling strategy and adopt non-linear EH at their end. We also derived the diversity order for this system as a function of the shape parameter. Furthermore, we developed a new closed-form upper bound on SE. We then extended our study to the scenario where the source is equipped with multiple antennas. Our numerical results validated the statistical modeling and rigorous mathematical analysis, and quantified the gain in performance with optimal phase shift configuration in terms of OP and SE compared to equal and random phase configurations. We also elucidated that a higher number of IoT users can be supported by increasing number of IRS elements while maintaining OP at a specific level. Furthermore, savings of transmit power can be obtained by equipping source with multiple antennas while keeping OP fixed.

6

Conclusions

Contents

It is expected that a large number of IoT devices will form a core component of next generation wireless systems. And providing high aggregate data rates, reliable connectivity and efficient wireless charging to these devices will be extremely vital. In this thesis, we investigated the fundamentals of wireless information and energy transfer to these devices and focused on aspects related to modeling, optimization and performance analysis.

We first investigated the viability of DL transmission from a BS with massive number of antennas jointly to support machine-centric communication among the IoT devices and human-centric communication among the mobile terminals. We derived an expression for the DL SE of the IoT devices with the proposed grouping based hybrid pilot assignment strategy. We also derived a DL SE expression for IoT devices based on non-orthogonal pilot assignment. We showed that under channel inversion based power control at the BS, the proposed strategy yields the highest sum SE and can serve the largest number of IoT devices when compared against orthogonal, non-orthogonal and distance-independent grouping based hybrid strategies. We then derived a new expression for the DL sum SE of mobile terminals in the presence of IoT devices. We evaluated the max-min SE of the IoT devices and saw that it is independent of the pilot assignment strategy used by the devices due to power control during the channel estimation phase.

We then elucidated feasibility of WET where a source equipped with multiple antennas and a single RF chain transfers energy to IoT devices. We proposed a low complexity rule that does joint AS at source and passive beamforming at IRS. We derived new expressions for OP in WET under perfect and estimated CSI and for both single and multiple users. We showed that the diversity order of a system with M antennas and N IRS elements equals $M + N$. We also generalized our model to study subset AS, discrete phase-shift design, and to evaluate performance under limited scattering. Our numerical results showed that the proposed AS rule yields near-optimal performance while requiring fewer pilot transmissions. We elucidated that we can trade-off active RF chains at source with passive elements at IRS to obtain improved performance both in terms of OP and PTE.

We saw that the outage performance with 3 bit IRS is close to that with a continuous phase

shift IRS. We also saw that as the inter-element spacing increases, the spatial correlation among the elements at IRS increases. And this can be exploited to program a larger number of adjacent elements with identical phase shifts. We also saw that significant savings of radiated power can be obtained at the source either by increasing number of IRS elements or by increasing number of antennas. And with estimated CSI, OP is high at low pilot powers due to poor channel estimates and at high pilot powers since the devices consume more than what they harvest.

Thereafter, we studied feasibility of WET from a source that is assisted by double IRS. We derived closed-form expressions for OP in WET under non-linear EH at the user for different channel fading scenarios. We also generalized our outage analysis to a scenario where all links via the direct path and via the cascaded paths along the two IRSs undergo Rician fading. This analysis involves developing a novel statistical model based on Gamma distribution for the sum of product of Rician fading envelopes corresponding to cascaded path. As benchmarks, we derived closed-form expressions for OP for single IRS-assisted configuration and massive MIMO configuration. We also studied the impact of four communication links between source and user on OP.

Furthermore, we determined the optimal number of IRS elements that minimizes the total power consumption for a given received power, thereby maximizing the PTE under double IRS-assisted configuration. As benchmarks, we also derived the corresponding new closed-form expressions with single IRS-assisted WET and massive MIMO enabled WET. Through our extensive analysis and simulations, we identified the operational regimes where double IRS aided WET outperforms single IRS configuration and massive MIMO enabled system in terms of both OP and PTE.

Finally, we investigated the fundamentals of SWIET to multiple IoT users using IRS under spatial correlation and optimal phase configuration. We derived a fairly tight upper bound on OP in the context of WET when the IoT users are served based on RR scheduling strategy. We then derived the diversity order for this system as a function of the shape parameter. We also derived an upper bound on SE for this system. The analysis takes into account developing a statistical model based on the Gamma distribution for the sum of product of Rayleigh fading

envelopes that are correlated across reflected paths via the IRS. We also extended our model to study the impact of multiple antennas at the source on OP. Through our numerical results, we validated the accuracy of our statistical modeling and novel analytical bounds and quantified the gain in performance relative to random and equal phase shift configurations in terms of OP and SE.

6.1 Directions for Future Research

The fundamental ideas and the mathematical analysis presented in this thesis can be extended in several ways. Some probable directions for future research are as follows:

(i) *Massive MIMO Enabled Joint Transmission to IoT Devices Under Spatial Correlation:* In Chapter 2, we analyzed joint machine centric communication among IoT devices and human centric communication among mobile terminals under spatially uncorrelated channel and where IoT users are grouped based on their relative distances from the BS. However, in practice, the channels from different antennas may be spatially correlated and more than two IoT devices may have to be grouped together to obtain substantial reduction in the estimation overhead. One possible direction for future work is to analyze this joint communication under spatially correlated channels, develop suitable power adaptation algorithms and design grouping strategies such that the multiple IoT devices that form a part of the group pose as little interference as possible to each other. Incorporating activity detection in the model and carrying out the corresponding performance analysis is also an interesting avenue for future research.

(ii) *Massive MIMO Enabled Joint Transmission to IoT Devices in the Presence of IRS:* In Chapter 2, we investigated simultaneous machine type communication among IoT devices and human type communication among mobile terminals in the absence of an IRS. One interesting avenue for future research can be to investigate this joint communication in the presence of IRS. Analyzing such configuration would involve design of active beamformer at the BS and phase shifts at IRS to maximize the sum SE of the IoT devices under power constraint at the BS, unit modulus constraint at IRS and SINR constraint at

every mobile terminal.

(iii) *IRS-Aided SWIET to Heterogeneous Sets of Users Under AS at Source:* An important generalization of the work presented in Chapter 3 is to develop the optimal AS rule, active beamformer at the source and phase shifts at the IRS to maximize the sum of the energy harvested by the energy users subject to constraints on the minimum SINR that must be maintained at every information user. Note that a user with EH capability is referred to as an energy user and a user with data decoding capability is referred to as the information user. The design of channel estimation strategies and trade-off between EE and PTE can as well be explored.

(iv) *Double IRS Aided WET Under Imperfect CSI:* In Chapter 4, we analyze the OP for double IRS-assisted WET for different channel fading scenarios under perfect CSI. However, in practice, CSI will have to be acquired. One possible generalization to this work could be to develop low overhead channel estimation algorithms and analyze the corresponding OP with imperfect CSI. Another extension could be to investigate the use of multiple IRSs in the network and resolve challenges associated with serving multiple users at the same time.

(v) *IRS-Aided SWIET Under Spatial Correlation and Imperfect CSI to Multiple Users:* In Chapter 5, we analyzed IRS-aided SWIET to multiple users under spatial correlation and optimal phase configuration at IRS. It will be of interest to understand the robustness of such systems to imperfections in CSI and develop a comprehensive performance analysis. Another generalization could be to include multiple antennas at the source and look at jointly designing active beamforming at source and phase shifts at IRS to maximize the sum of power received by the users.

A

Appendix

A.1 Proof of Lemma 2.1

Based on $y_{pdl}^{G_k}$, the MMSE estimate of the channel from the d^{th} IoT device in the G_k^{th} group to the l^{th} BS antenna is [38]

$$\hat{g}_{dl}^{G_k} = \mathbb{E}\left[g_{dl}^{G_k} \middle| y_{pdl}^{G_k}\right] = \frac{\sqrt{\tau_p q_d^{G_k}}\beta_d^{G_k} y_{pdl}^{G_k}}{\sigma^2 + \sum\limits_{d' \in G_k} \tau_p q_{d'}^{G_k} \beta_{d'}^{G_k}}. \tag{A.1}$$

Upon substituting $y_{pdl}^{G_k}$ from (2.4) in (A.1), we obtain

$$\hat{g}_{dl}^{G_k} = \frac{\sqrt{\tau_p q_d^{G_k}}\beta_d^{G_k} \left(\sum\limits_{d' \in G_k} \sqrt{\tau_p q_{d'}^{G_k}} g_{d'l}^{G_k} + n_{pdl}^{G_k} \right)}{\sigma^2 + \sum\limits_{d' \in G_k} \tau_p q_{d'}^{G_k} \beta_{d'}^{G_k}}. \tag{A.2}$$

The variance $\gamma_d^{G_k}$ of the estimated channel for the d^{th} IoT device belonging to the G_k^{th} group equals

$$\gamma_d^{G_k} = \mathbb{E}\left[\left|\hat{g}_{dl}^{G_k}\right|^2\right] = \frac{\tau_p q_d^{G_k} \left(\beta_d^{G_k}\right)^2 \mathbb{E}\left[\left|y_{pdl}^{G_k}\right|^2\right]}{\left(\sigma^2 + \sum\limits_{d' \in G_k} \tau_p q_{d'}^{G_k} \beta_{d'}^{G_k}\right)^2}. \tag{A.3}$$

This upon simplification yields $\gamma_d^{G_k}$ as stated in Lemma 2.1. To compute $\mathbb{E}\left[|\tilde{g}_{dl}^{G_k}|^2\right]$, we write $\tilde{g}_{dl}^{G_k} = \hat{g}_{dl}^{G_k} - g_{dl}^{G_k}$. By substituting $\hat{g}_{dl}^{G_k}$ from (A.2) and re-arranging terms we get,

$$\tilde{g}_{dl}^{G_k} = \left(\frac{\tau_p q_d^{G_k} \beta_d^{G_k}}{\sigma^2 + \sum\limits_{d' \in G_k} \tau_p q_{d'}^{G_k} \beta_{d'}^{G_k}} - 1 \right) g_{dl}^{G_k} + \sum_{d' \in G_k \setminus \{d\}} \frac{\sqrt{\tau_p q_d^{G_k} q_{d'}^{G_k}} \beta_d^{G_k}}{\sigma^2 + \sum\limits_{d'' \in G_k} \tau_p q_{d''}^{G_k} \beta_{d''}^{G_k}} + \frac{\sqrt{\tau_p q_d^{G_k}} \beta_d^{G_k} n_{pdl}^{G_k}}{\sigma^2 + \sum\limits_{d' \in G_k} \tau_p q_{d'}^{G_k} \beta_{d'}^{G_k}}. \quad \text{(A.4)}$$

Computing variance of each term in (A.4), yields $\mathbb{E}\left[|\tilde{g}_{dl}^{G_k}|^2\right] = \beta_d^{G_k} - \gamma_d^{G_k}$.

A.2 Proof of Theorem 2.1

To derive the SINR and the achievable rate for IoT devices based on hybrid pilot assignment strategy, we compute below the variance of each term in (2.18). The variance of the first term is given by

$$\text{var(I)} = \frac{p_d^{G_k}}{L\gamma_d^{G_k}} \left(\mathbb{E}\left[\left\| \hat{\boldsymbol{g}}_d^{G_k} \right\|^2 \right] \right)^2 \mathbb{E}\left[\left| s_d^{G_k} \right|^2 \right] = L\gamma_d^{G_k} p_d^{G_k}. \quad \text{(A.5)}$$

This is because $\mathbb{E}\left[|s_d^{G_k}|^2\right] = 1$ and $\mathbb{E}\left[\|\hat{\boldsymbol{g}}_d^{G_k}\|^2\right] = L\gamma_d^{G_k}$. Since, symbols intended for different IoT devices have zero mean and are independent of each other, variance of the second term is given by

$$\text{var(II)} = \sum_{d' \in G_k \setminus \{d\}} \text{var}\left(\sqrt{\frac{p_{d'}^{G_k}}{L\gamma_{d'}^{G_k}}} \left(\boldsymbol{g}_d^{G_k} \right)^T \left(\hat{\boldsymbol{g}}_{d'}^{G_k} \right)^* s_{d'}^{G_k} \right). \quad \text{(A.6)}$$

This can be further simplified to obtain

$$\text{var(II)} = \sum_{d' \in G_k \setminus \{d\}} \frac{p_{d'}^{G_k}}{L\gamma_{d'}^{G_k}} \mathbb{E}\left[\left| \left(\boldsymbol{g}_d^{G_k} \right)^T \left(\hat{\boldsymbol{g}}_{d'}^{G_k} \right)^* \right|^2 \right], \quad \text{(A.7)}$$

$$= \sum_{d' \in G_k \setminus \{d\}} \frac{p_{d'}^{G_k}}{L\gamma_{d'}^{G_k}} \chi_{d'}^{G_k}, \quad \text{(A.8)}$$

where

$$\chi_{d'}^{G_k} = \mathbb{E}\left| \left(\boldsymbol{g}_d^{G_k} \right)^T \eta_{d'}^{G_k} \left(\sum_{u \in G_k} \sqrt{\tau_p q_u^{G_k}} \left(\boldsymbol{g}_u^{G_k} \right)^* + \left(\boldsymbol{n}_{pd}^{G_k} \right)^* \right) \right|^2, \quad \text{(A.9)}$$

$$= \left(\eta_{d'}^{G_k} \right)^2 \left(\tau_p q_d^{G_k} L(L+1) \left(\beta_d^{G_k} \right)^2 + \sum_{u \in G_k \setminus \{d\}} \tau_p q_u^{G_k} L \beta_d^{G_k} \beta_u^{G_k} + L \beta_d^{G_k} \sigma^2 \right), \quad \text{(A.10)}$$

where $\eta_{d'}^{G_k}$ is as stated in the theorem. To derive $\chi_{d'}^{G_k}$, we have used the facts that the true channels of IoT devices are uncorrelated, $\mathbb{E}\left(\left\| \boldsymbol{g}_d^{G_k} \right\|^4 \right) = L(L+1) \left(\beta_d^{G_k} \right)^2$ and $\mathbb{E}\left(\left(\boldsymbol{g}_d^{G_k} \right)^T \boldsymbol{n}_{pd}^{G_k} \right) = 0$.

The variance of third term can be computed as follows:

$$\text{var(III)} = \sum_{\substack{k'=1 \\ k' \neq k}}^{D/N} \sum_{d' \in G_{k'}} \text{var}\left(\sqrt{\frac{p_{d'}^{G_{k'}}}{L\gamma_{d'}^{G_{k'}}}} \left(\boldsymbol{g}_d^{G_k}\right)^T \left(\hat{\boldsymbol{g}}_{d'}^{G_{k'}}\right)^* s_{d'}^{G_{k'}} \right). \tag{A.11}$$

This can be further simplified to obtain

$$\begin{aligned} \text{var(III)} &= \sum_{\substack{k'=1 \\ k' \neq k}}^{D/N} \sum_{d' \in G_{k'}} \frac{p_{d'}^{G_{k'}} \mathbb{E}\left[\left| \left(\boldsymbol{g}_d^{G_k}\right)^T \left(\hat{\boldsymbol{g}}_{d'}^{G_{k'}}\right)^* \right|^2 \right]}{L\gamma_{d'}^{G_{k'}}}, \\ &= \sum_{\substack{k'=1 \\ k' \neq k}}^{D/N} \sum_{d' \in G_{k'}} \frac{p_{d'}^{G_{k'}}}{L\gamma_{d'}^{G_{k'}}} \xi_{d'}^{G_{k'}}, \end{aligned} \tag{A.12}$$

where

$$\xi_{d'}^{G_{k'}} = \mathbb{E}\left| \left(\boldsymbol{g}_d^{G_k}\right)^T \eta_{d'}^{G_{k'}} \left(\sum_{u \in G_{k'}} \sqrt{\tau_p q_u^{G_{k'}}} \left(\boldsymbol{g}_u^{G_{k'}}\right)^* + \left(\boldsymbol{n}_{pd}^{G_{k'}}\right)^* \right) \right|^2, \tag{A.13}$$

$$= \left(\eta_{d'}^{G_{k'}}\right)^2 \left(\sum_{u \in G_{k'}} L\tau_p q_u^{G_{k'}} \beta_d^{G_k} \beta_u^{G_{k'}} + L\beta_d^{G_k} \sigma^2 \right), \tag{A.14}$$

The variance of the fourth term is given by

$$\text{var(IV)} = \sum_{m'=1}^{M} \text{var}\left(\sqrt{\frac{p_{m'}}{L\gamma_{m'}}} \left(\boldsymbol{g}_d^{G_k}\right)^T \hat{\boldsymbol{h}}_{m'}^* s_{m'} \right). \tag{A.15}$$

This upon further simplification yields

$$\begin{aligned} \text{var(IV)} &= \sum_{m'=1}^{M} \frac{p_{m'}}{L\gamma_{m'}} \mathbb{E}\left[s_{m'}^* \hat{\boldsymbol{h}}_{m'}^T \left(\boldsymbol{g}_d^{G_k}\right)^* \left(\boldsymbol{g}_d^{G_k}\right)^T \hat{\boldsymbol{h}}_{m'}^* s_{m'} \right], \\ &= \sum_{m'=1}^{M} \frac{p_{m'}}{L\gamma_{m'}} \beta_d^{G_k} L\gamma_{m'} \mathbb{E}\left[|s_{m'}|^2 \right] = \beta_d^{G_k} \sum_{m'=1}^{M} p_{m'}. \end{aligned} \tag{A.16}$$

We have used the facts that the true channel of IoT devices, channel estimates of mobile terminals and the transmit symbols are mutually independent of each other.

The fifth term captures receiver noise and channel estimation error and its variance calculation can be done in a similar fashion as is done in [37] by exploiting the fact that $\tilde{\boldsymbol{g}}_d^{G_k}$ and $\hat{\boldsymbol{g}}_d^{G_k}$ are independent of each other. The sixth term represents beamforming gain uncertainty and its

variance calculation involves the following steps:

$$\begin{aligned}\text{var(VI)} &= \frac{p_d^{G_k}}{L\gamma_d^{G_k}}\mathbb{E}\left[\left(\left(\|\hat{\boldsymbol{g}}_d^{G_k}\|^2 - \mathbb{E}\{\|\hat{\boldsymbol{g}}_d^{G_k}\|^2\}\right)s_d^{G_k}\right)^H\left(\left(\|\hat{\boldsymbol{g}}_d^{G_k}\|^2 - \mathbb{E}\{\|\hat{\boldsymbol{g}}_d^{G_k}\|^2\}\right)s_d^{G_k}\right)\right], \\ &= \frac{p_d^{G_k}}{L\gamma_d^{G_k}}\left[\mathbb{E}\left(\|\hat{\boldsymbol{g}}_d^{G_k}\|^4\right) - \left(\mathbb{E}\{\|\hat{\boldsymbol{g}}_d^{G_k}\|^2\}\right)^2\right] = p_d^{G_k}\gamma_d^{G_k}. \end{aligned} \tag{A.17}$$

A.3 Proof of Theorem 2.2

To derive the SINR and the achievable rate for IoT devices based on non-orthogonal pilot assignment strategy, we find below the variance of each term in (2.23). The variance of the first term is given by

$$\text{var(I)} = \frac{p_d}{L\gamma_d}\left(\mathbb{E}\left(\|\hat{\boldsymbol{g}}_d\|^2\right)\right)^2\mathbb{E}(|s_d|^2) = L\gamma_d p_d. \tag{A.18}$$

This is because $\mathbb{E}\left(|s_d|^2\right) = 1$ and $\mathbb{E}\left(\|\hat{\boldsymbol{g}}_d\|^2\right) = L\gamma_d$.

Using the fact that the symbols intended for different IoT devices have zero mean and are independent of each other, the variance of the second term simplifies to

$$\text{var(II)} = \sum_{\substack{d'=1\\d'\neq d}}^{D}\text{var}\left(\sqrt{\frac{p_{d'}}{L\gamma_{d'}}}\boldsymbol{g}_d^T\hat{\boldsymbol{g}}_{d'}^* s_{d'}\right). \tag{A.19}$$

This can be further simplified to obtain

$$\text{var(II)} = \sum_{\substack{d'=1\\d'\neq d}}^{D}\frac{p_{d'}}{L\gamma_{d'}}\mathbb{E}\left(|\boldsymbol{g}_d^T\hat{\boldsymbol{g}}_{d'}^*|^2\right) = \sum_{\substack{d'=1\\d'\neq d}}^{D}\frac{p_{d'}\chi_{d'}}{L\gamma_{d'}}, \tag{A.20}$$

where

$$\begin{aligned}\chi_{d'} &= \mathbb{E}\left[\left|\boldsymbol{g}_d^T\eta_{d'}\left(\sum_{u=1}^{D}\sqrt{q_u\tau_p}\boldsymbol{g}_u^*(\boldsymbol{\phi}_u^H\boldsymbol{\phi}_{d'})^* + \left(\boldsymbol{n}_{pd}\right)^*\right)\right|^2\right], \\ &= \eta_{d'}^2\left(q_d\tau_p L(L+1)\beta_d^2\left|\boldsymbol{\phi}_d^T\boldsymbol{\phi}_{d'}^*\right|^2 + \sum_{\substack{u=1\\u\neq d}}^{D}q_u\tau_p L\beta_d\beta_u\left|\boldsymbol{\phi}_u^T\boldsymbol{\phi}_{d'}^*\right|^2 + L\beta_d\sigma^2\right), \end{aligned} \tag{A.21}$$

and $\eta_{d'}$ is as given in Theorem 2.2. To derive $\chi_{d'}$, we have used the facts that the true channels of IoT devices are uncorrelated and $\mathbb{E}\left(\left\|\boldsymbol{g}_d\right\|^4\right) = L(L+1)\beta_d^2$.

Since symbols for different mobile terminals have zero mean and are independent of each

other, the variance of the third term is

$$\text{var(III)} = \sum_{m'=1}^{M} \text{var}\left(\sqrt{\frac{p_{m'}}{L\gamma_{m'}}} \boldsymbol{g}_d^T \hat{\boldsymbol{h}}_{m'}^* s_{m'} \right). \tag{A.22}$$

This can be simplified to obtain

$$\begin{aligned} \text{var(III)} &= \sum_{m'=1}^{M} \frac{p_{m'}}{L\gamma_{m'}} \mathbb{E}\left(s_{m'}^* \hat{\boldsymbol{h}}_{m'}^T \boldsymbol{g}_d^* \boldsymbol{g}_d^T \hat{\boldsymbol{h}}_{m'}^* s_{m'} \right), \\ &= \sum_{m'=1}^{M} \frac{p_{m'}}{L\gamma_{m'}} \mathbb{E}\left(s_{m'}^* \hat{\boldsymbol{h}}_{m'}^T \beta_d \boldsymbol{I}_L \hat{\boldsymbol{h}}_{m'}^* s_{m'} \right), \end{aligned} \tag{A.23}$$

where the last equality follows from the fact that $\boldsymbol{g}_d$ is independent of both $s_{m'}$ and $\hat{\boldsymbol{g}}_{m'}$. Upon further simplification, we obtain $\text{var(III)} = \beta_d \sum_{m'=1}^{M} p_{m'}$. The fourth term captures receiver noise and channel estimation error and its variance calculation can be done in a similar fashion as is done in [37]. The fifth term represents beamforming gain uncertainty and its variance calculation involves the following steps:

$$\begin{aligned} \text{var(V)} &= \frac{p_d}{L\gamma_d} \mathbb{E}\left(\left(\|\hat{\boldsymbol{g}}_d\|^2 - \mathbb{E}\{\|\hat{\boldsymbol{g}}_d\|^2\} \right) s_d \right)^H \left(\left(\|\hat{\boldsymbol{g}}_d\|^2 - \mathbb{E}\{\|\hat{\boldsymbol{g}}_d\|^2\} \right) s_d \right), \\ &= \frac{p_d}{L\gamma_d} \left[\mathbb{E}\left(\|\hat{\boldsymbol{g}}_d\|^4 \right) - \left(\mathbb{E}\{\|\hat{\boldsymbol{g}}_d\|^2\} \right)^2 \right] = p_d \gamma_d. \end{aligned} \tag{A.24}$$

A.4 Proof of Lemma 2.3

To derive the SINR and the achievable rate for mobile terminals based on orthogonal pilot assignment strategy, we find below the variance of each term in (2.27).The variance of the first term is

$$\text{var(I)} = \frac{p_m}{L\gamma_m} \left(\mathbb{E}\left(\|\hat{\boldsymbol{h}}_m\|^2 \right) \right)^2 \mathbb{E}\left[|s_m|^2 \right] = L\gamma_m p_m. \tag{A.25}$$

This is because $\mathbb{E}\left(|s_m|^2 \right) = 1$ and $\mathbb{E}\left(\|\hat{\boldsymbol{h}}_m\|^2 \right) = L\gamma_m$. Since symbols intended for different mobile terminals have zero mean and are uncorrelated to each other, the variance of the second term simplifies to

$$\text{var(II)} = \sum_{\substack{m'=1 \\ m' \neq m}}^{M} \text{var}\left(\sqrt{\frac{p_{m'}}{L\gamma_{m'}}} \boldsymbol{g}_m^T \hat{\boldsymbol{g}}_{m'}^* s_{m'} \right). \tag{A.26}$$

This can be further simplified as is done in Appendix A.3 as follows

$$\text{var(II)} = \sum_{\substack{m'=1 \\ m' \neq m}}^{M} \frac{p_{m'}}{L\gamma_{m,}} \mathbb{E}\left(|\boldsymbol{h}_m^T \hat{\boldsymbol{h}}_{m'}^* s_{m'}|^2\right), \tag{A.27}$$

$$= \beta_m \sum_{\substack{m'=1 \\ m' \neq m}}^{M} p_{m'}. \tag{A.28}$$

The variance of the third term is given by

$$\text{var(III)} = \sum_{d'=1}^{D} \text{var}\left(\sqrt{\frac{p_{d'}}{L\gamma_{d'}}} \boldsymbol{h}_m^T \hat{\boldsymbol{g}}_{d'}^* s_{d'}\right), \tag{A.29}$$

$$= \sum_{d'=1}^{D} \frac{p_{d'}}{L\gamma_{d'}} \mathbb{E}\left(|\boldsymbol{h}_m^T \hat{\boldsymbol{g}}_{d'}^* s_{d'}|^2\right). \tag{A.30}$$

Since $\boldsymbol{h}_m$, $\hat{\boldsymbol{g}}_{d'}$ and $s_{d'}$ are mutually independent of each other and using the facts that $\mathbb{E}\left(\boldsymbol{h}_m^* \boldsymbol{h}_m^T\right) = \beta_m \boldsymbol{I}_L$ and $\mathbb{E}\left(\hat{\boldsymbol{g}}_{d'}^T \hat{\boldsymbol{g}}_{d'}^*\right) = L\gamma_{d'}$, we obtain $\text{var(III)} = \beta_m \sum_{d'=1}^{D} p_{d'}$.

The fourth term captures receiver noise and error incurred during channel estimation and its variance can be computed as in [37]. And variance of the fifth term is

$$\text{var(V)} = \frac{p_m}{L\gamma_m} \mathbb{E}\left(\left(\left(\|\hat{\boldsymbol{h}}_m\|^2 - \mathbb{E}\{\|\hat{\boldsymbol{h}}_m\|^2\}\right) s_m\right)^H \left(\left(\|\hat{\boldsymbol{h}}_m\|^2 - \mathbb{E}\{\|\hat{\boldsymbol{h}}_m\|^2\}\right) s_m\right)\right),$$

$$= \frac{p_m}{L\gamma_m} \left[\mathbb{E}\left(\|\hat{\boldsymbol{h}}_m\|^4\right) - \left(\mathbb{E}\{\|\hat{\boldsymbol{h}}_m\|^2\}\right)^2\right] = p_m \gamma_m. \tag{A.31}$$

B

Appendix

B.1 Proof of Theorem 3.1

We are interested in evaluating

$$P_{\text{outage}} = \Pr\left(\gamma\left(\rho_{su}^{a} + \sum_{n=1}^{N} \rho_{siu}^{an}\right)^2 \leq E_{\text{th}}\right). \tag{B.1}$$

Let $X = \rho_{su}^{a} = \max\{\rho_{su}^{1}, \ldots, \rho_{su}^{M}\}$ and $Y = \sum_{n=1}^{N} \rho_{siu}^{an} = \sum_{n=1}^{N} \rho_{si}^{an}\rho_{iu}^{n}$. Thus, P_{outage} can be re-written as

$$P_{\text{outage}} = \int_{y=0}^{\infty} \Pr\left(X \leq \overline{E}_{\text{th}} - Y \mid Y = y\right) f_Y(y) dy \tag{B.2}$$

$$= \int_{y=0}^{\overline{E}_{\text{th}}} \int_{x=0}^{\overline{E}_{\text{th}}-y} f_X(x)\, f_Y(y)\, dx\, dy, \tag{B.3}$$

where $\overline{E}_{\text{th}} = \sqrt{\frac{E_{\text{th}}}{\gamma}}$, $f_X(x)$ is the PDF of X, $f_Y(y)$ is the PDF of Y. The equality in (B.3) holds since X and Y are mutually independent non-negative real RVs. To derive P_{outage} we need to compute $f_X(x)$ and $f_Y(y)$. Since X is the maximum of M i.i.d. Rayleigh RVs. Based on order

statistics, the PDF of X is given by [99]

$$f_X(x) = \frac{2Mx}{\beta_{su}}\left(1-\exp\left(\frac{-x^2}{\beta_{su}}\right)\right)^{M-1}\exp\left(\frac{-x^2}{\beta_{su}}\right), \quad x \geq 0. \tag{B.4}$$

To compute $f_Y(y)$, we invoke central limit theorem (CLT) [70]. Based on CLT, with large N, distribution of the sum of product of i.i.d. Rician RVs approaches Gaussian distribution and its PDF is given by

$$f_Y(y) = \frac{\psi}{\sqrt{2\pi\sigma_y^2}}\exp\left(\frac{-(y-\mu_y)^2}{2\sigma_y^2}\right), \quad y \geq 0, \tag{B.5}$$

where the scaling constant $\psi = Q^{-1}\left(\frac{-\mu_y}{\sigma_y}\right)$ ensures that $\int_0^\infty f_Y(y)\,dy = 1$. Based on the r^{th} moment of Rician RVs and exploiting the fact that ρ_{si}^{an} is independent of ρ_{iu}^{n}, μ_y and σ_y can be obtained as stated in Theorem 3.1.

Substituting the PDF of X in (B.3) and using binomial expansion to simplify,

$$P_{\text{outage}} = \int_{y=0}^{\overline{E}_{\text{th}}}\left(\int_{x=0}^{\overline{E}_{\text{th}}-y}\sum_{m=0}^{M-1}(-1)^m M\binom{M-1}{m}\frac{2x}{\beta_{su}}\exp\left(\frac{-x^2(m+1)}{\beta_{su}}\right)dx\right)f_Y(y)dy. \tag{B.6}$$

Solving the inner integral above with respect to x, we get

$$P_{\text{outage}} = \sum_{m=0}^{M-1}(-1)^m\frac{M}{m+1}\binom{M-1}{m}\left(\underbrace{\int_{y=0}^{\overline{E}_{\text{th}}}f_Y(y)dy}_{I_1} - \underbrace{\int_{y=0}^{\overline{E}_{\text{th}}}\exp\left(\frac{-(y-\overline{E}_{\text{th}})^2(m+1)}{\beta_{su}}\right)f_Y(y)dy}_{I_2}\right). \tag{B.7}$$

We next simplify I_1 and I_2 separately. Substituting the PDF of Y from (B.5), we can write

$$I_1 = \int_{y=0}^{\overline{E}_{\text{th}}}f_Y(y)dy = \int_{y=0}^{\overline{E}_{\text{th}}}\frac{\psi}{\sqrt{2\pi\sigma_y^2}}\exp\left(\frac{-(y-\mu_y)^2}{2\sigma_y^2}\right)dy = 1-\psi Q\left(\frac{\overline{E}_{\text{th}}-\mu_y}{\sigma_y}\right). \tag{B.8}$$

To compute I_2 we again substitute the PDF of Y from (B.5) to obtain

$$I_2 = \int_{y=0}^{\overline{E}_{\text{th}}}\exp\left(\frac{-(y-\overline{E}_{\text{th}})^2(m+1)}{\beta_{su}}\right)\frac{\psi}{\sqrt{2\pi\sigma_y^2}}\exp\left(\frac{-(y-\mu_y)^2}{2\sigma_y^2}\right)dy, \tag{B.9}$$

We replace $\left(\frac{2(m+1)}{\beta_{su}}+\frac{1}{\sigma_y^2}\right)$ with η, $\left(\frac{2(m+1)\overline{E}_{\text{th}}}{\beta_{su}}+\frac{\mu_y}{\sigma_y^2}\right)$ with ξ and $\left(\frac{2(m+1)\overline{E}_{\text{th}}{}^2}{\beta_{su}}+\frac{\mu_y^2}{\sigma_y^2}\right)$ with χ and further

simplify to write (B.9) as

$$I_2 = \frac{\psi}{\sqrt{2\pi\sigma_y^2}} \exp\left(\frac{\xi^2 - \eta\chi}{2\eta}\right) \int_{y=0}^{\overline{E}_{\text{th}}} \exp\left(\frac{-1}{2}\left(\sqrt{\eta}y - \frac{\xi}{\sqrt{\eta}}\right)^2\right) dy, \tag{B.10}$$

Upon expressing the integral in terms of Q-function, we get

$$I_2 = \frac{\psi}{\sqrt{\eta\sigma_y^2}} \exp\left(\frac{\xi^2 - \eta\chi}{2\eta}\right)\left(Q\left(\frac{-\xi}{\sqrt{\eta}}\right) - Q\left(\frac{\overline{E}_{\text{th}} - \mu_y}{\sigma_y^2\sqrt{\eta}}\right)\right). \tag{B.11}$$

Substituting I_1 from (B.8) and I_2 from (B.11) in (B.7), we obtain P_{outage} in (3.12).

B.2 Proof of Theorem 3.2

For $1 \leq k \leq K$, the events $\{E_k > E_{\text{th}}\}$ are not mutually independent. This is because the channel between source and IRS for different users may be exactly the same if source ends up selecting the same antenna for different users. Therefore, using Boole-Fréchet inequality,[1] an upper bound on probability of outage is given by

$$P_{\text{outage}} \leq 1 - \max\left(0, \sum_{k=1}^{K} \Pr\left(E_k > E_{\text{th}}\right) - K + 1\right), \tag{B.12}$$

$$= \min\left(1, K - \sum_{k=1}^{K} \Pr\left(E_k > E_{\text{th}}\right)\right). \tag{B.13}$$

Also, $\Pr\left(E_k > E_{\text{th}}\right) = 1 - \Pr\left(E_k \leq E_{\text{th}}\right)$. And remaining proof steps to evaluate $\Pr\left(E_k \leq E_{\text{th}}\right)$ is given in detail in Appendix B.1.

B.3 Proof of Lemma 3.1

Based on $\overline{\overline{y}}^{\hat{a}n}$, the linear MMSE estimate of $g_{siu}^{\hat{a}n}$ is given by [38]

$$\hat{g}_{siu}^{\hat{a}n} = \mathbb{E}\left(g_{siu}^{\hat{a}n}\right) + R_{g_{siu}^{\hat{a}n}\overline{\overline{y}}^{\hat{a}n}} R^{-1}_{\overline{\overline{y}}^{\hat{a}n}\overline{\overline{y}}^{\hat{a}n}} \left[\overline{\overline{y}}^{\hat{a}n} - \mathbb{E}\left(\overline{\overline{y}}^{\hat{a}n}\right)\right]. \tag{B.14}$$

[1] Let $\Pr\left(\bigcap_{i=1}^{r} Q_i\right)$ be the joint probability of the events $Q_1, \ldots, Q_r$, then according to Boole-Fréchet inequality [25], $\max\left(0, \Pr\left(Q_1\right) + \ldots + \Pr\left(Q_r\right) - (r-1)\right) \leq \Pr\left(\bigcap_{i=1}^{r} Q_i\right)$.

It can be shown that $\mathbb{E}\left(g_{siu}^{\hat{a}n}\right) = \mu_{siu}^{\hat{a}n}$ and $\mathbb{E}\left(\overline{\overline{y}}^{\hat{a}n}\right) = \sqrt{q}\left(\mu_{siu}^{\hat{a}n} - \tilde{\mu}_{su}^{\hat{a}}\right)$, where $\mu_{siu}^{\hat{a}n}$ and $\tilde{\mu}_{su}^{\hat{a}}$ are as stated in Lemma 3.1. Furthermore, the cross-correlation $R_{g_{siu}^{\hat{a}n}\overline{\overline{y}}^{\hat{a}n}}$ between the cascaded channel $g_{siu}^{\hat{a}n}$ and the observable $\overline{\overline{y}}^{\hat{a}n}$ is given by

$$R_{g_{siu}^{\hat{a}n}\overline{\overline{y}}^{\hat{a}n}} = \mathbb{E}\left(g_{siu}^{\hat{a}n}\overline{\overline{y}}^{\hat{a}n*}\right) - \mu_{siu}^{\hat{a}n}\mathbb{E}\left(\overline{\overline{y}}^{\hat{a}n}\right)^{*}. \tag{B.15}$$

Substituting $\overline{\overline{y}}^{\hat{a}n}$ from (3.31) and $\mathbb{E}\left(\overline{\overline{y}}^{\hat{a}n}\right)$ mentioned above, in (B.15), and simplifying, we get

$$R_{g_{siu}^{\hat{a}n}\overline{\overline{y}}^{\hat{a}n}} = \sqrt{q}\left(\left(\beta_{si} + \left|\mu_{si}^{\hat{a}n}\right|^2\right)\left(\beta_{iu} + \left|\mu_{iu}^{n}\right|^2\right) - \left|\mu_{siu}^{\hat{a}n}\right|^2\right). \tag{B.16}$$

Similarly, the auto-correlation $R_{\overline{\overline{y}}^{\hat{a}n}\overline{\overline{y}}^{\hat{a}n}}$ of the observable is given by

$$R_{\overline{\overline{y}}^{\hat{a}n}\overline{\overline{y}}^{\hat{a}n}} = q\left(\beta_{si} + \left|\mu_{si}^{\hat{a}n}\right|^2\right)\left(\beta_{iu} + \left|\mu_{iu}^{n}\right|^2\right) + \sigma^2 + q\left(\tilde{\sigma}_{su}^{\hat{a}}\right)^2 - q\left|\mu_{siu}^{\hat{a}n}\right|^2. \tag{B.17}$$

Substituting the cross-correlation from (B.16) and the auto-correlation from (B.17) in (B.14), and simplifying further, we obtain $\hat{g}_{siu}^{\hat{a}n}$ as stated in Lemma 3.1.

We next show steps involved in computing $\tilde{\mu}_{su}^{\hat{a}}$ and $\left(\tilde{\sigma}_{su}^{\hat{a}}\right)^2$, which in turn are required to compute $\mathbb{E}\left(\overline{\overline{y}}^{\hat{a}n}\right)$ above and the auto-correlation in (B.17). We first compute $\tilde{\mu}_{su}^{\hat{a}}$ as follows. We note that

$$\Re\left(\tilde{\mu}_{su}^{\hat{a}}\right) = \mathbb{E}\left(\Re\left(\tilde{h}_{su}^{\hat{a}}\right)\right) = \int_{-\infty}^{\infty} t f_{\Re\left(\tilde{h}_{su}^{\hat{a}}\right)}(t)\, dt. \tag{B.18}$$

Since $\tilde{h}_{su}^{\hat{a}}$ corresponds to the error induced in estimating the channel from U to the antenna $\hat{a}$ at S, its PDF corresponds to the PDF of the maximum of M i.i.d. Gaussian RVs each having mean zero and variance $\tilde{\sigma}_{su}^2$. Using this fact and results from order statistics, the PDF of $\Re\left(\tilde{h}_{su}^{\hat{a}}\right)$ is given by [99]

$$f_{\Re\left(\tilde{h}_{su}^{\hat{a}}\right)}(t) = \frac{M}{\sqrt{2\pi\tilde{\sigma}_{su}^2}} e^{-\frac{t^2}{2\tilde{\sigma}_{su}^2}}\left(1 - Q\left(\frac{t}{\tilde{\sigma}_{su}}\right)\right)^{M-1}. \tag{B.19}$$

Note that $\tilde{\sigma}_{su}^2 = \frac{\beta_{su}-\gamma_{su}}{2}$. Using this, we can write

$$\Re\left(\tilde{\mu}_{su}^{\hat{a}}\right) = \frac{M}{\sqrt{2\pi\tilde{\sigma}_{su}^2}} \int_{-\infty}^{\infty} t e^{-\frac{t^2}{2\tilde{\sigma}_{su}^2}}\left(1 - Q\left(\frac{t}{\tilde{\sigma}_{su}}\right)\right)^{M-1} dt. \tag{B.20}$$

This integral can be written down as the sum of two components and simplified further by

exploiting the symmetry property of Q-function [67] as

$$\Re\left(\tilde{\mu}_{su}^{\hat{a}}\right) = \frac{M}{\sqrt{2\pi\tilde{\sigma}_{su}^2}}\left(-\int_0^\infty te^{\frac{-t^2}{2\tilde{\sigma}_{su}^2}}\left(Q\left(\frac{t}{\tilde{\sigma}_{su}}\right)\right)^{M-1}dt + \int_0^\infty te^{\frac{-t^2}{2\tilde{\sigma}_{su}^2}}\left(1-Q\left(\frac{t}{\tilde{\sigma}_{su}}\right)\right)^{M-1}dt\right). \quad \text{(B.21)}$$

Approximating Q-function based on the identity in [100, Eqn. (14)], we obtain

$$\Re\left(\tilde{\mu}_{su}^{\hat{a}}\right) \simeq \frac{M}{\sqrt{2\pi\tilde{\sigma}_{su}^2}}\left(-\int_0^\infty te^{\frac{-t^2}{2\tilde{\sigma}_{su}^2}}\left(\frac{1}{12}e^{\frac{-t^2}{2\tilde{\sigma}_{su}^2}}+\frac{1}{4}e^{\frac{-2t^2}{3\tilde{\sigma}_{su}^2}}\right)^{M-1}dt + \int_0^\infty te^{\frac{-t^2}{2\tilde{\sigma}_{su}^2}}\left(1-\frac{1}{12}e^{\frac{-t^2}{2\tilde{\sigma}_{su}^2}}-\frac{1}{4}e^{\frac{-2t^2}{3\tilde{\sigma}_{su}^2}}\right)^{M-1}dt\right). \quad \text{(B.22)}$$

Using binomial expansion, and simplifying the integral further in (B.22), we obtain $\Re\left(\tilde{\mu}_{su}^{\hat{a}}\right)$ in simplified form as stated in (3.34). We know that $\Re\left(\tilde{h}_{su}^{\hat{a}}\right)$ and $\Im\left(\tilde{h}_{su}^{\hat{a}}\right)$ are identically distributed. Therefore $\Im\left(\tilde{\mu}_{su}^{\hat{a}}\right) = \Re\left(\tilde{\mu}_{su}^{\hat{a}}\right)$. And $\tilde{\mu}_{su}^{\hat{a}} = \Re\left(\tilde{\mu}_{su}^{\hat{a}}\right) + j\Im\left(\tilde{\mu}_{su}^{\hat{a}}\right)$.

In order to compute $\left(\tilde{\sigma}_{su}^{\hat{a}}\right)^2$, we first compute

$$\mathbb{E}\left(\Re\left(\tilde{h}_{su}^{\hat{a}}\right)\right)^2 = \int_{-\infty}^{\infty} t^2 f_{\Re\left(\tilde{h}_{su}^{\hat{a}}\right)}(t)\,dt. \quad \text{(B.23)}$$

Substituting the PDF of $\Re\left(\tilde{h}_{su}^{\hat{a}}\right)$ from (B.19), we get

$$\mathbb{E}\left(\Re\left(\tilde{h}_{su}^{\hat{a}}\right)\right)^2 = \frac{M}{\sqrt{2\pi\tilde{\sigma}_{su}^2}}\int_{-\infty}^{\infty} t^2 e^{\frac{-t^2}{2\tilde{\sigma}_{su}^2}}\left(1-Q\left(\frac{t}{\tilde{\sigma}_{su}}\right)\right)^{M-1}dt. \quad \text{(B.24)}$$

This integral can be written down as the sum of two components and simplified further using the symmetry property of Q-function as follows

$$\mathbb{E}\left(\Re\left(\tilde{h}_{su}^{\hat{a}}\right)\right)^2 = \frac{M}{\sqrt{2\pi\tilde{\sigma}_{su}^2}}\left(\int_0^\infty t^2 e^{\frac{-t^2}{2\tilde{\sigma}_{su}^2}}\left(Q\left(\frac{t}{\tilde{\sigma}_{su}}\right)\right)^{M-1}dt + \int_0^\infty t^2 e^{\frac{-t^2}{2\tilde{\sigma}_{su}^2}}\left(1-Q\left(\frac{t}{\tilde{\sigma}_{su}}\right)\right)^{M-1}dt\right). \quad \text{(B.25)}$$

We next approximate Q-function based on the identity in [100, Eqn. (14)] to yield

$$\mathbb{E}\left(\Re\left(\tilde{h}_{su}^{\hat{a}}\right)\right)^2 \simeq \frac{M}{\sqrt{2\pi\tilde{\sigma}_{su}^2}}\int_0^\infty t^2 e^{\frac{-t^2}{2\tilde{\sigma}_{su}^2}}\left(\left(\frac{1}{12}e^{\frac{-t^2}{2\tilde{\sigma}_{su}^2}}+\frac{1}{4}e^{\frac{-2t^2}{3\tilde{\sigma}_{su}^2}}\right)^{M-1}+\left(1-\frac{1}{12}e^{\frac{-t^2}{2\tilde{\sigma}_{su}^2}}-\frac{1}{4}e^{\frac{-2t^2}{3\tilde{\sigma}_{su}^2}}\right)^{M-1}\right)dt. \quad \text{(B.26)}$$

Using binomial expansion to simplify (B.26) further and using the fact that $\Re\left(\tilde{h}_{su}^{\hat{a}}\right)$ and $\Im\left(\tilde{h}_{su}^{\hat{a}}\right)$ are i.i.d. RVs, we get $\mathbb{E}\left(\left|\tilde{h}_{su}^{\hat{a}}\right|^2\right)$. Furthermore, $\left(\tilde{\sigma}_{su}^{\hat{a}}\right)^2 = \mathbb{E}\left(\left|\tilde{h}_{su}^{\hat{a}}\right|^2\right) - \left|\tilde{\mu}_{su}^{\hat{a}}\right|^2$, as in (3.35).

B.4 Proof of Theorem 3.3

With estimated CSI, the probability of outage in WET is given by

$$\hat{P}_{\text{outage}} \simeq \Pr\left(\widehat{\gamma}\left(\hat{\rho}_{su}^{\hat{a}} + \sum_{n=1}^{N}\left|\hat{g}_{siu}^{\hat{a}n}\right|\right)^2 \leq E_{\text{th}}\right). \tag{B.27}$$

Let $\hat{X} = \hat{\rho}_{su}^{\hat{a}} = \max\{\hat{\rho}_{su}^{1}, \ldots, \hat{\rho}_{su}^{M}\}$ and $\hat{Y} = \sum_{n=1}^{N}\left|\hat{g}_{siu}^{\hat{a}n}\right|$. Thus, $\hat{P}_{\text{outage}}$ with estimated CSI is

$$\hat{P}_{\text{outage}} \simeq \int_{\hat{y}=0}^{\infty} \Pr\left(\hat{X} \leq \hat{E}_{\text{th}} - \hat{Y} \mid \hat{Y} = \hat{y}\right) f_{\hat{Y}}(\hat{y}) d\hat{y}, \tag{B.28}$$

$$= \int_{\hat{y}=0}^{\hat{E}_{\text{th}}} \int_{\hat{x}=0}^{\hat{E}_{\text{th}}-\hat{y}} f_{\hat{X}}(\hat{x})\, f_{\hat{Y}}(\hat{y})\, d\hat{x}\, d\hat{y}, \tag{B.29}$$

where $\hat{E}_{\text{th}} = \sqrt{\frac{E_{\text{th}}}{\widehat{\gamma}}}$, $f_{\hat{X}}(\hat{x})$ is the PDF of $\hat{X}$, $f_{\hat{Y}}(\hat{y})$ is the PDF of $\hat{Y}$. The equality in (B.29) follows from the fact that $\hat{X}$ and $\hat{Y}$ are mutually independent non-negative real RVs under the assumption that the channel estimation error, $\tilde{h}_{su}^{\hat{a}}$ is negligibly small. Note that this is valid at typical energy levels [6, 71]. To derive P_{outage}, we first compute $f_{\hat{X}}(\hat{x})$ and $f_{\hat{Y}}(\hat{y})$. The RV $\hat{X}$ is the maximum of M i.i.d. Rayleigh distributed RVs. Using order statistics [99], it can be shown that

$$f_{\hat{X}}(\hat{x}) = \frac{2M\hat{x}}{\gamma_{su}}\left(1 - \exp\left(\frac{-\hat{x}^2}{\gamma_{su}}\right)\right)^{M-1} \exp\left(\frac{-\hat{x}^2}{\gamma_{su}}\right), \quad \hat{x} \geq 0. \tag{B.30}$$

To compute the PDF of $\hat{Y}$, we invoke CLT [70]. Based on CLT, with N large, the distribution of the sum of i.i.d. RVs approaches Gaussian distribution and its PDF is given by

$$f_{\hat{Y}}(\hat{y}) = \frac{\hat{\psi}}{\sqrt{2\pi\sigma_{\hat{y}}^2}} \exp\left(\frac{-(\hat{y} - \mu_{\hat{y}})^2}{2\sigma_{\hat{y}}^2}\right), \quad \hat{y} \geq 0, \tag{B.31}$$

where the scaling constant $\hat{\psi} = Q^{-1}\left(\frac{-\mu_{\hat{y}}}{\sigma_{\hat{y}}}\right)$ ensures that $\int_0^{\infty} f_{\hat{Y}}(\hat{y})\, d\hat{y} = 1$.

In order to compute the mean $\mu_{\hat{y}}$ and variance $\sigma_{\hat{y}}^2$ above, first we model the magnitude $\left|\hat{g}_{siu}^{\hat{a}n}\right|$ of the estimate of the cascaded channel coefficient via the n^{th} IRS element as a Rician

RV [101, 102].[2] Thereafter, we use (B.14) to compute $\mathbb{E}\left(\hat{g}_{siu}^{\hat{a}n}\right) = \mu_{siu}^{\hat{a}n}$ and

$$\text{var}\left(\hat{g}_{siu}^{\hat{a}n}\right) = \left(\frac{c_1}{c_2}\right)^2 \left(\mathbb{E}\left(\left|\bar{\bar{y}}^{\hat{a}n}\right|^2\right) - \left|\mathbb{E}\left(\bar{\bar{y}}^{\hat{a}n}\right)\right|^2\right) = \left(\frac{c_1}{c_2}\right)^2 c_2 = \frac{c_1^2}{c_2}, \tag{B.32}$$

where c_1 and c_2 are given in Theorem 3.3. Based on the r^{th} moment of the Rician RV, and exploiting the fact that the terms in $\sum_{n=1}^{N} \left|\hat{g}_{siu}^{\hat{a}n}\right|$ are mutually independent of each other, it can be shown that

$$\mu_{\hat{y}} = \sum_{n=1}^{N} \mathbb{E}\left(\left|\hat{g}_{siu}^{\hat{a}n}\right|\right) = N\sqrt{\frac{c_1^2\pi}{4c_2}} L_{\frac{1}{2}}\left(\frac{-\left|\mu_{siu}^{\hat{a}n}\right|^2 c_2}{c_1^2}\right), \tag{B.33}$$

and the variance,

$$\sigma_{\hat{y}}^2 = \sum_{n=1}^{N} \text{var}\left(\left|\hat{g}_{siu}^{\hat{a}n}\right|\right) = N\left(\frac{c_1^2}{c_2} + \left|\mu_{siu}^{\hat{a}n}\right|^2 - \frac{c_1^2\pi}{4c_2} L_{\frac{1}{2}}^2\left(\frac{-\left|\mu_{siu}^{\hat{a}n}\right|^2 c_2}{c_1^2}\right)\right). \tag{B.34}$$

Substituting the PDF of $\hat{X}$ from (B.30) and the PDF of $\hat{Y}$ from (B.31) in (B.29), and simplifying using similar steps as in Appendix B.1, we obtain $\hat{P}_{\text{outage}}$ in (3.43).

B.5 Proof of Theorem 3.4

To obtain diversity order of probability of outage in the high transmit power regime, it suffices to analyze behavior of PDF of power gain of each of the paths from S to U near origin [103]. We first analyze PDF of the power gain of the cascaded path from S to U via the n^{th} IRS element near origin. To this end, based on Figure 3.2, we model $\hat{g}_{siu}^{\hat{a}n} \sim \mathcal{CN}\left(\mu_{siu}^{\hat{a}n}, \nu_{siu}^{\hat{a}n}\right)$, where $\mu_{siu}^{\hat{a}n} = \mathbb{E}\left(\hat{g}_{siu}^{\hat{a}n}\right) = \mu_{si}^{\hat{a}n}\mu_{iu}^{n}$, and $\nu_{siu}^{\hat{a}n} = \text{var}\left(\hat{g}_{siu}^{\hat{a}n}\right) = \frac{c_1^2}{c_2}$. Thus, the PDF of $\left|\hat{g}_{siu}^{\hat{a}n}\right|^2$ is given by

$$f_{\left|\hat{g}_{siu}^{\hat{a}n}\right|^2}(y) = (1 + K_{siu})\, e^{-K_{siu}} e^{-(1+K_{siu})y} I_0\left(\sqrt{4K_{siu}(1 + K_{siu})y}\right), \tag{B.35}$$

where $K_{siu} = \frac{\left|\mu_{siu}^{\hat{a}n}\right|^2}{\nu_{siu}^{\hat{a}n}}$ is the corresponding Rician factor and $I_0(\cdot)$ is modified Bessel function of the first kind [68]. Upon using the series expansion for $\exp\left(-(1 + K_{siu})\, y\right)$, (B.35) can be expressed as

$$f_{\left|\hat{g}_{siu}^{\hat{a}n}\right|^2}(y) = (1 + K_{siu})\, e^{-K_{siu}} \left(1 + \sum_{i=1}^{\infty} \left(-(1 + K_{siu})\right)^i \frac{y^i}{i!}\right) I_0\left(\sqrt{4K_{siu}(1 + K_{siu})y}\right), \tag{B.36}$$

[2] Based on Figure 3.2, we see that modeling the magnitude of cascaded channel coefficient as a Rician RV is fairly accurate.

The PDF in (B.36) can be approximated as a single polynomial near the origin and

$$\lim_{y\to 0} f_{|\hat{g}_{siu}^{\hat{a}n}|^2}(y) = b_{siu} y^{t_{siu}} + O\left(y^{t_{siu}+\epsilon}\right), \tag{B.37}$$

where b_{siu} is a constant, the parameter t_{siu} captures the diversity order associated with probability of outage, $O(\cdot)$ denotes the big O notation and $\epsilon > 0$. Comparing (B.36) with (B.37) at $y \to 0$, we obtain $b_{siu} = (1 + K_{siu}) \exp(-K_{siu})$ and $t_{siu} = 0$. Using (B.37), the probability of outage in WET due the cascaded path via n^{th} IRS element is given by

$$p_{\text{outage}}^{\hat{a}n} = \int_0^{\frac{p_{\text{th}}}{p}} \left(b_{siu} y^{t_{siu}} + O\left(y^{t_{siu}+\epsilon}\right)\right) dy, \tag{B.38}$$

$$= \frac{b_{siu}}{t_{siu}+1} \left(\frac{p_{\text{th}}}{p}\right)^{t_{siu}+1} + O\left(\left(\frac{p_{\text{th}}}{p}\right)^{t_{siu}+1+\epsilon}\right), \tag{B.39}$$

where $p_{\text{th}} = \frac{E_{\text{th}}}{\eta_r(\tau_c-(M+N)\tau_p)}$ denotes the threshold power required at the user. Neglecting the higher order terms in (B.39), we can see that the probability of outage due to the reflected path via the n^{th} IRS element decays as $p^{-(t_{siu}+1)} = p^{-1}$. Since there are N independent cascaded paths from S to U via the IRS, the total contribution to the diversity order in probability of outage due to the N-element IRS equals N [103].

Furthermore, the PDF of channel power gain from the strongest antenna at S to U is given by

$$f_{|\hat{h}_{su}^{\hat{a}}|^2}(x) = \frac{2M}{\gamma_{su}} \left(1 - e^{\frac{-2x}{\gamma_{su}}}\right)^{M-1} e^{\frac{-2x}{\gamma_{su}}}, \tag{B.40}$$

$$= \frac{2M}{\gamma_{su}} \left(-\sum_{i=1}^{\infty} \left(\frac{-2}{\gamma_{su}}\right)^i \frac{x^i}{i!}\right)^{M-1} \left(\sum_{i=0}^{\infty} \left(\frac{-2}{\gamma_{su}}\right)^i \frac{x^i}{i!}\right), \tag{B.41}$$

where (B.41) is obtained by writing the series expansion for $\exp\left(\frac{-2x}{\gamma_{su}}\right)$. By writing the PDF in (B.41) as a single polynomial near the origin, we get

$$\lim_{x\to 0} f_{|\hat{h}_{su}^{\hat{a}}|^2}(x) = b_{su} x^{t_{su}} + O\left(x^{t_{su}+\epsilon}\right), \tag{B.42}$$

where b_{su} is a constant and the parameter t_{su} captures the diversity order of the probability of outage. Comparing (B.41) and (B.42) at $x \to 0$, we obtain $b_{su} = \frac{4M}{\gamma_{su}^2}$ and $t_{su} = M - 1$.

Algorithm 3 AO based algorithm to solve (P2) under subset AS

Select: subset of antennas $\mathcal{N}_{\mathrm{RF}} \subseteq \{1, \ldots, M\}$, obtain $\boldsymbol{h}_{su}, \boldsymbol{H}_{si}, \boldsymbol{h}_{iu}$, initialize $\boldsymbol{b} = \frac{\boldsymbol{h}_{su}}{\|\boldsymbol{h}_{su}\|}$.

1. Update θ_n, $\forall n = 1, \ldots, N$, using (B.49), for given $\boldsymbol{b}$.
2. Update $\boldsymbol{b}$ using (B.50), for given $\boldsymbol{\Theta}$.
3. Stop if increment in received power in (B.45) is below a threshold ϵ_0, where ϵ_0 is very small positive value. Else go to step 1.
4. Store final value of $\boldsymbol{\Theta}$ and $\boldsymbol{b}$.

Output: Optimal, $\boldsymbol{\Theta}$ and $\boldsymbol{b}$.

Using (B.42), the probability of outage in WET due to the direct path is given by

$$p_{\text{outage}}^{\hat{a}} = \int_0^{\frac{p_{\text{th}}}{p}} \left(b_{su} x^{t_{su}} + O\left(x^{t_{su}+\epsilon}\right)\right) dx = \frac{b_{su}}{t_{su}+1} \left(\frac{p_{\text{th}}}{p}\right)^{t_{su}+1} + O\left(\left(\frac{p_{\text{th}}}{p}\right)^{t_{su}+1+\epsilon}\right). \tag{B.43}$$

Neglecting the higher order terms in (B.43), we can see that the probability of outage due to the direct path decays as $p^{-(t_{su}+1)} = p^{-M}$. Since this path from the strongest antenna at S to U is independent of every cascaded path from S to U via the IRS elements, the total diversity order of probability of outage is equal to $M + N$ [103].

B.6 Subset AS: Transmit Beamformer and Passive Beamformer Design Based on AO

The signal received at the user for a scenario where the source is equipped with N_{RF} chains and M antennas is given by[3]

$$y_u = \left(\boldsymbol{h}_{su} + \boldsymbol{H}_{si}\boldsymbol{\Theta}\boldsymbol{h}_{iu}\right)^T x_s \boldsymbol{b} + w_u, \tag{B.44}$$

where $\boldsymbol{h}_{su} \in C^{N_{\mathrm{RF}} \times 1}$, $\boldsymbol{H}_{si} \in C^{N_{\mathrm{RF}} \times N}$, and $\boldsymbol{b} \in C^{N_{\mathrm{RF}} \times 1}$ denotes the transmit beamformer employed at the source. For subset AS, the channel gains of the direct links from the source to the user are arranged in descending order and N_{RF} antennas with the highest channel gains are selected and connected to the available for RF chains for energy beamforming. Using (B.44), the power received at the user is given by

$$p_u = p \left|\left(\boldsymbol{h}_{su} + \boldsymbol{H}_{si}\boldsymbol{\Theta}\boldsymbol{h}_{iu}\right)^T \boldsymbol{b}\right|^2, \tag{B.45}$$

[3]Note that for a full complexity system $N_{\mathrm{RF}} = M$.

where $p = |x_s|^2$. We neglect the contribution from noise since it is negligibly small [13, 71]. We design the transmit beamforming and the phase shifts at the IRS such that the received power is maximized. Mathematically, the optimization problem can be stated as follows:[4]

$$\begin{aligned} (\text{P1}): \quad & \max_{\boldsymbol{b},\boldsymbol{\Theta}} \left|(\boldsymbol{h}_{su} + \boldsymbol{H}_{si}\boldsymbol{\Theta}\boldsymbol{h}_{iu})^T \boldsymbol{b}\right|^2 \\ & \text{subject to } \|\boldsymbol{b}\|^2 \leq 1, \\ & \quad 0 \leq \theta_n \leq 2\pi, \ \forall n = 1, \ldots, N. \end{aligned} \tag{B.46}$$

Please note that for a given $\boldsymbol{b}$, the objective function in (P1) satisfies the following inequality

$$\left|(\boldsymbol{h}_{su} + \boldsymbol{H}_{si}\boldsymbol{\Theta}\boldsymbol{h}_{iu})^T \boldsymbol{b}\right| = \left|\boldsymbol{h}_{su}^T\boldsymbol{b} + \boldsymbol{h}_{iu}^T\boldsymbol{\Theta}\boldsymbol{H}_{si}^T\boldsymbol{b}\right| \leq \left|\boldsymbol{h}_{su}^T\boldsymbol{b}\right| + \left|\boldsymbol{h}_{iu}^T\boldsymbol{\Theta}\boldsymbol{H}_{si}^T\boldsymbol{b}\right|. \tag{B.47}$$

In the equation above, equality holds when $\angle\left(\boldsymbol{h}_{su}^T\boldsymbol{b}\right) = \angle\left(\boldsymbol{h}_{iu}^T\boldsymbol{\Theta}\boldsymbol{H}_{si}^T\boldsymbol{b}\right) \triangleq \phi_0$. Let $\boldsymbol{G}_{siu} = \boldsymbol{H}_{si}\text{diag}\left(\boldsymbol{h}_{iu}^T\right)$ and $\boldsymbol{f} \in C^{N\times 1}$ be a column vector comprising of the N diagonal elements of $\boldsymbol{\Theta}$. Then, the optimization problem (P1) can be re-formulated as

$$\begin{aligned} (\text{P2}): \quad & \max_{\boldsymbol{f}} \left|\boldsymbol{f}^T\boldsymbol{G}_{siu}^T\boldsymbol{b}\right| \\ & \text{subject to } |f_n| = 1, \ \forall n = 1, \ldots, N, \\ & \quad \angle\left(\boldsymbol{f}^T\boldsymbol{G}_{siu}^T\boldsymbol{b}\right) = \phi_0, \end{aligned} \tag{B.48}$$

where f_n denotes the n^{th} entry of $\boldsymbol{f}$. Based on the constraint $\angle\left(\boldsymbol{f}^T\boldsymbol{G}_{siu}^T\boldsymbol{b}\right) = \phi_0$ in (P2), we obtain $\boldsymbol{f} = \exp\left(j\left(\phi_0 - \angle\left(\boldsymbol{G}_{siu}^T\boldsymbol{b}\right)\right)\right)$. Thus,

$$\theta_n = \phi_0 - \angle\left(\boldsymbol{G}_{siu}^T\boldsymbol{b}\right)_n = \phi_0 - \angle\left(h_{iu}^n\left(\boldsymbol{h}_{si}^n\right)^T\boldsymbol{b}\right) = \phi_0 - \angle(h_{iu}^n) - \angle\left(\left(\boldsymbol{h}_{si}^n\right)^T\boldsymbol{b}\right), \ \forall n = 1, \ldots, N, \tag{B.49}$$

where $\boldsymbol{h}_{si}^n$ is the n^{th} column of $\boldsymbol{H}_{si}$. We consider MR transmission for transmit beamforming since it is optimal [14, 60]. Hence, the transmit beamforming for a given phase shift matrix $\boldsymbol{\Theta}$ is given by

$$\boldsymbol{b} = \frac{(\boldsymbol{h}_{su} + \boldsymbol{H}_{si}\boldsymbol{\Theta}\boldsymbol{h}_{iu})^*}{\|(\boldsymbol{h}_{su} + \boldsymbol{H}_{si}\boldsymbol{\Theta}\boldsymbol{h}_{iu})^*\|}\exp\left(j\alpha_0\right), \tag{B.50}$$

[4]Since the transmit signal power p does not affect the maximization, it is dropped.

where $\alpha_0 = -\angle\left(\boldsymbol{h}_{su}^T \overline{\boldsymbol{b}}\right)$, $\overline{\boldsymbol{b}} = \frac{(\boldsymbol{h}_{su}+\boldsymbol{H}_{si}\boldsymbol{\Theta}\boldsymbol{h}_{iu})^*}{\|(\boldsymbol{h}_{su}+\boldsymbol{H}_{si}\boldsymbol{\Theta}\boldsymbol{h}_{iu})^*\|}$. Note that α_0 is introduced to avoid computation of ϕ_0 every time $\boldsymbol{h}_{su}$ changes while solving the optimization problem and is adjusted such that $\phi_0 = \angle\left(\boldsymbol{h}_{su}^T \boldsymbol{b}\right) = 0$. The AO based algorithm to solve (P2) is given in Algorithm 3.

C

Appendix

C.1 Proof of Result

4.1 We are interested in evaluating

$$P_{\text{out}} = \Pr\left(\frac{P_0}{(1+\exp(-a_0(P_u-b_0)))\,(1-\Omega)} - \frac{P_0\Omega}{1-\Omega} \le P_{\text{th}}\right), \tag{C.1}$$

$$= \Pr\left(\exp(-a_0(P_u-b_0)) \ge \frac{P_0}{P_{\text{th}}(1-\Omega)+P_0\Omega} - 1\right), \tag{C.2}$$

$$= \Pr\left(P_u \le P'_{\text{th}}\right), \tag{C.3}$$

where $P'_{\text{th}} = b_0 - \frac{\ln\left(\frac{P_0 - P_{\text{th}}(1-\Omega)-P_0\Omega}{P_{\text{th}}(1-\Omega)+P_0\Omega}\right)}{a_0}$. Substituting P_u from (4.7) in (C.3), we obtain

$$P_{\text{out}} = \Pr\left(p\left(\rho_{su} + \sum_{n_1=1}^{N_1}\sum_{n_2=1}^{N_2} \rho_{si_1}^{n_1}\rho_{i_1i_2}^{n_1n_2}\rho_{i_2u}^{n_2}\right)^2 \le P'_{\text{th}}\right), \tag{C.4}$$

$$= \Pr\left(\rho_{su} \le \overline{P}_{\text{th}} - N_1N_2\sqrt{\beta_{si_1}\beta_{i_1i_2}\beta_{i_2u}}\right), \tag{C.5}$$

where $\overline{P}_{\text{th}} = \sqrt{\frac{P'_{\text{th}}}{p}}$, and we have used the fact that $\rho_{si_1}^{n_1} = \sqrt{\beta_{si_1}}$, $\rho_{i_1i_2}^{n_1n_2} = \sqrt{\beta_{i_1i_2}}$, and $\rho_{i_2u}^{n_2} = \sqrt{\beta_{i_2u}}$. Since ρ_{su} is Rayleigh distributed RV, hence its CDF, i.e., P_{out} can be obtained as given in Theorem 4.1.

C.2 Proof of Result

4.2 Upon performing similar initial steps as in Appendix C.1, we obtain

$$P_{\text{out}} = \Pr\left(P_u \leq P'_{\text{th}}\right), \tag{C.6}$$

Substituting P_u from (4.7) in (C.6), we obtain

$$P_{\text{out}} = \Pr\left(p\left(\rho_{su} + N_2\sqrt{\beta_{i_1i_2}\beta_{i_2u}}\sum_{n_1=1}^{N_1}\rho_{si_1}^{n_1}\right)^2 \leq P'_{\text{th}}\right), \tag{C.7}$$

where (C.7) follows from the fact that the link $S - I_1$ is Rician distributed and the other two links of the cascaded channel are pure LoS, hence $\rho_{i_1i_2}^{n_1n_2} = \sqrt{\beta_{i_1i_2}}$ and $\rho_{i_2u}^{n_2} = \sqrt{\beta_{i_2u}}$. To analyze further, let $X_0 = \rho_{su}$ and $Y_0 = N_2\sqrt{\beta_{i_1i_2}\beta_{i_2u}}\sum\limits_{n_1=1}^{N_1}\rho_{si_1}^{n_1}$. Thus, P_{out} can be re-written as

$$P_{\text{out}} = \int_{y_0=0}^{\infty}\Pr\left(X_0 \leq \overline{P}_{\text{th}} - Y_0 \mid Y_0 = y_0\right) f_{Y_0}(y_0)dy_0, \tag{C.8}$$

$$= \int_{y_0=0}^{\overline{P}_{\text{th}}}\int_{x_0=0}^{\overline{P}_{\text{th}}-y_0} f_{X_0}(x_0)\, f_{Y_0}(y_0)\, dx_0\, dy_0, \tag{C.9}$$

where $\overline{P}_{\text{th}} = \sqrt{\frac{P'_{\text{th}}}{p}}$, $f_{X_0}(x_0)$ is the PDF of X_0, $f_{Y_0}(y_0)$ is the PDF of Y_0. The equality in (C.9) follows from the fact that X_0 and Y_0 are mutually independent non-negative real RVs. To derive P_{out} we need to compute $f_{X_0}(x_0)$ and $f_{Y_0}(y_0)$. Note that X_0 is Rayleigh distributed and its PDF is given by

$$f_{X_0}(x_0) = \frac{2x_0}{\beta_{su}}\exp\left(\frac{-{x_0}^2}{\beta_{su}}\right), \quad x_0 \geq 0. \tag{C.10}$$

To compute $f_{Y_0}(y_0)$, we invoke CLT [70]. Based on CLT, with large N_1, the distribution of the sum of independent Rician RVs approaches Gaussian distribution and its PDF is given by

$$f_{Y_0}(y_0) = \frac{\psi_1}{\sqrt{2\pi\sigma_1^2}}\exp\left(\frac{-(y_0-\mu_1)^2}{2\sigma_1^2}\right), \quad y_0 \geq 0, \tag{C.11}$$

where the scaling constant $\psi_1 = Q^{-1}\left(\frac{-\mu_1}{\sigma_1}\right)$ ensures that $\int_0^{\infty} f_{Y_0}(y_0)\, dy_0 = 1$. Using the l^{th} moment of Rician RVs μ_1 and σ_1 can be obtained as stated in Theorem 4.2.

Substituting the PDF $f_{X_0}(x_0)$ from (C.10) in (C.9) and solving the integral with respect to x_0,

$$P_{\text{out}} = \underbrace{\int_{y_0=0}^{\overline{P}_{\text{th}}} f_{Y_0}(y_0)dy_0}_{S_1} - \underbrace{\int_{y_0=0}^{\overline{P}_{\text{th}}} \exp\left(\frac{-(y_0-\overline{P}_{\text{th}})^2}{\beta_{su}}\right) f_{Y_0}(y_0)dy_0}_{S_2}. \tag{C.12}$$

We next simplify S_1 and S_2 separately. Substituting the PDF of Y_0 from (C.11), we can write

$$S_1 = \int_{y_0=0}^{\overline{P}_{\text{th}}} \frac{\psi_1}{\sqrt{2\pi\sigma_1^2}} \exp\left(\frac{-(y_0-\mu_1)^2}{2\sigma_1^2}\right) dy_0 = 1 - \psi_1 Q\left(\frac{\overline{P}_{\text{th}}-\mu_1}{\sigma_1}\right). \tag{C.13}$$

To compute S_2 we again substitute the PDF of Y_0 from (C.11) to obtain

$$S_2 = \int_{y_0=0}^{\overline{P}_{\text{th}}} \exp\left(\frac{-(y_0-\overline{P}_{\text{th}})^2}{\beta_{su}}\right) \frac{\psi_1}{\sqrt{2\pi\sigma_1^2}} \exp\left(\frac{-(y_0-\mu_1)^2}{2\sigma_1^2}\right) dy_0, \tag{C.14}$$

We replace $\left(\frac{2}{\beta_{su}} + \frac{1}{\sigma_1^2}\right)$ with η_1, $\left(\frac{2\overline{P}_{\text{th}}}{\beta_{su}} + \frac{\mu_1}{\sigma_1^2}\right)$ with ξ_1 and $\left(\frac{2\overline{P}_{\text{th}}{}^2}{\beta_{su}} + \frac{\mu_1^2}{\sigma_1^2}\right)$ with χ_1 and further simplify to write (C.14) as

$$S_2 = \frac{\psi_1}{\sqrt{2\pi\sigma_1^2}} \exp\left(\frac{\xi_1^2 - \eta_1\chi_1}{2\eta_1}\right) \int_{y_0=0}^{\overline{P}_{\text{th}}} \exp\left(\frac{-1}{2}\left(\sqrt{\eta_1}y - \frac{\xi_1}{\sqrt{\eta_1}}\right)^2\right) dy_0, \tag{C.15}$$

Upon expressing the integral in terms of Q-function, we get

$$S_2 = \frac{\psi_1}{\sqrt{\eta_1\sigma_1^2}} \exp\left(\frac{\xi_1^2 - \eta_1\chi_1}{2\eta_1}\right)\left(Q\left(\frac{-\xi_1}{\sqrt{\eta_1}}\right) - Q\left(\frac{\overline{P}_{\text{th}}-\mu_1}{\sigma_1^2\sqrt{\eta_1}}\right)\right). \tag{C.16}$$

Substituting S_1 from (C.13) and S_2 from (C.16) in (C.12), it can be simplified further to obtain P_{out} in (4.13).

C.3 Proof of Theorem 4.1

We model Y as Gamma RV and find its shape parameter $k = \frac{r_1^2}{r_2 - r_1^2}$ and scale parameter $t = \frac{r_2 - r_1^2}{r_1}$ using moment matching method. We note that $r_1 = \mathbb{E}(Y) = \mathbb{E}\left(\sum_{n_1=1}^{N_1}\sum_{n_2=1}^{N_2} \rho_{si_1}^{n_1}\rho_{i_1i_2}^{n_1n_2}\rho_{i_2u}^{n_2}\right)$ can be re-written as

$$r_1 = \sum_{n_1=1}^{N_1}\sum_{n_2=1}^{N_2} \mathbb{E}\left(\rho_{si_1}^{n_1}\right)\mathbb{E}\left(\rho_{i_1i_2}^{n_1n_2}\right)\mathbb{E}\left(\rho_{i_2u}^{n_2}\right). \tag{C.17}$$

$$r_2 = \sum_{\substack{j=1\\ j=l}}^{N_1}\sum_{\substack{k=1\\ k=m}}^{N_2}\mathbb{E}\left(\left(\rho_{si_1}^{j}\right)^2\right)\mathbb{E}\left(\left(\rho_{i_1i_2}^{jk}\right)^2\right)\mathbb{E}\left(\left(\rho_{i_2u}^{k}\right)^2\right) + \sum_{\substack{j=1\\ j=l}}^{N_1}\sum_{k=1}^{N_2}\sum_{\substack{m=1\\ m\neq k}}^{N_2}\mathbb{E}\left(\left(\rho_{si_1}^{j}\right)^2\right)\mathbb{E}\left(\rho_{i_1i_2}^{jk}\right)\mathbb{E}\left(\rho_{i_1i_2}^{jm}\right)\mathbb{E}\left(\rho_{i_2u}^{k}\right)$$
$$\times\mathbb{E}\left(\rho_{i_2u}^{m}\right) + \sum_{j=1}^{N_1}\sum_{\substack{l=1\\ l\neq j}}^{N_1}\sum_{\substack{k=1\\ k=m}}^{N_2}\mathbb{E}\left(\rho_{si_1}^{j}\right)\mathbb{E}\left(\rho_{si_1}^{l}\right)\mathbb{E}\left(\rho_{i_1i_2}^{jk}\right)\mathbb{E}\left(\rho_{i_1i_2}^{lk}\right)\mathbb{E}\left(\left(\rho_{i_2u}^{k}\right)^2\right) + \sum_{j=1}^{N_1}\sum_{k=1}^{N_2}\sum_{\substack{l=1\\ l\neq j}}^{N_1}\sum_{\substack{m=1\\ m\neq k}}^{N_2}\mathbb{E}\left(\rho_{si_1}^{j}\right)\mathbb{E}\left(\rho_{si_1}^{l}\right)$$
$$\times\mathbb{E}\left(\rho_{i_1i_2}^{jk}\right)\mathbb{E}\left(\rho_{i_1i_2}^{lm}\right)\mathbb{E}\left(\rho_{i_2u}^{k}\right)\mathbb{E}\left(\rho_{i_2u}^{m}\right). \quad \text{(C.19)}$$

Note that (C.17) follows from the fact that for a given n_1 and n_2, the RVs $\rho_{si_1}^{n_1}$, $\rho_{i_1i_2}^{n_1n_2}$ and $\rho_{i_2u}^{n_2}$ are mutually uncorrelated to each other. Since, these are Rician distributed RVs, (C.17) can be simplified further to obtain r_1 as stated in Theorem 4.1.

And $r_2 = \mathbb{E}\left(Y^2\right) = \mathbb{E}\left(\left(\sum_{n_1=1}^{N_1}\sum_{n_2=1}^{N_2}\rho_{si_1}^{n_1}\rho_{i_1i_2}^{n_1n_2}\rho_{i_2u}^{n_2}\right)^2\right)$ can be re-written as

$$r_2 = \mathbb{E}\left(\left(\sum_{j=1}^{N_1}\sum_{k=1}^{N_2}\rho_{si_1}^{j}\rho_{i_1i_2}^{jk}\rho_{i_2u}^{k}\right)\left(\sum_{l=1}^{N_1}\sum_{m=1}^{N_2}\rho_{si_1}^{l}\rho_{i_1i_2}^{lm}\rho_{i_2u}^{m}\right)\right). \quad \text{(C.18)}$$

The second moment r_2 in (C.18) can be expanded as in (C.19) shown at the top of this page, since the entries of the channel vector from S to I_1 are uncorrelated, similarly, the entries of the channel matrix from I_1 to I_2 are uncorrelated and the entries of the channel vector from I_2 to U are also uncorrelated. Therefore, based on this, and using first and second moments of Rician RV, (C.19) can be simplified further to obtain r_2 as given in (4.25).

C.4 Proof of Theorem 4.2

Based on (4.22), we are interested in evaluating

$$P_{\text{out}} = \Pr\left(X + Y \leq \overline{\rho}_{\text{th}}\right), \quad \text{(C.20)}$$

where $X = \rho_{su}$, $Y = \sum_{n_1=1}^{N_1}\sum_{n_2=1}^{N_2}\rho_{si_1}^{n_1}\rho_{i_1i_2}^{n_1n_2}\rho_{i_2u}^{n_2}$ and $\overline{\rho}_{\text{th}} = \sqrt{\frac{\rho'_{\text{th}}}{\eta\rho}}$. Thus, P_{out} can be re-written as

$$P_{\text{out}} = \int_{y=0}^{\overline{\rho}_{\text{th}}}\int_{x=0}^{\overline{\rho}_{\text{th}}-y} f_X(x)\, f_Y(y)\, dx\, dy, \quad \text{(C.21)}$$

where $f_X(x)$ is the PDF of X and $f_Y(y)$ is the PDF of Y. The equality in (C.21) holds since X and Y are mutually independent non-negative real RVs. To derive P_{out}, we need to compute $f_X(x)$ and $f_Y(y)$. Note that X is Rician distributed and its PDF is given by

$$f_X(x) = \frac{2x}{\zeta_{su}} \exp\left(\frac{-\left(x^2+\mu_{su}^2\right)}{\zeta_{su}}\right) I_0\left(\frac{2x\mu_{su}}{\zeta_{su}}\right), \quad x \geq 0, \tag{C.22}$$

where I_0 denotes the zeroth order modified Bessel function of the first kind [68, Eqn. (8.447.1)]. And, to obtain the PDF of Y, we cannot apply CLT since the terms inside the summation in Y are correlated across n_1 and n_2. Therefore, we model Y statistically as a Gamma RV[1] and derive its shape and scale parameters as given in Appendix C.3. Thus, the PDF of Y is given by

$$f_Y(y) \approx \frac{1}{t^k \Gamma(k)} y^{k-1} \exp\left(\frac{-y}{t}\right), \quad y \geq 0, \tag{C.23}$$

where k and t denote the shape and scale parameters, respectively, as given in Theorem 4.1. Substituting the PDF $f_X(x)$ from (C.22) in (C.21) and simplifying the integral with respect to x, we obtain

$$P_{\text{out}} = \int_{y=0}^{\overline{p}_{\text{th}}} f_Y(y)dy - \int_{y=0}^{\overline{p}_{\text{th}}} Q_1\left(\sqrt{2K_{su}}, \frac{\overline{p}_{\text{th}} - y}{\sqrt{\zeta_{su}/2}}\right) f_Y(y)dy, \tag{C.24}$$

where $Q_1(\cdot,\cdot)$ denotes the first order Marcum Q-function [67, Eqn. (4.34)]. Substituting $f_Y(y)$ from (C.23) in (C.24) and simplifying further, we obtain P_{out} in (4.26).

C.5 Proof of Theorem 4.4

Upon performing similar initial steps as in Appendix C.1, we obtain

$$P_{\text{out}} = \Pr\left(P_u^m \leq P'_{\text{th}}\right), \tag{C.25}$$

Substituting P_u^m from (4.33) in (C.25), we obtain

$$P_{\text{out}} = \Pr\left(p\|\boldsymbol{h}_{su}\|^2 \leq P'_{\text{th}}\right) = \Pr\left(\left\|\frac{\boldsymbol{h}_{su}}{\sqrt{\beta_{su}/2}}\right\|^2 \leq \frac{2P'_{\text{th}}}{p\beta_{su}}\right). \tag{C.26}$$

[1]Based on Figure 4.2, we observe that modeling Y as a Gamma RV is fairly accurate.

Since, $\left\| \frac{\boldsymbol{h}_{su}}{\sqrt{\beta_{su}/2}} \right\|^2$ is the sum of the squares of $2M$ $\mathcal{N}(0,1)$ i.i.d. RVs, it is Chi-square distributed RV with $2M$ degrees of freedom, hence its P_{out} can be obtained as given in Theorem 4.4.

C.6 Proof of Theorem 4.5

Based on (4.7) and using the fact that $N_1 = N_2 = \frac{N}{2}$ minimizes the OP, the average received power at the user is given by

$$p_1^u = p\left(\sqrt{\beta_{su}} + \frac{N^2}{4}\sqrt{\beta_{si_1}\beta_{i_1i_2}\beta_{i_2u}}\right)^2. \tag{C.27}$$

Using (C.27), transmit power p can be expressed in terms of number of IRS elements as

$$p(N) = \frac{p_1^u}{\left(\sqrt{\beta_{su}} + \frac{N^2}{4}\sqrt{\beta_{si_1}\beta_{i_1i_2}\beta_{i_2u}}\right)^2}. \tag{C.28}$$

Based on the power consumption model discussed in (4.60) and using (C.28), we write the total power consumption as a function of total number of IRS elements N as

$$P_{\text{c}}(N) = \frac{p_1^u}{\eta_{\text{pa}}^{\text{bs}}\left(\sqrt{\beta_{su}} + \frac{N^2}{4}\sqrt{\beta_{si_1}\beta_{i_1i_2}\beta_{i_2u}}\right)^2} + p_{\text{fix}} + p_{\text{s}} + p_{\text{lp}} + Np_e. \tag{C.29}$$

We obtain the critical points by differentiating $P_c(N)$ with respect to N and equating it to zero

$$\frac{\partial P_{\text{c}}(N)}{\partial N} = -\frac{p_1^u N\sqrt{\beta_{si_1}\beta_{i_1i_2}\beta_{i_2u}}}{\eta_{\text{pa}}^{\text{bs}}\left(\sqrt{\beta_{su}} + \frac{N^2}{4}\sqrt{\beta_{si_1}\beta_{i_1i_2}\beta_{i_2u}}\right)^3} + p_e. \tag{C.30}$$

Equating this to zero, we obtain

$$\eta_{\text{pa}}^{\text{bs}}p_e\left(\sqrt{\beta_{su}} + \frac{N^2}{4}\sqrt{\beta_{si_1}\beta_{i_1i_2}\beta_{i_2u}}\right)^3 - p_1^u N\sqrt{\beta_{si_1}\beta_{i_1i_2}\beta_{i_2u}} = 0. \tag{C.31}$$

Since the polynomial equation in (C.31) is a sixth degree polynomial equation, therefore, we evaluate its roots numerically. And from these roots, we can choose the valid root, i.e., the optimal number of IRS elements that minimizes the total power consumption in (C.29).

C.7 Proof of Theorem 4.6

Based on (4.30), average received power at U is given by

$$p_2^u = p\left(\sqrt{\beta_{su}} + N\sqrt{\beta_{si}\beta_{iu}}\right)^2. \tag{C.32}$$

Therefore, the transmit power p can be expressed in terms of the number of IRS elements as

$$p(N) = \frac{p_2^u}{\eta_{\text{pa}}^{\text{bs}}\left(\sqrt{\beta_{su}} + N\sqrt{\beta_{si}\beta_{iu}}\right)^2}. \tag{C.33}$$

Based on (4.60) and using (C.33), we can write the total power consumption as a function of number of IRS elements N as

$$P_{\text{c}}(N) = \frac{p_2^u}{\eta_{\text{pa}}^{\text{bs}}\left(\sqrt{\beta_{su}} + N\sqrt{\beta_{si}\beta_{iu}}\right)^2} + p_{\text{fix}} + p_{\text{s}} + p_{\text{lp}} + Np_e. \tag{C.34}$$

To obtain critical points, we differentiate $P_{\text{c}}(N)$ with respect to N and equate this to zero, i.e., $\frac{\partial P_{\text{c}}(N)}{\partial N} = 0$, to obtain

$$\frac{2p_2^u\sqrt{\beta_{si}\beta_{iu}}}{\eta_{\text{pa}}^{\text{bs}}\left(\sqrt{\beta_{su}} + N\sqrt{\beta_{si}\beta_{iu}}\right)^3} = p_e. \tag{C.35}$$

We observe that $\frac{\partial^2 P_{\text{c}}(N)}{\partial N^2} > 0$, therefore $P_{\text{c}}(N)$ is a convex function with respect to N and minimizes power consumption. Upon simplification of (C.35), we obtain optimal N as given in (4.63).

C.8 Proof of Theorem 4.7

From (4.64), we can write average received power at the user as $P_3^u = pM\beta_{su}$. Therefore, transmit power p as a function of M can be expressed as

$$p(M) = \frac{p_3^u}{M\beta_{su}}. \tag{C.36}$$

Based on the power consumption model discussed in (4.60) and using (C.36), we write the total power consumption as a function of number of antennas M at the source to obtain

$$P_{\text{c}}(M) = \frac{p_3^u}{\eta_{\text{pa}}^{\text{bs}}M\beta_{su}} + p_{\text{fix}} + M\left(p_{\text{s}} + p_{\text{lp}}\right). \tag{C.37}$$

Differentiating $P_{\mathrm{c}}(M)$ with respect to M, we obtain

$$\frac{\partial P_{\mathrm{c}}(M)}{\partial M} = -\frac{p_3^u}{\eta_{\mathrm{pa}}^{\mathrm{bs}} M^2 \beta_{su}} + p_{\mathrm{s}} + p_{\mathrm{lp}}. \tag{C.38}$$

Since, $\frac{\partial^2 P_{\mathrm{c}}(M)}{\partial M^2} > 0$, therefore $P_{\mathrm{c}}(M)$ is a convex function with respect to M and minimizes power consumption. Then, from (C.38), $\frac{\partial P_{\mathrm{c}}(M)}{\partial M} = 0$, gives $M_{\mathrm{opt}} = \sqrt{\frac{p_3^u}{\eta_{\mathrm{pa}}^{\mathrm{bs}} \beta_{su}(p_{\mathrm{s}}+p_{\mathrm{lp}})}}$ that minimizes the power consumption.

D Appendix

D.1 Proof of Lemma 5.1

We model Y_u as Gamma RV and find its shape parameter $k_u = \frac{r_{1_u}^2}{r_{2_u} - r_{1_u}^2}$ and scale parameter $t_u = \frac{r_{2_u} - r_{1_u}^2}{r_{1_u}}$ using moment matching method. We note that

$$r_{1_u} = \mathbb{E}(Y_u) = \mathbb{E}\left(\sum_{n=1}^{N} \rho_{si}^n \rho_{iu}^n\right) = \sum_{n=1}^{N} \mathbb{E}\left(\rho_{si}^n\right) \mathbb{E}\left(\rho_{iu}^n\right) = N\mu_{si}\mu_{iu}, \tag{D.1}$$

where $\mu_{si} = \sqrt{\frac{\pi\beta_{si}}{4}}$, $\mu_{iu} = \sqrt{\frac{\pi\beta_{iu}}{4}}$ and (D.1) follows from the fact that ρ_{si}^n and ρ_{iu}^n are independent Rayleigh RVs. And $r_{2_u} = \mathbb{E}\left(Y_u^2\right) = \mathbb{E}\left(\left(\sum_{n=1}^{N} \rho_{si}^n \rho_{iu}^n\right)^2\right)$ can be re-written as

$$r_{2_u} = \sum_{m,n=1}^{N} \mathbb{E}(\rho_{si}^m \rho_{si}^n)\, \mathbb{E}\left(\rho_{iu}^m \rho_{iu}^n\right) = \sum_{m,n=1}^{N} \left(\hat{R}_{si}^{mn} + \mu_{si}^2\right)\left(\hat{R}_{iu}^{mn} + \mu_{iu}^2\right), \tag{D.2}$$

where $\hat{R}_{si}^{mn}$ and $\hat{R}_{iu}^{mn}$ denote the $(m,n)^{\text{th}}$ element of the correlation matrices of the Rayleigh envelopes corresponding to $\beta_{si}\boldsymbol{G}_{si}$ and $\beta_{iu}\boldsymbol{G}_{iu}$, respectively. The $(m,n)^{\text{th}}$ element R_{si}^{mn} of the normalized correlation matrix can be expressed in terms of $\hat{R}_{si}^{mn}$ as $R_{si}^{mn} = \frac{\hat{R}_{si}^{mn}}{\sqrt{\text{var}(\rho_{si}^m)\text{var}(\rho_{si}^n)}} = \frac{4\hat{R}_{si}^{mn}}{(4-\pi)\beta_{si}}$.

Thus, (D.2) can be re-written in terms of R_{si}^{mn} and R_{iu}^{mn} as

$$r_{2_u} = \sum_{m,n=1}^{N} \left(\frac{(4-\pi)\beta_{si} R_{si}^{mn}}{4} + \mu_{si}^2 \right) \left(\frac{(4-\pi)\beta_{iu} R_{iu}^{mn}}{4} + \mu_{iu}^2 \right). \tag{D.3}$$

To obtain r_{2_u}, we need to determine R_{si}^{mn} and R_{iu}^{mn}. We note that

$$R_{si}^{mn} = \frac{\mathbb{E}\left(\rho_{si}^m \rho_{si}^n\right) - \mathbb{E}\left(\rho_{si}^m\right)\mathbb{E}\left(\rho_{si}^n\right)}{\sqrt{\text{var}\left(\rho_{si}^m\right)\text{var}\left(\rho_{si}^n\right)}} = \frac{4\mathbb{E}\left(\rho_{si}^m \rho_{si}^n\right) - \pi\beta_{si}}{(4-\pi)\beta_{si}}. \tag{D.4}$$

To further simplify (D.4), we need to obtain

$$\mathbb{E}\left(\rho_{si}^m \rho_{si}^n\right) = \int_0^\infty \int_0^\infty q_m q_n f_{\rho_{si}^m \rho_{si}^n}(q_m, q_n) dq_m dq_n. \tag{D.5}$$

We substitute the joint PDF $f_{\rho_{si}^m \rho_{si}^n}(q_m, q_n)$ from [104, Eqn. (1.5-22)] in (D.5) to obtain

$$\mathbb{E}\left(\rho_{si}^m \rho_{si}^n\right) = \int_0^\infty \int_0^\infty \frac{4q_m^2 q_n^2}{\beta_{si}^2\left(1-\left|G_{si}^{mn}\right|^2\right)} e^{\frac{-\left(q_m^2+q_n^2\right)}{\beta_{si}\left(1-\left|G_{si}^{mn}\right|^2\right)}} I_0\left(\frac{2q_m q_n \left|G_{si}^{mn}\right|}{\beta_{si}\left(1-\left|G_{si}^{mn}\right|^2\right)}\right) dq_m dq_n, \tag{D.6}$$

where $I_0(\cdot)$ denotes the zeroth order modified Bessel function of the first kind [68, Eqn. (8.447.1)]. We simplify the integral with respect to q_n further in (D.6) using [68, Eqn. (6.643.2)] to obtain

$$\mathbb{E}\left(\rho_{si}^m \rho_{si}^n\right) = \int_0^\infty \frac{\sqrt{\pi}\left(1-\left|G_{si}^{mn}\right|^2\right) q_m}{\left|G_{si}^{mn}\right|} e^{\frac{-q_m^2\left(2-\left|G_{si}^{mn}\right|^2\right)}{2\beta_{si}\left(1-\left|G_{si}^{mn}\right|^2\right)}} M_{-1,0}\left(\frac{q_m^2\left|G_{si}^{mn}\right|^2}{\beta_{si}\left(1-\left|G_{si}^{mn}\right|^2\right)}\right) dq_m, \tag{D.7}$$

where, $M_{\nu,\lambda}(\cdot)$ denotes the Whittaker function [68, Eqn. (9.221)]. We then use [68, Eqn. (7.621.1)] to obtain

$$\mathbb{E}\left(\rho_{si}^m \rho_{si}^n\right) = \frac{\pi\beta_{si}}{4} F\left(-0.5, -0.5; 1; \left|G_{si}^{mn}\right|^2\right). \tag{D.8}$$

Substituting $\mathbb{E}\left(\rho_{si}^m \rho_{si}^n\right)$ in (D.4), we obtain R_{si}^{mn} as given in (5.14). We can obtain R_{iu}^{mn} using similar ideas.

D.2 Proof of Theorem 5.1

We are interested in evaluating

$$\psi_u = \Pr\left(X_u + Y_u \le \overline{p}_{\text{th}}\right), \tag{D.9}$$

where $X_u = \rho_{su}$, $Y_u = \sum_{n=1}^{N} \rho_{si}^n \rho_{iu}^n$ and $\overline{p}_{\text{th}} = \sqrt{\frac{p'_{\text{th}}}{\eta p}}$. We can re-write ψ_u in integral form as

$$\psi_u = \int_{y=0}^{\overline{p}_{\text{th}}} \int_{x=0}^{\overline{p}_{\text{th}}-y} f_{X_u}(x)\, f_{Y_u}(y)\, dx\, dy, \tag{D.10}$$

where $f_{X_u}(x)$ is the PDF of X_u and $f_{Y_u}(y)$ is the PDF of Y_u. The equality in (D.10) holds since X_u and Y_u are mutually independent non-negative real RVs. To derive ψ_u, we need to compute $f_{X_u}(x)$ and $f_{Y_u}(y)$. Note that X_u is Rayleigh distributed and its PDF is given by

$$f_{X_u}(x) = \frac{2x}{\beta_{su}} \exp\left(\frac{-x^2}{\beta_{su}}\right), \quad x \geq 0. \tag{D.11}$$

And, we approximate Y_u as Gamma RV and show that this modeling is reasonably tight in Figure 5.1. Thus, the PDF of Y_u is given by

$$f_{Y_u}(y) \approx \frac{1}{t_u^{k_u}\Gamma(k_u)} y^{k_u-1} \exp\left(\frac{-y}{t_u}\right), \quad y \geq 0. \tag{D.12}$$

where k_u and t_u denote the shape and scale parameters, respectively, as given in Lemma 5.1. Substituting the PDF of X from (D.11) in (D.10) and solving the integral with respect to x, we obtain

$$\psi_u = \int_{y=0}^{\overline{p}_{\text{th}}} f_Y(y)dy - \int_{y=0}^{\overline{p}_{\text{th}}} \exp\left(\frac{-(y-\overline{p}_{\text{th}})^2}{\beta_{su}}\right) f_Y(y)dy. \tag{D.13}$$

Substituting $f_Y(y)$ from (D.12) in (D.13) and simplifying further, we obtain ψ_u in (5.16).

D.3 Proof of Theorem 5.2

To obtain diversity order, we analyze ψ_u for small values of channel gain in the high transmit power regime [97, 103]. We first derive the diversity order due to the cascaded path followed by the diversity order due to the direct path [103]. Based on Lemma 5.1, we model Y_u as a Gamma RV. Thus, the contribution to ψ_u due to the cascaded path equals

$$\psi_u^c = \int_{0}^{\overline{p}_{\text{th}}} \frac{1}{t_u^{k_u}\Gamma(k_u)} y^{k_u-1} e^{\frac{-y}{t_u}} dy. \tag{D.14}$$

By substituting $z = \frac{y}{t_u}$, (D.14) can be further simplified to obtain

$$\psi_u^c = \int_0^{\frac{\overline{p}_{\text{th}}}{t}} \frac{1}{\Gamma(k_u)} z^{k_u-1} \exp(-z)\, dz. \tag{D.15}$$

For small values of z, ψ_u^c above can be approximated as

$$\psi_u^c \approx \int_0^{\frac{\overline{p}_{\text{th}}}{t}} \frac{z^{k_u-1}}{\Gamma(k_u)} dz = \frac{1}{t_u^{k_u}\Gamma(k_u)} \left(\frac{p'_{\text{th}}}{\eta}\right)^{\frac{k_u}{2}} \left(\frac{1}{p}\right)^{\frac{k_u}{2}}. \tag{D.16}$$

From (D.16), we see that the exponent of p equals $\frac{-k_u}{2}$, therefore, diversity order due to the cascaded channels equals $\frac{k_u}{2}$.

We next derive the diversity order due to the direct path. The contribution to ψ_u due to the direct channel is given by

$$\psi_u^d = \int_0^{\frac{p'_{\text{th}}}{\eta p}} \frac{2}{\beta_{su}} e^{\frac{-2x}{\beta_{su}}} dx. \tag{D.17}$$

For small values of x, ψ_u^d in (D.17) can be approximated as

$$\psi_u^d \approx \int_0^{\frac{p'_{\text{th}}}{\eta p}} \frac{2}{\beta_{su}} dx = \frac{2p'_{\text{th}}}{\eta p \beta_{su}}. \tag{D.18}$$

Based on this, the diversity order due to direct channel equals 1. Since the direct channel is independent of the cascaded channels, therefore, the overall diversity order equals $1 + \frac{k_u}{2}$.

D.4 Proof of Lemma 5.2

Exploiting concave nature of the logarithmic function and using Jensen's inequality [98], we obtain

$$C_u \leq \log_2 \left(1 + \mathbb{E}\left(\frac{(1-\eta)p\left(\rho_{su} + \sum_{n=1}^{N} \rho_{si}^n \rho_{iu}^n\right)^2}{(1-\eta)\sigma^2 + \sigma_d^2}\right)\right). \tag{D.19}$$

Note that

$$\mathbb{E}\left((1-\eta)p\left(\rho_{su} + \sum_{n=1}^{N} \rho_{si}^n \rho_{iu}^n\right)^2\right) = (1-\eta)p\mathbb{E}\left((X_u + Y_u)^2\right). \tag{D.20}$$

This can be simplified further using Lemma 5.1 and the facts that $\mathbb{E}(X_u) = \sqrt{\frac{\pi\beta_{su}}{4}}$, $\mathbb{E}\left(X_u^2\right) = \beta_{su}$, $\mathbb{E}(Y_u) = r_{1_u}$, $\mathbb{E}\left(Y_u^2\right) = r_{2_u}$, and X_u and Y_u are independent.

Bibliography

[1] "Cisco visual networking index: Forecast and trends, 2017–2022," *White Paper*, 2018.

[2] R. Du, M. Xiao, and C. Fischione, "Optimal node deployment and energy provision for wirelessly powered sensor networks," *IEEE J. Sel. Areas Commun.*, vol. 37, no. 2, pp. 407–423, Feb. 2019.

[3] Z. Dawy, W. Saad, A. Ghosh, J. G. Andrews, and E. Yaacoub, "Toward massive machine type cellular communications," *IEEE Trans. Wireless Commun.*, vol. 24, no. 1, pp. 120–128, Feb. 2017.

[4] A. Osseiran *et al.*, "Scenarios for 5G mobile and wireless communications: the vision of the METIS project," *IEEE Commun. Mag.*, vol. 52, no. 5, pp. 26–35, May 2014.

[5] Z. Popovic, E. A. Falkenstein, D. Costinett, and R. Zane, "Low-power far-field wireless powering for wireless sensors," *Proc. IEEE*, vol. 101, no. 6, pp. 1397–1409, Jun. 2013.

[6] S. Kashyap, E. Björnson, and E. G. Larsson, "On the feasibility of wireless energy transfer using massive antenna arrays," *IEEE Trans. Wireless Commun.*, vol. 15, no. 5, pp. 3466–3480, May 2016.

[7] Q. Wu, X. Guan, and R. Zhang, "Intelligent reflecting surface-aided wireless energy and information transmission: An overview," *Proc. IEEE*, vol. 110, no. 1, pp. 150–170, Jan. 2022.

[8] T. L. Marzetta, "Massive MIMO: An introduction," *Bell Labs Tech. J.*, vol. 20, pp. 11–22, Mar. 2015.

[9] E. G. Larsson, O. Edfors, F. Tufvesson, and T. L. Marzetta, "Massive MIMO for next generation wireless systems," *IEEE Commun. Mag.*, vol. 52, no. 2, pp. 186–195, Feb. 2014.

[10] E. Björnson, E. G. Larsson, and T. L. Marzetta, "Massive MIMO: ten myths and one critical question," *IEEE Commun. Mag.*, vol. 54, no. 2, pp. 114–123, Feb. 2016.

[11] T. L. Marzetta, "Noncooperative cellular wireless with unlimited numbers of base station antennas," *IEEE Trans. Wireless Commun.*, vol. 9, no. 11, pp. 3590–3600, Nov. 2010.

[12] K. Senel, E. Björnson, and E. G. Larsson, "Human and machine type communications can coexist in uplink massive MIMO systems," in *Proc. ICASSP*, Apr. 2018, pp. 6613–6617.

[13] M. K. Sarangi and S. Kashyap, "Impact of pilot allocation strategies on outage in wireless energy transfer using massive antenna arrays," *IEEE Trans. Wireless Commun.*, vol. 20, no. 2, pp. 942–954, Feb. 2021.

[14] D. Mishra and H. Johansson, "Channel estimation and low-complexity beamforming design for passive intelligent surface assisted MISO wireless energy transfer," in *Proc. ICASSP*, Apr. 2019, pp. 4659–4663.

[15] D. Mishra and E. G. Larsson, "Passive intelligent surface assisted MIMO powered sustainable IoT," in *Proc. ICASSP*, May 2020, pp. 8961–8965.

[16] Q. Wu, S. Zhang, B. Zheng, C. You, and R. Zhang, "Intelligent reflecting surface-aided wireless communications: A tutorial," *IEEE Trans. Commun.*, vol. 69, no. 5, pp. 3313–3351, May 2021.

[17] Ö. Özdogan, E. Björnson, and E. G. Larsson, "Intelligent reflecting surfaces: Physics, propagation, and pathloss modeling," *IEEE Wireless Commun. Lett.*, vol. 9, no. 5, pp. 581–585, May 2020.

[18] "ISO/IEC/IEEE - international standard - telecommunications and information exchange between systems-specific requirements for local and metropolitan area networks-part 11: Wireless LAN medium access control (MAC) and physical layer (PHY) specifications," *ISO/IEC/IEEE 8802-11: 2022 (E)*, pp. 1–4382, Oct. 2022.

[19] R. Sarvendranath and A. K. R. Chavva, "Low-complexity joint antenna selection and beamforming for an IRS assisted system," in *Proc. WCNC*, Apr. 2021, pp. 1–6.

[20] Z. Abdullah, G. Chen, S. Lambotharan, and J. Chambers, "Low-complexity antenna selection and discrete phase-shifts design in IRS-assisted multiuser massive MIMO networks," *IEEE Trans. Veh. Technol.*, vol. 71, no. 4, pp. 3980–3994, Apr. 2022.

[21] X. Lu, I. Flint, D. Niyato, N. Privault, and P. Wang, "Self-sustainable communications with RF energy harvesting: Ginibre point process modeling and analysis," *IEEE J. Sel. Areas Commun.*, vol. 34, no. 5, pp. 1518–1535, May 2016.

[22] Z. Yang, Z. Ding, P. Fan, and G. K. Karagiannidis, "Outage performance of cognitive relay networks with wireless information and power transfer," *IEEE Trans. Veh. Technol.*, vol. 65, no. 5, pp. 3828–3833, May 2016.

[23] A. N. Abdulfattah, C. C. Tsimenidis, B. Z. Al-Jewad, and A. Yakovlev, "Performance analysis of MICS-based RF wireless power transfer system for implantable medical devices," *IEEE Access*, vol. 7, pp. 11 775–11 784, Jan. 2019.

[24] M. Najafi, V. Jamali, R. Schober, and H. V. Poor, "Physics-based modeling and scalable optimization of large intelligent reflecting surfaces," *IEEE Trans. Commun.*, vol. 69, no. 4, pp. 2673–2691, Apr. 2021.

[25] M. Fréchet, "Généralisation du théoréme des probabilités totales," *Fundamenta Mathematicae*, vol. 25, no. 1, pp. 379–387, 1935.

[26] E. D. Carvalho, E. Björnson, J. H. Sorensen, P. Popovski, and E. G. Larsson, "Random access protocols for massive MIMO," *IEEE Commun. Mag.*, vol. 55, no. 5, pp. 216–222, May 2017.

[27] E. D. Carvalho, E. Björnson, J. H. Sorensen, E. G. Larsson, and P. Popovski, "Random pilot and data access in massive MIMO for machine-type communications," *IEEE Trans. Wireless Commun.*, vol. 16, no. 12, pp. 7703–7717, Dec. 2017.

[28] L. Liu and W. Yu, "Massive connectivity with massive MIMO- Part I: Device activity detection and channel estimation," *IEEE Trans. Signal Process.*, vol. 66, no. 11, pp. 2933–2946, Jun. 2018.

[29] ——, "Massive connectivity with massive MIMO- Part II: Achievable rate characterization," *IEEE Trans. Signal Process.*, vol. 66, no. 11, pp. 2947–2959, Jun. 2018.

[30] L. Liu, E. G. Larsson, W. Yu, P. Popovski, C. Stefanovic, and E. D. Carvalho, "Sparse signal processing for grant-free massive connectivity: A future paradigm for random access protocols in the internet of things," *IEEE Signal Process. Mag.*, vol. 35, no. 5, pp. 88–99, Sep. 2018.

[31] K. Kim, D. J. Lee, and J. Choi, "Deep learning based pilot allocation scheme (DL-PAS) for 5G massive MIMO system," *IEEE Commun. Lett.*, vol. 22, no. 04, pp. 828–831, Apr. 2018.

[32] M. Sadeghi, E. Björnson, E. G. Larsson, C. Yuen, and T. Marzetta, "Joint unicast and multigroup multicast transmission in massive MIMO systems," *IEEE Trans. Wireless Commun.*, vol. 17, no. 10, pp. 6375–6388, Oct. 2018.

[33] D. Christopoulos, S. Chatzinotas, and B. Ottersten, "Multicast multigroup beamforming for per-antenna power constrained large-scale arrays," in *Proc. SPAWC*, Jun. 2015, pp. 271–275.

[34] Z. Xiang, M. Tao, and X. Wang, "Massive MIMO multicasting in noncooperative multicell networks," in *Proc. ICC*, Aug. 2014, pp. 4777–4782.

[35] M. Sadeghi, L. Sanguinetti, R. Couillet, and C. Yuen, "Reducing the computational complexity of multicasting in large-scale antenna systems," *IEEE Trans. Wireless Commun.*, vol. 16, no. 5, pp. 2963–2975, May 2017.

[36] M. Sadeghi, E. Björnson, E. G. Larsson, C. Yuen, and T. L. Marzetta, "Max-min fair transmit precoding for multi-group multicasting in massive MIMO," *IEEE Trans. Wireless Commun.*, vol. 17, no. 2, pp. 1358–1373, Feb. 2018.

[37] T. L. Marzetta, E. G. Larsson, H. Yang, and H. Q. Ngo, *Fundamentals of Massive MIMO*, Cambridge University Press, 2016.

[38] S. M. Kay, *Fundamentals of Statistical Signal Processing: Estimation Theory*, 1st ed. Prentice Hall Signal Processing Series, 1993, vol. 1.

[39] H. Q. Ngo, E. G. Larsson, and T. L. Marzetta, "Energy and spectral efficiency of very large multiuser MIMO systems," *IEEE Trans. Commun.*, vol. 61, no. 4, pp. 1436–1449, Apr. 2013.

[40] E. Becirovic, E. Björnson, and E. G. Larsson, "How much will tiny IoT nodes profit from massive base station arrays?" in *Proc. EUSIPCO*, Sep. 2018, pp. 832–836.

[41] S. Waldron, "Generalized welch bound equality sequences are tight frames," *IEEE Trans. Inf. Theory*, vol. 49, no. 9, pp. 2307–2309, Sep. 2003.

[42] E. Björnson, J. Hoydis, and L. Sanguinetti, "Massive MIMO networks: Spectral, energy, and hardware efficiency," *Found. and Trends Signal Process.*, vol. 11, no. 3, pp. 154–655, Nov. 2017.

[43] E. Björnson and E. Jorswieck, "Optimal resource allocation in coordinated multi-cell systems," *Found. and Trends Commun. and Inf. Theory*, vol. 9, no. 2, pp. 113–381, 2013.

[44] M. Grant and S. Boyd, *CVX: Matlab software for disciplined convex programming Version 2.1*, Mar. 2014.

[45] F. E. Bouanani, S. Muhaidat, P. C. Sofotasios, O. A. Dobre, and O. S. Badarneh, "Performance analysis of intelligent reflecting surface aided wireless networks with wireless power transfer," *IEEE Commun. Lett.*, vol. 25, no. 3, pp. 793–797, Mar. 2021.

[46] L. Zhao, Z. Wang, and X. Wang, "Wireless power transfer empowered by reconfigurable intelligent surfaces," vol. 15, no. 2, pp. 2121–2124, Jun. 2021.

[47] H. Yang, X. Yuan, J. Fang, and Y.-C. Liang, "Reconfigurable intelligent surface aided constant-envelope wireless power transfer," *IEEE Trans. Signal Process.*, vol. 69, pp. 1347–1361, Feb. 2021.

[48] Z. Feng, B. Clerckx, and Y. Zhao, "Waveform and beamforming design for intelligent reflecting surface aided wireless power transfer: Single-user and multi-user solutions," *IEEE Trans. Wireless Commun.*, vol. 21, no. 7, pp. 5346–5361, Jul. 2022.

[49] Y. Zheng, S. Bi, Y. J. Zhang, Z. Quan, and H. Wang, "Intelligent reflecting surface enhanced user cooperation in wireless powered communication networks," *IEEE Wireless Commun. Lett.*, vol. 9, no. 6, pp. 901–905, Jun. 2020.

[50] D. Xu, V. Jamali, X. Yu, D. W. K. Ng, and R. Schober, "Optimal resource allocation design for large IRS-assisted SWIPT systems: A scalable optimization framework," *IEEE Trans. Commun.*, vol. 70, no. 2, pp. 1423–1441, Feb. 2022.

[51] Q. Wu and R. Zhang, "Joint active and passive beamforming optimization for intelligent reflecting surface assisted SWIPT under QoS constraints," *IEEE J. Sel. Areas Commun.*, vol. 38, no. 8, pp. 1735–1748, Aug. 2020.

[52] S. Zargari, A. Khalili, and R. Zhang, "Energy efficiency maximization via joint active and passive beamforming design for multiuser MISO IRS-aided SWIPT," *IEEE Wireless Commun. Lett.*, vol. 10, no. 3, pp. 557–561, Mar. 2021.

[53] J. Liu, K. Xiong, Y. Lu, D. W. K. Ng, Z. Zhong, and Z. Han, "Energy efficiency in secure IRS-aided SWIPT," *IEEE Wireless Commun. Lett.*, vol. 9, no. 11, pp. 1884–1888, Nov. 2020.

[54] D. Gunasinghe and G. A. A. Baduge, "Performance analysis of SWIPT for intelligent reflective surfaces for wireless communication," *IEEE Commun. Lett.*, vol. 25, no. 7, pp. 2201–2205, Jul. 2021.

[55] S. Zargari, S. Farahmand, B. Abolhassani, and C. Tellambura, "Robust active and passive beamformer design for IRS-aided downlink MISO PS-SWIPT with a nonlinear energy harvesting model," vol. 5, no. 4, pp. 2027–2041, Dec. 2021.

[56] S. Gong, Z. Yang, C. Xing, J. An, and L. Hanzo, "Beamforming optimization for intelligent reflecting surface-aided SWIPT IoT networks relying on discrete phase shifts," vol. 8, no. 10, pp. 8585–8602, May 2021.

[57] A. Khalili, S. Zargari, Q. Wu, D. W. K. Ng, and R. Zhang, "Multi-objective resource allocation for IRS-aided SWIPT," *IEEE Wireless Commun. Lett.*, vol. 10, no. 6, pp. 1324–1328, Jun. 2021.

[58] J. He, K. Yu, Y. Shi, Y. Zhou, W. Chen, and K. B. Letaief, "Reconfigurable intelligent surface assisted massive MIMO with antenna selection," *IEEE Trans. Wireless Commun.*, vol. 21, no. 7, pp. 4769–4783, Jul. 2022.

[59] X. Pei, H. Yin, L. Tan, L. Cao, Z. Li, K. Wang, K. Zhang, and E. Björnson, "RIS-aided wireless communications: Prototyping, adaptive beamforming, and indoor/outdoor field trials," *IEEE Trans. Commun.*, vol. 69, no. 12, pp. 8627–8640, Dec. 2021.

[60] Q. Wu and R. Zhang, "Intelligent reflecting surface enhanced wireless network: Joint active and passive beamforming design," in *Proc. Globecom*, Dec. 2018, pp. 1–6.

[61] Q.-U.-A. Nadeem, H. Alwazani, A. Kammoun, A. Chaaban, M. Debbah, and M.-S. Alouini, "Intelligent reflecting surface-assisted multi-user MISO communication: Channel estimation and beamforming design," *IEEE Open J. Commun. Society*, vol. 1, pp. 661–680, May 2020.

[62] T. L. Jensen and E. De Carvalho, "An optimal channel estimation scheme for intelligent reflecting surfaces based on a minimum variance unbiased estimator," in *Proc. ICASSP*, May 2020, pp. 5000–5004.

[63] H. Shen, W. Xu, S. Gong, C. Zhao, and D. W. K. Ng, "Beamforming optimization for IRS-aided communications with transceiver hardware impairments," *IEEE Trans. Commun.*, vol. 69, no. 2, pp. 1214–1227, Feb. 2021.

[64] J. M. Kang, I. M. Kim, and D. I. Kim, "Joint Tx power allocation and Rx power splitting for SWIPT system with multiple nonlinear energy harvesting circuits," *IEEE Wireless Commun. Lett.*, vol. 8, no. 1, pp. 53–56, Feb. 2019.

[65] M. A. Abouzied, K. Ravichandran, and E. Sanchez-Sinencio, "A fully integrated reconfigurable self-startup RF energy-harvesting system with storage capability," *IEEE J. Solid-State Circuits*, vol. 52, no. 3, pp. 704–719, Mar. 2017.

[66] Y. Zeng and R. Zhang, "Optimized training design for wireless energy transfer," *IEEE Trans. Commun.*, vol. 63, no. 2, pp. 536–550, Feb. 2015.

[67] M. Simon and M.-S. Alouini, *Digital Communication over Fading Channels*, 2nd ed. Wiley-Interscience, 2005.

[68] I. S. Gradshteyn and I. M. Ryzhik, *Table of Integrals, Series and Products*, 4th ed. Academic Press, 1980.

[69] Q. Tao, J. Wang, and C. Zhong, "Performance analysis of intelligent reflecting surface aided communication systems," *IEEE Commun. Lett.*, vol. 24, no. 11, pp. 2464–2468, Nov. 2020.

[70] A. Papoulis, *Probability, Random Variables and Stochastic Processes*, 3rd ed. McGraw Hill, 1991.

[71] T. A. Khan, A. Yazdan, and R. W. Heath, "Optimization of power transfer efficiency and energy efficiency for wireless-powered systems with massive MIMO," *IEEE Trans. Wireless Commun.*, vol. 17, no. 11, pp. 7159–7172, Nov. 2018.

[72] H. J. Visser and R. J. M. Vullers, "RF energy harvesting and transport for wireless sensor network applications: Principles and requirements," *Proc. IEEE*, vol. 101, no. 6, pp. 1410–1423, Jun. 2013.

[73] E. Björnson, Ö. Özdogan, and E. G. Larsson, "Intelligent reflecting surface versus decode-and-forward: How large surfaces are needed to beat relaying?" *IEEE Wireless Commun. Lett.*, vol. 9, no. 2, pp. 244–248, Feb. 2020.

[74] P. Wang, J. Fang, H. Duan, and H. Li, "Compressed channel estimation for intelligent reflecting surface-assisted millimeter wave systems," *IEEE Signal Process. Lett.*, vol. 27, pp. 905–909, May 2020.

[75] Y. Yang, B. Zheng, S. Zhang, and R. Zhang, "Intelligent reflecting surface meets OFDM: Protocol design and rate maximization," *IEEE Trans. Commun.*, vol. 68, no. 7, pp. 4522–4535, Jul. 2020.

[76] A. A. Nasir, H. D. Tuan, T. Q. Duong, and L. Hanzo, "Transmitter-side wireless information- and power-transfer in massive MIMO systems," *IEEE Trans. Veh. Technol.*, vol. 69, no. 2, pp. 2322–2326, Feb. 2020.

[77] L. Zhao and X. Wang, "Massive MIMO downlink for wireless information and energy transfer with energy harvesting receivers," *IEEE Trans. Commun.*, vol. 67, no. 5, pp. 3309–3322, May 2019.

[78] Y. Alsaba, S. K. A. Rahim, and C. Y. Leow, "Beamforming in wireless energy harvesting communications systems: A survey," *IEEE Commun. Surv. Tuts.*, vol. 20, no. 2, pp. 1329–1360, 2nd Quart. 2018.

[79] L. Yang, Y. Yang, M. O. Hasna, and M. S. Alouini, "Coverage, probability of SNR gain, and DOR analysis of RIS-aided communication systems," *IEEE Wireless Commun. Lett.*, vol. 9, no. 8, pp. 1268–1272, Aug. 2020.

[80] Y. Han, S. Zhang, L. Duan, and R. Zhang, "Cooperative double-IRS aided communication: Beamforming design and power scaling," *IEEE Wireless Commun. Lett.*, vol. 9, no. 8, pp. 1206–1210, Aug. 2020.

[81] A. Papazafeiropoulos, P. Kourtessis, S. Chatzinotas, and J. M. Senior, "Coverage probability of double-IRS assisted communication systems," *IEEE Wireless Commun. Lett.*, vol. 11, no. 1, pp. 96–100, Jan. 2022.

[82] L. Dong, H.-M. Wang, J. Bai, and H. Xiao, "Double intelligent reflecting surface for secure transmission with inter-surface signal reflection," *IEEE Trans. Veh. Technol.*, vol. 70, no. 3, pp. 2912–2916, Mar. 2021.

[83] B. Zheng, C. You, and R. Zhang, "Double-IRS assisted multi-user MIMO: Cooperative passive beamforming design," *IEEE Wireless Commun. Lett.*, vol. 20, no. 7, pp. 4513–4526, Jul. 2021.

[84] H. Niu, Z. Chu, F. Zhou, C. Pan, D. W. K. Ng, and H. X. Nguyen, "Double intelligent reflecting surface-assisted multi-user MIMO mmwave systems with hybrid precoding," *IEEE Trans. Veh. Technol.*, vol. 71, no. 2, pp. 1575–1587, Feb. 2022.

[85] W. Mei and R. Zhang, "Cooperative beam routing for multi-IRS aided communication," *IEEE Wireless Commun. Lett.*, vol. 10, no. 2, pp. 426–430, Feb. 2021.

[86] E. Boshkovska, D. W. K. Ng, N. Zlatanov, and R. Schober, "Practical non-linear energy harvesting model and resource allocation for SWIPT systems," *IEEE Commun. Lett.*, vol. 19, no. 12, pp. 2082–2085, Dec. 2015.

[87] X. Bai, J. Shao, J. Tian, and L. Shi, "Power-splitting scheme for nonlinear energy harvesting AF relaying with direct link," *Wireless Commun. Mobile Comput.*, vol. 2018, pp. 1–8, Jul. 2018.

[88] T. Le, K. Mayaram, and T. Fiez, "Efficient far-field radio frequency energy harvesting for passively powered sensor networks," *IEEE J. Solid-State Circuits*, vol. 43, no. 5, pp. 1287–1302, May 2008.

[89] X. Yu, D. Xu, and R. Schober, "MISO wireless communication systems via intelligent reflecting surfaces," in *Proc. IEEE/CIC Int. Conf. Commun. China (ICCC)*, Aug. 2019, pp. 735–740.

[90] P.-A. Absil, R. Mahony, and R. Sepulchre, *Optimization algorithms on matrix manifolds*, Princeton University Press, 2009.

[91] J. C. Bezdek and R. J. Hathaway, "Some notes on alternating optimization," in *Proc. Conf. Adv. Soft Comput.*, 2002, pp. 288–300.

[92] "Evolved Universal Terrestrial Radio Access (E-UTRA); Further Advancements for E-UTRA Physical Layer Aspects (Release 9)," *Tech. Rep. 36.814*, Mar. 2010.

[93] T. Van Chien, A. K. Papazafeiropoulos, L. T. Tu, R. Chopra, S. Chatzinotas, and B. Ottersten, "Outage probability analysis of IRS-assisted systems under spatially correlated channels," *IEEE Wireless Commun. Lett.*, vol. 10, no. 8, pp. 1815–1819, Aug. 2021.

[94] C. Psomas and I. Krikidis, "SWIPT with intelligent reflecting surfaces under spatial correlation," *IEEE Wireless Commun. Lett.*, vol. 10, no. 9, pp. 1924–1928, Sep. 2021.

[95] M.-M. Zhao, Q. Wu, M.-J. Zhao, and R. Zhang, "Intelligent reflecting surface enhanced wireless networks: Two-timescale beamforming optimization," *IEEE Trans. Wireless Commun.*, vol. 20, no. 1, pp. 2–17, Jan. 2021.

[96] A. P. Ajayan, S. P. Dash, and B. Ramkumar, "Performance analysis of an IRS-aided wireless communication system with spatially correlated channels," *IEEE Wireless Commun. Lett.*, vol. 11, no. 3, pp. 563–567, Mar. 2022.

[97] C. Kumar, S. Kashyap, R. Sarvendranath, and S. K. Sharma, "On the feasibility of wireless energy transfer based on low complexity antenna selection and passive IRS beamforming," *IEEE Trans. Commun.*, vol. 70, no. 8, pp. 5663–5678, Aug. 2022.

[98] T. M. Cover and J. A. Thomas, *Elements of Information Theory*, Wiley series in telecommunications, 1991.

[99] H. A. David and H. N. Nagaraja, *Order Statistics*, 3rd ed. Wiley Series in Probability and Statistics, 2003.

[100] M. Chiani, D. Dardari, and M. K. Simon, "New exponential bounds and approximations for the computation of error probability in fading channels," *IEEE Trans. Wireless Commun.*, vol. 2, no. 4, pp. 840–845, Jul. 2003.

[101] S. Bharadwaj and N. B. Mehta, "Accurate performance analysis of single and opportunistic AF relay cooperation with imperfect cascaded channel estimates," *IEEE Trans. Commun.*, vol. 61, no. 5, pp. 1764–1775, May 2013.

[102] C. S. Patel and G. L. Stuber, "Channel estimation for amplify and forward relay based cooperation diversity systems," *IEEE Trans. Wireless Commun.*, vol. 6, no. 6, pp. 2348–2356, Jun. 2007.

[103] Z. Wang and G. Giannakis, "A simple and general parameterization quantifying performance in fading channels," *IEEE Trans. Commun.*, vol. 51, no. 8, pp. 1389–1398, Aug. 2003.

[104] W. C. Jakes, *Microwave Mobile Communications*, IEEE Press, 1993.